Emissions, Properties and Mixing State of Aerosols in a Range of Combustion Sources

A thesis submitted to the University of Manchester for the degree of Doctor of Philosophy in the Faculty of Science and Engineering

2018

Yu-Chieh Ting

School of Earth and Environmental Sciences
University of Manchester

Contents

Abstract

Atmospheric aerosols are ubiquitous in the atmosphere and have an impact on human health and atmospheric energy balance. Black carbon (BC) is the highly light-absorbing aerosol that affects climate warming by absorbing solar radiation, which is mainly produced by incomplete combustion of carbonaceous matter, including mobile sources, solid fuel burning and open biomass burning. The BC from solid fuel burning has been paid increased attention due to its strong emission at highly populated region, causing both climatic and health effect. Due to the changes in energy sources, biomass burning emissions have been globally identified to be a major source of the atmospheric aerosols. However, because of the complexity to characterise the emissions of biomass burning and the limitation of the previous instrumentation, the uncertainties of the BC properties and source apportionment for solid fuel burning still exist.

This project provides the insights on investigating a variety of BC sources by three experiments. First, comparisons were made between source apportionment techniques to investigate the causes of the difference between different source apportionment techniques, using the data from a comprehensive suite of aerosol measurements and the outputs from various source apportionment studies obtained from the cooperated groups of the Clean Air for London (ClearfLo) project. Data from a single particle soot photometer (SP2), Aethalometer, the outputs of positive matrix factorisation (PMF) of organic aerosol mass spectra measured by a high-resolution aerosol mass spectrometer (HR-AMS) and chemical mass balance (CMB) were used in this study. The results presented here indicated that oxygenated organic aerosols (OOA) and the assumption of absorption Angstrom exponent (α_{wb}) for wood burning have an effect on Aethalometer model, estimating the contribution of the biomass burning emissions to BC. In addition, it was found that the estimate of the carbonaceous matter contributed by wood burning derived by Aethalometer model in the previous studies were likely to be overestimated due to the attribution of the non-biomass burning organic matter to the biomass burning emissions.

Second, a cruise campaign was carried out along the Yangtze River (YR), where one of the most polluted regions in China. The first time continuous measurements of BC and gaseous pollutants over YR on the regional scale

indicated that the shipping emissions significantly contributed to air pollution during the highly polluted periods. BC with smaller mass median core diameter (MMD) of 120-180nm was found to be largely produced by the local sources, whereas a larger MMD of ~200nm was found for mixed sources from the regional transport. The consistency between the $PM_{2.5}$ from the measurements on the river and the official monitoring sites in the coastal cities supported the inference that the YR basin was strongly affected by the regional pollution.

Finally, laboratory experiments were conducted to characterise the solid fuel combustion emissions at source, using three commercial cookstoves with various solid fuels, which have been widely used in developing countries. The results provided a useful insight into interactions between BC and OM, which were parameterised according to modified combustion efficiency. In addition, the finding of the relationship between the OM fraction in PM_1 and mixing state of BC can aid in assessment of the absorption enhancement of BC in models, where the BC source profile of solid fuel combustion emissions is not available.

In summary, these findings provide an in-depth understanding of BC emissions from a variety of sources in real world, which can underpin either the future research or the mitigation strategies.

Declaration

No portion of the work referred to in this thesis has been submitted in support of an application for another degree or qualification of this or any other university or other institute of learning.

Copyright statement

i. The author of this thesis (including any appendices and/or schedules to this thesis) owns certain copyright or related rights in it (the “Copyright”) and she has given The University of Manchester certain rights to use such Copyright, including for administrative purposes.

ii. Copies of this thesis, either in full or in extracts and whether in hard or electronic copy, may be made only in accordance with the Copyright, Designs and Patents Act 1988 (as amended) and regulations issued under it or, where appropriate, in accordance Presentation of Theses Policy You are required to submit your thesis electronically Page 11 of 25 with licensing agreements which the University has from time to time. This page must form part of any such copies made.

iii. The ownership of certain Copyright, patents, designs, trademarks and other intellectual property (the “Intellectual Property”) and any reproductions of copyright works in the thesis, for example graphs and tables (“Reproductions”), which may be described in this thesis, may not be owned by the author and may be owned by third parties. Such Intellectual Property and Reproductions cannot and must not be made available for use without the prior written permission of the owner(s) of the relevant Intellectual Property and/or Reproductions.

iv. Further information on the conditions under which disclosure, publication and commercialisation of this thesis, the Copyright and any Intellectual Property and/or Reproductions described in it may take place is available in the University IP Policy (see http://documents.manchester.ac.uk/DocuInfo.aspx? DocID=24420), in any relevant Thesis restriction declarations deposited in the University Library, The University Library’s regulations (see http://www. library.manchester.ac.uk/about/regulations/) and in The University’s policy on Presentation of Theses

Acknowledgements

I am incredibly grateful to my supervisors Prof. Hugh Coe and Dr. James Allan for their guidance, support and encouragement throughout my PhD. Hugh, I am really thankful for your support and that always finding time to discuss my work and provided much appreciated advice about my future. I am eternally grateful to James for not only teaching me the operation of the instruments I needed for my PhD, but always providing me with valuable advice when I was confused about my work.

I would like to thank the aerosol group. I really enjoyed the group meetings every Monday. The friendly atmosphere and the opportunity to listen to the different research topics from others helped me to think about my research from different ways. Special thanks must go to Dantong not only for his endless help in my research but also in life throughout my PhD.

Thank you Ernesto, Mike, Zixia and Nick. Your company and assistance make me not alone during the period of my PhD.

Finally but definitely not least, I would like to thank to my family for their unlimited support, whether financial or spiritual. I really would not be where I am today without them.

Thesis overview

In this thesis, the investigation of the characteristics of carbonaceous aerosols from combustion sources is provided by the field measurements in the UK and China, and the laboratory work. This thesis is structured following the journal format, which includes the results section comprising scientific papers. **Chapter 1** gives an overview of the aerosol properties, sources and the effects on human health and air quality. More importantly, it highlights the importance of studying carbonaceous aerosols, which provides the fundamental basis for this work. An overview of the aerosol community and air quality in the UK and China is aslo provided in this chapter. It emphasizes the current issues regarding black carbon (BC), which the UK and China are facing. **Chapter 2** presents an overview of the current BC measurements and highlights the problem that this work aims to deal with. A review of the instruments utilised in this work is presented in **Chapter 3**, comprising the analysis techniques used to process dataset. A brief description of the source apportionment techniques is presented here as well, although only the outputs of these models are used in this study.

Chapter 4 consists of three scientific papers. **Paper I** shows the comparison of the outputs from the different analysis techniques based on a suite of the comprehensive measurements in London. The components of the atmospheric particles affecting the measurement and estimation of the biomass burning emissions are investigated here. In **Paper II**, BC properties and gaseous pollutants over the Yangtze River are investigated during wintertime. The cruiser campaign is firstly to continuously measure the shipping emissions and the air pollution of the complex sources transported from the coastal cities along the river in order to investigate the characteristics of BC and infer the sources which may affect the air quality in this area on the regional scale. In **Paper III**, a laboratory-based experiment was conducted in order to investigate the primary emissions from solid fuel combustion at source. The interaction of BC and OM according to combustion efficiency was explored to provide a common metric for the atmospheric emission community. Finally, the implications of these findings and recommendations for future research are provided in **Chapter 5**.

Chapter 1

Introduction

1.1 Atmospheric Aerosols

Aerosols are defined as suspensions of clusters of liquid or/and solid particles in a gaseous medium (Seinfeld and Pandis, 2006). Aerosols have been found to have a negative effect on climate change (Seinfeld and Pandis, 2012), air quality (Fuzzi et al., 2015), and particularly to human health (Pöschl, 2005). Thus, it is important to completely understand the physical and chemical properties of aerosols and with their processes in the atmosphere. The physical characteristics such as particle size, number and shape are required to enable the basic understanding of the role of aerosols in the atmosphere. The chemical compositions of aerosols are of importance as they determine the optical properties and different components present diverse effects on human health; moreover, aerosols are also classified by their chemical composition as organics or inorganics and have significantly different properties due to the complex chemical compositions.

1.1.1 Aerosol effects

Atmospheric aerosols are of central importance for atmospheric chemistry, physics, air quality, human health, and climate change; the effects of aerosols on the air quality, climate, and public health have been a concern for decades and have become an issue of political and global interest. The main impacts of aerosol pollution observed on air quality are the degradation of visibility (Watson, 2002) and harm to human health. Poor visibility caused by haze, consisting of fine particles and gaseous air pollution in the atmosphere, is not only an aesthetic problem but also a safety issue of traffic. Growing evidence of the correlation between adverse effects on human health and fine particulate matter (Chow et al., 2006; Pope and Dockery, 2006; Ramgolam et al., 2009) is illustrated by the fact that ambient air pollution has been characterized as carcinogenic since December 2013 by the International Agency for Research on Cancer (Loomis et al., 2013). However, the “aerosol cocktail effect”, directly linked to the complexity of the chemical composition and sources of the particulate phase, remains poorly understood. In addition, aerosols also play important roles in diverse chemical and physical processes in the atmosphere. The Earth’s climate, hydrological cycle and

various ecosystems are all known to be affected by atmospheric aerosols through changing the Earth's radiative balance, the deposition of acids and toxins, and other species onto soils and into aquatic systems. As aerosol sources are not uniformly distributed geographically, the distribution of atmospheric aerosols is fairly inhomogeneous and so these aerosols have both global and regional effects on climate. The adverse effects of aerosols on visibility, air quality and human health are of principal concern in urban areas, particularly as both the emission rates of aerosols and the number of people exposed to urban pollution are likely to increase in the future.

1.1.2 Aerosol Sources

Aerosols, depending on their origins, are classified into natural or anthropogenic. Natural sources of aerosols include mineral dust, sea salt spray, volcanic eruptions and vegetation (Monks et al., 2009). Anthropogenic sources include traffic emissions, fuel combustion, industrial processes, biomass burning and cooking (Seinfeld and Pandis, 2006, Jimenez et al., 2009). Secondary aerosols are mainly formed by condensation in the atmosphere from chemical processes involving a set of the gaseous precursors (Fuzzi et al., 2006), such as sulphur dioxide (SO_2) generated predominantly by solid fuel combustion, nitrogen oxides (NO_x) generated by combustion of fossil fuel and ammonia (NH_3) originating from synthetic fertilizers, which may react with other gases or materials, such as ozone (O_3) and hydroxyl radical (·OH), forming secondary inorganic aerosols (SIA). In addition, secondary organic aerosols (SOA) are formed by the condensation of volatile organic compounds (VOCs) emitted by the biosphere (BVOCs) acting as both biogenic and anthropogenic sources.

1.1.3 Particle Size

In the atmosphere, aerosol particles span a very wide range of sizes from a few nanometres (nm) to tens of micrometres (μm), which can be roughly split into three groups: ultrafine particles, which have an aerodynamic diameter less than 0.1 μm, fine particles, which have an aerodynamic diameter of less than 2.5 μm, and coarse particles with an aerodynamic diameter greater than 2.5 μm. Figure 1.1 illustrates typical PM volume and number distribution according to size showing multimodal nature of the ambient aerosols.

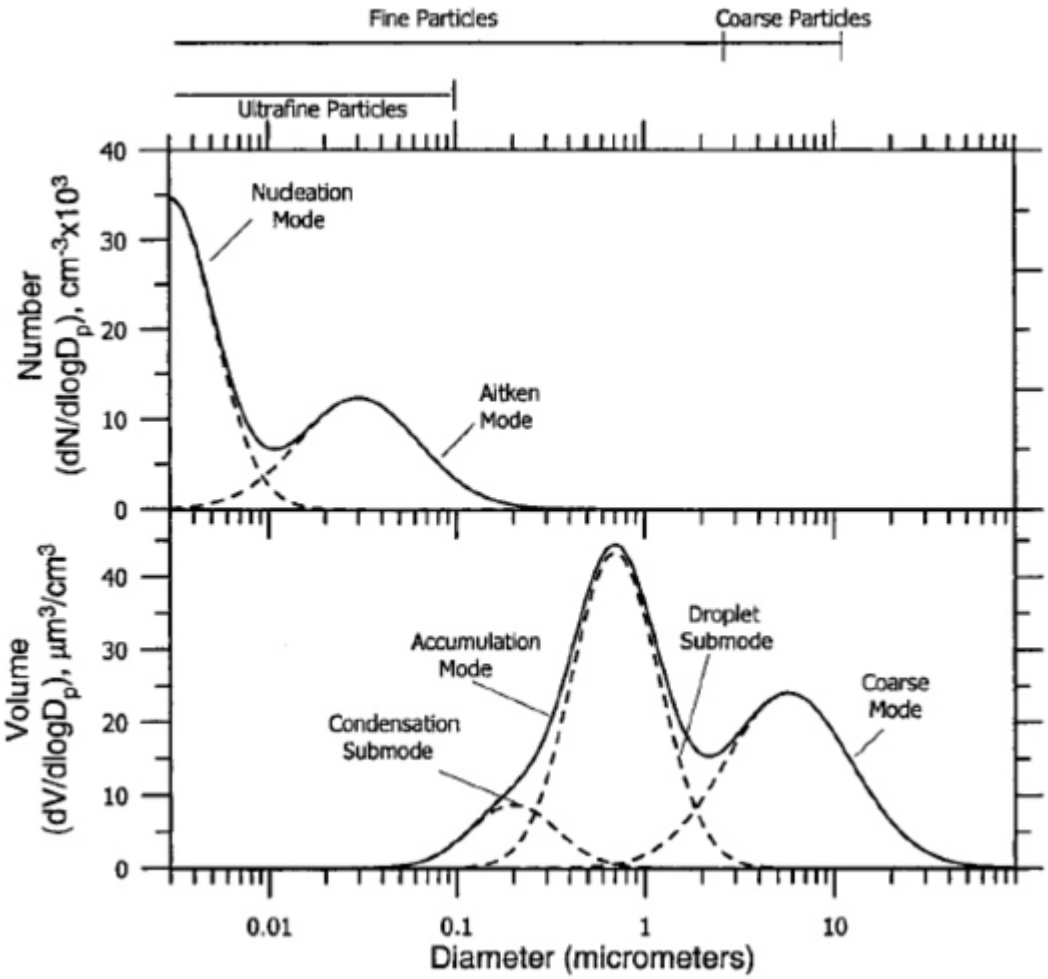

Figure 1.1 Typical particulate number and volume distributions with the different particle sizes and modes (Seinfeld and Pandis, 2006).

In the volume distribution, particles in the accumulation (an aerodynamic diameter from around 0.1 to 2.5 µm) and coarse (an aerodynamic diameter greater than 2.5 µm) modes are dominating in the ambient aerosols (Seinfeld and Pandis, 2006). Particles prevail in the accumulation mode as they are formed as a result of primary emissions and condensation of secondary aerosols, e.g. sulfates, nitrates and organics, from the gas phase. Moreover, coagulation of smaller particles also result in the formation of the accumulation mode particles. To increase the diameter of larger particles requires more mass so there is a limit to the growth of accumulation mode particles by either condensation of coagulation and this leads to a well characterised submicron mode. There are two overlapping sub-modes included in the accumulation mode: the condensation sub-mode particles which are formed as a result of the growth of smaller particles by coagulation and vapour condensation, and the droplet sub-mode particles are created by chemical reactions in cloud droplets and thus contribute to the accumulation mode particles (Heintzenberg et al., 2003). Particles in the accumulation mode are long-lived in

the atmosphere as the removal mechanisms are least efficient compared to coarse mode. Therefore, the lifetime of the accumulation mode particles is significantly longer than those in other modes.

The coarse mode particles originate mainly from mechanical processes such as the mechanism in the fragmentation of bulk materials or from sea spray (Seinfeld and Pandis, 2006). These particles contribute substantially to the total mass, although the number of such particles often presents a small value. Furthermore, the coarse mode particles are shorter-lived in the atmosphere, over a short timescale of a few hours to days, due to their size causing high sedimentation velocities.

Another view of the ambient aerosol distribution is obtained if one focuses on the number of particles (Figure 1.1, upper panel). While particles with diameters larger than 0.1 μm are the main contributors to the aerosol volume, they are negligible in number compared to those of the diameter smaller than 0.1 μm. Two modes dominate the aerosol number distribution - the nucleation mode where the diameters of particles are smaller than 10 nm and the Aitken mode where the diameters of the particles are between 10 and 100 nm. However, due to the small size, particles in the nucleation mode do not have an important contribution to volume, although they have a high contribution in number.

Particles in the nucleation mode are usually formed from gaseous species by nucleation depending on the atmospheric conditions. Most of the Aitken mode particles are formed as primary particles condensed subsequently by secondary species as they are transported through the atmosphere. They can also be formed as a result of the coagulation of nucleation mode particles. Mass of the nucleation mode particles are negligible, e.g. 100,000 particles cm^{-3} with a diameter equal to 10 nm have a mass concentration of lower than 0.05 μg m^{-3} (Seinfeld and Pandis, 2006), while the larger Aitken nuclei contribute to the mass distribution due to the formation of the accumulation mode.

Overall, particulate matter (PM) is categorised according to the aerodynamic diameter and can overlap to comprise a broad range of size distribution observed in the atmosphere. PM_{10} represents the particles with an aerodynamic diameter less than 10 μm, $PM_{2.5}$ describes the particles with an aerodynamic diameter less than 2.5 μm and PM_1 stands for those particles with an aerodynamic diameter less

than 1 μm. Although atmospheric PM pollution levels are generally determined based on the PM_{10} and $PM_{2.5}$ (Pope and Dockery, 2006), PM_1 particles have been increasingly pointed out that they account for a large fraction of $PM_{2.5}$ (Liu et al., 2004). It is therefore more effective to carry out the measurement of PM_1 and investigate the characteristics of the aerosols.

1.1.4 Aerosol Chemical Compositions

Chemical composition of atmospheric aerosols is very complex and variable due to the various sources and transformations of their components. A recent overview indicated that atmospheric PM predominantly comprises nitrate, sulphate, ammonium, sea salt, mineral dust, organic compounds and black carbon (Monks et al., 2009). It is estimated that each of the chemical compounds typically contribute approximately 10-30% to the total mass loading depending on the locations, meteorological conditions, times and particle size fractions (Monks et al., 2009). The dominant components of the fine particles are inorganic aerosols, including nitrate, sulphate and ammonium, and carbonaceous aerosols, comprising organic species and black carbon.

1.1.4.1 Inorganic aerosols

Sulphate (SO_4^{2-}), nitrate (NO_3^-) and ammonium (NH_4^+) are the main secondary inorganic aerosol components, which are formed from the oxidation of gaseous precursors, existing mainly as ammonium sulphate ($(NH_4)_2SO_4$) and ammonium nitrate (NH_4NO_3) which are generated respectively by the neutralization of sulphuric acid (H_2SO_4) and nitric acid (HNO_3) with ammonia (NH_3) (Stockwell et al., 2003). The formation of sulphate aerosols is from both natural, such as the eruption of volcanoes and forest fires, and anthropogenic sources where sulphur dioxide (SO_2) is the predominantly anthropogenic precursor of fossil fuel combustion and biomass burning emissions. The neutralization of H_2SO_4 generally predominates over the neutralization of HNO_3 (Seinfeld and Pandis, 2006). However, the production of sulphate and/or nitrate aerosols strongly depends on certain factors of micro-meteorology and chemical, such as the ambient temperature, relative humidity, the amount of gaseous precursors, the concentrations of oxidants and the properties of pre-existing aerosols (Baek et al., 2004, Pathak et al., 2009).

1.1.4.2 Carbonaceous aerosols

The carbonaceous species of atmospheric aerosols, which include organic matter (OM) and black carbon (BC) or elemental carbon (EC), typically constitute a dominant fraction of the fine particle mass. BC is a primary aerosol emitted directly from incomplete combustion processes, such as fossil fuel and biomass burning. BC has been found to be the most strongly light-absorbing component of soot (e.g. Schwarz et al. (2008b)). The terminology in this field varies depending on the measurement methodologies used, where the definitions are based on optical properties, morphological discrepancies, sources and chemical composition. BC or EC is terms frequently used for the major light absorbing component of combustion aerosols while the most commonly used term is BC which is similar to soot carbon in terms of optical properties and composition (Andreae and Gelencsér, 2006).

OM, another component of the carbonaceous fraction (Quincey et al., 2009), is a complex mixture of numerous of carbon-containing compounds. Organic aerosols (OA) comprise substantial fraction (~20-90%) of submicron aerosol mass (Kanakidou et al., 2005, Zhang et al., 2007) and approximately 10-70% of the total dry fine particle mass respectively in the atmosphere (Turpin et al., 2000); they are composed of tens of thousands of compounds (Hamilton et al., 2004) with a wide range of properties such as oxidation state and volatility (Goldstein and Galbally, 2007), results in being challenging to analyse, particularly the discrepancies between different thermal-optical organic matter (OM) quantification and artificial removal techniques (Turpin et al., 2000, Kanakidou et al., 2005).

OA originate from both natural and anthropogenic sources and can be classified as primary OA (POA) emitted directly in particulate form typically by vehicular transport and solid fuel burning, and secondary OA (SOA), the dominant portion of organic aerosols, formed from the gas-phase oxidation of volatile organic compounds (VOCs) (Kanakidou et al., 2005, Shiraiwa et al., 2013). Nevertheless, the knowledge of organic aerosols' composition, properties and sources in the atmosphere is still extremely limited, and the precursors of SOA have currently become a major research topic (Fuzzi et al., 2006). Moreover, Goldstein and Galbally (2007) inferred that 10,000-100,000 different organic species have been measured in the atmosphere. While these species may account for a small fraction

in the atmosphere, they may have potential negative effects on human health and air quality.

1.1.4.3 Carbonaceous aerosols spatial concentrations

The importance of understanding carbonaceous aerosols composition, sources and contribution to air pollution is due to that a large proportion of submicron particulate matter is composed of them (Kanakidou et al., 2005, Zhang et al., 2007). Figure 1.2 shows the fractional composition of the non-refractory submicron particle mass from different studies at the various stations (Zhang et al., 2007). The average mass concentrations range from 2.6 μg m^{-3} at a rural site in Finland to 71 μg m^{-3} in an urban area in China. In most of the monitoring sites, OA contributed to a large fraction of PM_1. Moreover, the chemical composition of aerosols varies greatly from place to place, and high mass concentrations of particles are generally present in urban cities.

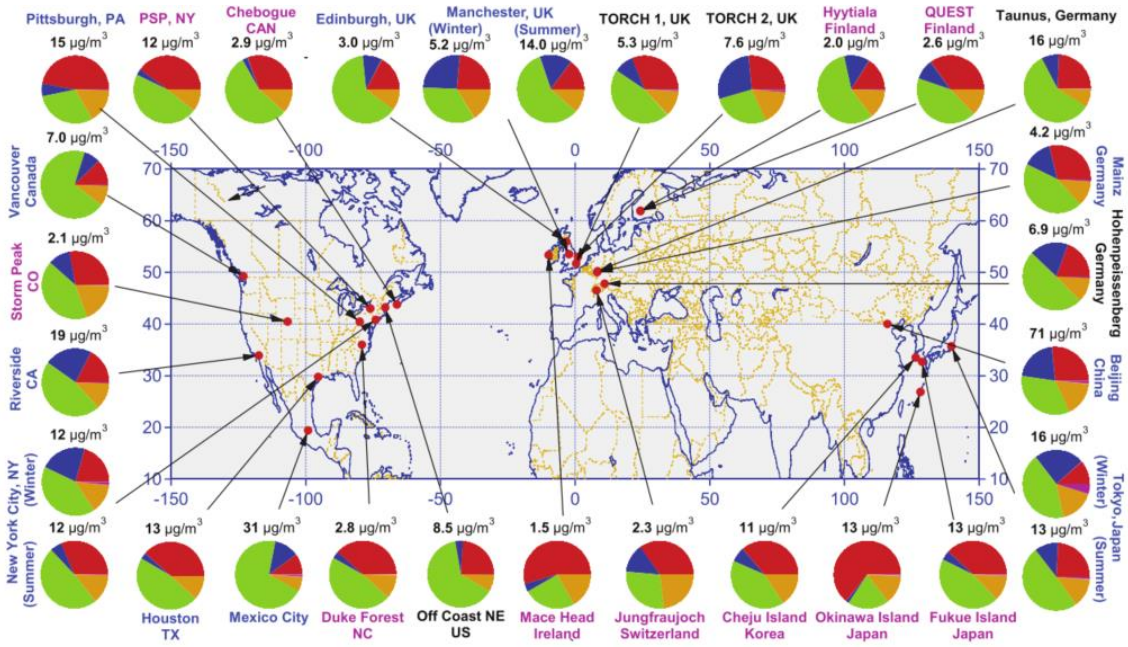

Figure 1.2 Average mass concentration of the non-refractory submicron particle mass (NR-PM_1) at the various locations, reproduced from Zhang et al. (2007). Colours for the study locations indicate the type of sampling site. Urban areas (blue), <100 miles downwind of major cities (black), and rural/remote areas >100 miles downwind (pink). Pie chart colours indicate the average mass concentration of chemical composition, which are organics (green), sulphate (red), nitrate (blue), ammonium (orange), and chloride (purple), of NR-PM_1.

In recent year, BC emission has increasingly received attention of people due to the evidence of its effect on human health (Smith et al., 2009), air quality and global climate (Ramanathan and Carmichael, 2008, Bond et al., 2013). However, there is no agreement on measuring methods that lead to high uncertainty of the

estimation of BC emission in the atmosphere. Moreover, the shortage of characterization studies on BC emissions from the various emission sources makes is even difficult to obtain accurate estimation of BC emissions in developing countries (Ni et al., 2014). An observation in winter at an Beijing urban site in China showed that the average mass concentrations of rBC were 7.6 μg m^{-3} and 0.4 μg m^{-3} on the polluted days and clean days, respectively (Wu et al., 2017). A long-term measurement in an urban area in Shanghai showed an average BC mass concentration of 2.6 μg m^{-3} in 2013 and 2.1 μg m^{-3} in 2014. In Africa urban site, BC mass concentrations ranged from lower about 8 μg m^{-3} to higher 13 μg m^{-3} due to regional transport of polluted air masses over West Africa (Doumbia et al., 2012). The sources of BC emissions vary with the lifestyle in different regions and the types of fuel used. Figure 1.3 illustrates the structure of the global BC emission sources. Mobile-related sources account for about 24% of the global BC emissions, and approximately 24% and 10% are related to residential emissions and industry and power generation, respectively.

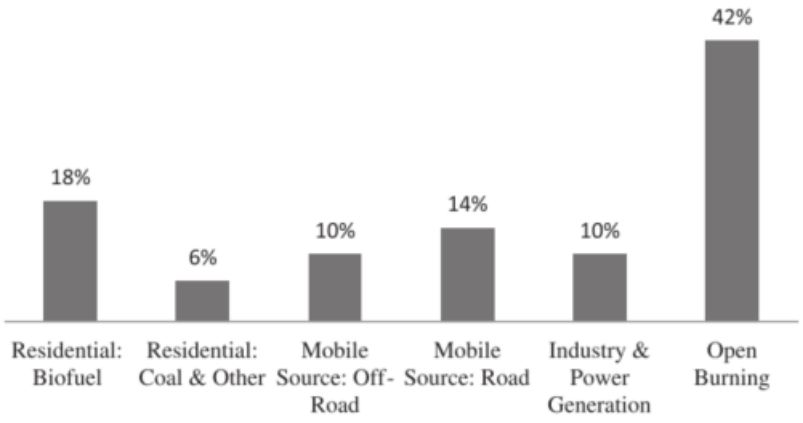

Figure 1.3 Global contribution of sources to BC emissions. Reprinted from Ni et al. (2014).

1.2 Air quality

1.2.1 In the UK

Air pollution in the UK has been considered to have negative effects on the ambient environment and public health for decades. In the UK, air pollution is a major cause of diseases such as lung disease, cardiovascular disease, respiratory disease, asthma, and stroke (Brook et al., 2004). As a consequence of the public's increasing reliance for energy upon the burning of fossil and solid fuels throughout the Industrial Revolution, there were more and more occurrences of urban smog events. According to the historical records, particulate air pollution, black smoke, was first measured in the 1920s (Quincey, 2007); the first air quality network, UK Black Smoke Network was established. Owing to the infamous smog events in 1950s and 1960s, which finally precipitated public concern, the UK government introduced its first Clean Air Act in 1956 (https://uk-air.defra.gov.uk/networks/brief-history). In 1961, the UK established the first coordinate national air pollution monitoring network, named the National Survey, which monitored BC and sulphur dioxide (SO_2) throughout the UK and provided valuable datasets revealing the impacts of the Clear Air Acts (Bryner, 1993). In 2008, the manual black smoke samplers were replaced by Automatic Magee AE22 Aethalometer black carbon analysers to quantify the BC based on the transmission of light on a filter sample. The BC network comprised 14 sites making measurements in 2015 (Butterfield et al., 2016).

The monitoring data demonstrated that the legislation and the development of cleaner fuels successfully decreased the black smoke and sulphur dioxide concentrations. However, with the dramatic increase in road traffic, focus shifted progressively to the pollutants from vehicular emissions, including nitrogen dioxide, ozone and fine particulate matter. This led the UK to establish an automatic urban monitoring network in 1987, to monitor the emerging directive with EC limit values on air quality. In the coming years, the UK government expanded unban monitoring and improved the availability of air quality information for the population. In 1998, these separated UK urban and rural monitoring sites were combined to form the Automatic Urban and Rural Network (AURN), currently operating with 108 sites (DEFRA, 2017).

1.2.1.1 London

The population of London was estimated to be 7.6 million in 2007 (Wroth and Wiles, 2009), whilst Greater London, including the surrounding areas has a population over 13 million, making it the largest megacity in the European Union. London has experienced substantial air quality problems mainly produced by anthropogenic sources. One of the worst air quality events, the great smog, happened in 1952, when in winter a cold weather outbreak combined with an anticyclone and low wind speeds led to optimal conditions for accumulation of pollutants particularly particulate matter and sulphur dioxide resulting in high concentrations of air pollutants. The main source of pollution was coal combustion due to heating in the cold weather which is estimated to cause 4000 deaths (Brunekreef and Holgate, 2002). Smokeless fuel regulation and the consumption of cleaner energy from gas or liquid were legislated to improve this severe situation leading to a rapid decline in air pollutants in London through 1960s and 1970s. However, a massive growth in road traffic was accompanied by this change in emissions, resulting in problems with emissions of other pollutants such as carbon monoxide (CO) and nitrogen oxides (NO_x), which caused an occurrence of pollution episode in London in 1991 causing significant impacts on air quality (Harrison et al., 2012). Previous studies in London indicated that a large fraction of particulate matter arises from regional transport rather than from formation within London itself (Charron et al., 2007, Abdalmogith and Harrison, 2006). Moreover, the impacts on formation of secondary inorganic aerosol (SIA) are uncertain due to the nonlinear correlation between SIA concentrations and the reduction in precursor emissions (AQEG, 2012). In winter, air quality in the London urban area is significantly influenced by solid fuel combustion, such as wood burning for residential heating (Allan et al., 2010). Despite stricter emission standards for particulate matter and precursors of secondary aerosols from various sources, concentrations of airborne particles have not significantly reduced in London as the processes of particle formation and transport from sources are still poorly understood (Harrison et al., 2008).

In the UK, the emissions of domestic wood burning has been systematically underestimated in the national inventory (Water, 2016), and it is therefore essential to properly quantify its contribution to the ambient environment. In addition to quantify BC concentrations, Aethalometers in cities in the UK measure

light absorption of the collected particles at two different wavelengths, which can be processed to quantify the particle matter from wood burning. However, there have been literatures indicating that non-BC absorbing particles can affect Aethalometer measurements to a certain extent (Wang et al., 2014a, Saleh et al., 2013). Therefore, the need to better understand the contribution of sources to PM for environmental policies is essential.

1.2.2 In China

China has been and continuous to be a rapidly developing country and has suffered from severe air pollution, which has been a major issue, posing a great risk to public health. In China, during 2010, air pollution was found to be the fourth highest factor of deaths due to the inhalation of particulate matter (Wong, 2013). It is estimated that air pollution contributes to 1.2 to 2 million deaths annually (Yang et al., 2013, Rohde and Muller, 2015). In 2012, Zhong Nanshan, the president of the China Medical Association, warned that air pollution would be the biggest health issue if the government was still reluctant to investigate and publicly disclose the medical consequences (Watts, 2012). In the same year, China adopted the Ambient Air Quality Standard (China, 2012) and developed a national Air Reporting System that currently comprises 945 sites in 190 cities. These automated stations report hourly data and focus on six pollutants: $PM_{2.5}$, PM_{10}, carbon monoxide (CO), ozone (O_3), nitrogen dioxide (NO_2) and sulphur dioxide (SO_2). Previous air pollution studies in regional scale generally relied on satellite data (Zhang et al., 2012) or modelling (Liu et al., 2010, Lei et al., 2011), but the high density of monitoring data from the ground in China now allows the regional patterns to be constructed.

China is the largest user of coal as a source of energy production in the world. China is the worst fossil fuel for local and global pollutant emissions (Benjamin 2016). The origin of the poor air quality in China can be traced back to the 1950s following the Second World War, when China was making massive efforts to rapidly develop its economy and reconstruct the country. The poor air quality did not receive the attention of Chinese government until 1980s, when the population increased rapidly so did the level of air pollution. The debate of the environmental issues intensified in 1980s, as some people believed that sustained economic growth could not continue without considering the environmental impacts it has, while others believed that China should follow “pollute first and clean up later”

pattern (Edmonds, 1999). The first efforts dealing with ecological problems began around 1972 when the Republic of China sent a delegation to the First United Nation Conference on Human Environment in Stockholm (Edmonds, 1999). In 1979, the government promulgated the Environmental Protection Law for trial implementation and the purpose of harmonious development. There has been stronger determination to deal with environmental problem, and the full Environmental Protection Law was adopted in 1989, although environmental policy was still held back by prioritization of economic growth. The upgrade from the National Environmental Protection Agency to the State Environmental Protection Administration (SEPA) in 1998 revealed an attempt by the government to put more efforts into environmental plans. In 2008, the SEPA was further changed to the Ministry of Environmental Protection (MEP) and set a goal to reduce 10% of the national SO2 emission level by 2005 (i.e. 18.0 Tg/year) compared to 2000 (20 Tg/year).

In 2013, measurements by the Beijing municipal government showed that the highest recorded level of $PM_{2.5}$ was at nearly 1000 μg m^{-3}. Based on the particle sampling, chemical analysis and source apportionment models, the primary sources of $PM_{2.5}$ in China have been identified to be vehicle emissions, coal combustion and industrial sources (Zhang et al., 2012, Pui et al., 2014).

There has been sufficient evidence that exposure to air pollution is harmful to health in China. Although China has made immense amounts of progress in slowing down air pollution and preventing mortality from this pollution, it still faces the worst air pollution problems in the world (Kan et al., 2009). Air pollution in China is currently a major concern as the Chinese population accounts for nearly one-fourth of the world population.

1.2.2.1 Yangtze River

"Yangtze River (YR)" was actually the name of Chang Jiang for the lower part from Nanjing to the river mouth at Shanghai. However, due to the fact that Christian missionaries carried out their activities mainly in this area and were familiar with the name of this part of Chang Jiang, "Yangtze River" was used to represent the whole Chang Jiang in the English language. In modern Chinese, "Yangtze River" still stands for the lower part of Chang Jiang from Nanjing to the river mouth, but not the whole Chang Jiang.

The YR, which is about 6,380 kilo-meter long, is the longest river in Asia and the third-longest worldwide. The river is also the longest in the world to flow entirely within one country. It accounts for one-fifth of the national area and its river basin is home to approximately one-third of the national population (quote="Today, the Yangtze region is home to more than 400 million people, or nearly one-third of China's population. Some of China's largest cities" [1]. Accessed 10 Sept 2010. (in Chinese)). The cities Shanghai, Nanjing and Wuhan all have populations in excess of 8 million people and many other cities still in development along the YR have populations of more than 1 million people making the region one of the most polluted in China (Fu et al., 2013). The YR plays an important role in connecting the inland with overseas shipping, which contributes to non-negligible impact on air quality in both the entire YR region and the East China (Fan et al., 2016, Zhang et al., 2017).

The prosperous area of the Yangtze River Delta (YRD) is a triangle-shaped metropolitan region comprising Shanghai, southern Jiangsu and northern Zhejiang provinces. It contributes over 20% of the total national gross domestic product (GDP) in 2007 (National Bureau of Statistics of China, 2008). This region lies in the heart of the Jiangnan region, where Yangtze River drains into the East China Sea. The population in the built-up urban area has been increasing to possibly be the largest adjacent metropolitan areas in the world. In 2013, it covered 99,600 kilometers and was home to over 115 million people, including an estimated 83 million in urban area (*"Yangtze (Yangzi, Changjiang) River Delta"*. *China Today*. *Retrieved 27 March 2013*).

During the past few years, the occurrence of the $PM_{2.5}$ pollution events on a large scale in China has been increasingly frequent (Fu et al., 2008, Hu et al., 2014). YR region has been experiencing serious air pollution and is subject of concern worldwide (Geng et al., 2009). To understand the transport and transformation processes of atmospheric pollution, and to evaluate the impacts of aerosol on climate and cloud formation, many studies have been conducted in eastern China (Lin et al., 2011, Huang et al., 2011, Huang et al., 2013, Ding et al., 2013, Hua et al., 2015, Li et al., 2015a, Zhang et al., 2015). Nanjing, an important city and economic center of the YRD, is suffering from the severe air pollution associated with urbanization development. The source apportionment analysis of the VOCs showed that the contributors to air pollution in Nanjing consisted of

automobile emission sources, combustion sources, industrial production sources and biogenic emission sources (An et al., 2014). The dominated primary sources of PM in Nanjing were mobile exhaust, coal combustion, biomass burning and construction dust (Chen et al., 2015). Joint field observations were conducted in Shanghai, Suzhou, Nanjing and Hangzhou to explore haze pollution in the YRD (Hua et al., 2015). Source apportionment indicated that the five cities had similar pollution sources of $PM_{2.5}$ and the main contributors to $PM_{2.5}$ are secondary pollutants and primary emissions from vehicles and biomass burning. A regional emission inventory developed for the input emissions data to a modelling system indicated that air quality in winter in YRD is generally worse than in summer (Li et al., 2011, Chen et al., 2017). In winter, the air pollution transport from Northern China to the YRD reinforces the pollution caused by local sources (Li et al., 2011). In general, it was found that the occurrence of air pollution episodes depended on the synoptic patterns and anthropogenic emission intensity (Ji et al., 2012). It has been evidenced that emissions of ships at ports or along the shipping route have impacts on the air quality on local, regional and global scale (Liu et al., 2016). An extremely high $PM_{2.5}$ pollution episode in the YRD was investigated, the results of which showed that the mitigation strategy of air pollution in this region should focus on the joint control of combustion emissions, mobile source emissions, industrial processing emissions and fugitive dust. It was also indicated that regional transport of air pollution was prominent, and the implementation of the joint prevention and control of air pollution on a regional scale will aid to mitigate $PM_{2.5}$ concentrations under heavy pollution events significantly (Li et al., 2015b).

The influence of air pollution from anthropogenic emissions on the YR region has increased over the past decade (Feng et al., 2009; Shen et al., 2014). There have been many observational studies focusing on air pollution and its influences on the YR region (Huang et al., 2012b, Li et al., 2015a, Chen et al., 2015, Chen et al., 2017, Ming et al., 2017). Previous studies mainly concentrated on a specific city as a whole, and few focused on the comparison between cities (Wang et al., 2012; Fu et al., 2013; Song et al., 2015; Wang et al., 2015). However, the effects of the regional air pollution on the air quality in the YR regions have been increasingly frequent in recent years (Fu et al., 2008, Wang et al., 2015).

In inland rivers, ship emissions have become one of the main anthropogenic sources of air pollution, with a large number of different kinds of diesel-powered offshore and sea-going vessels operating along waterways, differing in technical level and operation conditions. Recently, the impact of ship emissions on the atmospheric environment has attracted an increasingly level of attention (Liu et al., 2011; Zhao et al., 2013; Ye et al., 2014). However, there are very few studies sampling when cruising on rivers to investigate the impacts of shipping emissions on the air quality in coastal cities, especially on the Yangtze River as one of the largest river in the world. It is imperative to conduct comprehensive measurements when cruising on the river to better understand the impacts of the shipping emissions on the air pollution in the coastal cities.

BC has been recognized as the most important anthropogenic contributor of particulate matter to climate forcing only after CO_2 (Bond et al., 2013, Ramanathan and Carmichael, 2008) due to its physicochemical properties. In the Yangtze River basin, a couple of studies (Huang et al., 2012a, Huang et al., 2013, Zhuang et al., 2014, Gong et al., 2016) have investigated BC particles in the coastal cities and provide valuable insight into the impact of BC on air pollution and human health on the local scale. As BC has lifetime in the atmosphere for several days, the effect of BC on climate depends crucially on its temporal and spatial variations. The measurements of BC on the regional scale in eastern China, where the sources of BC are complex, therefore are essential to assess the sources and characteristics of BC for formulating proper mitigation strategies of air pollution.

Chapter 2

Recent studies of BC measurements and motivation

2.1 Aethalometer and SP2 application

Source apportionment is widely used to identify the possible sources of the atmospheric aerosols and their contributions to the particulate matter (PM). In addition to assessing the health effects and risks of the exposure to these pollution components, the scientific knowledge of the sources of the PM, the level of their contributions to PM mass, and associated health risks is required for the policy-makers to develop and implement the strategies to control air pollutants and mitigate their effects on air quality. Thus, using more appropriate source apportionment methods under different conditions will lead to a more accurate estimation of the contributions of the specific sources to PM.

Aethalometer is a filter-based instrument, which collects $PM_{2.5}$ particles on to a quartze tape, used to measure light attenuation through the sampled filter at different wavelengths. Aethalometers have been widely used to measure light absorption of the atmospheric aerosols at either two wavelengths (370 and 880 nm) or seven wavelengths (370, 470, 520, 590, 660, 880 and 950 nm) and are used to estimate concentrations of BC using a conversion factor, the mass absorption coefficient (Quincey et al., 2009, Hyvärinen et al., 2011, Crilley et al., 2015), which is highly variable depending on the source emissions, transportation, and the absorption efficiency and magnitude at different wavelengths (Bond and Bergstrom, 2006). It has been recognised that Aethalometer are affected by multiple scattering by the filter fibres and light-absorbing particles accumulating in the filter (shadowing effect), with corrections being proposed and widely applied to overcome this problem (Weingartner et al., 2003, Collaud Coen et al., 2010, Drinovec et al., 2015). A source apportionment model, often called the Aethalometer model, was introduced and applied to estimate the contributions of traffic and wood burning emissions to carbonaceous matter concentrations (Sandradewi et al., 2008a, Sandradewi et al., 2008b, Harrison et al., 2012, Harrison et al., 2013, Favez et al., 2010). In these studies, traffic and wood burning emissions were considered as the main sources of the particles in winter and accounted for the most contribution of the Aethalometer measurements at

wavelengths of 470 and 950 nm. In addition, the model was not only used to apportion the contributions of the traffic and wood burning emissions to PM but also the BC, which are BC_{tra} and BC_{wb} (Favez et al.,2010; Herich et al., 2011; Crilley et al., 2015). However, these studies were mainly based on the filter-based techniques measuring bulk aerosol absorption rather than direct BC mass concentrations. As there is no agreement on the measurement methods of BC with a specific definition, Petzold et al. (2013) and Lack et al. (2014) presented a recommended terminology to clarify the terms and the measurement techniques for BC in atmospheric research. In the scientific literature, the SP2 has been increasingly recognised as an appropriate instrument for characterising refractory BC–containing particles (Schwarz et al., 2006), and there have been more and more studies investigating the physical properties of rBC using the SP2, which can provide continuously high-resolve size and mixing state information for individual rBC-containing particles over a range of mass concentration (Stephens et al., 2003, Schwarz et al., 2008a). Comparison between the Aethalometer and SP2, therefore, was made and indicated that non-rBC absorbing particles, referred to as brown carbon (BrC), have a significant effect on the Aethalometer measurements in the sampling area (Wang et al., 2014a). Saleh et al. (2013) found that both primary organic aerosol (POA) emitted directly by solid fuels combustion and secondary organic aerosol (SOA) produced by photochemical aging processes comprise brown carbon, and exhibit the properties of light absorption at different wavelengths to a significant extent. Besides, there are also studies indicating that the BrC is mainly produced from biomass burning/biofuel combustion (Washenfelder et al., 2015) and also generated from the photo-oxidation of anthropogenic and biogenic volatile organic compounds (VOCs) (Ervens et al., 2011). Liu et al. (2014) found a discrepancy between the attribution by the SP2 and Aethalometer methods in winter when the air mass was easterly and mostly influenced by solid fuel sources. In this study, it was found that the BC_{sf} (BC contributed by solid fuel combustion attributed by SP2) correlated better with $SFOA_{total}$ (OM contributed by solid fuel combustion attributed by AMS-PMF) but not with Aethalometer attribution, indicating that the absorption Angstrom exponent (α) for the contributions of the solid fuel was not correspondingly high.

2.2 In the Yangtze River region

Severe air pollution in China has been of great concern, especially carbonaceous aerosols, since these are one of the major pollutants. (Wang and Hao, 2012; Zhang et al., 2012). Moreover, China has been considered as one of the major regions contributing to the BC particles in the world, approximately 30% of BC emissions of the global anthropogenic sources (Bond et al., 2004). The Yangtze River region in eastern China, a basin of one of the longest rivers in the world, is suffering the highest particle concentrations and most pollution episodes resulting from the contributions of various sources, i.e. traffic, power generation plant, biomass burning, industry and non-road transportation. (Fu et al., 2013, Wang et al., 2014b, Wang et al., 2016, Xu et al., 2016). In general, air quality in winter in YRD is worse than in summer (Chen et al., 2017; Ming et al., 2017) due to the transport of the pollution caused by considerable local emissions from Northern China to the YRD (Li e t al., 2011).

Solid fuel combustion has been found to be an important source largely contributing to the air pollution in YRD (Cheng et al., 2014). The results in this study suggested that the impact of the biomass burning is regional, due to the substantial transport of air pollution between the provinces. Gong et al. (2016) investigated the physical properties of rBC in urban Shanghai during a regional air pollution episode in winter using a SP2. The rBC particles contributed by biomass burning had a larger core size and thicker coating compared to those from traffic. Continuous measurements of BC and related gases were conducted in urban Nanjing in 2012 (Zhuang et al., 2014). It was suggested that the high levels of BC concentrations mainly resulted from local and regional emissions, and the dominating BC sources were likely to be bio-fuel, industry-coal and vehicle-gasoline combustions. Huang et al. (2013) characterised the PM_1 during the summer and winter campaigns at a suburban site in Jiaxing in the central YRD using a HR-ToF-AMS and a SP2. The results showed that the BC fraction in PM_1 was much higher in winter than in summer, and both of them were significantly higher than that in urban Shanghai (Huang et al., 2012), which implied that combustion sources, e.g. biomass burning and coal combustion, played an important role in winter and in suburban areas in YRD.

2.3 Cookstove emissions

In addition to the open burning of biomass and the solid fuel combustion required for the supply of industrial energy, household cookstoves consuming solid fuel contribute approximately 20-25% of globally anthropogenic BC emissions (Garland et al., 2017). Approximately 41% of households in the world, about 2.8 billion people, rely on solid fuels to deliver the energy of cooking and heating (Amegah and Jaakkola, 2016). For the year 2012, exposure to household air pollution from cooking resulted in approximately 4.3 million premature deaths worldwide (WHO, 2014).

Policies aiming to reduce the BC emissions from cookstove have attracted great attention owing to their potential impacts on both climate and human health (Janssen et al., 2012, Grahame et al., 2014, Venkataraman et al., 2010, Anenberg et al., 2013). In addition to the impacts of the BC particles on climate forcing, the co-emitted OM also affects the optical properties of emitted BC particles when the components are internally mixed (Liu et al., 2015, Saliba et al., 2016, Flato et al., 2013). There is a high variability in the chemical composition of solid fuel combustion emissions from the cookstoves depending on the fuel type, source loading and burning condition (Venkataraman et al., 2010, Pettersson et al., 2011, Vicente et al., 2015, Nyström et al., 2017), and a large number of studies have investigated the performance of different varieties of cookstoves and fuels widely used in developing countries. For instance, Kar et al. (2012) studied the BC emissions from one traditional and four improved cookstoves and indicated that the BC concentrations varied significantly for repeated combustion cycles with same stove, emphasizing the inherent uncertainties in cookstove performance. Just et al. (2013) compared the ultrafine particulate emissions from a traditional cookstove to those from two improved cookstoves. The results showed that the improved cookstoves produced less OC but uniform EC compared to the traditional cookstove. There is a large effect on emissions caused by even a small alteration in the way which a fuel burns, making it difficult to study the composition of particles from biomass burning mechanically. Haslett et al. (2018) conducted several burns with small wood samples in a highly constrained combustion environment to address this gap. The study showed remarkable repeatability of the results, allowing the variations of particulate emissions to be clearly observed according to different burning phases.

There have been many previous studies characterising the BC and OM of solid fuel combustion; however, the source profile of BC from solid fuel burning is still lacking (Nielsen et al., 2017, Martinsson et al., 2015). While the absorption enhancement of BC particles is determined by the mixing state of BC and non-BC materials in a BC-containing particle (Flato et al., 2013, Liu et al., 2015, Saliba et al., 2016, Liu et al., 2017), this is still uncertain, particularly for the emissions of solid fuel combustion, and is currently mostly simplified in models (Koch et al., 2009, Reddington et al., 2013).

2.4 Motivation

Atmospheric aerosols are ubiquitous on Earth and a large proportion of them are produced by anthropogenic combustion sources. These aerosols have been found to affect human health and air quality. In recent years, black carbon (BC) particles, emitted from incomplete combustion of fossil fuel and biomass, have been of great concern owing to their significant impacts on human health and climate forcing. However, due to the limitation of the measurement techniques, the past studies mostly used the filter-based techniques, which were often incapable of capturing the details of the BC properties. An Aethalometer, a filter-based instrument, has been widely used to perform on-line measurements of the light absorption of the fine particles, and further to convert to the BC loadings by applying the BC mass absorption cross section, which can be affected by the compositions of the atmospheric aerosols. This method is currently employed by the Department for Environment, Food and Rural Affairs (DEFRA) across the UK Black Carbon Network. Recently, a state of the art instrument, Single Particle Soot Photometer (SP2), has been used to directly measure the mass concentration of the rBC, which can also provide the core size and mixing state of the BC particles. In order to obtain more accurate attribution of BC particles, it is essential to understand the factors resulting in the differences between the attributions of BC from both instruments/technologies. This study has a unique opportunity to apply the comprehensive data to determine the factors and provided the parameters, which can be used as references for future studies to estimate the mass loadings and source contribution of the BC, where such a comprehensive suite of aerosol measurements may not be available.

The contribution of BC emissions in China to the global anthropogenic emissions has been considerable, and the sources of BC are complex, especially in

the Yangtze River regions in eastern China with a large population, where the emissions of industry, biomass burning and power generation plant are massive. In the last decade, there have been studies indicating that the air quality in these areas has been increasingly affected by regional transport. However, most of the studies were confined in individual cities, which could not systematically provide the characteristics of BC over a regional scale. To have an insight into the properties of BC in the regions of eastern China and thereby underpin the constitution of mitigation strategies, a cruise campaign with continuously on-line measurements of the BC and related gases was carried out on the Yangtze River.

In addition to being important in the ambient environment, the characteristics of BC of primary emissions from solid fuel combustion at sources are also critical, especially for the climate models, as the BC size and mixing state at source, which are the initialized inputs determining the subsequent aging process, is a fundamental basis for any model to estimate its atmospheric lifetime. Many global models currently assume the same size and mixing state of BC for all type of solid fuel sources. Although some models could incorporate realistic source profiles, the BC profiles of solid fuel at sources are scarce. In order to better estimate the impacts of BC particles on the climate, this study implemented a series of experiments of solid fuel combustion using different commercial cookstoves, and investigated the composition and mixing state of carbonaceous aerosols.

Chapter 3

Instrumentation and data analysis techniques

3.1 Aerosol Mass Spectrometer (AMS)

The Aerodyne Aerosol Mass Spectrometer (AMS) has been designed and developed by Aerodyne Research, Inc. It combines a unique aerodynamic lens inlet focusing particles into a narrow beam, aerodynamic sizing area, high vacuum thermal vaporization, electron impact ionization and mass spectrometer (Jayne et al., 2000, Allan et al., 2003, Jimenez et al., 2003, Canagaratna et al., 2007). The AMS on-line instrument can quantitatively measure size-resolved mass loadings and chemical composition of non-refractory submicron particulate matter (PM_1) with high time resolution based on the standard configuration of operation, which has demonstrated its capability in a wide range of environmental studies (Jayne et al., 2000, Canagaratna et al., 2007). The AMS with a Quadrupole mass spectrometer (Q-AMS) was the earliest version, which was developed to provide ensemble data of the measured aerosols. However, an advancement in the development of AMS has been introduced that improves the sensitivity and time resolution of measurements. There are three main versions of the AMS developed predominantly depending on the different type of mass spectrometer employed, which are the Quadruple AMS (Q-AMS) (Jayne et al., 2000), the compact Time-of-Flight AMS (cToF-AMS) (Drewnick et al., 2005) and the high-resolution Time-of-Flight AMS (HR-ToF-AMS) (DeCarlo et al., 2006). Despite the different mass spectrometers used in these versions of AMS, the fundamental principle of measurement remains the same. The following will describe the design and operation of the AMS commonly used for all three versions. Moreover, as the data used in this work were measured by the cToF-AMS, the technical aspects of the version and the techniques for the data analysis will be described in details.

3.1.1 Instrument description and operation

The AMS has three main sections as illustrated in Figure 3.1: the particle beam generation, the aerodynamic sizing, and the particle composition, where the mass spectrometer is located so that the particle composition can be determined.

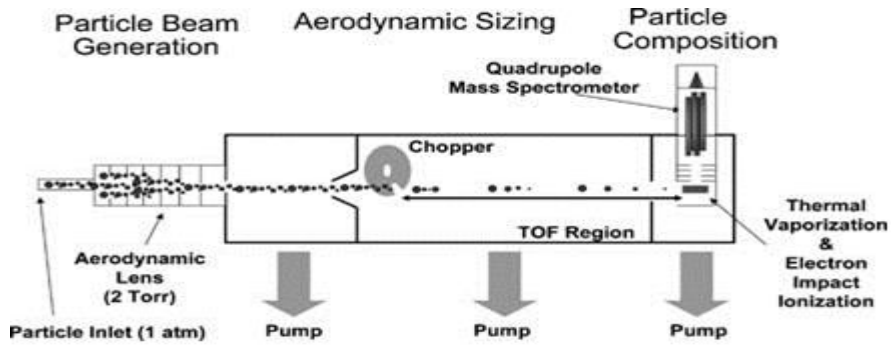

Figure 3.1 Schematic of the Q-AMS, demonstrating the three main sections of the AMS Reprinted from Canagaratna et al. (2007).

In the particle beam generation section of the AMS, submicron particles are sampled from the atmosphere by the particle inlet into the AMS through the aerodynamic lens, where the narrow particle beam is formed and subsequently transmitted into the detection region. A critical orifice with a diameter of 100 µm or 120 µm is typically used, resulting in a flow rate of 1.5 cm^3 s^{-1} or 2 cm^3 s^{-1}, respectively (Allan et al., 2003). The orifice also reduces the ambient atmospheric pressure to approximately 267 Pa. An aerodynamic lens system focuses the sampled air into a narrow beam through a series of apertures of progressively smaller diameters (Liu et al., 1995). A combination of the passage through each aperture and entering the differentially pumped vacuum chamber upon exiting the aerodynamic lens system results in the divergence of gas phase molecules. The majority of the gaseous composition in the beam is removed by a skimmer cone before entering the particle sizing region. Consequently, the sampled particles have formed a narrow and collimated particle beam, which is enriched by a factor of approximately 10^7 compared to the air sampled at the entrance of the inlet. However, the gas phase material still dominates the mass of the beam rather than particulate matter.

Computational fluid dynamic simulations of the inlet system have shown that particles with aerodynamic diameters between 70 nm and 500 nm can be transmitted to the detection system with 100% efficiency (Jayne et al., 2000, Zhang et al., 2002, Zhang et al., 2004). Furthermore, particles in the ranges of 30-70 nm and 500-2500 nm have shown significant transmission efficiency, while particles smaller than the size cut-off are lost because of following the gas streamlines in the lens system. Larger particles are lost as a result of deposition on the walls of the apertures in the lens system. The transmission efficiencies have been based on a priori assumption that the particles are spherical or near-

spherical. However, highly non-spherical particles and long chain agglomerates such as BC have been known to be inefficiently focused by the lens system (Liu et al., 1995). It has been shown that the transmission efficiency for the particles with aerodynamic diameters of 1 μm is approximately 50% in the AMS (Canagaratna et al., 2007).

After exiting the aerodynamic lens system, the particle beam enters the aerodynamic sizing section of the AMS, which is a vacuum chamber comprising a mechanical chopper. The chopper wheel contains two radial slits and rotates at a rate of 100-150 Hz to modulate the particle beam via being operated in one of the three modes. The chopper in the 'open' position allows particles to pass through freely to the detection region, whereas in the 'blocked' position it completely blocks the particle beam for the background measurements. The chopped position, which is related to the detection of the particle size, is used to measure the time at which a particle travel from the chopper to the end of the chamber. Upon exiting the aerodynamic lens, the particle beam travels into the vacuum chamber, where particles with a smaller aerodynamic diameter have a greater velocity than those with a larger diameter.

When the particles enter the particle composition section of the AMS, non-refractory components are flash vaporized on impact upon a resistively heated porous tungsten surface (～600°C) under high vacuum and ionized via electron impact at 70 eV before the determination of particle composition by the mass spectrometer shown as Figure 3.2. This thermal vaporization method limits the AMS to detection of non-refractory components including organic matter, and major inorganics like $(NH_4)_2SO_4$, NH_4NO_3 and NH_4Cl. A Soot Particle AMS (SP-AMS) (Onasch et al., 2012) has been developed that has the ability to measure the refractory components like black carbon, using laser-based vaporization.

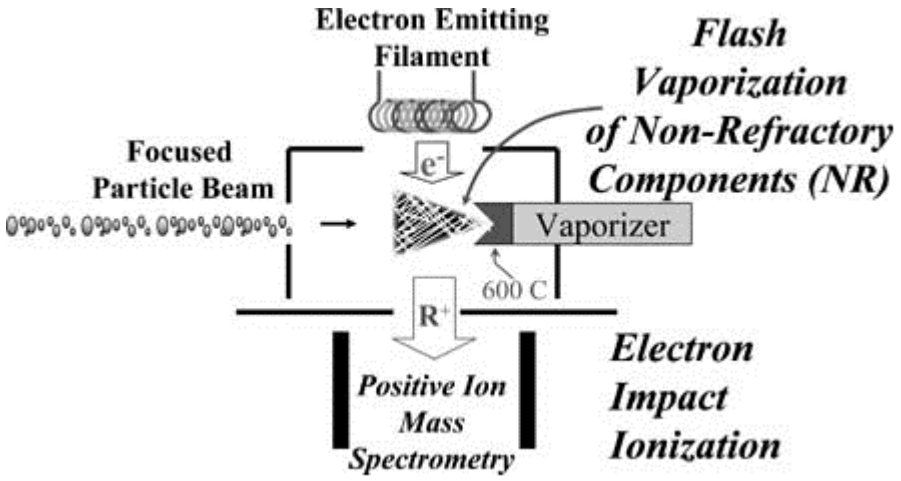

Figure 3.2 Schematic of the detection scheme in the AMS (Canagaratna et al., 2007).

The AMS alternates between two modes during operation: the Mass Spectrum (MS) and Particle Time-of-Flight (PToF) modes (Jimenez et al., 2003). In the MS mode of operation, the chopper alternates between the open and blocked positions. An ensemble average mass spectrum of the both particle and gas species is obtained by subtracting the average background mass spectrum acquired when the chopper is in the blocked position from the average spectrum acquired when the chopper is in the open position. This can therefore remove any contribution from background gases in the detector. As a result of the ensemble average mass spectra obtained, the ambient mass concentrations of chemical species can be derived. The process of data processing is presented in the Section 3.1.3.

The mass spectra of air samples at any particular m/z can be contributed by different ions. Furthermore, due to the strong electron ionisation resulting in fragmentation, the particles tend to present as their constituent ions, making the AMS analysis challenging. A fragmentation table, containing some of the key ion fragments and their corresponding molecular mass used to aerosol species from AMS mass spectra, was developed to improve the AMS data analysis (Allan et al., 2004). The fragmentation table can be user-defined by the AMS analysis toolkit, with the availability of being updated or edited depending on the need of the case study. Table 1 shows the key ion fragments for the identification of the aerosol species, where the particles are typically detected in the atmospheric environment.

Table 1. Main ion fragments used to identify organic and inorganic aerosols species in AMS mass spectra. Reproduced from (Canagaratna et al. 2007).

Group	Molecule/Species	Ion Fragments	Mass Fragments
Water	H_2O	$\mathbf{H_2O^+}$, HO^+, O^+	**18**, 17, 16
Ammonium	NH_3	NH_3^+, $\mathbf{NH_2^+}$, NH^+	17, **16**, 15
Nitrate	NO_3	HNO_3^+, $\mathbf{NO_2^+}$, $\mathbf{NO^+}$	63, **46, 30**
Sulphate	H_2SO_4	$H_2SO_4^+$, HSO_3^+, SO_3^+, $\mathbf{SO_2^+}$, $\mathbf{SO^+}$	98, 81, 80, **64, 48**
Organic (oxygenated)	$C_nH_mO_y$	H_2O^+, CO^+, CO_2^+, $\mathbf{H_3C_2O^+}$, HCO_2^+, $C_nH_m^+$	18, 28, **44**, **43**, 45, ….
Organic (Hydrocarbon)	C_nH_m	$C_nH_m^+$	27, 29, **41**, **43**, **55**, **57**, 69, 71, …

In the PToF mode operation, the mass spectrometer is set to one of several mass/charge ratios (m/z) programmed for a period of time and sampled at a user-defined rate, and then transformed into the next m/z. The chopper is set to the chopped position and an optical sensor positioned on the chopper mount detecting when the slit of chopper is positioned to allow aerosol beam to pass. The delay time between the aerosol beam passing through the slit of the chopper and the ion detection in the mass spectrometer is the particle time of flight. Several signal distributions of the different m/z are obtained over many chopped cycles. Since the time of flight is dependent on the particle's aerodynamic diameter, these signals are subsequently used to calculate mass distributions for particular chemicals versus aerodynamic diameters.

3.1.2 Compact Time-of-Flight Aerosol Mass Spectrometer (cToF-AMS)

The cToF-AMS incorporates the three main sections of the AMS, where the particle focusing, particle sizing and the combination of the vaporisation and ionisation steps are utilised in the Q-AMS as described above (Steiner et al., 2001). After the vaporisation and ionisation processes, the ions are transported into an orthogonal time-of flight extractor, where they are then orthogonally transferred from the extractor to time-of flight section by a high pulsed voltage. The flight path is around 430 mm resembling a 'C' shape shown as Figure 3.3, which is controlled by a two-stage gridded ion reflector. The extraction period is typically about 12 μs, whilst the Q-AMS takes 300ms to scan at m/z 1-300. The

cToF-AMS therefore allows the generation of approximately 83,300 complete mass spectra every second, whereas only about 3 generated by the Q-AMS in that time. The long flight path and large temporal resolution in the cTof-AMS improves the sensitivity and time resolution of the instrument compared the Q-AMS (Drewnick et al., 2005). After the extraction and ion reflector stages, the ions are collected and detected by the Multi-Channel Plate (MCP) detector. The cTof-AMS has a detection limit of 0.03 μg m^{-3} for organics compared to a value of 0.5 μg m^{-3} for the Q-AMS (Drewnick et al., 2009).

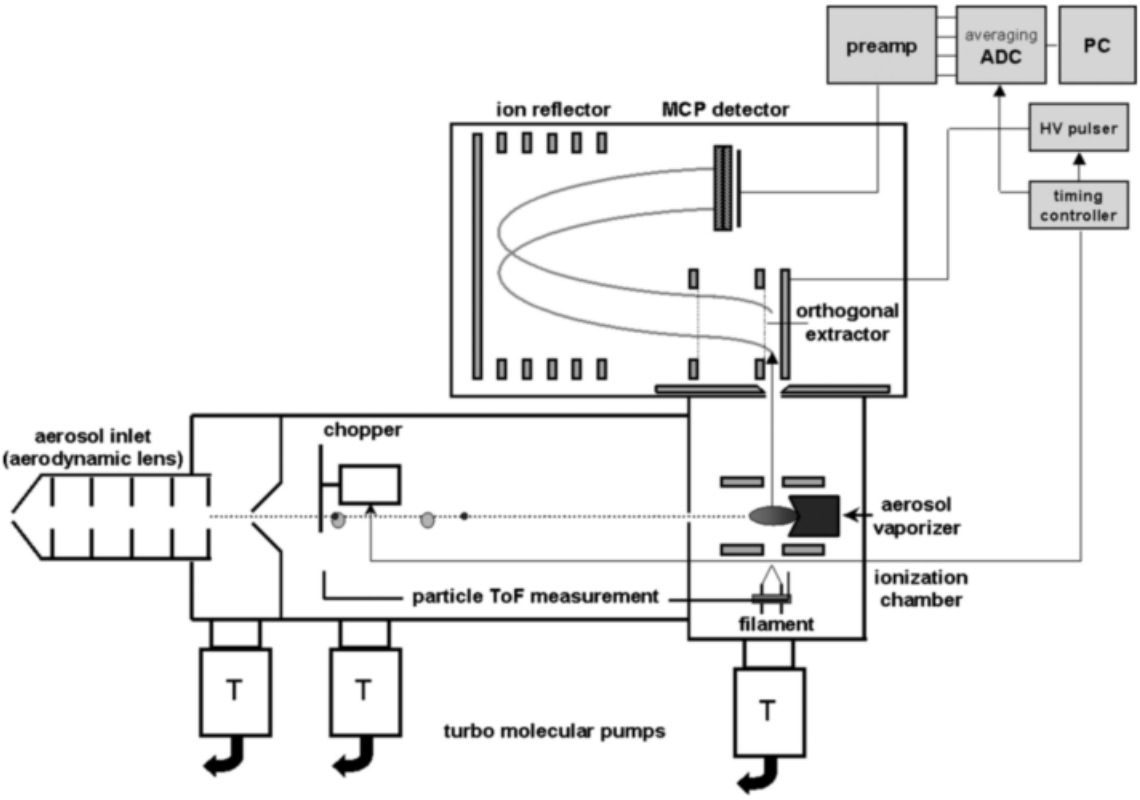

Figure 3.3 Schematic of the cToF-AMS. Reprinted from Drewnick et al. (2005)

3.1.3 Data quantification

In order to derive quantitative information of chemical species from detected ion signals from the C-ToF-AMS, a number of processes are required, which has been discussed in Jayne et al. (2000), Jimenez et al. (2003) and Allan et al. (2003).

Voltage signals from the pre-amplifier ('preamp' in Figure 3.3) are proportional to the electrical current outputs of the MCP (Figure 3.3). The detected ion rates (*I*, Hz) are derived via division of the average single ion strength, which is determined by the daily calibration during the period of measurement that allows the signals of single ions to be distinguished from the background material. The

peaks of the individual ion signals are then averaged before conversion into mass concentration (C, µg m^{-3}), which is achieved via the following formula, presented by Jimenez et al. (2003):

$$C = \frac{MW}{IE.Q.N_A} I \times 10^{12} \quad (3.1)$$

Where MW is the molecular weight of the parent species (g mol^{-1}), IE is the ionisation efficiency, Q is the volumetric flow rate of the instrument (cm^3 s^{-1}), NA is Avogadro's number (6.023×10^{23} mol^{-1}) and the factor 10^{12} is used to convert from g cm^{-3} to µg m^{-3}. Equation 3.1 is used to calculate the mass concentration at a particular m/z. In order to obtain the total mass concentration for a specific species, the ion signals for each mass fragment are summed as equation 3.2.

$$C_S = \left(\frac{MW_S}{IE_S.Q.N_A} \sum_{alli} I_{S,i}\right) \times 10^{12} \quad (3.2)$$

Where the subscript S represents a particular species and I denotes the mass fragments of species S.

The IE is a species specific dimensionless quantity defined as the number of ions detected per molecule of the parent species (Canagaratna et al., 2007). It describes the probability that a particle is ionised, transmitted through the mass spectrometer and subsequently detected by the MCP.

While quantification of IE for a specific species is very difficult due to the complex aerosol particles, the IE of ammonium nitrate (NH_3NO_4), which is efficiently volatilised upon contact with the vaporiser, is used as a standard. IE_{NO_3} is calculated regularly during AMS operation from routine calibration using a well-documented experimental methodology (e.g. Jayne et al., 2000, Allan et al., 2003, Canagaratna et al., 2007). Principally, monodisperse NH_4NO_3 particles are generated from a nebulizer using an aqueous ammonium nitrate solution, which are then dried before size selection via a Differential Mobility Analyser (DMA). A mobility diameter of 350 nm is considered an optimum diameter and selected because ions of the particles at this size are reliably distinguished and counted. The sample is introduced into the AMS and the number of ion signals at m/z 30 and 46 are then counted in PToF mode via single particle vaporisation events. As the size of the particle for calibration has been pre-selected, and the bulk density of 1.725 g cm^{-3} and Jayne shape factor (0.8, Jayne et al., 2000) for NH_4NO_3 are

known, the average mass concentration of the sampled particles can be determined.

The IE_{NO_3} is then used to calculate the ionisation efficiency of other chemical species on the basis of the assumption that the ionisation cross section of the parent molecules is proportional to the number of molecules present (Jimenez et al., 2003). In addition, the ionisation cross section is assumed to be proportional to the molecular weight (MW_s) of the species. The IE of a particular chemical species can then be calculated as the following equation:

$$\frac{MW_S}{IE_S} = RIE_S \frac{MW_{NO_3}}{IE_{NO_3}} \tag{3.3}$$

Where RIEs is the relative ionisation efficiency of a specific species (Alfarra et al., 2004), which is calculated by laboratory experiments or from the routine IE calibration of specific species as described above. For the calculation of the mass loadings, equation 3.3 is substituted into equation 3.2 as follows:

$$C_S = \left(\frac{1}{RIE_S} \frac{MW_{NO_3}}{IE_{NO_3}.Q.N_A} \sum_{alli} I_{S,i}\right) \times 10^{12} \tag{3.4}$$

As only a fraction of the particles entering the AMS are successfully transmitted through the mass spectrometer, vaporised, ionised and detected. The collection efficiency (CE) has to be taken into account as the following equation:

$$CE(d_{va}) = E_L(d_{va}) \times E_s(d_{va}) \times E_b(d_{va}) \tag{3.5}$$

Where E_L is the transmission efficiency of the aerodynamic lens, E_s is the efficiency of the particle beam reaching the vaporiser, and E_b represents the detection efficiency of the particles which impact the vaporiser being detected (Huffman et al., 2005). The CE can be dependent on particle size, particle phase, humidity and morphology (Allan et al., 2004, Quinn et al., 2006, Weimer et al., 2006, Crosier et al., 2007, Middlebrook et al., 2012). For the internally mixed aerosols, the same CE can be assumed for all chemical composition (Alfarra et al., 2004). A default CE of 0.5 has been applied to a number of field measurements and provided reasonable results (Alfarra et al., 2004, Topping et al., 2004, Takegawa et al., 2005, Aiken et al., 2009). However, CE has been found to be dependent on individual pollution events. Therefore, Middlebrook et al. (2012) developed an algorism to estimate the CE for a given dataset, which improved the quantification of the mass loadings compared to that when the default value was

used. In the specific case of solid fuel combustion from residential stoves, there has been no defined CE. However, the CE of 1 has often assumed in previous studies regarding the emissions of residential stove combustion (Heringa et al., 2012, Brito et al., 2014, Haslett et al., 2018), which is the case in this study.

3.2 Aethalometer

The 7-wavelength Aethalometer (AE31, Magee Scientific) measures the light absorbing coefficients of particles collected onto a quartz fibre filter at seven wavelengths (λ = 370, 470, 520, 590, 660, 880 and 950 nm) covering the ultra-violet (UV) to the near-infrared wavelength range, and is often used to derive the mass concentration of light absorbing BC particles. The measured aerosol light absorption coefficients were corrected for multiple scattering by the filter fibres (C value) and shadowing effects (f value) caused by the accumulating particles in the filter which may shadow the newly collected ones so that the new particles cannot exposed to the same intensity of light. The procedure of correction is described by Weingartner et al. (2003) and the values of 1.2 and 3.095 for f and C were used to correct the absorption coefficients in this study. The C value was determined based on the comparison between the uncorrected Aethalometer data and that of a Thermo Scientific Multi-Angle Absorption Photometer (MAAP) measured at λ = 630 nm using data with attenuation values only smaller than 10 (Collaud Coen et al., 2010), where the shadowing effect is not expected. As the correction was done by Crilley et al. (2015), the processes of the correction related to this work are only briefly described here.

The light attenuation (ATN) through a quartz filter was defined in equation 3.6, where I_0 is the intensity of the incoming light, and I is the remaining light intensity after passing through the loaded filter.

$$ATN = \ln(\frac{I_0}{I}) \tag{3.6}$$

The absorption coefficients (b_{ATN}) measured by the Aethalometer need to be corrected for calculating the real absorption coefficients (b_{abs}) as shown in equation 3.7.

$$b_{abs,\lambda} = \frac{b_{ATN,\lambda}}{C * R} \tag{3.7}$$

Where C is for the correction of the scattering effect; R is a wavelength dependent parameter for the correction of the shadowing effect.

C value is obtained by the ratio of $b_{ATN,630}$ from Aethalometer and babs_630 from MAAP. As the Aethalometer does not measure at wavelength of 630 nm, The absorption Angstrom exponent, $b_{ATN,630}$ is calculated as shown in equation 3.9 using the absorption Angstrom exponent (α), which is calculated as shown in equation 3.8.

$$\alpha = \frac{\ln(\frac{b_{ATN,470}}{b_{ATN,950}})}{\ln(\frac{950}{470})} \tag{3.8}$$

$$b_{ATN,630} = b_{ATN,660} * (\frac{630}{660})^{-\alpha} \tag{3.9}$$

The shadowing correction (*f*) was calculated by the ratio of the absorption coefficients before and after each filter tape advance. The f value, which gives the median ratio over all tape advances closest to 1 for each wavelength, was taken. R is calculated as the following equation 3.10.

$$R = \left(\frac{1}{f} - 1\right)\frac{\ln(ATN) - \ln(10\%)}{\ln(50\%) - \ln(10\%)} + 1 \tag{3.10}$$

Finally, the b_{abs} for each wavelength has been determined, and the BC mass concentrations can be calculated by the conversion from b_{abs} using the mass absorption and attenuation cross section (σ_{ATN}, m^2g^{-1}) for each wavelength as reported in the Aethalometer manual (MAC EC Magee) using the equation 3.11 and 3.12, where M_{BC} ($g\ m^{-3}$) is the mass concentration of BC.

$$\sigma_{ATN,\tau} = \frac{14625}{\tau} \tag{3.11}$$

$$M_{BC} = \frac{b_{abs}}{\sigma_{abs}} \tag{3.12}$$

3.2.1 Black carbon and carbonaceous matter Source apportionment by Aethalometer model

3.2.1.1 Methodology

The Aethalometer was originally developed to quantify light absorption by black carbon (BC), which is considered as the predominant light absorbing particulate species at visible wavelengths (Hansen et al., 1984). However, there have been several studies pointing out that brown carbon, which is the absorbing part of organic matter, could significantly absorb light at wavelengths in the 400-500nm region (Kirchstetter et al., 2004). This approach has been used to calculate the contribution of fossil fuel and wood burning sources to carbonaceous matter concentration in ambient air according to their different optical properties (Sandradewi et al., 2008b; Favez et al., 2010). The parameterized aerosol absorption coefficients are proportional to $\lambda^{-\alpha}$, where λ is wavelength and α is the Ångström absorption exponent which is constant for pure traffic (α_{tr}) and pure wood burning (α_{wb}) measured at λ = 470 and 950 nm (Sandradewi et al., 2008b). Based on the assumptions that during winter FF and WB combustion are the dominating sources of total carbonaceous matter (CM_{total}), ambient CM_{total} can be modelled by the light absorption coefficients of aerosols emitted by these two sources. The above assumptions imply that the aerosol absorption coefficient (babs (λ)) at a given λ can represent the sum of the light absorption of aerosols emitted by these two sources as equation 3.13. Both quantities can be calculated from light absorption with given α_{tr} and α_{wb} for both sources with equation 3.14 and 3.15:

$$b_{abs}(\lambda) = b_{abs}(\lambda)_{traffic} + b_{abs}(\lambda)_{wb} \quad (3.13)$$

$$\frac{b_{abs}(470nm)_{traffic}}{b_{abs}(950nm)_{traffic}} = \left(\frac{470}{950}\right)^{-\alpha_{traffic}} \quad (3.14)$$

$$\frac{b_{abs}(470nm)_{wb}}{b_{abs}(950nm)_{wb}} = \left(\frac{470}{950}\right)^{-\alpha_{wb}} \quad (3.15)$$

With given α_{tr} and α_{wb} values and using the field data of the light absorption measurements at 470 and 950 nm, the values for $b_{abs,traffic,470nm}$, $b_{abs,traffic,950nm}$, $b_{abs,wb,470nm}$, and $b_{abs,wb,950nm}$ can be computed with equation (3.13)-(3.15). In this study, the values of the absorption Angstrom exponent of traffic and wood

burning are set at 1 (Bond and Bergstrom, 2006) and 2 (Kirchstetter et al., 2004, Bond and Bergstrom, 2006, Lewis et al., 2008, Crilley et al., 2015), respectively. In the following, the contribution of wood burning and traffic emission aerosols to the carbonaceous matter within PM_1 is estimated by a linear regression of the light absorption of the two sources combined with the measurements of AMS (Young et al., 2015) and SP2 (Liu et al., 2014). The equations are as follows:

$$\begin{aligned} CM_{total} &= OM + BC \\ &= CM_{traffic} + CM_{wb} + CM_{other} \\ &= C_1 * b_{abs,tr,950nm} + C_2 * b_{abs,wb,470nm} + C_3 \end{aligned} \quad (3.16)$$

Where OM is the organic mass measured by the AMS, BC is the black carbon measured directly by the SP2 rather than Aethalometer as the uncertainties of the assumed α will lead to considerable variations of the model outputs (Harrison et al., 2012a, 2013), $b_{abs,tr,950nm}$ represents the absorption coefficient of carbonaceous matter originating from fossil fuel combustion ($CM_{traffic}$) at wavelength 950 nm, $b_{abs,wb,470nm}$ represents the absorption coefficient of wood-burning carbonaceous matter (CM_{wb}) at wavelength 470nm, the calculated parameters C_1 and C_2 relate the light absorption to the particulate mass of both sources. The third constant, C_3, which accounts for the background concentration/offset.

Combining factors derived using AMS-PMF (Young et al., 2015), BC_{tr} and BC_{wb} were separated by Liu et al, (2014), using a reformulation of equation 4.16 which can be rewritten as follows:

$$\begin{aligned} CM_{traffic} &= HOA + BC_{tr} \\ &= C_1 * b_{abs,tr,950nm} + C_3 \end{aligned} \quad (3.17)$$

$$\begin{aligned} CM_{wb} &= SFOA_1 + SFOA_2 + BC_{wb} \\ &= C_2 * b_{abs,wb,470nm} + C_3 \end{aligned} \quad (3.18)$$

3.3 Single particle soot photometer

A single particle soot photometer (SP2, manufactured by Droplet Measurement Technology, Inc., Boulder, CO, USA) measures the mass of individual refractory black carbon (rBC) particles (Petzold et al., 2013) based on the detection of the incandescence radiation at high temperatures induced by a laser. Moreover, the

SP2 can also determine the scattered light emitted by non-refractory materials, enabling the calculation of the fraction of non-refractory materials to rBC in a rBC-containing particle (Schwarz et al., 2008a). Regarding the detection limit, the SP2 is able to measure the absorbing particles with volume equivalent diameters from 0.15 μm to 0.7 μm.

Figure 3.4 is a schematic of the SP2 optical head. An air jet containing sample aerosols is drawn into the instrument and intersects with a 1064 nm intra-cavity Nd:YAG laser beam, which has a power of about 1 MW cm^{-2} with a Gaussian intensity distribution (Schwarz et al., 2006). The air jet is approximately ¼ the width of the laser beam, which ensures that all particles can see the same laser intensity. In the interaction with the laser beam, BC particles absorb energy and are heated to vaporization temperatures, emitting measurable incandescent radiation. The incandescent and scattering light is measured by four avalanche photo-detectors (APD) behind complex lenses, which are positioned around the intersection of the particle and laser beams in order to capture the largest light intensity emitted by particles. Two of the APD are used to detect incandescent light either over a narrowband (~630-800 nm) or broadband (~350-800 nm) wavelength interval via the use of the optical filters. The measured intensity of the incandescent light is proportional to rBC mass (Slowik et al., 2007). Aquadag sample black carbon particle (Aqueous Deflocculated Acheson Graphite, manufactured by Acheson Inc., USA) is typically used to calibrate the incandescence signal, as it has shown to produce a stable signal of the particles with a mobility diameter of 300nm (Laborde et al., 2012a). Aquadag suspension is nebulised and the aerosols enter through a dryer, followed by a Differential Mobility Analyser (DMA) selecting particles of certain sizes, which are sampled by SP2. The mass of these particles is derived by the mobility diameters corresponding to the signal strength from the instrument in order to obtain a calibration constant. As the generated rBC particle standards from Aquadag do not represent the ambient rBC, a further correction of 0.75 is employed with the calibration curve to obtain more reliable rBC mass determination (Moteki et al., 2010, Baumgardner et al., 2012, Laborde et al., 2012b).

The other two APDs are used to detect scattered light at a wavelength interval of ~850-1200 nm and operate at two different gain settings to optically size particles that only scatter laser light. A similar process is used to calibrate the

scattering channels, although in this case the calibration is based entirely on 300 nm particles. The size and refractive index of polystyrene latex spheres (PSLs) is known, although a DMA is still used to remove interference at different sizes. In addition to calibrating the scattering channels, this process provides a check on the alignment of the beam within the instrument. A Gaussian signal distribution is generated and provides information about particle size. The scattering signal of an rBC-containing particle can be distorted because of the mass loss of an rBC-containing particle by laser heating when it passes through the laser beam. When a coated rBC-containing particle passes through the laser beam, it initially acts as a purely scattering particle and the Gaussian scattering signal is detected. When the coatings vaporise, the rBC core begins to incandesce and the Gaussian scattering signal decays. However, the Gaussian scattering signal can be reconstructed by the baseline offset, amplitude, centre position and width by the 'leading edge only' (LEO) method. Thus, the LEO fitted scattering signal can be used to obtain the size and the thickness of the rBC-containing particle's coating (Gao et al., 2007).

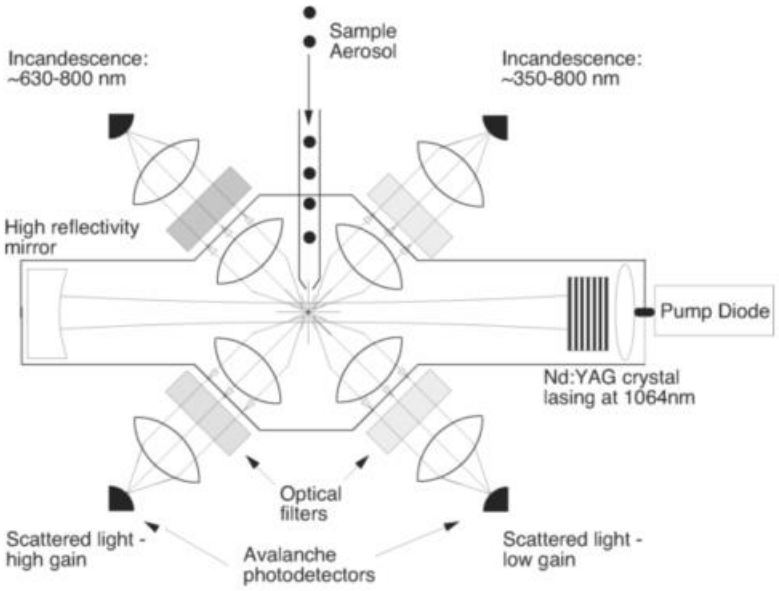

Figure 3.4 Schematic of the SP2 optical head illustrating the basic optics and detectors for incandescence and scattering light induced by a laser. The aerosol jet here is drawn for simplicity, and it is vertical to APDs, reproduced from Gao et al. (2007).

3.3.1 Black carbon source apportionment by SP2 method

The overall rBC size (D_p), including the BC core and coatings, can therefore be provided by a core-shell Mie model with the input of the LEO fitted scattering

signal and BC core size, accompanied with the assumption of an rBC core refractive index of 2.26 – 1.26i and a coating refractive index of 1.5 + 0i (Moteki et al., 2010). The relative coating thickness of an rBC particle is calculated as D_p/D_c. The optical size of a non-rBC particle can also be calculated using Mie theory with a coating refractive index of 1.5 + 0i, which makes the optical sizes of rBC-containing and non-rBC particles directly comparable. Given the coating thickness of individual rBC particles is Dc size dependent, the bulk coating thickness is calculated as the cubed root by the total volume of the rBC particles divided by the total volume of the BC cores, as shown in Eq (3.19):

$$\frac{D_p}{D_c} = \left(\frac{\sum_i D_{p,i}^3}{\sum_i D_{c,i}^3}\right)^{\frac{1}{3}} \tag{3.19}$$

Where D_p and D_c are the coated BC diameter and BC core diameter, respectively; *i* denotes the *i*th single BC particle. The volume weighted bulk D_p/D_c is considered to be a representative diagnostic for the overall mixing state of the entire population of BC particles.

In order to identify the sources of the BC, a parameter of scattering enhancement, E_s, was introduced, which is defined as the Eq. (3.20):

$$E_s = \frac{S_{coated}}{S_{uncoated}} \tag{3.20}$$

Where S_{coated} is the scattering signal measured by the SP2 and then LEO fitted; $S_{uncoated}$ is the scattering signal of the corresponding BC core, which is derived using the Mie single particle scattering solutions.

According to the Eq. 3.20, a value of 1 for E_s means that the scattering signal of a BC particle equals to that of only a BC core, which also means zero coating or $D_p/D_c = 1$. Actually, particles with any coatings will scatter more the corresponding core, and E_s therefore will be necessarily greater than 1. However, S_{coated} will also be subject to the uncertainties of the instrument measurement. Thus, a proportion of particles with E_s less than 1 would be expected. In general, an increase in Es will indicate a thicker coating for a specified D_c. Figure 3.5 shows the variation of E_s as a function of BC core diameter (D_c) for the BC particles, when the traffic source mostly dominated and BC particles were least coated during the experiment. The coatings on these BC particles are considered to be completely removed after thermal desorption at 250 °C (TD250 °C), in other

words, no coating should yield a value of 1 for E_s. For the particles with smaller D_c (< 110 nm), the low signal-to-noise ratio in the scattering signal related to the SP2 detectors, thus causing a failed LEO fit, or the scattering signal of measured particles falling outside of the Mie-calculation predictable range. In addition, it is expected that the scattering signal for a proportion of BC particles with core diameter less than 110 nm with thin coatings will also not be efficiently detected, resulting in a bias towards the particles with larger cores that were successfully fitted.

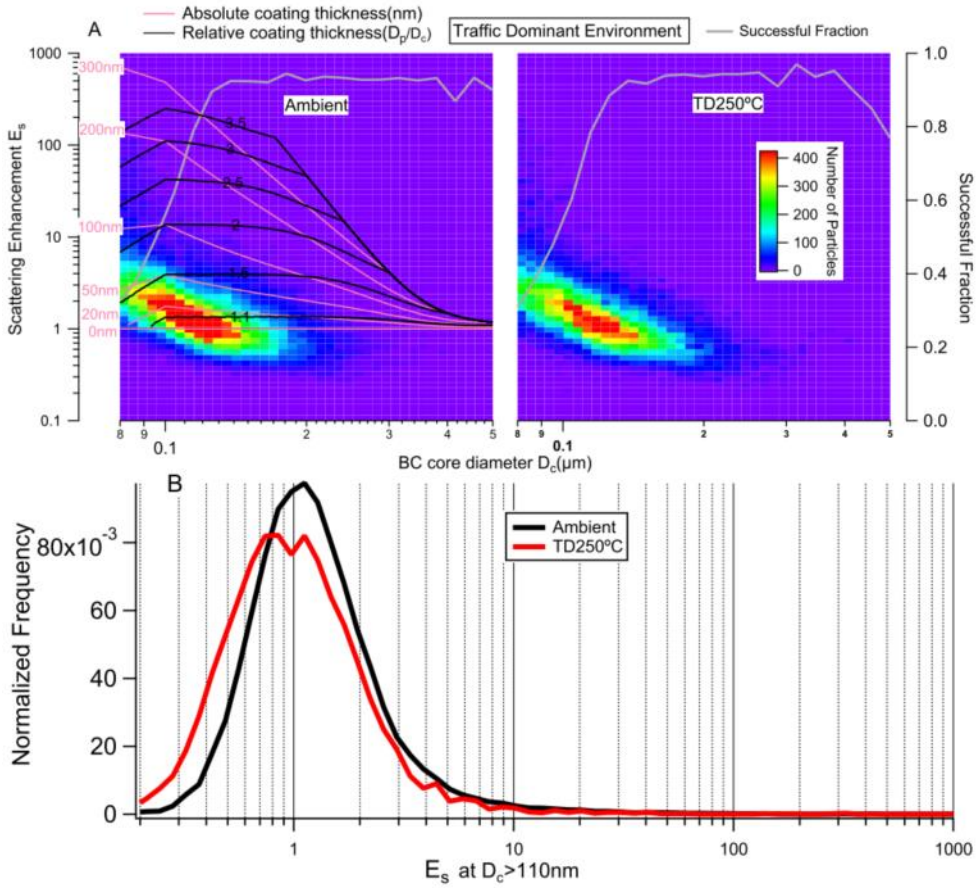

Figure 3.5. BC optical properties when the environment is dominated by traffic source. (a) The scattering enhancement (Es) as a function of BC core diameter (Dc). The image plot is a two dimensional histogram for the detected particles. The solid grey line, with corresponding scale on right axis, shows the number fraction of BC particles that were successfully determined according to their scattering signal at each Dc size. The left panel is for the ambient data, whereas the right panel is the same group of BC particles after passing through the thermodenuder (TD) at 250 ◦C. The thinner red and black contours show the corresponding absolute coating thickness (in nm, (Dp−Dc)/2) and relative coating thickness (Dp/Dc), respectively. (b) The area normalised histogram of Es for the particles with Dc >110nm. Reprinted from Liu et al. (2014).

For BC particles associated with the solid fuel burning, the coatings were not completely removed under the TD250 °C setting, as shown in Figure 3.6. The BC particles after the exposure to TD250 °C appeared to be compacted to a single defined mode; however, a significant tail is observed in the E_s distribution (Figure 3.6b). The remaining coatings on the BC particles, which are dominated by the solid fuel burning, may still contain a certain fraction of less-volatile OM. For the ambient data, which was largely affected by solid fuel burning, two modes of BC particle populations were observed (Figure 3.6a). The mode with smaller BC core size and thinner coatings agrees well with the mode only dominated by traffic source (Figure 3.5a), whereas the other mode with larger BC core size and thicker coatings are deemed to be from solid fuel burning. It has been indicated that BC particles from biomass burning are primarily thickly coated using SP2 measurements (Schwarz et al., 2008). The results in this study are consistent with it and support the argument that the emissions of solid fuel combustion have a great influence on the variation of BC core size and coating thickness, i.e. significantly increase the core size and coating thickness of BC.

According to the derived E_s as a function of D_c, at each bin of D_c, a threshold of E_s, E_{s_thre}, can be obtained at a specified D_c, as the example shown (Figure 3.6c). The E_{s_thre} as a function of D_c can therefore be empirically fitted as the following function:

$$E_{s-thre} = 1.0637 + 0.012343 \times D_c^{-2.6131} \quad (3.21)$$

Based on the assumption that the distribution of coating thickness is unimodal for a given source, any BC particle with a given D_c and $E_s > E_{s\_thre}$ is considered to be contributed by non-traffic sources in this model. The E_{s_thre} as a function of D_c is the dark dotted line, as shown in left panel of Fig. 3.6a. The BC particles with the characteristics above the dotted line are classified as the BC contributed by solid fuel combustion (BC_{sf}) and below the line are the BC from traffic source (BC_{tr}). Further details have been presented in Liu et al. (2014). The source apportionment technique based on the SP2 measurements is called the SP2 method in this study.

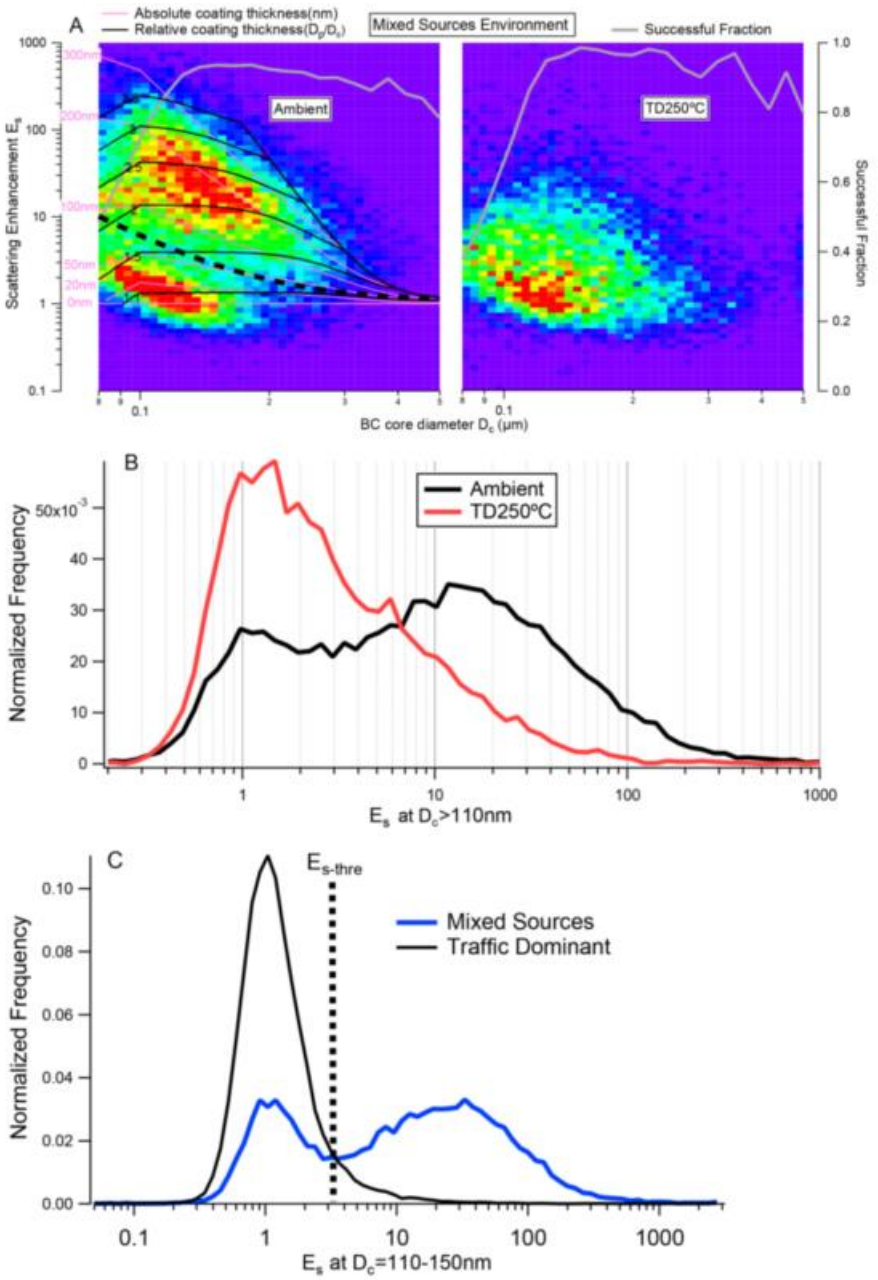

Figure 3.6. BC optical properties when environment is significantly influenced by solid fuel burning (31 January to 1 February when E air mass). The legends in the plot are identical with Fig. 4. In particular, the thick dotted black line on the left panel of (a) shows the reference line used to discriminate the BC from traffic or solid fuel burning source. (c) the Es distribution atDc =110–150nm for the traffic and mixed sources, with the dotted line showing the determination of Es-thre. Reprinted from Liu et al. (2014).

3.4 Source Apportionment models

In order to build an effective air quality management system, assessment of the sources of atmospheric pollutants is necessary and knowledge of how much each of the sources is contributing to ambient concentrations of particles is required. Source apportionment models based on different techniques to re-construct the contribution of emissions from different sources of atmospheric pollutants are

now well established. Although the receptor models for source apportionment were not used in this study, the source apportionment techniques are described briefly in this section as the outcomes of the models have been used in this research.

There are three main techniques generally categorized for source apportionment. First, numerical data obtained directly from the monitor is treated to identify sources, e.g. correlation between wind direction and the concentrations of measured pollutants to identify source locations (Henry et al., 2002). Another example of identifying the contributions of different sources is to subtract the concentrations measured at the regional background from the urban background and the kerbside levels (Yin et al., 2010). The main advantage of the methods is that there is not much complex calculation so that the possibility of artificial errors could be lower (Hopke et al., 2006).

Second, detailed emission inventories are needed to stimulate aerosol emissions, formation, transportation and deposition (Kulmala et al., 2011, Beevers et al., 2013). The principal advantage of these methods is that they can be applied to evaluate the concentrations of emissions reduction or increment in scenarios studies. However, these models are constrained by the accuracy of emission inventories and the availability of detailed emission inventories required (Viana et al., 2008).

Finally, the assumption of mass and species conservation is the fundamental principle of receptor modelling which can be used to identify and apportion the concentrations of pollutants to different sources in the atmosphere (Hopke et al., 2003, 2006). Receptor models can be generally described by the following equation based on the mass balance of elements between the measured concentrations and source contributions.

$$X_{ij} = \sum_{k=1}^{p} f_{ik} g_{kj} + e_{ij} \qquad (3.22)$$

Where X_{ij} is the measured concentration of the jth pollutant in the ith sample, f_{ik} is the mass concentration from the kth source contributing to the ith sample, and g_{kj} is the mass fraction of the jth pollutant from the kth source, e_{ij} is regarded as the residual.

3.4.1 Chemical Mass Balance (CMB)

The CMB model is based on the principle of mass conservation and is constrained by the major assumptions of (1) compositions of source emissions are constant. (2) species included in the source profiles are not reactive. (3) all sources contributing to the receptor have been included in the calculations. (4) the source uncertainties are independent. (5) the number of sources is less than or equal to the number of species. (6) measurement uncertainties are random, uncorrelated and normally distributed (Seinfeld and Pandis, 2006). The assumptions of CMB mean that a number of sources P contributing to the measured concentrations X at the receptor sites have been identified without any interaction between sources resulting in decrease and increase in their concentrations. If the mass fractions of the pollutant compositions from the sources in the region are known (f_{ik} in equation 3.22), the only unknown for the source apportionment of the measured concentration X_{ij} is the mass contribution of each source to each sample (g_{kj} in equation 3.22). The total aerosol concentration X can be expressed as the sum of the contributions of the individual sources c_k:

$$X = \sum_{k=1}^{p} C_k + e_k \tag{3.23}$$

In addition to the above assumptions of the method, there are still a number of difficulties in the application of CMB. Firstly, there is a need to determine which sources should be included in the model. If the emission inventory exists for the measured region, it can be used to determine the main sources. The second issue is the source profiles that should be used as profiles may be applicable to only the certain source in the specific area. Moreover, emission profiles often change with time and are usually different from location to location. Therefore, uncertainties in the CMB results can be reduced significantly by conducting source profile measurements corresponding to the period of the atmospheric measurements (Glover et al., 1991). It is absolutely essential for CMB modelling to know the area which is to be modelled (Hopke, 1985).

3.4.2 Positive Matrix Factorisation (PMF)

Positive Matrix Factorisation (PMF), which is like PCA in that does not use a priori knowledge of pollutants, is a multivariate factor analysis model which was first applied successfully by Paatero et al., (1991) and subsequently developed and

refined by Paatero and Tapper (1994) and Paatero (1997). This model can be utilized to process data in order to further explore the chemical constituents and investigate the potential sources. The fundamental principle of PMF is that mass conservation can be assumed and it has been referred to receptor-only model identifying and apportioning sources of airborne particulate matter in the atmosphere (Hopke, 2003) with no need of a priori information of source profiles. The PMF model uses a least squares algorithm in which the non-negativity of the solutions has been constrained because negative values of the factors are not meaningful in many physical situations.

With the elemental index notation, the bilinear model is defined as:

$$X_{ij} = \sum_{k=1}^{p} \mathrm{W}_{ik} \mathrm{P}_{kj} + e_{ij} \tag{3.24}$$

Where W_{ik} represents factor loading of the *i*th pollutant to the *k*th source; P_{kj} is called the score of the *k*th source of the *j*th sample; e_{ij} is regarded as the residual based on the same bilinear model as PCA (Tauler et al., 2009).

In spectroscopy, for example, X_{ij} is the spectral signal observed from the measurement, W_{ik} is the concentration of factor *k* at time step *i*, and P_{kj} is the fractional contribution of ion fragment *j* in the mass spectrum of factor *k*. In matrix form, the equation can be written as:

$$\mathrm{X} = \mathrm{GF} + \mathrm{E} \tag{3.25}$$

Where X is the measured dataset, G is the matrix of the concentrations of the factors, F is the matrix of the constant contributions, and E is the matrix of residuals that cannot be fitted by the model (Hopke et al., 2006).

Since the model uses a least squares approach to solve the factor analysis, G and F are constrained to be non-negative that there would be certain bias against the solutions. In order to get the optimal solutions, the "loss function" Q is defined as:

$$Q = \sum_{i=1}^{m} \sum_{j=1}^{n} \left(\frac{e_{ij}}{\sigma_{ij}} \right)^2 \tag{3.26}$$

Where the values σ_{ij} are estimated errors (standard deviations) of the data matrix in the *i*th variable measured in the *j*th sample. The factor analysis problem is to minimize Q which is used to determine the quality of fit of the PMF solution for

the chosen number of factors to the data. The degree of freedom of the fitted data (Paatero et al., 2002) is an important parameter calculated by subtracting the number of free parameters from the number of data points and consequently the expected Q is given as follows:

$$Q_{\text{exp}} \cong (nm) - P(n+m) \tag{3.27}$$

Where P is the number of factors, n is the number of samples and m is the mass spectra.

Several criteria are used to choose the appropriate number of factors from the model, and furthermore this is the most subjective part of PMF analysis and the most critical decision in order to fully interpret the results. Basically, the value of Q/Qexp is expected to be close to 1 if the model accurately represents the variability of the measured data. For AMS datasets, mn >> p(m+n), so $Q_{\text{exp}} \approx mn$, the number of points in the data matrix. However, an underestimation of the errors or variability unaccounted for in the factor profiles is indicated by values of Q/Q_{exp} greater than 1. Conversely, if values are less than 1, an overestimation of the errors of the input data has been indicated. As the degrees of freedom increase when additional factors are considered, Q is expected to decrease as more of the data should be allowed to be fitted. PMF solutions may not be unique as there may be linear transformations or rotations of the factor time series and mass spectra resulting in an identical fit to the data (Paatero et al., 2002). The transformation is defined as:

$$G = \text{GT} \quad \text{and} \quad F = \text{T}^{-1}\text{F} \tag{3.28}$$

Where T is a non-singular square matrix and T^{-1} is the inverse of the transformation matrix. *G* and *F* are the rotated matrices of G and F matrices respectively. As $GF=\text{GTT}^{-1}\text{F}=\text{GIF}=\text{GF}$, the products of multiplication of GF and *GF* are equal. However, an infinite number of rotations may still exist and the constraint of non-negativity of all elements of factor matrices could still be met (Paatero et al., 2002).

With such an approximate rotation, Q stays unchanged in a pure rotation. However, factor matrices only comply with the rotation equation, and therefore the objective function Q will increase from its minimum value. The rotation is

considered acceptable when the value of Q does not increase significantly (Paatero et al., 2009).

It is clear that there is rotational ambiguity as an infinite number of rotations may exist. The user defined rotational parameter Φ, call FPEAK can therefore be used to explore the ambiguity and indicate the suitable solutions by imposing rotations to the emerging solutions throughout the iteration processes (Paatero et al.,2002).

3.4.3 Multilinear engine (ME-2)

The multilinear engine algorithm (ME-2) (Paatero, 1999) is a computer program designed to solve multivariate receptor models, e.g. Chemical Mass Balance (CMB) and PMF, using an efficient least square algorithm. In the CMB model, a priori information of sources has to be known in advance, but one of the uncertainties in CMB modelling is the variable source compositions (Marmur et al., 2007). The bilinear model (PMF), on the other hand, gives an estimate of source profiles without a priori knowledge of emission sources, but the rotational ambiguity exists in the result. However, the rotational ambiguity of PMF can be reduced by ME-2 utilizing a priori knowledge of source profiles or time series (Paatero and Hopke, 2009); indeed, ME-2 can be regarded as a hybrid model of CMB and bilinear model (PMF). The advantage of ME-2 over PMF can range from the fully constrained profiles in CMB to fully unconstrained PMF solutions using a least squares algorithm to iteratively minimize the quantity Q (Canonaco et al., 2013).

There are two methods to constrain the factor profiles (elements of the F matrix) and/or factor time series (elements of the G matrix) called the a-value approach and the pulling approach (Canonaco et al., 2013).

With the a-value approach, the user inputs a constraint defined by the a value which determines the degree of the variation from the input F matrix and/or G matrix to the output F matrix and/or G matrix. The equation is:

$$\begin{aligned} \mathrm{W}_{i,solution} &= \mathrm{W}_i \pm a \cdot \mathrm{W}_i \\ \mathrm{P}_{j,solution} &= \mathrm{P}_j \pm a \cdot \mathrm{P}_j \end{aligned} \tag{3.29}$$

Where W and P represent a row and a column of the F and G matrices, respectively. The index *i* represents the *i*th variable and *j* represents the *j*th measured point.

In terms of the pulling approach, the pulling equations are utilised into the model by the user to pull profile factor elements towards predefined values. The equation is:

$$a_i = W_i + r_i \tag{3.30}$$

The equation only shows a row of the F matrix, where a_i represents the anchor which the model uses to pull the iterative value W_i, and r_i represents the residual. The more detailed introduction of ME-2 is described by Canonaco et al. (2013).

3.5 The strengths and weaknesses of the different models

CMB and PMF models have been applied in numerous studies for source apportionment of atmospheric pollutants investigated by Viana et al. (2008). In the previous studies, CMB was commonly applied to the data obtained from the filter samples (Docherty et al., 2008; Stone et al., 2008, 2009; El Haddad et al., 2011; Yin et al., 2010, 2015), whereas PMF has been developed to identify sources and contributions of organic aerosols acquired from highly time-resolved aerosol mass spectra (Lanz et al., 2007; Song et al., 2008; Allan et al., 2010; Zhang et al., 2011; Saarikoski et al., 2012; Young et al., 2014), besides being applied to the data from filter samples (Bullock et al., 2008; Lee et al., 2008; Chen et al., 2011; Heo et al., 2013) . However, the choice of CMB and PMF depends on various factors. First of all, the main difference between CMB and PMF is the fact that the application of CMB requires detailed a priori knowledge of the emission source profiles, whereas PMF only requires quantitatively a posteriori knowledge of the emission sources (Viana et al., 2008, Gianini et al., 2013). From the view of the application of the models, the CMB result for fine fraction was not satisfactory due to higher ratio of secondary particles (Okamoto et al., 2012). Although several studies suggested that the unapportioned OC from the CMB model can be a good estimate of SOA (Lee et al., 2008, Stone et al., 2008, Yin et al., 2015), a number of neglected POA sources may account for a fraction of unapportioned OC without SOA source profiles which have not been established in CMB. Furthermore, deviations of the selected input source profiles can also cause great uncertainties of SOA estimation (Robinson et al., 2006); however, PMF can provide a method to separate POA and SOA, which commonly accounts for a large part of the airborne OA (Zhang et al., 2009).

On the other hand, PMF requires a large number of ambient samples to resolve sources of atmospheric aerosols and their profile (mass fractions of species in sources), whereas CMB can be applied to any number of samples as long as the source profiles have already been known (Lee et al., 2008). The application of PMF also has limitations when source emissions have a strong correlation with time, and/or when meteorology and atmospheric processing have a great impact on particulate matter variability (Gianini et al., 2013). In these situations, the application of PMF can lead to mixed source profiles and consequently result in the under- or overestimation of the real contributions of sources (Canonaco et al., 2013).

ME-2, which has a priori information of source profiles added to the model, has been utilized in several studies to find better solutions which PMF does not represent (Lanz et al., 2008, Amato and Hopke, 2012). With the known source profiles input, the ME-2 solver can make a large improvement for hydrogen-like OA (HOA) due to the better separation of HOA and cooking OA (COA) by constraining these factors (Canonaco et al., 2013). Furthermore, ME-2 can provide a better resolution in result compared to that acquired from PMF as BBOA which has a high diurnal correlation with another factor exists. In this situation, the time series could not be separated using PMF (Lanz et al., 2008). Although several studies have indicated that ME-2 can reduce the rotational ambiguity compared to PMF, there is currently very little research regarding a priori knowledge of sources profiles included in the source apportionment for aerosol mass spectrum data. Therefore, further exploration for the application of ME-2 is needed and its pros and cons compared to different models for source apportionment of ambient aerosols for aerosol mass spectra should be tested and presented in future work.

Chapter 4

Results

4.1 Paper I: Intercomparison of different analysing approaches of source apportionment for wood burning aerosols in London

Authors: Y. Ting, D. Liu, J. D. Allan, D. E. Young, J. Yin[4], P. Zotter, S. Visser, A. S. H. Prevot, H. Coe

Publication: The manuscript has been under review by other co-authors.

Research highlights:

- Intercomparison was made based on a comprehensive suite of the dataset derived at a London urban site during wintertime.
- Factors affecting the data derived from Aethalometer were investigated.
- More accurate parameters for the estimation of the contribution of wood burning emissions to particulate matter were derived by a suite of pre-apportioned data.

Author's contribution: I led the data analysis and manuscript preparation.

Co-author contributions: Liu, Allan, Young, Yin, Zotter, Prevot and Coe participated in the field work/ data acquisition. Liu was responsible for quality assurance and provision of SP2. Young was responsible for the data of AMS-PMF, Yin was responsible for the outputs of CMB. Zotter and Prevot were for assurance of the Aethalometer data. Liu, Allan and Coe assisted in preparation of the manuscript.

Intercomparison of different analysis approaches of source apportionment for wood burning aerosols in London

Y. Ting[1], D. Liu[1], J. D. Allan[1], D. E. Young[3], J. Yin[4], P. Zotter[5], S. Visser[5], A. S. H. Prevot[5], H. Coe[1]

1. School of Earth and Environmental Sciences, University of Manchester, Manchester M13 9PL, UK
2. National Centre for Atmospheric Science, University of Manchester, Manchester M13 9PL, UK
3. Department of Environmental Toxicology, University of California, Davis, CA 95616, USA
4. Division of Environmental Health and Risk Management, School of Geography, Earth and Environmental Sciences, University of Birmingham, Edgbaston, Birmingham B15 2TT, UK
5. Laboratory of Atmospheric Chemistry, Paul Scherrer Institute, Villigen, Switzerland

Correspondence: Hugh Coe (hugh.coe@manchester.ac.uk)

Abstract. Determining the contribution of the wood burning to air pollution has become increasingly important due to the changings in energy sources in London. In winter, in particular, biomass burning emissions have been identified to be a major source of the atmospheric aerosols. Due to the complexity to characterise the mass concentrations of the solid fuel burning emissions, there have been several source apportionment techniques to estimate their contribution to particulate matter. However, as there is no agreement on the analysis techniques, the estimates of the contribution obtained from these methods are quantitatively different. The aim of this work is to investigate the potential factors resulting in the difference between the outputs of Aethalometer model and single particle soot photometer (SP2) method, using the data from a comprehensive suite of aerosol measurements and the outputs from various source apportionment studies obtained from the cooperated groups of the Clean Air for London (ClearfLo) project. The contribution of the wood burning to the BC apportioned by the Aethalometer model (BC_{wb_Aeth}) is less than ~38% of that attributed by SP2 method, resulting from the oxygenated organic aerosols (OOA). In addition, a lower absorption Angstrom exponent value for wood burning (α_{wb}) is expected depending on the burning conditions, fuel types or other non-traffic sources, such as coal and wood burning, which can affect the estimate of the BC_{wb_Aeth}.

For the estimate of the carbonaceous matter contributed by wood burning (CM_{wb}), the results indicate that an overestimation in CM_{wb} would be expected using the poly-linear regression in Aethalometer model, which has been widely used in most previous studies. The OM contributed by the other sources, such as cooking and OOA, is likely to be attributed to CM_{wb}. The findings and the parameters derived in this study could have implications when considering the mitigation strategies during winter in the future and may be a reference for better determining the contribution of wood burning.

1. Introduction

High concentrations of anthropogenic aerosols have been known to contribute to severe air quality, climate change and adverse human health (Lim et al., 2012, Butt et al., 2016) particularly in urbanised cities with high population densities. Black carbon (BC), mainly emitted from incomplete combustion of fossil fuel and biomass (Bond et al., 2004), is the principal source of the light-absorbing carbonaceous matter in aerosols (Bond et al., 2013a), only second to carbon dioxide (CO_2). BC has been found to be a contributor to positive radiative forcing, which has a strong effect on globe and regional warming (Ramana et al.,

2010, Ramanathan and Carmichael, 2008). Reducing air pollution has been a matter of concern, mainly in urban environments. However, the source contributions are not easily to be evaluated accurately as pollutants emitted by various sources have different properties, with further physical and chemical processes involved. BC is the prevailing indicator of the adverse health effect caused by the particulate air pollution (Janssen et al., 2012, Grahame et al., 2014), and therefore the quantification and source apportionment of the BC and their concentration are essential, especially in winter when wood burning has been found to be a major contributor to air pollution in residential areas (Lanz et al., 2008, Sandradewi et al., 2008b, Favez et al., 2010, Crippa et al., 2013). As there is no agreement on particulate measuring technique with a specific definition, various techniques for the measurement of the refractory BC have been developed and used in the recent studies (Petzold et al., 2013).

In the UK, a 2-wavelength Aethalometer (AE22, Magee Scientific) has been principal BC analyser, quantifying the optically absorbing BC particles according to the transmission of light on a filter sample (Butterfield et al., 2016). Moreover, a 7-wavelength Aethalometer based on filter technique has been widely used for the measurements of the BC mass concentration and the light absorption coefficients of aerosols (Sandradewi et al., 2008b, Favez et al., 2010, Hyvärinen et al., 2011, Patrón et al., 2017). From a wide range of measurement methods/ instruments used in the scientific literature, the Single Particle Soot Photometer (SP2) has been increasingly recognised as a more appropriate tool for characterizing refractory BC-containing particles (Schwarz et al., 2006).

The Aethalometer model has been used to evaluate the contributions of traffic-related and solid fuel sources to carbonaceous matter concentrations (Sandradewi et al., 2008b, Favez et al., 2010). The key factor for the accuracy of the model is to assign appropriate α values for the traffic and wood burning sources, and therefore the uncertainties of the assumed α will lead to considerable variations of the model outputs (Harrison et al., 2013). Recently, a source apportionment methodology for BC attribution has been developed based on the measured BC size distribution and mixing state by SP2 (Liu et al., 2014). It was the first time to directly attribute the quantity of BC sources from their physical properties. A comparison of the SP2 and Aethalometer measurements indicated that non-BC species, referred to as brown carbon (BrC), significantly affect the Aethalometer measurements in the sampling area (Wang et al., 2014). It was found that both primary organic aerosol (POA), emitted directly by the sources, and secondary organic aerosol (SOA), produced by photochemical aging processes, comprise brown carbon, and exhibit the properties of light absorption at different

wavelengths to a significant extent (Saleh et al., 2013). Besides, there are studies indicating that BrC is mainly produced from biomass burning/biofuel combustion (Washenfelder et al., 2015) and generated from the photo-oxidation of anthropogenic and biogenic volatile organic compounds (VOCs) (Ervens et al., 2011).

To explore the difference of the source apportionment from the various approaches in this study, the comprehensive data from Chemical Mass Balance (CMB) receptor model (Yin et al., 2015), Aerosol Mass Spectrometer Positive Matrix Factorisation (AMS-PMF) (Young et al., 2015), Multilinear Engine (ME-2), SP2 (Liu et al., 2014) and Aethalometer models were used. The aim of the study is to estimate the contributions of wood burning and traffic to carbonaceous matter using Aethalometer model and explore the relationships between the results derived by different source apportionment models. The resulting coefficients from the Aethalometer model can be used as references for future studies, where such a comprehensive suite of aerosol measurements may not be available. In addition, there is a discrepancy between the BC_{wb} attributions apportioned by SP2 (BC_{wb_SP2}) according to the coating thickness and core size (Liu et al., 2014), and Aethalometer method (BC_{wb_Aeth}) using absorption Angstrom exponent (AAE), which describes the dependency of aerosol optical thickness on wavelength, during the winter intensive observation period (Monks et al., 2009). As Aethalometer has been widely applied to quantify the light absorption by BC and the contributions of the carbonaceous matter by pollution sources, the cause of the difference between the attributions apportioned by SP2 and Aethalometer has to be identified to be used as a reference for future research. To find out the reasons of the difference between the contributions of BC from wood burning apportioned by Aethalometer method and SP2, the ratios of levoglucosan/potassium, SFOA1/SFOA2 as well as various pollutants have been used. This is a unique opportunity to apply the datasets measured by various instruments at the same site during the same period and analysed by different source apportionment models to compare the source contributions of the carbonaceous matter (CM). This study will provide a method to determine which model is more appropriate depending on different conditions. In previous studies, the estimated contributions of wood burning and traffic to CM by the Aethalometer model were performed with the combination of the off-line (i.e. the concentration of CM) and on-line (i.e. light absorption coefficients) measured data (Sandradewi et al., 2008b, Sandradewi et al., 2008c, Favez et al., 2010), which may cause more sampling and analysed artefacts than that of the all on-line measured data. This study can provide a relatively high time-solution data for a better estimate with the on-line

measurement of CM (i.e. OA from AMS; BC from SP2) and the light absorption coefficients measured by Aethalometer. The resulting coefficients from linear regressions can be used as references for future studies, where such a comprehensive suite of aerosol measurements may not be available.

2. Experiment and data analysis

This study reports the continuous measurements from the Clean Air for London (ClearfLo) campaign conducted in 2012 with an intensive observation period (IOP). An overview of the projected is detailed in Bohnenstengel et al. (2015) and (http://www.clearflo.ac.uk). The experiment in this study was conducted at an urban background site in the grounds of a school in North Kensington (51.521055_ N, 0.213432_W), which is identified as an urban background site. The IOP lasted for 4 weeks and was conducted in winter (11 Janurary to 8 February) to investigate the range of sources and the ambient pollutants to which the London population are exposed to and provide comprehensive gaseous pollutant and aerosol data for tackling air quality issue. The sources of the outputs of different models used in this study are shown in the following section.

2.1 The sources of the data

The Chemical Mass Balance (CMB) model: This model was applied to aerosols collected on filter. The 24 h fine particles ($PM_{2.5}$) were collected onto 150 mm diameter quartz filters, which were analysed for ions (SO_4^{2-}, NO_3^-, Cl^-, Na^+, K^+, Ca^{2+}, Mg^{2+} and NH_4^+) using a Dionex ion chromatograph. OC and EC were analysed by Sunset Laboratory thermal-optial OC/EC analyser, and organic markers were analysed by GC-MS. The methods for the sample extraction and analysis procedures have been reported by Yue and Fraser (2004) and Yin et al. (2010). A modified quantification method for the secondary biogenic markers was used as described by Wagener et al. (2012a).

The results of the CMB modelling are from Yin et al. (2015) calculating related organic matter (OM) components by multiplying by OM/OC ratios considered suitable for the source. In brief, the US EPA CMB8.2 software was used for CMB modelling, with similar source profile to previous works, including traffic (Pant et al., 2014), food cooking (Zhao et al., 2007), wood smoke/biomass burning (Fine et al., 2004), coal combustion (Zhang et al., 2008), dust/soil (Schauer, 1998), vegetative detritus, natural gas combustion (Rogge et al., 1993a, Rogge et al., 1993b) and secondary biogenic emissions (Wagener et al., 2012a,

Wagener et al., 2012b). The model performance and measurements can be found in detail in Yin et al. (2010) and Yin et al. (2015).

The AMS data and PMF analysis: The chemical composition of non-refractory PM_1 was measured by an on-line instrument, the Aerodyne high-resolution time-of flight aerosol mass spectrometer (HR-ToF-AMS, hereafter AMS). The AMS data has been analysed and apportioned by Young et al. (2014) using Positive Matrix Factorisation (PMF) model based on the method described by Allan et al. (2010). Further details about the operation, measurements and data analysis of the AMS have been presented in Young et al. (2015), but a brief description relevant to this work is provided here.

Positive matrix factorisation (PMF), which can be used to identify potential pollutant sources, was performed on the organic data from the "V-mode", allowing analysis of peaks according to elemental composition (Sun et al., 2011). Although the "W-mode" data could provide a more detailed analysis theoretically, the fractions of peaks were too low to permit a meaningful PMF analysis. A computer program for using the multilinear engine algorithm (ME-2) (Paatero, 1999) is currently available (Canonaco et al., 2013), which can provide a better resolution in result in some circumstances. However, the advantages of this approach are most significant when applied to the unit mass resolution data (e.g. Quadruple AMS, compact ToF-AMS), where the key peaks of the ion fragments (such as $C_3H_7^+$ and $C_2OH_3^+$) cannot be explicitly separated and thus result in the contribution to rotational ambiguity under PMF analysis. As this is not an issue to apply the PMF to the HR-ToF-AMS data presented here, it would be more appropriate to use PMF. The results therefore would not be affected by a priori assumptions upon the composition of the aerosols.

The data were processed according to the recommended method as described by Ulbrich et al. (2009). A five factor solution for the AMS-PMF results was identified that contribute to organic aerosols OA, including oxygenated organic aerosols (OOA), traffic related/hydrocarbon-like organic aerosols (HOA), cooking organic aerosols (COA) and two solid fuel burning organic aerosols (SFOA1 and SFOA2), which had a split factor of SFOA. While the SFOA in the four-factor solution (only one SFOA factor was identified) seemed to be valid, it was deemed that the five-factor solution (the split SFOA factors were identified) was more appropriate as the sum of the SFOA factors better correlated with the gas tracers. Further details have been presented in Young et al. (2015).

The trace element and ME-2 analysis: The trace elements (Na, Mg, Al, Si, P, S, Cl, K, Ca, Ti, V, Cr, Mn, Fe, Ni, Cu, Zn, Br, Sr, Zr, Mo, Sn, Sb, Ba and Pb), which can be used as the tracers of the source contribution, were collected using rotating drum impactors (RDIs) described in Bukowiecki et al. (2009a) and subsequently analysed by synchrotron radiation induced X-ray fluorescence spectrometry (SR-XRF) described in Flechsig et al. (2009a) and Visser et al. (2015b). ME-2 was further applied to estimate the contributions of different sources (Visser et al., 2015a). The contributions of the traffic-related and solid fuel combustion sources to PM_1 are utilised in the study.

The single particle soot photometer: In this study, the physical properties of individual refractory BC (rBC) particles (Petzold et al., 2013) was characterised by a single particle soot photometer (SP2). The detailed operation of the instrument and data analysis procedures of the specific SP2 in Manchester have been described in previous studies (McMeeking et al., 2010), but a brief description related to this study is given here. The SP2 determines the mass of refractory particle by detection of the incandescence radiation induced by a 1064 nm intra-cavity Nd:YAG laser when a light-absorbing particle passes through. The main light-absorbing component in the atmosphere at this wavelength is BC. Therefore, the incandescence signal was converted to the mass of single particle rBC based on the calibration using Aquadag sample black carbon particle standards (Aqueous Deflocculated Acheson Graphite, manufactured by Acheson Inc., USA). The generated rBC particle standards from Aquadag do not represent the ambient rBC, thus a further correction of 0.75 is employed with the calibration curve to obtain more reliable rBC mass determination (Moteki et al., 2010, Baumgardner et al., 2012, Laborde et al., 2012). The determined rBC mass is used to calculate a mass-equivalent diameter, assuming a density of 1.8 g cm^{-3} for atmospheric BC (Bond and Bergstrom, 2006a), termed as the BC core diameter (Dc), which is the diameter of a sphere containing the same mass of measured rBC. The total rBC concentration is the sum of rBC masses of all detected single particles. As the core sizes of some particles are too small to being detected, or too large thus saturating the detector, a certain amount of rBC mass is missed. These undetected masses are estimated based on a log-normal fit of the D_c mass distribution. The missing masses can be derived by the extrapolation of the log-normal fit on the Dc mass distribution (Liu et al., 2014).

The scattering signal of an rBC-containing particle can be distorted because of the mass loss of a BC particle by laser heating when it passes through the laser beam. Thus, the ‘leading

edge only' (LEO) method is utilised to reconstruct the scattering signal of an rBC-containing particle (Gao et al., 2007). The details for the LEO fitting are described by Liu et al. (2014) and Taylor et al. (2015). The overall rBC size (D_p), including the BC core and coatings, can therefore be provided by a core-shell Mie model with the input of the LEO fitted scattering signal and BC core size, accompanied with the assumption of an rBC core refractive index of 2.26 – 1.26i and a coating refractive index of 1.5 + 0i (Moteki et al., 2010). The relative coating thickness of an rBC particle is calculated as D_p/D_c. The optical size of a non-rBC particle can also be calculated using Mie theory with a coating refractive index of 1.5 + 0i, which makes the optical sizes of rBC-containing and non-rBC particles directly comparable. Given the coating thickness of individual rBC particles is Dc size dependent, the bulk coating thickness is calculated as the cubed root by the total volume of the rBC particles divided by the total volume of the BC cores, as shown in Eq (1):

$$\frac{D_p}{D_c} = \left(\frac{\sum_i D_{p,i}^3}{\sum_i D_{c,i}^3}\right)^{\frac{1}{3}} \quad (1)$$

Where D_p and D_c are the coated BC diameter and BC core diameter, respectively; *i* denotes the *i*th single BC particle. The volume weighted bulk D_p/D_c is considered to be a representative diagnostic for the overall mixing state of the entire population of BC particles.

In order to identify the sources of the BC, a parameter of scattering enhancement, E_s, was introduced, which is defined as the Eq. (2):

$$E_s = \frac{S_{coated}}{S_{uncoated}} \quad (2)$$

Where S_{coated} is the scattering signal measured by the SP2 and then LEO fitted; $S_{uncoated}$ is the scattering signal of the corresponding BC core, which is derived using the Mie single particle scattering solutions.

According to the Eq. 2, a value of 1 for E_s means that the scattering signal of a BC particle equals to that of only a BC core, which also means zero coating or $D_p/D_c = 1$. Actually, particles with any coatings will scatter more the corresponding core, and E_s therefore will be necessarily greater than 1. However, S_{coated} will also be subject to the uncertainties of the instrument measurement. Thus, a proportion of particles with E_s less than 1 would be expected. In general, an increase in Es will indicate a thicker coating for a specified D_c.

Figure S1 shows the variation of E_s as a function of BC core diameter (D_c) for the BC particles, when the traffic source mostly dominated and BC particles were least coated during the experiment. The coatings on these BC particles are considered to be completely removed after thermal desorption at 250 °C (TD250 °C), in other words, no coating should yield a value of 1 for E_s. For the particles with smaller D_c (< 110 nm), the low signal-to-noise ratio in the scattering signal related to the SP2 detectors, thus causing a failed LEO fit, or the scattering signal of measured particles falling outside of the Mie-calculation predictable range. In addition, it is expected that the scattering signal for a proportion of BC particles with core diameter less than 110 nm with thin coatings will also not be efficiently detected, resulting in a bias towards the particles with larger cores that were successfully fitted.

For BC particles associated with the solid fuel burning, the coatings were not completely removed under the TD250 °C setting, as shown in Figure S2. The BC particles after the exposure to TD250 °C appeared to be compacted to a single defined mode; however, a significant tail is observed in the E_s distribution (Figure S2b). The remaining coatings on the BC particles, which are dominated by the solid fuel burning, may still contain a certain fraction of less-volatile OM. For the ambient data, which was largely affected by solid fuel burning, two modes of BC particle populations were observed (Figure S2a). The mode with smaller BC core size and thinner coatings agrees well with the mode only dominated by traffic source (Figure S1a), whereas the other mode with larger BC core size and thicker coatings are deemed to be from solid fuel burning. It has been indicated that BC particles from biomass burning are primarily thickly coated using SP2 measurements (Schwarz et al., 2008). The results in this study are consistent with it and support the argument that the emissions of solid fuel combustion have a great influence on the variation of BC core size and coating thickness, i.e. significantly increase the core size and coating thickness of BC.

According to the derived E_s as a function of D_c, at each bin of D_c, a threshold of E_s, E_{s_thre}, can be obtained at a specified D_c, as the example shown (Figure S2c). The E_{s_thre} as a function of D_c can therefore be empirically fitted as the following function:

$$E_{s-thre} = 1.0637 + 0.012343 \times D_c^{-2.6131} \quad (3)$$

Based on the assumption that the distribution of coating thickness is unimodal for a given source, any BC particle with a given D_c and $E_s > E_{s\_thre}$ is considered to be contributed by non-traffic sources in this model. The E_{s_thre} as a function of D_c is the dark dotted line, as

shown in left panel of Fig. S2a. The BC particles with the characteristics above the dotted line are classified as the BC contributed by solid fuel combustion (BC_{sf}) and below the line are the BC from traffic source (BC_{tr}). Further details have been presented in Liu et al. (2014). The source apportionment technique based on the SP2 measurements is called the SP2 method in this study.

Aethalometer

A 7-wavelength Aethalometer (AE31, Magee Scientific) was used to measure the light absorption coefficients (b_{abs}, in Mm^{-1}) at seven different wavelengths from which the mass concentrations of BC can be derived (Petzold et al., 2013) by assuming a mass absorption cross section (MAC, m^2 g^{-1}). The measured aerosol light absorption coefficients (b_{abs}) were corrected for multiple scattering effect (C value) by the filter fibres and the shadowing effect caused by the accumulation of light absorbing particles in the filter (f value), which may shadow the newly collected ones so that could not be exposed to the same intensity of light. A value of 1.2 (f value) was used for the correction of shadowing effect based on the procedure described in Weingartner et al. (2003), and a C value of 3.095 was determined based on the comparison between the uncorrected b_{abs} and that of a Multi-Angle Absorption Photometer (MAAP) measured at λ = 630 nm using data with attenuation values only smaller than 10 (Collaud Coen et al., 2010), where the shadowing effect is not expected (Crilley et al., 2015).

Aethalometer model

The Aethalometer was originally developed to quantify light absorption by black carbon (BC), which is considered as the predominant light absorbing particulate species at visible wavelengths (Hansen et al., 1984). The parameterized aerosol absorption coefficients are proportional to $\lambda^{-\alpha}$, where λ is wavelength and α is the Ångström absorption exponent which can be calculated by the Eq. (1). It has been proved that α can be assumed to be constant for pure traffic (α_{tr}) and pure wood burning (α_{wb}) measured at λ 470 and 950 nm (Harrison et al., 2012, Sandradewi et al., 2008b). Wavelengths of 470 and 950 nm were chosen here as Liu et al. (2014) has examined the two-wavelength Aethalometer measurement at wavelengths of 370 and 880 nm, which is also routinely used for the estimates of the contribution of the traffic and solid fuel combustion. It was found that fewer residuals resulted from the use of wavelengths at 470 and 950 nm compared to that from the

wavelengths of 370 and 880 nm (Zotter et al., 2017). In this study, the value of 1 (Bond and Bergstrom, 2006a) for α_{tr} and 2 (Kirchstetter et al., 2004, Bond and Bergstrom, 2006a, Lewis et al., 2008, Crilley et al., 2015) for α_{wb} was used, and the b_{abs} for traffic ($b_{abs,tr}$) and wood burning (b_{abs_wb}) were derived by Eq. (2-4). The derived b_{abs} were then used to apportion the total BC to the contribution of traffic ($BC_{traffic\_Aeth}$) and wood burning (BC_{wb_Aeth}) according to Sandradewi et al. (2008b, c) by the Eq. (5).

$$\alpha = \frac{\ln(\frac{b_{ATN,470}}{b_{ATN,950}})}{\ln(\frac{950}{470})} \quad (1)$$

$$b_{abs}(\lambda) = b_{abs}(\lambda)_{traffic} + b_{abs}(\lambda)_{wb} \quad (2)$$

$$\frac{b_{abs}(470nm)_{traffic}}{b_{abs}(950nm)_{traffic}} = \left(\frac{470}{950}\right)^{-\alpha_{traffic}} \quad (3)$$

$$\frac{b_{abs}(470nm)_{wb}}{b_{abs}(950nm)_{wb}} = \left(\frac{470}{950}\right)^{-\alpha_{wb}} \quad (4)$$

$$BC_{tra} = \frac{b_{abs(950nm)tra}}{b_{abs(950nm)total}} \quad (5)$$

With given α_{tr} and α_{wb} values and using the field data of the light absorption measurements at 470 and 950 nm, the values for $b_{abs,traffic,470nm}$, $b_{abs,traffic,950nm}$, $b_{abs,wb,470nm}$, and $b_{abs,wb,950nm}$ can be computed with equation (2)-(4). In this study, the BC mass concentration (BC_{total}) is presented as the rBC measured by the SP2 instrument rather than the Aethalometer derived BC mass.

Based on the a priori assumptions that during winter fossil fuel and wood combustion are the dominating sources of total carbonaceous matter (CM_{total}), ambient CM_{total} can be modelled by the light absorption coefficients of aerosols emitted by these two sources (Sandradewi et al., 2008b, Favez et al., 2010), as shown in Eq. (6). In the following, the contribution of wood burning and traffic emission aerosols to the carbonaceous matter within PM_1 is estimated by a linear regression of the light absorption of the two sources combined with AMS (Young et al., 2015) and SP2 (Liu et al., 2014) measurements. The equations are as follows:

$$CM_{total} = OM + BC$$
$$= CM_{traffic\_Aeth} + CM_{wb,Aeth} + CM_{residual} \quad (6)$$
$$= C_1 * b_{abs,traffic,950nm} + C_2 * b_{abs,wb,470nm} + C_3$$

Where OM is the organic mass measured by the AMS, BC is the black carbon measured directly by the SP2 rather than Aethalometer as the uncertainties of the assumed α will lead to considerable variations of the model outputs (Harrison et al., 2012, Harrison et al., 2013), $b_{abs,tr,950nm}$ represents the absorption coefficient of carbonaceous matter originating from traffic emissions ($CM_{traffic\_Aeth}$) at wavelength 950 nm, $b_{abs,wb,470nm}$ represents the absorption coefficient of wood-smoke containing carbonaceous matter (CM_{wb_Aeth}) at wavelength 470nm, the calculated parameters C_1 and C_2 relate the light absorption to the particulate mass of both sources. The third constant, C_3, accounts for the background concentration/non-combustion OM.

With AMS-PMF (Young et al., 2015), BC_{tr_SP2} and BC_{wb_SP2} separated by Liu et al. (2014), the equation (6) can be rewritten as Eq. (7)-(8). As OM and BC contributed by the specific sources have been attributed, which are primary aerosols, C3 in Eq. (7)-(8) is set to be zero.

$$CM_{traffi\_SP2} = HOA + BC_{tr} \quad (7)$$
$$= C_1^* * b_{abs,traffic,950nm}$$
$$CM_{wb\_SP2} = SFOA1 + SFOA2 + BC_{wb} \quad (8)$$
$$= C_2^* * b_{abs,wb,470nm}$$

Where $CM_{traffic\_SP2}$ is the carbonaceous matter contributed by the traffic and CM_{wb_SP2} is the carbonaceous matter contributed by the wood burning apportioned by the AMS-PMF and SP2 methods. C_1^* and C_2^* are the parameters associated with the light absorption to the particulate mass of both sources.

3. Results and Discussion

Investigation of the difference between BC source attribution from SP2 and Aethalometer model

Figure 1 shows the time series of the species derived by different receptor models, and certain correlations between $BC_{wb\_difference}$ and coal/wood smoke/solid fuel organic aerosol 1 (SFOA1)/SFOA2/oxygenated organic aerosol (OOA)/solid fuel trace element are observed,

especially in the CMB time series with lower time-resolved data. As the relationships between $BC_{wb\_difference}$ and the chemical components are not normally distributed and/or linear, the spearman rank correlation method (described in Supplement) was used to investigate the relationships between them, which are showed in Appendix (Table S1 with lower time resolution based on the filter measurements and Table S2 with higher time resolution according to the AMS measurements). The correlation coefficient of the spearman rank correlation test (r_s) between the OOA and $BC_{wb\_difference}$ is highest among these tests in Table S1 and S2, which means that the OOA is likely to be the main factor causing the discrepancy between the results apportioned by different models. Although the r_s between the coal combustion emissions, water-soluble potassium ion and $BC_{wb\_difference}$ are high, the both p-value are higher than 0.05 which mean they are not significant. However, the coal combustion emissions and potassium may still be the factors causing the differences as the higher p-value are possibly due to the less number of the data.

As there are many possible reasons resulting in the discrepancy between the different BC_{wb} attributions, the absorption Angstrom exponent of wood burning (α_{wb}) was further evaluated by the Eq. (1) – (4).

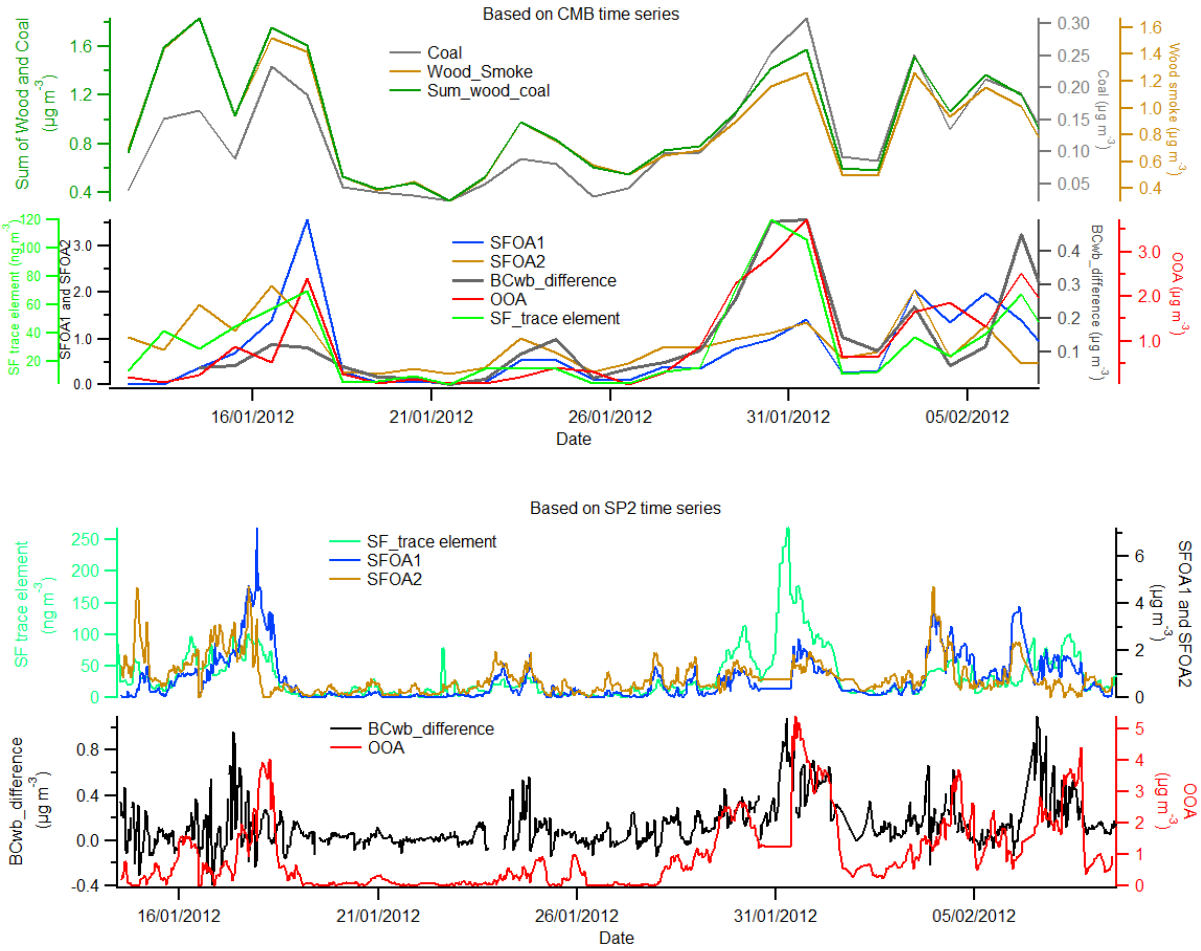

Figure 1. The upper plot is based on the CMB time series and shows certain correlations between $BC_{wb\_difference}$ and coal/wood smoke/SFOA1/SFOA2/OOA/solid fuel trace element, while the lower one is based on the SP2 time series with higher time resolution and illustrates lower correlation between the species. (Note: $BC_{wb\_difference} = BC_{wb\_SP2} - BC_{wb\_Aeth}$)

BC_{tra} apportioned by the SP2 (Liu et al., 2014) and Aethalometer methods shown in Appendix have a high correlation ($r^2 = 0.96$), and the slope of the linear regression is close to 1 (1.07), whereas the BC_{wb} attributions have only moderate correlation ($r^2 = 0.53$), and the slope is 0.49, which means BC_{wb} attribution with Aethalometer model are mostly lower than that with SP2.

The key factor for the accuracy of the outcome of the Aethalometer model attribution is to assign appropriate α_{tra} and α_{wb}; otherwise the uncertainties of the assumed α will result in the considerable variations of the model outputs (Harrison et al., 2013). In this study, the α_{tra} value of 1 and α_{wb} of 2 are set according to Crilley et al. (2015), which are consistent to the values introduced in Sandradewi et al. (2008b) and Favez et al. (2010). However, the α_{wb} has been shown to be of a large range of dependence on the burning phase, conditions, fuel types

as well as aging level of the biomass burning emissions (Saleh et al., 2013; Garg et al., 2016 and references therein). Therefore, the α_{wb} during the IOP are calculated using the given BC_{wb} obtained by SP2 and fixed α_{tra} being 1 to explore the factors causing the discrepancy between the BC_{wb} attributions apportioned by SP2 and Aethalometer model shown in Figure 2.

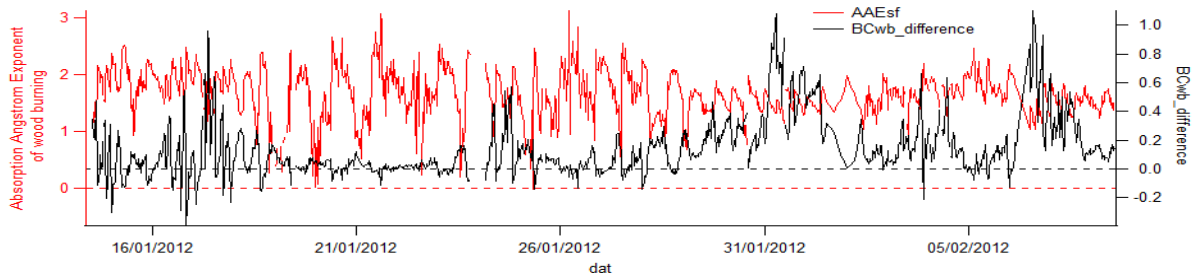

Figure 2. The time series of the absorption Angstrom exponent (AAE) of solid fuel and $BC_{wb\_difference}$.

As the correlations between α_{wb} and different pollutants are not significant throughout the IOP, and the characteristics of the pollutants transmitted from different regional sources are not completely the same, the data sets are separated based on the origin of air masses (Liu et al., 2014) to explore the relationship of the diurnal patterns between them showed in Figure 3.

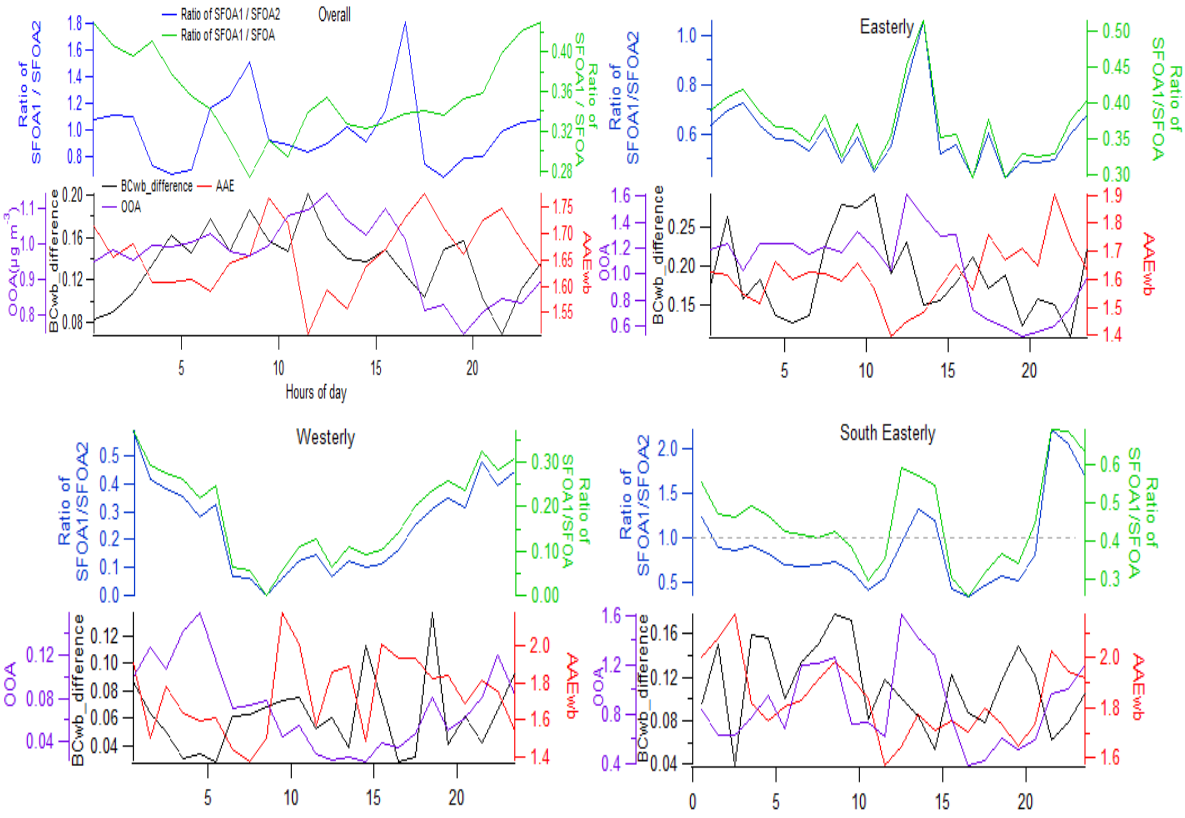

Figure 3. The diurnal patterns of the α_{wb}, $BC_{wb\_difference}$, OOA, ratios of SFOA1/SFOA2 and SFOA1/SFOA based on the origin of air masses. The overall period is 32 days.

There is a high correlation between the ratios of SFOA1/SFOA2 and SFOA1/SFOA when they are divided into three datasets based on the origin of air masses compared to the entire time series. This indicates that there are different properties of the solid fuel combustion emissions from various areas. AAE_{wb} and $BC_{wb\_difference}$ have moderately negative correlations regardless of the origin of air masses (Easterly, r = - 0.63; Westerly, r = - 0.59; South Easterly, r = - 0.70), showing the need of the decrease in α_{wb} depending on the air mass rather than assumed value of 2 during the whole period.

Figure 4 displays the relationships between the differences of the BC_{wb} apportioned by the two methods and the OOA concentrations according to the origin of air masses. BC_{wb_Aeth} are significantly lower than BC_{wb_SP2} when the high OOA concentrations occur wherever the air masses come from. It is consistent with the result of the spearman rank test that OOA is likely to be the factor causing the discrepancy between the attributions of these two methods.

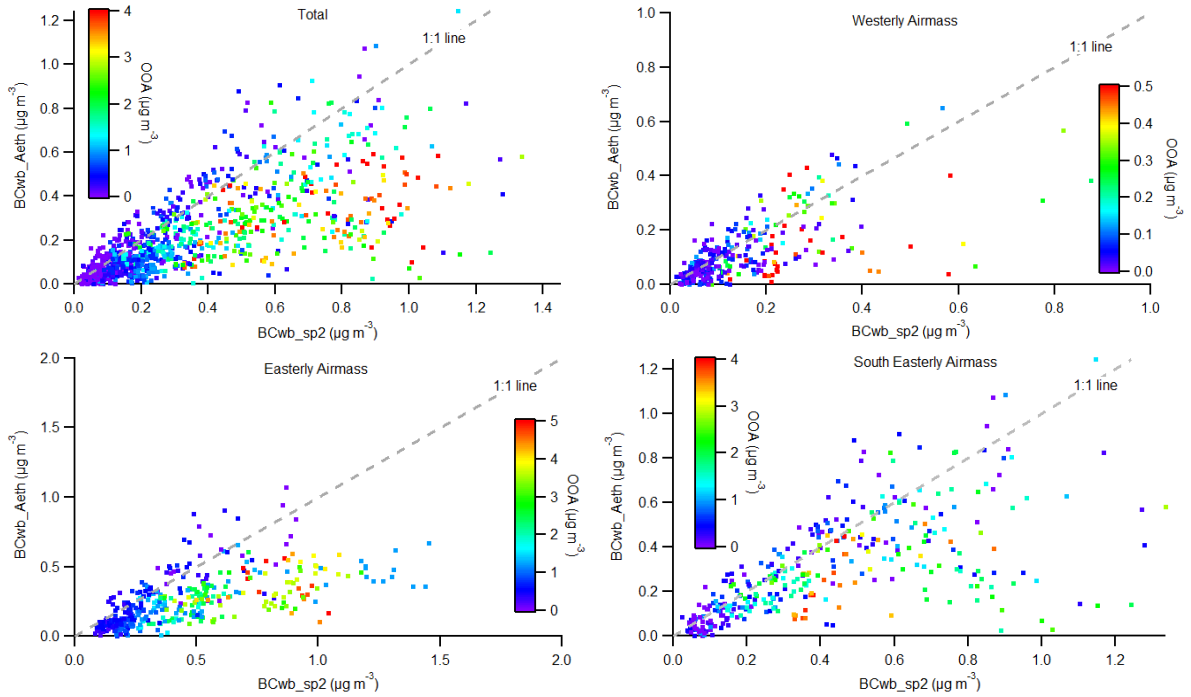

Figure 4. Comparisons between BC_{wb_Aeth} and BC_{wb_SP2} with the variations of OOA concentrations based on the origin of air masses. The BC_{wb_SP2} are larger than BC_{wb_Aeth} when the high OOA concentrations occur.

Inter-comparison of source apportionment of carbonaceous matter

In this study, according to equations (7) and (8), Figure 5 exhibits a very high correlation between $CM_{traffic}$ (HOA+BC_{tr}) and $b_{abs,traffic,950nm}$ (r^2 = 0.90), which means that $b_{abs,traffic,950nm}$ can effectively represent the most absorption of carbonaceous matter from traffic emissions. Although Figure 5 indicates that the correlation between CM_{wb} (SFOA1+SFOA2+BC_{wb}) and $b_{abs,wb,470nm}$ is just moderate (r^2 = 0.68), $b_{abs,wb,470nm}$ can generally represent the absorption of carbonaceous matter from wood burning emissions.

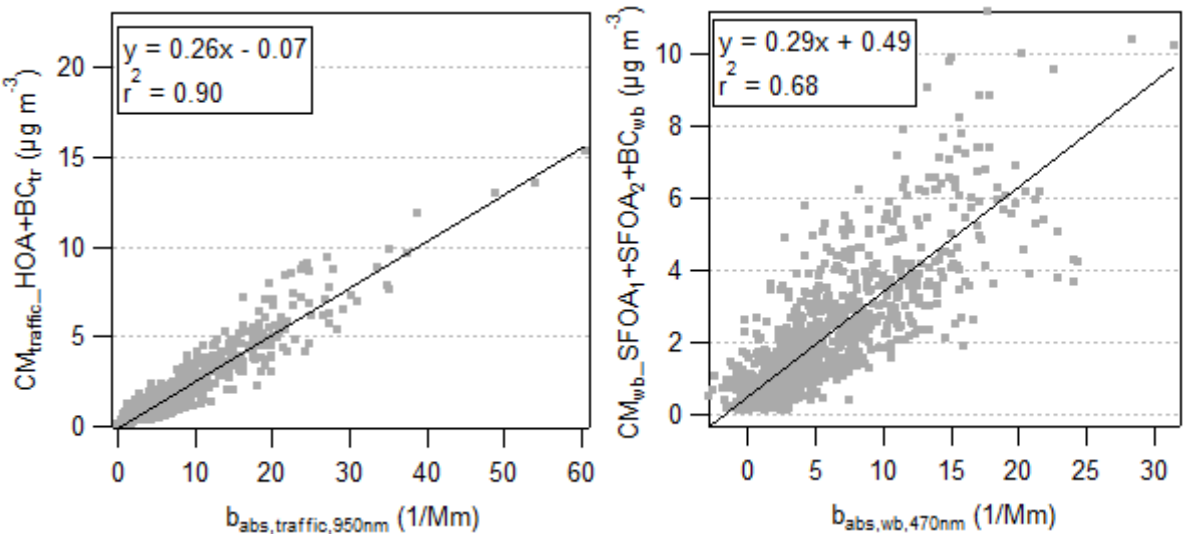

Figure 5. The correlations between $CM_{traffic\_HOA+BCtr}$ and $b_{abs,traffic,950nm}$ and between $CM_{wb\_SFOA1+SFOA2+BCwb}$ and $b_{abs,wb,470nm}$.

The intercomparisons of $CM_{traffic}$ and CM_{wb} between the measured data (from AMS-PMF and SP2) and the estimates calculated by the poly-linear regression equations derived from using $b_{abs,traffic,950nm}$ ($CM_{traffic\_Aeth}$) and $b_{abs,wb,470nm}$ (CM_{wb_Aeth}) (from Aethalometer) are made in time series and the results are presented in Figure 6 and Table 1, which illustrates the daily concentrations of $CM_{traffic}$, CM_{wb} and the discrepancies between the estimates from two methods. From the upper plot of Figure 6, the $CM_{traffic\_Aeth}$ is extremely similar to that of the combination of AMS-PMF and SP2 attribution (r^2 = 0.90) even if the slight discrepancies denoted by $CM_{traffic\_offset}$ between the apportionment of the two methods occurred at certain times during the winter IOP. As to the attribution of the CM_{wb} showed at the bottom of Figure 6, the correlation between the results of two methods is not that high as $CM_{traffic}$ but still significant (r^2 =0.67). However, the differences denoted by CM_{wb_offset} between the apportionments of the two methods vary remarkably at several points in time series. Figure 7 illustrates diurnal variations of $CM_{traffic\_offset}$ and CM_{wb_offset}, and both the offsets are generally close to 0. It is interesting that there is variation of CM_{wb_offset} in time series, however there is no obvious diurnal pattern as shown in Figure 8. The discovery indicates that the contributions of wood burning sources in North Kensington during the winter IOP might be influenced by meteorological condition such as the wind direction, which is consistent with Liu et al. (2014).

To date, this is the first time to apply the Aethalometer model using the combination of OM and BC attributions from AMS-PMF and SP2. The derived C_1^* of 254,260, which is related to traffic source, is very close to those proposed by Favez et al. (2009, 2010) and Sandradewi

et al. (2008c) with the values of 264,895 and 258,831, respectively. However, the C_2^* of 338,740, which is associated with the emissions from solid fuel burning, is significantly lower than those with the values of 724,256 (Favez et al., 2009), ~630,000 (Sandradewi et al., 2008c) and ~670,000. In this study, the OM and BC contributed by the traffic and solid fuel burning has been pre-attributed by the AMS-PMF and SP2 methods rather than assuming total CM only contributed by both traffic and solid fuel burning, which means that the estimates of the solid fuel burning contribution to CM in the previous studies could be overestimated. In this case, approximately 38.6% of carbonaceous aerosols in PM_1 was contributed by the traffic source, while around 32.7% of those was attributed to solid fuel burning in London during wintertime in 2012.

Table 1. The linear regression equations of $CM_{traffic}$ and CM_{wb}.

Traffic-related	Wood burning
$CM_{traffic}\_SP2\_AMS = 254{,}260 * b_{abs,traffic,950nm}$	$CM_{wb}\_SP2\_AMS = 338{,}740 * b_{abs,wb,470nm}$
$CM_{traffic}\_Aeth = 344{,}850 * b_{abs,traffic,950nm}$	$CM_{wb}\_Aeth = 453080 * b_{abs,wb,470nm}$
$CM_{traffic}\_offset = CM_{traffic}\_SP2\_AMS - CM_{traffic}\_Aeth$	$CM_{wb}\_offset = CM_{wb}\_SP2\_AMS - CM_{wb}\_Aeth$

Note: $CM_{traffic}\_SP2\_AMS = HOA + BC_{tr}$

$CM_{wb}\_SP2\_AMS = SFOA1 + SFOA2 + BC_{wb}$

$CM_{total} = OM + BC = 344{,}850 * b_{abs,traffic,950nm} + 453{,}080 * b_{abs,wb,470nm} + 0.84$

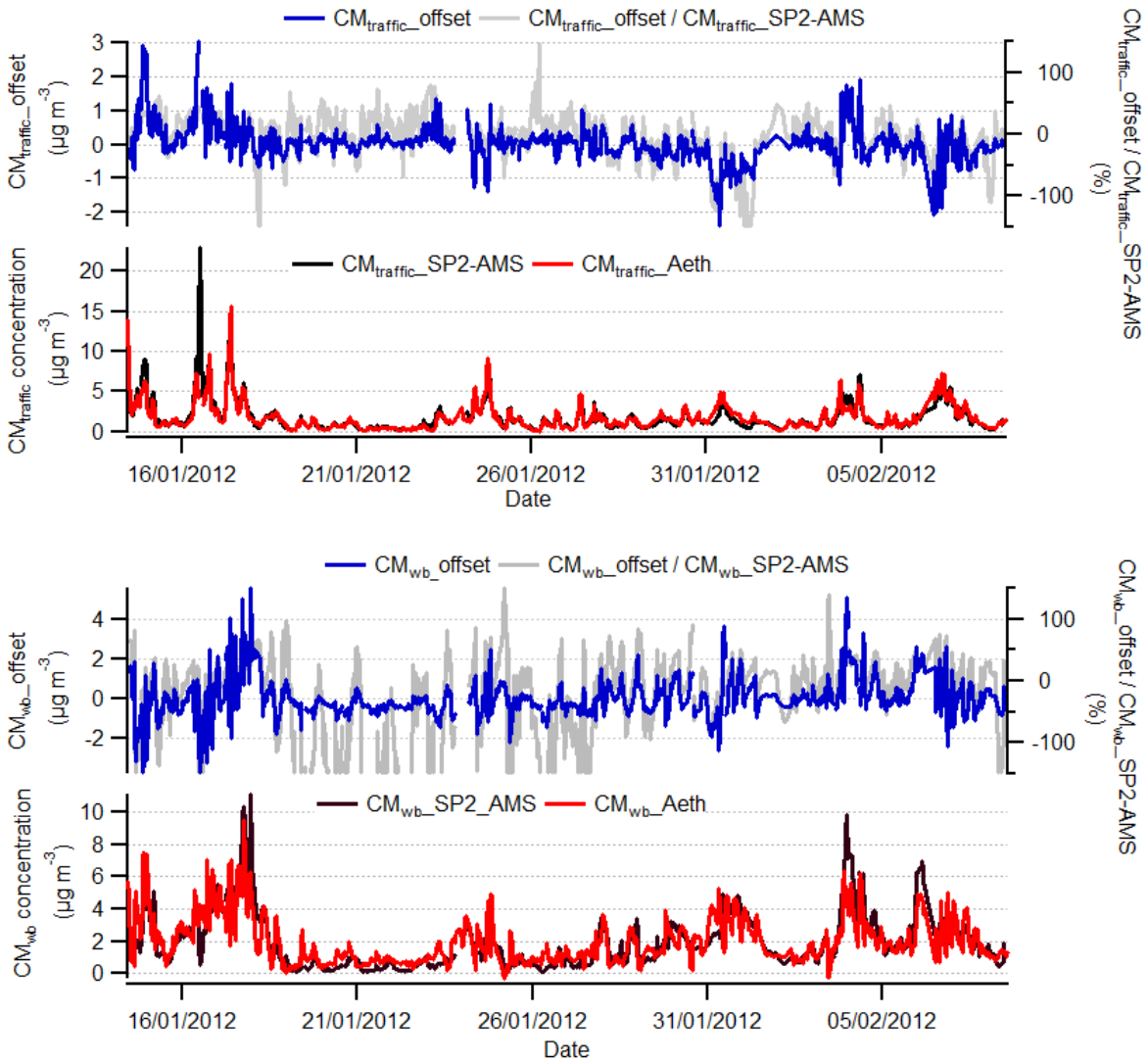

Figure 6. The differences of $CM_{traffic}$ and CM_{wb} between measured data and the estimates from Aethalometer model. $CM_{traffic}$_offset = $CM_{traffic}$_SP2_AMS - $CM_{traffic}$_Aeth; CM_{wb}_offset = CM_{wb}_SP2_AMS - CM_{wb}_Aeth. The percentage (%) represents that how much the offset accounts for in the measured

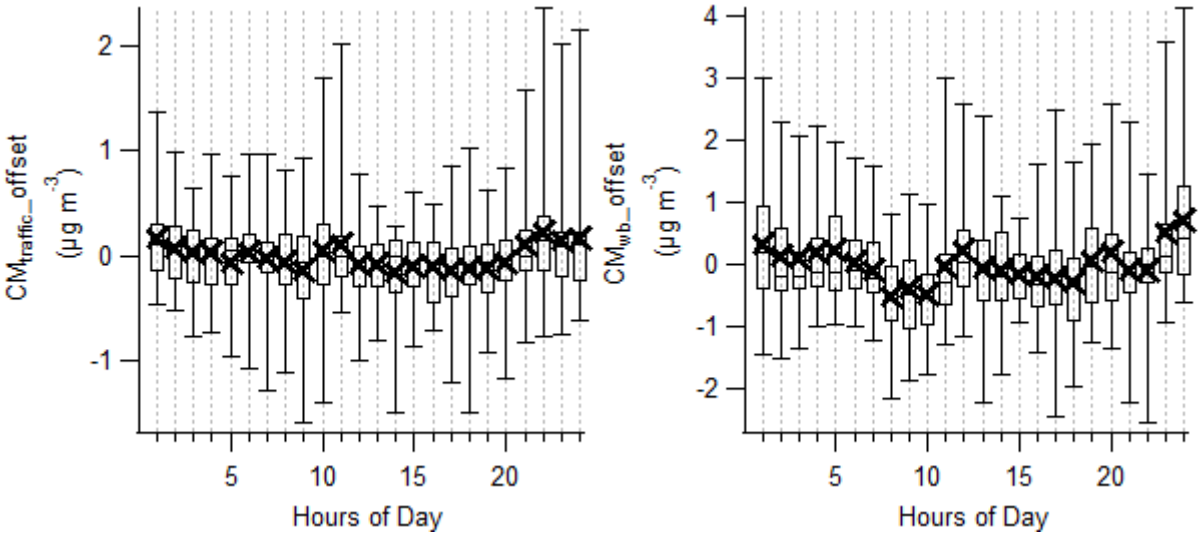

Figure 7. The diurnal variations of $CM_{traffic}$_offset and CM_{wb}_offset

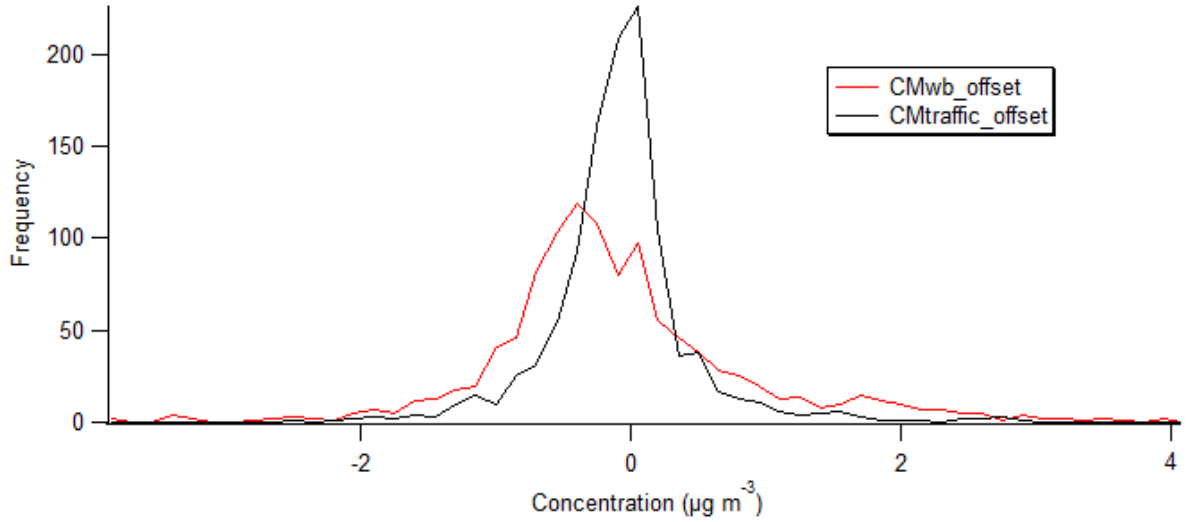

Figure 8. The frequencies of concentrations of $CM_{traffic}$_offset and CM_{wb}_offset in time series.

Relationship between the species from different source apportion methods

The average concentrations of trace elements from traffic emissions (TE_{tr}) and solid fuel combustion (TE_{sf}) during the winter intensive observation period were 28.80 and 32.89 ng m^{-3} derived from ME-2, respectively. The correlation between different compositions from traffic-related sources and solid fuel combustion derived from various source apportionment methods is shown in Table 2. The correlation between TE_{tr} and BC_{tr} is the highest (r^2 = 0.72) among the traffic-related emissions. Moreover, the correlation between TE_{sf} and BC_{wb} is also the highest (r^2 = 0.68) among the solid fuel combustion emissions. The reason for the results may be because trace elements and BC are both primary emissions and do not easily react with other substances. Organic matter derived from AMS-PMF, in contrast, has a lower

correlation with trace elements (0.32 for HOA and 0.20 for SFOA) as organic matter in the atmosphere is more varied and has the more complex mechanism of formation.

Table 2. The correlation between trace elements and BC and OM from different methods.

ME-2 / Others	Trace elements (TE_{tr})	ME-2 / Others	Trace elements (TE_{sf})
BCtr (SP2)	$r^2 = 0.72$	BCwb (SP2)	$r^2 = 0.68$
CMB_traffic	$r^2 = 0.55$	CMB_(WS+Coal)	$r^2 = 0.51$
HOA	$r^2 = 0.32$	SFOA	$r^2 = 0.20$
$CM_{traffic\_Aeth}$	$r^2 = 0.68$	CMwb_Aeth	$r^2 = 0.31$

Conclusion

The comprehensive suite of dataset used in this study was based on the ClearfLo project in 2012. The Aethalometer model was applied to quantify the CM from traffic and solid fuel sources during wintertime, using the aerosol light absorption coefficients at different wavelengths measured by Aethalometer accompanied with the two on-line measurements by AMS-PMF and SP2 in a London urban background site in 2012. In the comparison between the contributions of BC sources, the BC_{tra_SP2} agrees well with BC_{tra_Aeth}, whereas BC_{wb_Aeth} is less than BC_{wb_SP2} with increasing OOA and the solid fuel combustion emissions (coal and wood smoke). The results imply that the higher OOA, coal and wood burning emissions have an impact on the absorption of the BC associated with the solid fuel combustion (Saleh et al., 2013) by the Aethalometer model. On the other hand, lower α_{wb} would be expected according to the emissions of solid fuel burning coming from different air masses, indicating that solid fuel burning with different burning conditions, fuel types or other non-traffic sources could also affect the estimates of the contribution of the BC solid fuel sources (Liu et al., 2014)

The derived parameter for the estimates of the $CM_{traffic}$ with the pre-attributed AMS-PMF and SP2 data is consistent with those of the previous studies, whereas the parameter derived from the CM_{wb}^{*} indicates that an overestimation can be expected compared to the parameters

derived from the poly-linear regression using unapportioned data as the OM in CM_{total} comprises not only HOA and SFOA but also COA and OOA, which may lead to the attribution of the unassociated solid fuel burning emissions to the solid fuel burning emissions. The results in this study shows that the traffic and solid fuel burning accounted for approximately 71.3% (38.6% from traffic and 32.7% from solid fuel burning) of carbonaceous aerosols in PM_1, which meant that there were still about 30% of them contributed by the other sources, e.g. cooking and OOA. It is helpful and useful with the parameters derived in this study that the more accurate estimates of the contribution from the combustion sources can underpin the mitigation strategy in the future, although more work in different regions is still needed to further investigate the complex non-traffic sources and to obtain the appropriate α_{wb} and the parameters for the more reliable outputs from the Aethalometer model.

List of acronyms

BC_{wb}: the contribution of the wood burning to the BC.

BC_{wb_SP2}: the contribution of the wood burning to the BC apportioned by SP2 (BC_{wb_SP2}) according to the coating thickness and core size.

BC_{wb_Aeth}: the contribution of the wood burning to the BC apportioned by the Aethalometer model

OOA: oxygenated organic aerosols.

α_{wb}: absorption Angstrom exponent for traffic-related emissions.

α_{wb}: absorption Angstrom exponent for wood burning.

CM_{wb}: carbonaceous matter contributed by wood burning.

BC_{tra}: BC particles dominated by the traffic source.

BC_{sf}: BC particles dominated by solid fuel burning, same as wood burning in this study.

AMS-PMF: Aerosol Mass Spectrometer Positive Matrix Factorisation.

SFOA1: OM contributed by more efficient solid fuel combustion.

SFOA2: OM contributed by less efficient solid fuel combustion.

$SFOA_{total}$: OM contributed by solid fuel combustion attributed by AMS-PMF, e.g. $SFOA_{total}$ = SFOA1 + SFOA2

References

ALLAN, J. D., WILLIAMS, P. I., MORGAN, W. T., MARTIN, C. L., FLYNN, M. J., LEE, J., NEMITZ, E., PHILLIPS, G. J., GALLAGHER, M. W. & COE, H. 2010. Contributions from transport, solid fuel burning and cooking to primary organic aerosols in two UK cities. *Atmos. Chem. Phys.,* 10**,** 647-668.

BAUMGARDNER, D., POPOVICHEVA, O., ALLAN, J., BERNARDONI, V., CAO, J., CAVALLI, F., COZIC, J., DIAPOULI, E., ELEFTHERIADIS, K., GENBERG, P. J., GONZALEZ, C., GYSEL, M., JOHN, A., KIRCHSTETTER, T. W., KUHLBUSCH, T. A. J., LABORDE, M., LACK, D., MULLER, T., NIESSNER, R., PETZOLD, A., PIAZZALUNGA, A., PUTAUD, J. P., SCHWARZ, J., SHERIDAN, P., SUBRAMANIAN, R., SWIETLICKI, E., VALLI, G., VECCHI, R. & VIANA, M. 2012. Soot reference materials for instrument calibration and intercomparisons: a workshop summary with recommendations. *Atmos. Meas. Tech.,* 5**,** 1869- 1887.

BOHNENSTENGEL, S., BELCHER, S., AIKEN, A., ALLAN, J., ALLEN, G., BACAK, A., BANNAN, T., BARLOW, J., BEDDOWS, D. & BLOSS, W. 2015. Meteorology, air quality, and health in London: The ClearfLo project. *Bulletin of the American Meteorological Society,* 96**,** 779-804.

BOND, T. C. & BERGSTROM, R. W. 2006a. Light Absorption by Carbonaceous Particles: An Investigative Review. *Aerosol Sci. Technol.,* 40**,** 27-67.

BOND, T. C. & BERGSTROM, R. W. 2006b. Light Absorption by Carbonaceous Particles: An Investigative Review. *Aerosol Science and Technology,* 40**,** 27-67.

BOND, T. C., DOHERTY, S. J., FAHEY, D., FORSTER, P., BERNTSEN, T., DEANGELO, B., FLANNER, M., GHAN, S., KÄRCHER, B. & KOCH, D. 2013a. Bounding the role of black carbon in the climate system: A scientific assessment. *J. Geophys. Res.,* 118**,** 5380-5552.

BOND, T. C., DOHERTY, S. J., FAHEY, D., FORSTER, P., BERNTSEN, T., DEANGELO, B., FLANNER, M., GHAN, S., KÄRCHER, B. & KOCH, D. 2013b. Bounding the role of black carbon in the climate system: A scientific assessment. *Journal of Geophysical Research: Atmospheres,* 118**,** 5380-5552.

BOND, T. C., STREETS, D. G., YARBER, K. F., NELSON, S. M., WOO, J. H. & KLIMONT, Z. 2004. A technology-based global inventory of black and organic carbon emissions from combustion. *J. Geophys. Res.,* 109.

BUKOWIECKI, N., LIENEMANN, P., HILL, M., FIGI, R., RICHARD, A., FURGER, M., RICKERS, K., FALKENBERG, G., ZHAO, Y. & CLIFF, S. S. 2009a. Real-world emission factors for antimony and other brake wear related trace elements: size-segregated values for light and heavy duty vehicles. *Environmental science & technology,* 43**,** 8072-8078.

BUKOWIECKI, N., RICHARD, A., FURGER, M., WEINGARTNER, E., AGUIRRE, M., HUTHWELKER, T., LIENEMANN, P., GEHRIG, R. & BALTENSPERGER, U. 2009b. Deposition Uniformity and Particle Size Distribution of Ambient Aerosol Collected with a Rotating Drum Impactor. *Aerosol Science and Technology,* 43**,** 891-901.

BUTT, E. W., RAP, A., SCHMIDT, A., SCOTT, C. E., PRINGLE, K. J., REDDINGTON, C. L., RICHARDS, N. A. D., WOODHOUSE, M. T., RAMIREZ-VILLEGAS, J., YANG, H., VAKKARI, V., STONE, E. A., RUPAKHETI, M., S. PRAVEEN, P., G. VAN ZYL, P., P. BEUKES, J., JOSIPOVIC, M., MITCHELL, E. J. S., SALLU, S. M., FORSTER, P. M. & SPRACKLEN, D. V. 2016. The impact of residential combustion emissions on atmospheric aerosol, human health, and climate. *Atmos. Chem. Phys.,* 16**,** 873-905.

BUTTERFIELD, D., BECCACECI, S., QUINCEY, P., SWEENEY, B., WHITESIDE, K., FULLER, G., GREEN, D. & GRIEVE, A. 2016. 2014 Annual Report for the UK Black Carbon Network.

CANONACO, F., CRIPPA, M., SLOWIK, J. G., BALTENSPERGER, U. & PREVOT, A. S. H. 2013. SoFi, an IGOR-based interface for the efficient use of the generalized multilinear engine (ME-2) for the source apportionment: ME-2 application to aerosol mass spectrometer data. *Atmospheric Measurement Techniques,* 6**,** 3649-3661.

COLLAUD COEN, M., WEINGARTNER, E., APITULEY, A., CEBURNIS, D., FIERZ-SCHMIDHAUSER, R., FLENTJE, H., HENZING, J., JENNINGS, S. G., MOERMAN, M. & PETZOLD, A. 2010. Minimizing light absorption measurement artifacts of the Aethalometer: evaluation of five correction algorithms. *Atmospheric Measurement Techniques,* 3**,** 457-474.

CRILLEY, L. R., BLOSS, W. J., YIN, J., BEDDOWS, D. C. S., HARRISON, R. M., ALLAN, J. D., YOUNG, D. E., FLYNN, M., WILLIAMS, P., ZOTTER, P., H. PREVOT, A. S., HEAL, M. R., BARLOW, J. F., HALIOS, C. H., LEE, J. D., SZIDAT, S. & MOHR, C. 2014. Sources and contributions of wood smoke during winter in London: assessing local and regional influences. *Atmos. Chem. Phys. Discuss.,* 14**,** 27459-27530.

CRILLEY, L. R., BLOSS, W. J., YIN, J., BEDDOWS, D. C. S., HARRISON, R. M., ALLAN, J. D., YOUNG, D. E., FLYNN, M., WILLIAMS, P., ZOTTER, P., PREVOT, A. S. H., HEAL, M. R., BARLOW, J. F., HALIOS, C. H., LEE, J. D., SZIDAT, S. & MOHR, C. 2015. Sources and contributions of wood smoke during winter in London: assessing local and regional influences. *Atmos. Chem. Phys.,* 15**,** 3149-3171.

CRIPPA, M., DECARLO, P. F., SLOWIK, J. G., MOHR, C., HERINGA, M. F., CHIRICO, R., POULAIN, L., FREUTEL, F., SCIARE, J., COZIC, J., DI MARCO, C. F., ELSASSER, M., NICOLAS, J. B., MARCHAND, N., ABIDI, E., WIEDENSOHLER, A., DREWNICK, F., SCHNEIDER, J., BORRMANN, S., NEMITZ, E., ZIMMERMANN, R., JAFFREZO, J. L., PRÉVÔT, A. S. H. & BALTENSPERGER, U. 2013. Wintertime aerosol chemical composition and source apportionment of the organic fraction in the metropolitan area of Paris. *Atmos. Chem. Phys.,* 13**,** 961-981.

ERVENS, B., TURPIN, B. J. & WEBER, R. 2011. Secondary organic aerosol formation in cloud droplets and aqueous particles (aqSOA): a review of laboratory, field and model studies. *Atmospheric Chemistry and Physics,* 11**,** 11069-11102.

FAVEZ, O., CACHIER, H., SCIARE, J., SARDA-ESTÈVE, R. & MARTINON, L. 2009. Evidence for a significant contribution of wood burning aerosols to PM2.5 during the winter season in Paris, France. *Atmospheric Environment,* 43**,** 3640-3644.

FAVEZ, O., EL HADDAD, I., PIOT, C., BOREAVE, A., ABIDI, E., MARCHAND, N., JAFFREZO, J. L., BESOMBES, J. L., PERSONNAZ, M. B., SCIARE, J., WORTHAM, H., GEORGE, C. & D'ANNA, B. 2010. Inter-comparison of source apportionment models for the estimation of wood burning aerosols during wintertime in an Alpine city (Grenoble, France). *Atmospheric Chemistry and Physics,* 10**,** 5295-5314.

FINE, P. M., CASS, G. R. & SIMONEIT, B. R. 2004. Chemical characterization of fine particle emissions from the fireplace combustion of wood types grown in the Midwestern and Western United States. *Environmental Engineering Science,* 21**,** 387-409.

FLECHSIG, U., JAGGI, A., SPIELMANN, S., PADMORE, H. & MACDOWELL, A. 2009a. The optics beamline at the Swiss Light Source. *Nuclear Instruments and Methods in Physics Research Section A: Accelerators, Spectrometers, Detectors and Associated Equipment,* 609**,** 281-285.

FLECHSIG, U., JAGGI, A., SPIELMANN, S., PADMORE, H. A. & MACDOWELL, A. A. 2009b. The optics beamline at the Swiss Light Source. *Nuclear Instruments and Methods in Physics Research Section A: Accelerators, Spectrometers, Detectors and Associated Equipment,* 609**,** 281-285.

GAO, R. S., SCHWARZ, J. P., KELLY, K. K., FAHEY, D. W., WATTS, L. A., THOMPSON, T. L., SPACKMAN, J. R., SLOWIK, J. G., CROSS, E. S., HAN, J. H., DAVIDOVITS, P., ONASCH, T. B. & WORSNOP, D. R. 2007. A Novel Method for Estimating Light-Scattering Properties of Soot Aerosols Using a Modified Single-Particle Soot Photometer. *Aerosol Science and Technology,* 41**,** 125-135.

GARG, S., CHANDRA, B. P., SINHA, V., SARDA-ESTEVE, R., GROS, V. & SINHA, B. 2016. Limitation of the Use of the Absorption Angstrom Exponent for Source Apportionment of Equivalent Black Carbon: a Case Study from the North West Indo-Gangetic Plain. *Environmental Science & Technology,* 50**,** 814-824.

GRAHAME, T. J., KLEMM, R. & SCHLESINGER, R. B. 2014. Public health and components of particulate matter: The changing assessment of black carbon. *Journal of the Air & Waste Management Association,* 64**,** 620-660.

HANSEN, A. D. A., ROSEN, H. & NOVAKOV, T. 1984. The aethalometer — An instrument for the real-time measurement of optical absorption by aerosol particles. *Science of The Total Environment,* 36**,** 191-196.

HARRISON, R. M., BEDDOWS, D. C. S., HU, L. & YIN, J. 2012. Comparison of methods for evaluation of wood smoke and estimation of UK ambient concentrations. *Atmos. Chem. Phys.,* 12**,** 8271-8283.

HARRISON, R. M., BEDDOWS, D. C. S., JONES, A. M., CALVO, A., ALVES, C. & PIO, C. 2013. An evaluation of some issues regarding the use of aethalometers to measure woodsmoke concentrations. *Atmospheric Environment,* 80**,** 540-548.

HYVÄRINEN, A. P., KOLMONEN, P., KERMINEN, V. M., VIRKKULA, A., LESKINEN, A., KOMPPULA, M., HATAKKA, J., BURKHART, J., STOHL, A., AALTO, P., KULMALA, M., LEHTINEN, K. E. J., VIISANEN, Y. & LIHAVAINEN, H. 2011. Aerosol black carbon at five background measurement sites over Finland, a gateway to the Arctic. *Atmospheric Environment,* 45**,** 4042-4050.

JANSSEN, N., GERLOFS-NIJLAND, M., LANKI, T., SALONEN, R., CASSEE, F., HOEK, G., FISCHER, P., BRUNEKREEF, B. & KRZYZANOWSKI, M. 2012. Health effects of black carbon, The WHO European Centre for Environment and Health, Bonn, Germany. *World Health Organisation Regional Office for Europe, Copenhagen, Denmark*.

KIRCHSTETTER, T. W., NOVAKOV, T. & HOBBS, P. V. 2004. Evidence that the spectral dependence of light absorption by aerosols is affected by organic carbon. *Journal of Geophysical Research: Atmospheres (1984–2012),* 109.

LABORDE, M., SCHNAITER, M., LINKE, C., SAATHOFF, H., NAUMANN, K. H., MÖHLER, O., BERLENZ, S., WAGNER, U., TAYLOR, J. W., LIU, D., FLYNN, M., ALLAN, J. D., COE, H., HEIMERL, K., DAHLKÖTTER, F., WEINZIERL, B., WOLLNY, A. G., ZANATTA, M., COZIC, J., LAJ, P., HITZENBERGER, R., SCHWARZ, J. P. & GYSEL, M. 2012. Single Particle Soot Photometer intercomparison at the AIDA chamber. *Atmos. Meas. Tech.,* 5**,** 3077-3097.

LANZ, V. A., ALFARRA, M. R., BALTENSPERGER, U., BUCHMANN, B., HUEGLIN, C., SZIDAT, S., WEHRLI, M. N., WACKER, L., WEIMER, S., CASEIRO, A., PUXBAUM, H. & PREVOT, A. S. H. 2008. Source Attribution of Submicron Organic Aerosols during Wintertime Inversions by Advanced Factor Analysis of Aerosol Mass Spectra. *Environmental Science & Technology,* 42**,** 214-220.

LEWIS, K., ARNOTT, W. P., MOOSMÜLLER, H. & WOLD, C. E. 2008. Strong spectral variation of biomass smoke light absorption and single scattering albedo observed with a novel dual-wavelength photoacoustic instrument. *Journal of Geophysical Research: Atmospheres (1984–2012),* 113.

LIM, S. S., VOS, T., FLAXMAN, A. D., DANAEI, G., SHIBUYA, K., ADAIR-ROHANI, H., ALMAZROA, M. A., AMANN, M., ANDERSON, H. R., ANDREWS, K. G., ARYEE, M., ATKINSON, C., BACCHUS, L. J., BAHALIM, A. N., BALAKRISHNAN, K., BALMES, J., BARKER-COLLO, S., BAXTER, A., BELL, M. L., BLORE, J. D., BLYTH, F., BONNER, C., BORGES, G., BOURNE, R., BOUSSINESQ, M., BRAUER, M., BROOKS, P., BRUCE, N. G., BRUNEKREEF, B., BRYAN-HANCOCK, C., BUCELLO, C., BUCHBINDER, R., BULL, F., BURNETT, R. T., BYERS, T. E., CALABRIA, B., CARAPETIS, J., CARNAHAN, E., CHAFE, Z., CHARLSON, F., CHEN, H., CHEN, J. S., CHENG, A. T.-A., CHILD, J. C., COHEN, A., COLSON, K. E., COWIE, B. C., DARBY, S., DARLING, S., DAVIS, A., DEGENHARDT, L., DENTENER, F., DES JARLAIS, D. C., DEVRIES, K., DHERANI, M., DING, E. L., DORSEY, E. R., DRISCOLL, T., EDMOND, K., ALI, S. E., ENGELL, R. E., ERWIN, P. J., FAHIMI, S., FALDER, G., FARZADFAR, F., FERRARI, A., FINUCANE, M. M., FLAXMAN, S., FOWKES, F. G. R., FREEDMAN, G., FREEMAN, M. K., GAKIDOU, E., GHOSH, S., GIOVANNUCCI, E., GMEL, G., GRAHAM, K., GRAINGER, R., GRANT, B., GUNNELL, D., GUTIERREZ, H. R., HALL, W., HOEK, H. W., HOGAN, A., HOSGOOD, H. D., III, HOY, D., HU, H., HUBBELL, B. J., HUTCHINGS, S. J., IBEANUSI, S. E.,

JACKLYN, G. L., JASRASARIA, R., JONAS, J. B., KAN, H., KANIS, J. A., KASSEBAUM, N., KAWAKAMI, N., KHANG, Y.-H., KHATIBZADEH, S., KHOO, J.-P., KOK, C., et al. 2012. A comparative risk assessment of burden of disease and injury attributable to 67 risk factors and risk factor clusters in 21 regions, 1990–2010: a systematic analysis for the Global Burden of Disease Study 2010. *The Lancet,* 380**,** 2224-2260.

LIU, D., ALLAN, J. D., YOUNG, D. E., COE, H., BEDDOWS, D., FLEMING, Z. L., FLYNN, M. J., GALLAGHER, M. W., HARRISON, R. M., LEE, J., PREVOT, A. S. H., TAYLOR, J. W., YIN, J., WILLIAMS, P. I. & ZOTTER, P. 2014. Size distribution, mixing state and source apportionment of black carbon aerosol in London during wintertime. *Atmos. Chem. Phys.,* 14**,** 10061-10084.

LIU, D., FLYNN, M., GYSEL, M., TARGINO, A., CRAWFORD, I., BOWER, K., CHOULARTON, T., JURÁNYI, Z., STEINBACHER, M., HÜGLIN, C., CURTIUS, J., KAMPUS, M., PETZOLD, A., WEINGARTNER, E., BALTENSPERGER, U. & COE, H. 2010. Single particle characterization of black carbon aerosols at a tropospheric alpine site in Switzerland. *Atmos. Chem. Phys.,* 10**,** 7389-7407.

MCMEEKING, G. R., HAMBURGER, T., LIU, D., FLYNN, M., MORGAN, W. T., NORTHWAY, M., HIGHWOOD, E. J., KREJCI, R., ALLAN, J. D., MINIKIN, A. & COE, H. 2010. Black carbon measurements in the boundary layer over western and northern Europe. *Atmos. Chem. Phys.,* 10**,** 9393-9414.

MONKS, P. S., GRANIER, C., FUZZI, S., STOHL, A., WILLIAMS, M. L., AKIMOTO, H., AMANN, M., BAKLANOV, A., BALTENSPERGER, U., BEY, I., BLAKE, N., BLAKE, R. S., CARSLAW, K., COOPER, O. R., DENTENER, F., FOWLER, D., FRAGKOU, E., FROST, G. J., GENEROSO, S., GINOUX, P., GREWE, V., GUENTHER, A., HANSSON, H. C., HENNE, S., HJORTH, J., HOFZUMAHAUS, A., HUNTRIESER, H., ISAKSEN, I. S. A., JENKIN, M. E., KAISER, J., KANAKIDOU, M., KLIMONT, Z., KULMALA, M., LAJ, P., LAWRENCE, M. G., LEE, J. D., LIOUSSE, C., MAIONE, M., MCFIGGANS, G., METZGER, A., MIEVILLE, A., MOUSSIOPOULOS, N., ORLANDO, J. J., O'DOWD, C. D., PALMER, P. I., PARRISH, D. D., PETZOLD, A., PLATT, U., PÖSCHL, U., PRÉVÔT, A. S. H., REEVES, C. E., REIMANN, S., RUDICH, Y., SELLEGRI, K., STEINBRECHER, R., SIMPSON, D., TEN BRINK, H., THELOKE, J., VAN DER WERF, G. R., VAUTARD, R., VESTRENG, V., VLACHOKOSTAS, C. & VON GLASOW, R. 2009. Atmospheric composition change – global and regional air quality. *Atmospheric Environment,* 43**,** 5268-5350.

MOTEKI, N., KONDO, Y. & NAKAMURA, S.-I. 2010. Method to measure refractive indices of small nonspherical particles: Application to black carbon particles. *J. Aerosol Sci.,* 41**,** 513-521.

PAATERO, P. 1999. The Multilinear Engine—A Table-Driven, Least Squares Program for Solving Multilinear Problems, Including the n-Way Parallel Factor Analysis Model. *Journal of Computational and Graphical Statistics,* 8**,** 854-888.

PANT, P., YIN, J. & HARRISON, R. M. 2014. Sensitivity of a Chemical Mass Balance model to different molecular marker traffic source profiles. *Atmospheric environment,* 82**,** 238-249.

PATRÓN, D., LYAMANI, H., TITOS, G., CASQUERO-VERA, J. A., CARDELL, C., MOČNIK, G., ALADOS-ARBOLEDAS, L. & OLMO, F. J. 2017. Monumental heritage exposure to urban black carbon pollution. *Atmospheric Environment,* 170**,** 22-32.

PETZOLD, A., OGREN, J. A., FIEBIG, M., LAJ, P., LI, S. M., BALTENSPERGER, U., HOLZER-POPP, T., KINNE, S., PAPPALARDO, G., SUGIMOTO, N., WEHRLI, C., WIEDENSOHLER, A. & ZHANG, X. Y. 2013. Recommendations for reporting "black carbon" measurements. *Atmos. Chem. Phys.,* 13**,** 8365-8379.

RAMANA, M. V., RAMANATHAN, V., FENG, Y., YOON, S. C., KIM, S. W., CARMICHAEL, G. R. & SCHAUER, J. J. 2010. Warming influenced by the ratio of black carbon to sulphate and the black-carbon source. *Nature Geosci,* 3**,** 542-545.

RAMANATHAN, V. & CARMICHAEL, G. 2008. Global and regional climate changes due to black carbon. *Nature geoscience,* 1**,** 221.

ROGGE, W. F., HILDEMANN, L. M., MAZUREK, M. A., CASS, G. R. & SIMONEIT, B. R. 1993a. Sources of fine organic aerosol. 4. Particulate abrasion products from leaf surfaces of urban plants. *Environmental Science & Technology,* 27**,** 2700-2711.

ROGGE, W. F., HILDEMANN, L. M., MAZUREK, M. A., CASS, G. R. & SIMONEIT, B. R. 1993b. Sources of fine organic aerosol. 5. Natural gas home appliances. *Environmental Science & Technology,* 27**,** 2736-2744.

SALEH, R., HENNIGAN, C. J., MCMEEKING, G. R., CHUANG, W. K., ROBINSON, E. S., COE, H., DONAHUE, N. M. & ROBINSON, A. L. 2013. Absorptivity of brown carbon in fresh and photo-chemically aged biomass-burning emissions. *Atmos. Chem. Phys.,* 13**,** 7683-7693.

SANDRADEWI, J., PRÉVÔT, A. S. H., ALFARRA, M. R., SZIDAT, S., WEHRLI, M. N., RUFF, M., WEIMER, S., LANZ, V. A., WEINGARTNER, E., PERRON, N., CASEIRO, A., KASPER-GIEBL, A., PUXBAUM, H., WACKER, L. & BALTENSPERGER, U. 2008c. Comparison of several wood smoke markers and source apportionment methods for wood burning particulate mass. *Atmos. Chem. Phys. Discuss.,* 8**,** 8091-8118.

SANDRADEWI, J., PRÉVÔT, A. S. H., SZIDAT, S., PERRON, N., ALFARRA, M. R., LANZ, V. A., WEINGARTNER, E. & BALTENSPERGER, U. 2008b. Using Aerosol Light Absorption Measurements for the Quantitative Determination of Wood Burning and Traffic Emission Contributions to Particulate Matter. *Environmental Science & Technology,* 42**,** 3316-3323.

SCHAUER, J. J. 1998. *Source contributions to atmospheric organic compound concentrations: emissions measurements and model predictions.* California Institute of Technology.

SCHWARZ, J., GAO, R., FAHEY, D., THOMSON, D., WATTS, L., WILSON, J., REEVES, J., DARBEHESHTI, M., BAUMGARDNER, D. & KOK, G. 2006. Single-particle measurements of midlatitude black carbon and light-scattering aerosols from the boundary layer to the lower stratosphere. *Journal of Geophysical Research: Atmospheres (1984–2012),* 111.

SUN, Y. L., ZHANG, Q., SCHWAB, J. J., DEMERJIAN, K. L., CHEN, W. N., BAE, M. S., HUNG, H. M., HOGREFE, O., FRANK, B., RATTIGAN, O. V. & LIN, Y. C. 2011. Characterization of the sources and processes of organic and inorganic aerosols in New York city with a high-resolution time-of-flight aerosol mass apectrometer. *Atmos. Chem. Phys.,* 11**,** 1581-1602.

TAYLOR, J., ALLAN, J., LIU, D., FLYNN, M., WEBER, R., ZHANG, X., LEFER, B., GROSSBERG, N., FLYNN, J. & COE, H. 2015. Assessment of the sensitivity of core/shell parameters derived using the single-particle soot photometer to density and refractive index. *Atmos. Meas. Tech.,* 8**,** 1701-1718.

ULBRICH, I. M., CANAGARATNA, M. R., ZHANG, Q., WORSNOP, D. R. & JIMENEZ, J. L. 2009. Interpretation of organic components from Positive Matrix Factorization of aerosol mass spectrometric data. *Atmospheric Chemistry and Physics,* 9**,** 2891-2918.

VISSER, S., SLOWIK, J. G., FURGER, M., ZOTTER, P., BUKOWIECKI, N., CANONACO, F., FLECHSIG, U., APPEL, K., GREEN, D. C., TREMPER, A. H., YOUNG, D. E., WILLIAMS, P. I., ALLAN, J. D., COE, H., WILLIAMS, L. R., MOHR, C., XU, L., NG, N. L., NEMITZ, E., BARLOW, J. F., HALIOS, C. H., FLEMING, Z. L., BALTENSPERGER, U. & PRÉVÔT, A. S. H. 2015a. Advanced source apportionment of size-resolved trace elements at multiple sites in London during winter. *Atmos. Chem. Phys. Discuss.,* 15**,** 14733-14781.

VISSER, S., SLOWIK, J. G., FURGER, M., ZOTTER, P., BUKOWIECKI, N., DRESSLER, R., FLECHSIG, U., APPEL, K., GREEN, D. C., TREMPER, A. H., YOUNG, D. E., WILLIAMS, P. I., ALLAN, J. D., HERNDON, S. C., WILLIAMS, L. R., MOHR, C., XU, L., NG, N. L., DETOURNAY, A., BARLOW, J. F., HALIOS, C. H., FLEMING, Z. L., BALTENSPERGER, U. & PRÉVÔT, A. S. H. 2014. Kerb and urban increment of highly time-resolved trace elements in PM10, PM2.5 and PM1.0 winter aerosol in London during ClearfLo 2012. *Atmos. Chem. Phys. Discuss.,* 14**,** 15895-15951.

VISSER, S., SLOWIK, J. G., FURGER, M., ZOTTER, P., BUKOWIECKI, N., DRESSLER, R., FLECHSIG, U., APPEL, K., GREEN, D. C., TREMPER, A. H., YOUNG, D. E., WILLIAMS, P. I., ALLAN, J. D., HERNDON, S. C., WILLIAMS, L. R., MOHR, C., XU, L., NG, N. L., DETOURNAY, A., BARLOW, J. F.,

HALIOS, C. H., FLEMING, Z. L., BALTENSPERGER, U. & PRÉVÔT, A. S. H. 2015b. Kerb and urban increment of highly time-resolved trace elements in PM10, PM2.5 and PM1.0 winter aerosol in London during ClearfLo 2012. *Atmos. Chem. Phys.,* 15**,** 2367-2386.

WAGENER, S., LANGNER, M., HANSEN, U., MORISKE, H.-J. & ENDLICHER, W. R. 2012a. Source apportionment of organic compounds in Berlin using positive matrix factorization—Assessing the impact of biogenic aerosol and biomass burning on urban particulate matter. *Science of the Total Environment,* 435**,** 392-401.

WAGENER, S., LANGNER, M., HANSEN, U., MORISKE, H.-J. & ENDLICHER, W. R. 2012b. Spatial and seasonal variations of biogenic tracer compounds in ambient PM10 and PM1 samples in Berlin, Germany. *Atmospheric environment,* 47**,** 33-42.

WANG, Q., SCHWARZ, J. P., CAO, J., GAO, R., FAHEY, D. W., HU, T., HUANG, R. J., HAN, Y. & SHEN, Z. 2014. Black carbon aerosol characterization in a remote area of Qinghai–Tibetan Plateau, western China. *Science of The Total Environment,* 479–480**,** 151-158.

WASHENFELDER, R., ATTWOOD, A., BROCK, C., GUO, H., XU, L., WEBER, R., NG, N., ALLEN, H., AYRES, B. & BAUMANN, K. 2015. Biomass burning dominates brown carbon absorption in the rural southeastern United States. *Geophysical Research Letters,* 42**,** 653-664.

WEINGARTNER, E., SAATHOFF, H., SCHNAITER, M., STREIT, N., BITNAR, B. & BALTENSPERGER, U. 2003. Absorption of light by soot particles: determination of the absorption coefficient by means of aethalometers. *Journal of Aerosol Science,* 34**,** 1445-1463.

YIN, J., CUMBERLAND, S. A., HARRISON, R. M., ALLAN, J., YOUNG, D. E., WILLIAMS, P. I. & COE, H. 2015. Receptor modelling of fine particles in southern England using CMB including comparison with AMS-PMF factors. *Atmos. Chem. Phys.,* 15**,** 2139-2158.

YIN, J., HARRISON, R. M., CHEN, Q., RUTTER, A. & SCHAUER, J. J. 2010. Source apportionment of fine particles at urban background and rural sites in the UK atmosphere. *Atmospheric Environment,* 44**,** 841-851.

YOUNG, D., ALLAN, J., WILLIAMS, P., GREEN, D., FLYNN, M., HARRISON, R., YIN, J., GALLAGHER, M. & COE, H. 2015. Investigating the annual behaviour of submicron secondary inorganic and organic aerosols in London. *Atmospheric Chemistry and Physics,* 15**,** 6351-6366.

YOUNG, D. E., ALLAN, J. D., WILLIAMS, P. I., GREEN, D. C., FLYNN, M. J., HARRISON, R. M., YIN, J., GALLAGHER, M. W. & COE, H. 2014. Investigating the annual behaviour of submicron secondary inorganic and organic aerosols in London. *Atmos. Chem. Phys. Discuss.,* 14**,** 18739-18784.

YUE, Z. & FRASER, M. P. 2004. Polar organic compounds measured in fine particulate matter during TexAQS 2000. *Atmospheric Environment,* 38**,** 3253-3261.

ZHANG, Y., SCHAUER, J. J., ZHANG, Y., ZENG, L., WEI, Y., LIU, Y. & SHAO, M. 2008. Characteristics of particulate carbon emissions from real-world Chinese coal combustion. *Environmental science & technology,* 42**,** 5068-5073.

ZHAO, Y., HU, M., SLANINA, S. & ZHANG, Y. 2007. Chemical compositions of fine particulate organic matter emitted from Chinese cooking. *Environmental science & technology,* 41**,** 99-105.

ZOTTER, P., HERICH, H., GYSEL, M., EL-HADDAD, I., ZHANG, Y., MOČNIK, G., HÜGLIN, C., BALTENSPERGER, U., SZIDAT, S. & PRÉVÔT, A. S. 2017. Evaluation of the absorption Ångström exponents for traffic and wood burning in the Aethalometer-based source apportionment using radiocarbon measurements of ambient aerosol. *Atmospheric chemistry and physics,* 17**,** 4229-4249.

SUPPORTING INFORMATION

Intercomparison of different analysis approaches of source apportionment for wood burning aerosols in London.

Y. Ting[1], D. Liu[1], J. D. Allan[1], D. E. Young[3], J. Yin[4], P. Zotter[5], S. Visser[5], A. S. H. Prevot[5], H. Coe[1]

1. School of Earth and Environmental Sciences, University of Manchester, Manchester M13 9PL, UK

2. National Centre for Atmospheric Science, University of Manchester, Manchester M13 9PL, UK

3. Department of Environmental Toxicology, University of California, Davis, CA 95616, USA

4. Division of Environmental Health and Risk Management, School of Geography, Earth and Environmental Sciences, University of Birmingham, Edgbaston, Birmingham B15 2TT, UK

5. Laboratory of Atmospheric Chemistry, Paul Scherrer Institute, Villigen, Switzerland

Correspondence: Hugh Coe (hugh.coe@manchester.ac.uk)

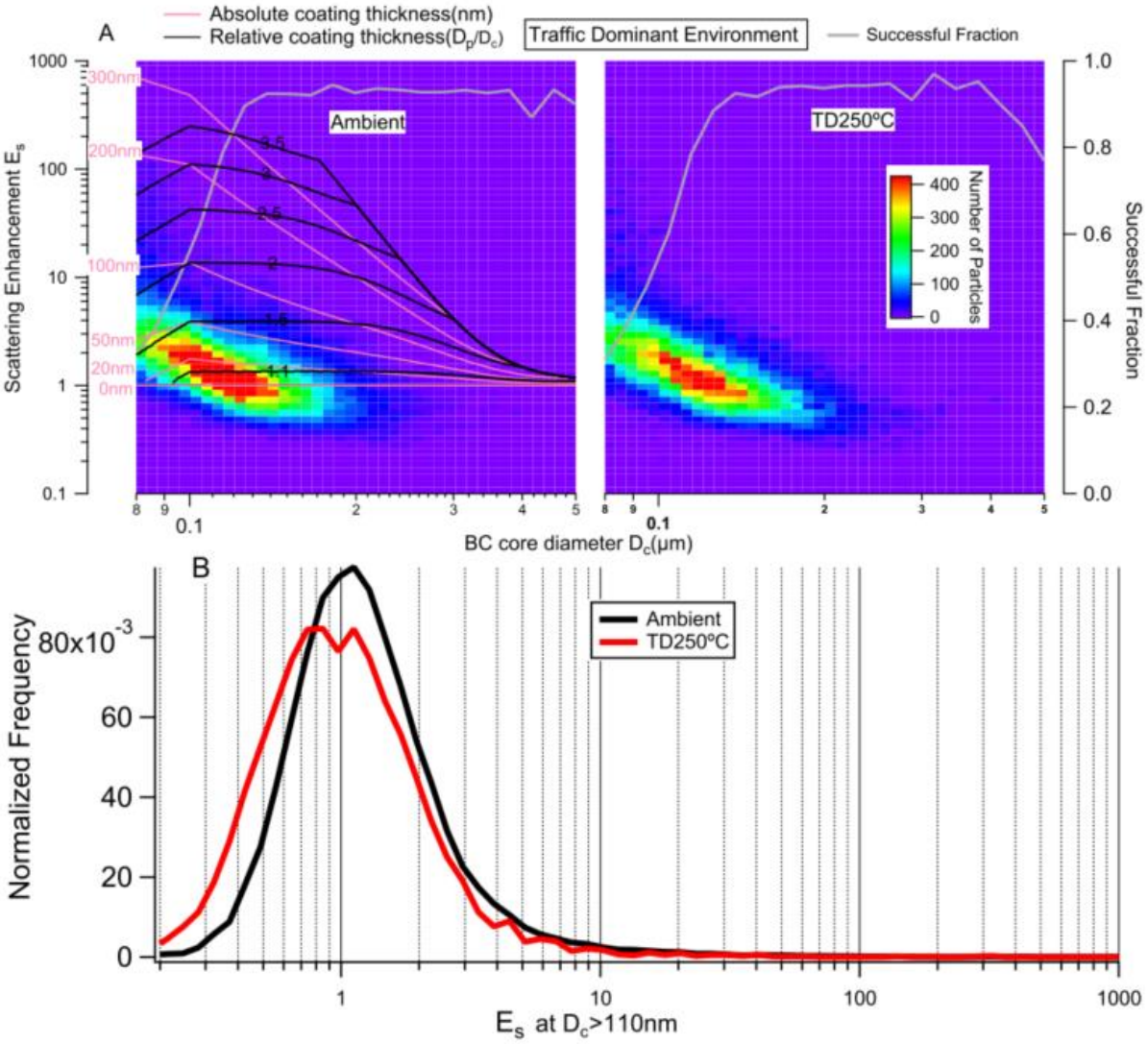

Figure S1. BC optical properties when the environment is dominated by traffic source. (a) The scattering enhancement (Es) as a function of BC core diameter (Dc). The image plot is a two dimensional histogram for the detected particles. The solid grey line, with corresponding scale on right axis, shows the number fraction of BC particles that were successfully determined according to their scattering signal at each Dc size. The left panel is for the ambient data, whereas the right panel is the same group of BC particles after passing through the thermodenuder (TD) at 250 ◦C. The thinner red and black contours show the corresponding absolute coating thickness (in nm, (Dp−Dc)/2) and relative coating thickness (Dp/Dc), respectively. (b) The area normalised histogram of Es for the particles with Dc >110nm. Reprinted from Liu et al. (2014).

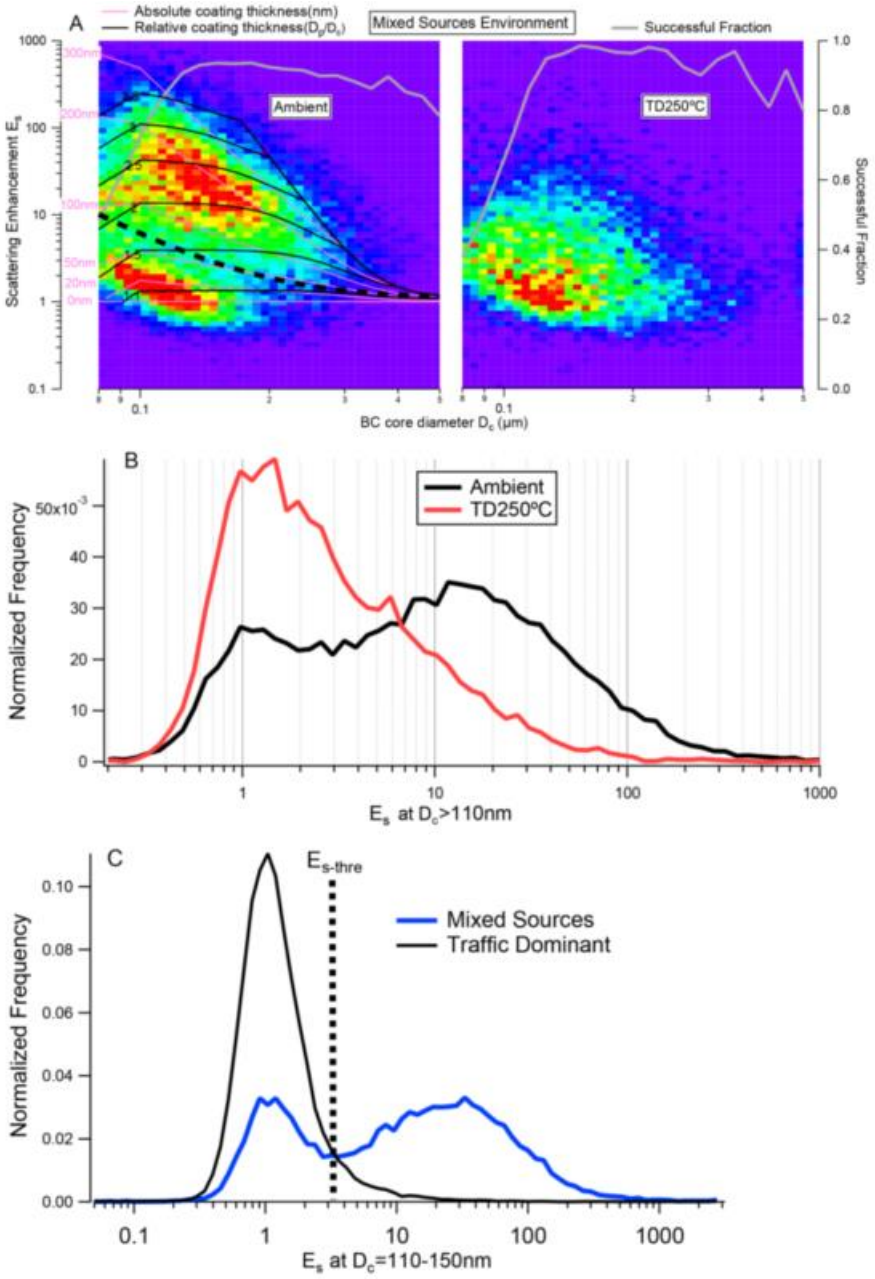

Figure S2. BC optical properties when environment is significantly influenced by solid fuel burning (31 January to 1 February when E air mass). The legends in the plot are identical with Fig. 4. In particular, the thick dotted black line on the left panel of (a) shows the reference line used to discriminate the BC from traffic or solid fuel burning source. (c) the Es distribution atDc =110–150nm for the traffic and mixed sources, with the dotted line showing the determination of Es-thre. Reprinted from Liu et al. (2014).

Spearman rank correlation test

$$r_s = \rho_{\mathrm{rg}_X, \mathrm{rg}_Y} = \frac{\mathrm{cov}(\mathrm{rg}_X, \mathrm{rg}_Y)}{\sigma_{\mathrm{rg}_X} \sigma_{\mathrm{rg}_Y}}$$

where

- ρ denotes the usual Pearson correlation coefficient, but applied to the rank variables.
- $\mathrm{cov}(\mathrm{rg}_X, \mathrm{rg}_Y)$ is the covariance of the rank variables.
- σ_{rgX} and σ_{rgY} are the standard deviations of the rank variables.

$$r_s = 1 - \frac{6 \sum d_i^2}{n(n^2 - 1)}.$$

where

- $d_i = rg(X_i) - rg(Y_i)$, is the difference between the two ranks of each observation.
- n is the number of observations

To determine if the r_s are significant, the p-value tests have been conducted.

$$p\ Value_{(r,df)} = 1 - F.DIST\left(\left(\frac{df * r^2}{1 - r^2}\right), 1, df, TRUE\right)$$

Note: r_s is significant at $\alpha = 0.05$ if the p-value is lower than α (0.05).

Table S1. The spearman rank correlation coefficients between the $BC_{wb\_difference}$ and organics.

Correlation coefficient / Variables	Pearson's r	r^2	Spearmen rank correlation r_s	P-value
$BC_{wb\_difference}$ V.S. Coal	0.76	0.58	0.79	0.63 > 0.05
$BC_{wb\_difference}$ V.S. Wood smoke	0.43	0.18	0.59	< 0.001
$BC_{wb\_difference}$ V.S. Levoglucosan	0.42	0.18	0.61	0.04 < 0.05
$BC_{wb\_difference}$ V.S. Potassium	0.52	0.27	0.71	0.08 > 0.05
$BC_{wb\_difference}$ V.S. SFOA1	0.38	0.15	0.74	< 0.001
$BC_{wb\_difference}$ V.S. SFOA2	0.30	0.09	0.55	< 0.001
$BC_{wb\_difference}$ V.S. SFOA1 – SFOA2	0.23	0.05	0.34	0.12 > 0.05
$BC_{wb\_difference}$ V.S. OOA	0.86	0.74	0.83	< 0.001
$BC_{wb\_difference}$ V.S. SF trace elements	0.85	0.73	0.75	< 0.001
$BC_{wb\_difference}$ V.S. SFOA1/SFOA	0.53	0.28	0.69	< 0.001
$BC_{wb\_difference}$ V.S. SFOA2/SFOA	-0.53	0.28	-0.25	< 0.001
$BC_{wb\_difference}$ V.S. Levo/K	-0.34	0.11	-0.185	< 0.001

*Time series is based on the CMB (24 hours).

Table S2. The spearman rank correlation coefficients between the $BC_{wb\_difference}$ and organics and inorganics.

Correlation coefficient / Variables	Pearson's r	r^2	Spearmen rank correlation r_s	P-value
$BC_{wb\_difference}$ V.S. OOA	0.52	0.27	0.52	< 0.001
$BC_{wb\_difference}$ V.S. SFOA1	0.20	0.04	0.37	< 0.001
$BC_{wb\_difference}$ V.S. SFOA2	0.14	0.02	0.27	< 0.001
$BC_{wb\_difference}$ V.S. Solid fuel trace element	0.66	0.43	0.50	< 0.001
$BC_{wb\_difference}$ V.S. SFOA1 – SFOA2	0.12	0.01	0.11	< 0.001
$BC_{wb\_difference}$ V.S. Non-volatile PM2.5	0.67	0.45	0.42	< 0.001
$BC_{wb\_difference}$ V.S. SO4	0.61	0.37	0.49	< 0.001
$BC_{wb\_difference}$ V.S. NO3	0.58	0.33	0.54	< 0.001
$BC_{wb\_difference}$ V.S. NH4	0.64	0.41	0.55	< 0.001

*Time series is based on the AMS (30 minutes).

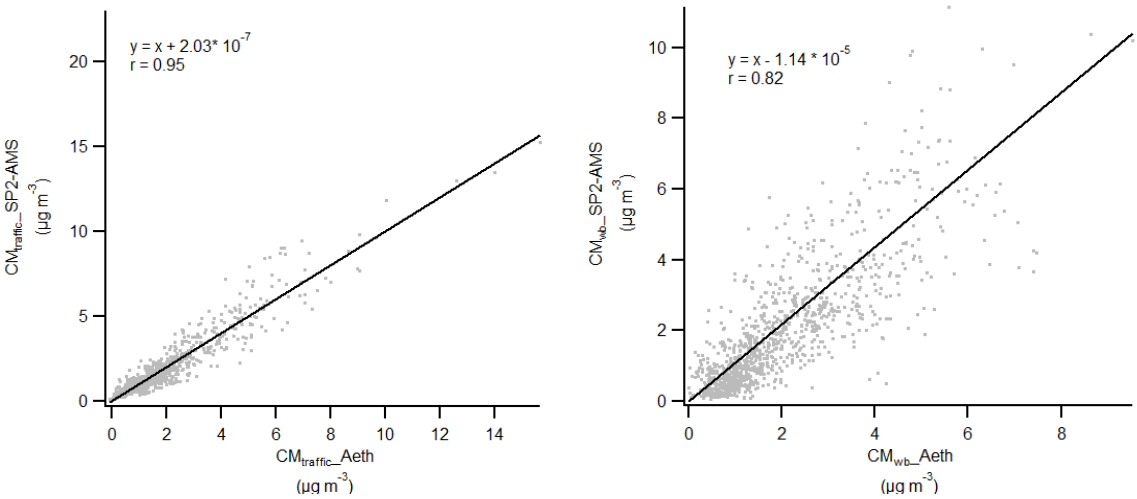

Figure S3. The estimate of carbonaceous matter for traffic and wood burning by pre-apportioned data as a function of that by traditional method.

4.2 Paper II: Characterising the Black Carbon and gaseous pollutants on the Yangtze River in Eastern China.

Authors: Y. Ting, D. Liu, W.T. Morgan, J.D. Allan, H. Coe, C. Li, X. Wang, X. Ye, J. Chen.

Publication: The manuscript has been under review by other co-authors. It is planned for the Science of the Total Environment.

Research highlights:

- On-line measurements of black carbon (BC) and gaseous pollutants were performed in winter over the Yangtze River in China.
- The effects of the shipping emissions and regional pollutants in the coastal cities on the air pollution over the Yangtze River were investigated.
- The characteristics of BC and gases for the background and high pollution periods were presented.

Author's contribution: I led the data analysis and manuscript preparation.

Co-author contributions: Morgan, Li, Wang and Ye participated in the field work/data acquisition. Morgan helped to set up the instrument of SP2 on the ship. Li was responsible for the work on the river. Wang was responsible for ensuring the SP2 operation. Ye was responsible for the work during the cruiser campaign. Chen was the PI of this project. Liu, Allan and Coe assisted in preparation of the manuscript.

Characterising Black Carbon and gaseous pollutants on the Yangtze River in Eastern China.

Y. Ting[1], D. Liu[1], W.T. Morgan[1], J.D. Allan[1,2], H. Coe[1], C. Li[3], X. Wang[3], X. Ye[3] and J. Chen[3]

[1]School of Earth and Environmental Science, University of Manchester, Manchester, UK

[2]National Centre for Atmospheric Science, Manchester, UK

[3]Department of Environmental Science & Engineering, Fudan University, Shanghai, China

Abstract. The Yangtze River region and cities along the river have severe deterioration of air quality due to urbanization and economic development. Black carbon (BC) has important radiative impact at this region however has yet to be characterised and included in the emission inventory. Here we report the first time continuous measurements of BC and gaseous pollutants over Yangtze River in wintertime covering ~7° longitude over continent. The river was influenced by a combination of complex sources such as shipping emissions, power plants, surrounding industries as well as regional transport from the cities along the river. The highly polluted periods (HPP) with NO_x > 80 μg m^{-3} (above 75th percentile) conditions correlated with high SO_2 > 10 μg m^{-3}, which indicated more localized emissions, e.g. mainly from shipping emissions on the river or local industry sources along the river. These HPP also corresponded with high BC number concentrations, but had no apparent correlation with CO (due to higher background level) or PM_1 (as dominated by secondary formation). For the region in inner land (longitude < 118°E) mostly influenced by terrain height and regional transport, and outer land (longitude > 118°E) influenced by easterly oceanic or westerly continental air mass, the HPP significantly decreased the BC core size by 5.39-19.41% for all air mass conditions. BC with smaller core size, at a mode of mass median diameter 120-180 nm, was found to importantly contribute to the local sources, contrasting with a more consistent mode ~200nm for mixed sources. Overall, the dominating shipping activities increased BC number by 17.49-115.77% with low contribution to BC mass (5.62-51.19%) because of the smaller size. A comparison of simultaneously measured data from the official monitoring stations in the 9 cities along the river determined a high consistency of $PM_{2.5}$ over the river (slope = 0.96, R^2 = 0.75), which reflects the important regional impact on the particulate mass. This study serves a metric to evaluate the possible shipping emission and regional influence over the Yangtze River and may guide the policy making on mitigating air pollution.

Introduction

The Yangtze River (YR) basin is located in eastern China, and includes the cities of Shanghai, Nanjing and Wuhan all having population in excess of 8 million people. Other cities along the YR include more than 1 million people, making the region one of the most polluted in China (Fu et al., 2013). As one of the longest rivers in the world, YR is a severely polluted channel, which has been heavily suffering from air pollution from both the surrounding areas and local vessels.

Black carbon (BC) is the dominating light absorbing particle, which is estimated to be the most important anthropogenic contributor to global warming after CO_2 (Ramanathan and Carmichael, 2008, Bond et al., 2013) and widely recognised as having adverse effects on human health of the exposed population (Koelmans et al., 2006, Kandlikar et al., 2009, Shrestha et al., 2010, Grahame et al., 2014). BC not only affects the optical properties of clouds (Lohmann and Feichter, 2005, Riemer et al., 2010, Rose et al., 2011) but also atmospheric chemistry (Deng et al., 2010, Ding et al., 2016). China is one of the major regions of the sources of BC aerosol, with a contribution of approximately 30% of anthropogenic global BC concentrations (Bond et al., 2004). In the last few years, severe air pollution episodes have occurred frequently in China due to the rapid industrialisation and economic development. The YR region, including Yangtze River Delta (YRD), a basin of one of the longest rivers in the world, is even suffering from air pollutants from various sources, such as traffic, power plant, biomass burning, industry and non-road transportation (e.g. shipping emissions) (Fu et al., 2013, Wang et al., 2016, Xu et al., 2016). As a result of the large uncertainties of the emission inventories, estimation of the impact of BC on climate radiative forcing varies dramatically (Wang et al., 2017). Therefore, it is essential to clarify the characteristics of BC from different sources to aid accessing the impact of optical and physical properties of BC on climate forcing and the establishment of the mitigation strategy.

Air pollution over the YR has been severe in the recent year due to the high levels of energy consumption (Fu et al., 2008, Fu et al., 2013), which results in a large amount of emissions of atmospheric pollutants. The influence of the regional/long-range transport of pollutants in the YR region has been of more and more concern in the last decade (Huang et al., 2011, Wang et al., 2014, Huang et al., 2013, Xu et al., 2016). From 2010, the YRD region has been identified as a key area for joint prevention and control of air pollution, as part of an important air pollution control plan for China (Wang and Hao, 2012). However, due to the

complex sources of the air pollution, it has been still a challenge for policy makers and researchers to identify emission sources, understand the contamination processes, and develop effective air pollution control strategies.

Shipping emissions, including SO_2, NO_x, organic carbon (OC), black carbon (BC) and particulate matter (PM), have a significant contribution to the impacts on climate, air quality and human health (Capaldo et al., 1999, Fuglestvedt et al., 2009, Lu et al., 2006, Lonati et al., 2010). Over the last two decades, the global shipping emissions and their impacts on global climate, air quality and human health have been of great interest worldwide (Corbett et al., 2007, Lu et al., 2006, Isakson et al., 2001, Kim and Hopke, 2008, Agrawal et al., 2009, Hellebust et al., 2010, Matthias et al., 2010). Previous studies indicate that shipping emissions along the shipping routes have contributed to the degradation of the current air pollution situation (MOT, 2015, Zhang et al., 2017). In the recent years, shipping emissions in the East Asia have rapidly increased (Liu et al., 2016). Hazardous emissions from ships result in increasing impacts on the air quality of local, regional and global atmosphere. Particularly in the YRD (Fan et al., 2016), one of the five major port clusters in China, where with the significant development of the economy and vessel traffic, has been increasingly busy and features a dense distribution of ports and a large throughput. Previous studies have investigated the physical-chemical properties, sources and formation mechanisms of particles in the YRD on a city-level scale, such as Shanghai, Nanjing, Jiaxing, Suzhou, Ningbo and Hangzhou, (Ding et al., 2013, Hua et al., 2015, Li et al., 2015, Chen et al., 2015, Gong et al., 2016, Huang et al., 2012b, Huang et al., 2013), however very few researches have been conducted on a regional scale considering the impacts of local activities in the YR region. Furthermore, there has not been study investigating the air pollution on the Yangtze River, where has been polluted by the emission sources from the surrounding cities, the shipping routes and regional transport. Influenced by the local emissions (e.g., ship and traffic exhaust) as well as regional transport of air pollutants from the surrounding heavily polluted areas, the physicochemical properties of ambient BC aerosols in the YR region are highly varied.

This cruiser campaign was the first time to continually measure the shipping emissions and air pollutants simultaneously on the Yangtze River in order to better understand the impacts of shipping emissions to the atmospheric environment. Moreover, this study is a good opportunity to investigate systematically the regional transport in the eastern China. Here, the mass-equivalent size distributions of refractory BC (rBC, Petzold et al. (2013)) were first

revealed in the extensive YR region based on the SP2 measurements. The characteristics of rBC particles were also investigated, accompanied by an analysis of their relation with gaseous emissions and their potential source contributions. A novel approach was employed to evaluate the contribution of local traffic to the rBC concentration based on the measured rBC sizes and reasonable assumptions; including a deductive mean diameter of rBC from local traffic and relatively stable rBC sizes in the air masses transported over certain regions. The aim of this study is to report the direct measurements of BC mass loadings and properties from different sources in eastern China, which underpins the mitigation strategy of air pollution.

Methodology

The Yangtze River experiment

The YR observation campaign took place along the Yangtze River in winter 2015 within the scope of the regional transport and transformation of air pollution in eastern China. The cruise measurements were conducted along the YR between Shanghai and Wuhan from 21st November and 4th December 2015. The measurement campaign started at 11:30 UTC (+ 8 hours for local time) on 21 November 2015 from Shanghai (31.36°N, 121.62°E), one of the major industrial and commercial hubs in eastern China, and arrived in Wuhan (30.62°N, 114.33°E) at 07:42 UTC on 29 November 2015. The carrier ship then sailed back and finally arrived in Shanghai at 12:30 UTC on 4 December 2015. The cruise campaign, including a departing journey from Shanghai to Wuhan and a returning journey from Wuhan to Shanghai, covered the river with about 2150 km passing over the major industrial and transportation hubs in eastern China, such as Shanghai, Nanjing, Jiujiang, Huanghang and Wuhan. Details of the cruise route is shown in Figure 1.

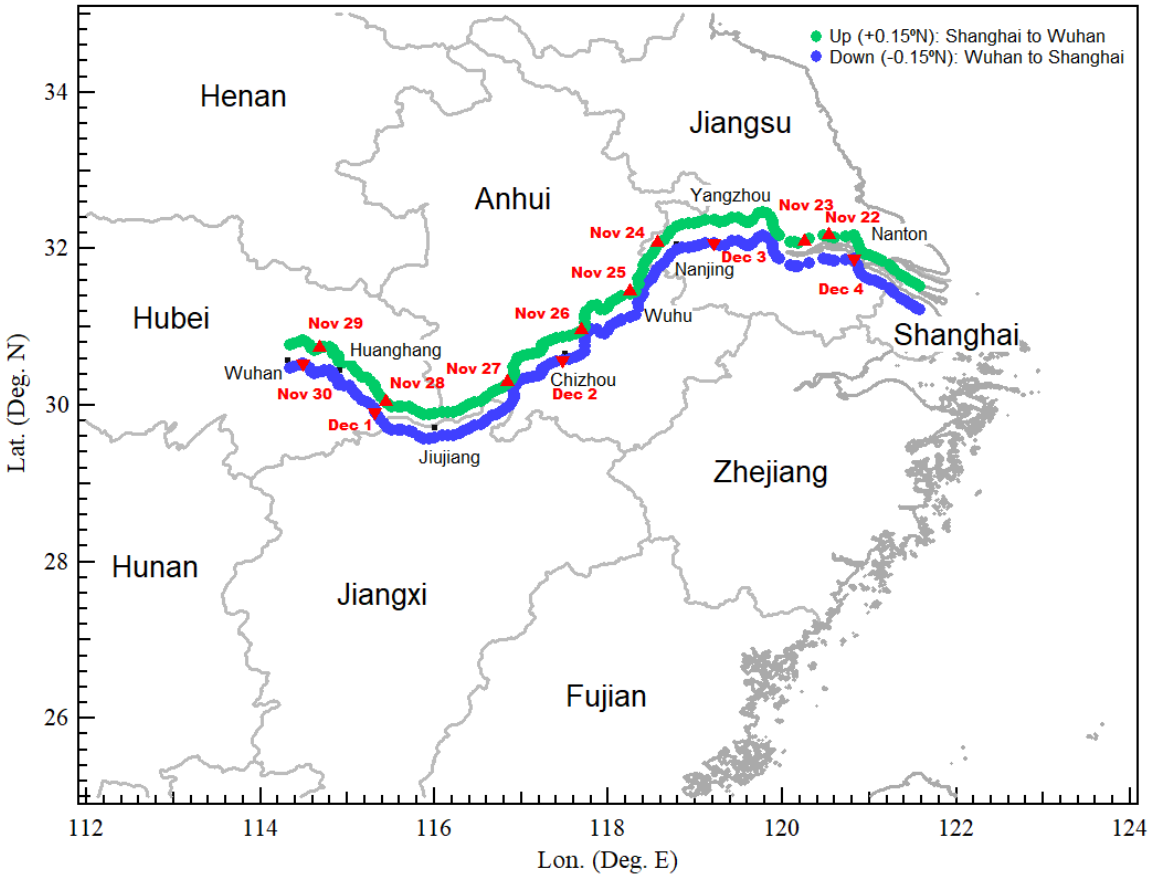

Figure 1. The cruise tracks of the departing journey from Shanghai to Wuhan (green line) and the returning journey from Wuhan to Shanghai (blue line). The red symbols represent the date of arrival.

Instrumentation and data analysis

The physical properties of individual rBC particles were characterised using a single particle soot photometer (SP2, Droplet Measurement Technology, Inc., Boulder, CO, USA). The SP2 determines the mass of refractory particles by detection of the incandescence radiation induced by a 1064 nm intra-cavity Nd:YAG laser when a light-absorbing particle passes through. The main light-absorbing component in the atmosphere at this wavelength is BC. Therefore, the incandescence signal was converted to the mass of single particle rBC based on the calibration using Aquadag sample black carbon particle standards (Aqueous Deflocculated Acheson Graphite, manufactured by Acheson Inc., USA). The generated rBC particle standards from Aquadag do not represent the ambient rBC, thus a further correction of 0.75 is employed in the calibration curve to obtain a more reliable rBC mass determination (Moteki et al., 2010, Baumgardner et al., 2012, Laborde et al., 2012). An rBC sphere-equivalent core diameter (D_c) can be derived by the conversion of rBC mass, assuming a density of 1.8 g cm^{-3} for atmospheric rBC (Bond and Bergstrom, 2006). Any particles with

the detectable incandescence signals are referred to as the rBC-containing particles and the particles that only present the scattering signals are termed as the non-BC particles. As a certain amount of rBC particles has either too small core sizes to be detected or too large thereby saturating the detector, the extrapolation of log-normal fit on the Dc mass distribution is applied to predict the missing masses.

The scattering signal of an rBC-containing particle can be distorted because of the mass loss of a BC particle by laser heating when it passes through the laser beam. Thus, the 'leading edge only' (LEO) method is utilised to reconstruct the scattering signal of an rBC-containing particle (Gao et al., 2007). The details for the LEO fitting are described into detail by Liu et al. (2014) and Taylor et al. (2015). The overall size (D_p) of the rBC particle, including the BC core and coatings, can therefore be provided by a core-shell Mie model with the input of the LEO fitted scattering signal and BC core size, accompanied with the assumption of an rBC core refractive index of 2.26 – 1.26i and a coating refractive index of 1.5 + 0i (Moteki et al., 2010). The relative coating thickness of an rBC particle is calculated as D_p/D_c. The optical size of a non-rBC particle can also be calculated using the Mie theory with a coating refractive index of 1.5 + 0i, which makes the optical sizes of rBC-containing and non-rBC particles directly comparable. Given the coating thickness of individual rBC particles is Dc size dependent, the bulk coating thickness is calculated as the cubed root by the total volume of the rBC particles divided by the total volume of the BC cores, as shown in Eq. (1). The more detailed information of the instrument operation and data interpretation procedures of the SP2 used in this study has been described in McMeeking et al. (2010) and Liu et al. (2010).

$$\frac{D_p}{D_c} = \left(\frac{\sum_i D_{p,i}^3}{\sum_i D_{c,i}^3}\right)^{\frac{1}{3}} \quad (1)$$

Where Dp and Dc are the coated rBC diameter and rBC core diameter, respectively; *i* denotes the *i*th single rBC particle. The bulk of volume weight, D_p/D_c, is considered to be a representative diagnostic for the overall mixing state of the whole population of BC particles.

NO and NO_2 concentrations were monitored by a chemiluminescent NO-NO_2-NO_x analyser (Thermo Fisher Scientific, Model 42i), SO_2 concentrations were monitored by a pulsed fluorescence SO_2 analyzer (Thermo Fisher Scientific, Model 43i). The CO concentrations were monitored by a non-dispersive infrared CO analyser (Thermo Fisher Scientific, Model 48i), and O_3 concentrations were measured by a UV photometric O_3 analyser (Nodel 49I,

Thermo-Fisher Scientific, USA). The concentrations of particulate matter (PM_1 and $PM_{2.5}$) was measured using TSI SidePak AM510 Personal Aerosol Monitors. SO_2, CO, NO_2, O_3 and $PM_{2.5}$ mass concentrations from the monitoring site in the cities were obtained from the China National Environmental Monitoring Centre (http://www.cnemc.cn/).

The Hybrid Single-Particle Lagrangian Integrated Trajectory (HYSPLIT) model (Draxler and Hess, 1998) was used to compute back trajectories of air parcel and transport. Real-time back trajectories were generated every 1 h and calculated 3 days backward in time. The horizontal and vertical wind fields for trajectory calculations were provided by the 1*1, 3-hourly GDAS reanalysis meteorology (Global Data Assimilation System; NOAA Air Resources Laboratory, Boulder, CO, USA). The emissions inventory of BC, which includes the major anthropogenic sources in the regions in China, used in this study is part of the mosaic inventory, named MIX, which was developed by Li et al. (2017).

Results and discussion

Overview of the campaign

A cruise campaign was conducted from the estuary at Shanghai to Wuhan and then back to Shanghai in order to characterise rBC and its related gaseous pollution over the YR in eastern China. Figure 1 shows the time series of the rBC properties and the mass concentrations of the other pollutants during the sampling period. Over the cruise of this study, there were many simultaneous spikes of the rBC mass and number concentrations with NO_x and SO_2 mass concentrations, corresponding to fresh rBC particles with smaller core size and thinner coatings during the periods of cruising. This situation implies that the sources dominating these plumes might come from local activities with less aging process, which could be mainly the shipping emissions.

During the period from Shanghai to Wuhan, the average rBC mass concentration and number concentration were 2.04 ± 1.27 (0.13 ~ 11.99) μg m^{-3} and 1246.99 ± 934.51 (76.60 ~ 5062.45) cm^{-3}. The average MMD and coating thickness of BC particles were 186.10 ± 22.17 (123.04 ~ 238.00) nm and 1.38 ± 0.01 (1.16 ~ 1.63). The average mass concentrations of NO_x, SO_2, CO and $PM_{2.5}$ were, 68.95 ± 82.89 (0.93 ~ 372.49), 11.64 ± 11.40 (0.02 ~ 52.20). 411.95 ± 185.00 (82.33 ~ 1523.21) and 37.88 ± 21.09 (2.59 ~ 107.73) μg m^{-3}, respectively. A moderate correlation (r = 0.49) between $PM_{2.5}$ and rBC indicated that the concentrations of rBC increased with $PM_{2.5}$ during this period over the river. NO_x showed a strong correlation with SO_2 (r = 0.83) but not with CO, indicating the possible sources of both SO_2 and NO_x

emissions were likely to be sulphur-containing fossil fuel combustion from the ships, power generation plants or industrial facilities (Lu et al., 2006).

In the return way from Wuhan to Shanghai, the average BC mass concentration and number concentration were 2.70 ± 1.36 (0.66 ~ 11.29) μg m^{-3} and 1308.9 ± 973.76 (295.45 ~ 5730.04) cm^{-3}. The average MMD and coating thickness of BC particles were 198.59 ± 12.11 (158.34 ~ 219.99) nm and 1.42 ± 0.14 (1.17 ~ 1.79). The average mass concentrations of NO_x, SO_2, CO and $PM_{2.5}$ were, 53.92 ± 69.10 (3.24 ~ 292.31), 10.76 ± 8.67 (0.61 ~ 44.12). 616.52 ± 247.07 (210.56 ~ 1913.79) and 47.62 ± 19.04 (20.52 ~ 148.15) μg m^{-3}, respectively. A weak correlation (r = 0.21) between $PM_{2.5}$ and rBC was observed during this period, which was different from that for the route from Shanghai to Wuhan. In general, sulphur-containing fossil fuel combustion was also the main source during this period, implied by the moderate correlation between NO_x and SO_2, but not with CO, which was the same as that measured from Shanghai to Wuhan.

Figure 3 shows BC mass concentrations on the topographical map, which reveals the spatial distribution of the concentrations during the sampling period. It can be noticed that about 118 °E can be used as a boundary between terrain, which might affect the diffusion and transmission of air pollution, to explore the characteristics of the emissions of the sources from different regions. Thus, the measured data was divided into four sections according to 118 °E to investigate the potential sources and characteristics of the air pollutants in the following sections, which are depart_I, depart_II, return_I and return_II.

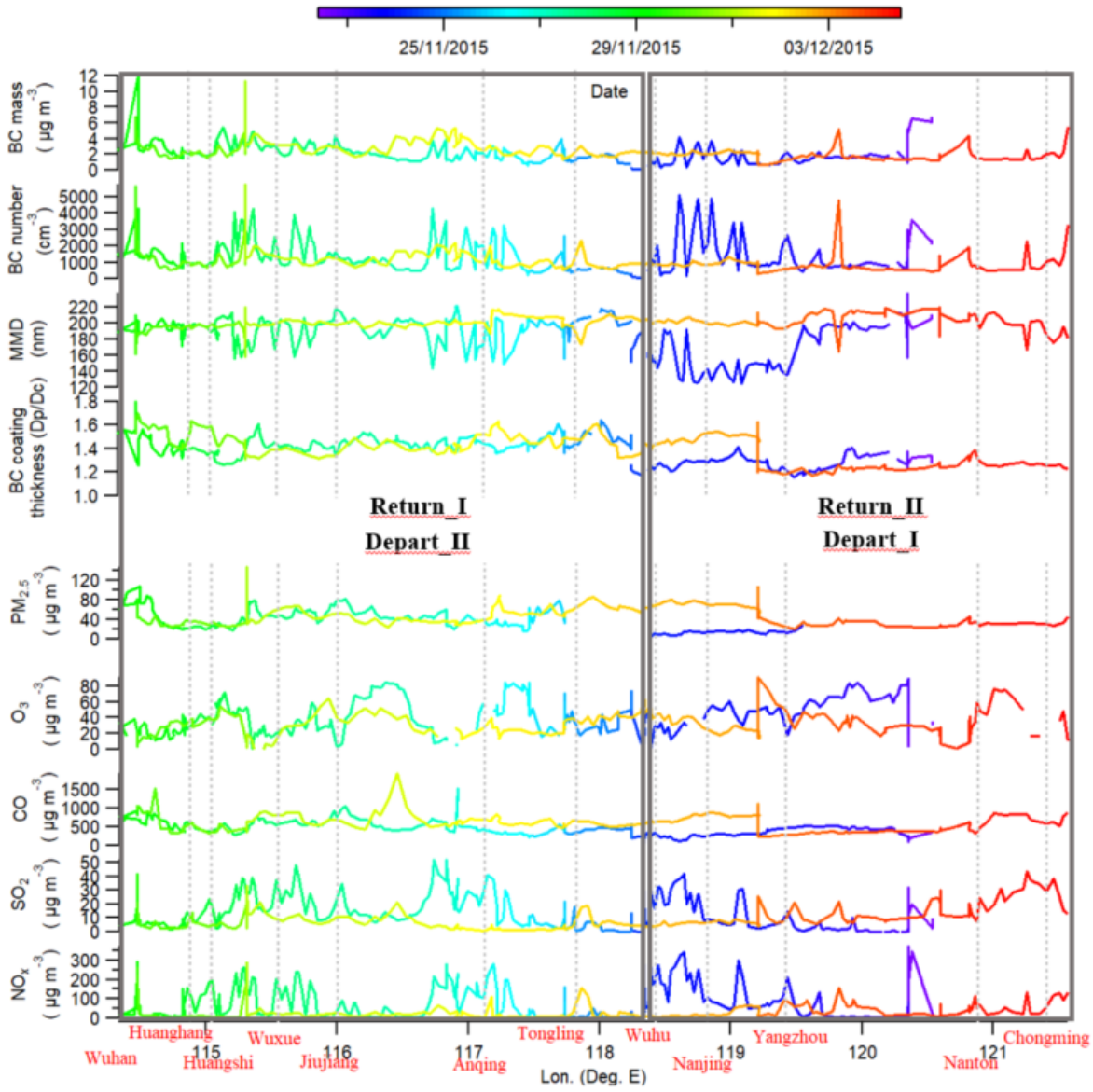

Figure 2. Top panel: Mass and number concentrations, mass median diameter (MMD) and coating thickness of BC particles. Bottom: Mass concentrations of pollutants at different longitude during the round cruise. Depart_I: 120.53 °E to 118.34 °E; Depart_II: 118.33 °E to 114.34 °E; Return_I: 114.37 °E to 118.34 °E; Return_II: 118.34 °E to 121.57 °E.

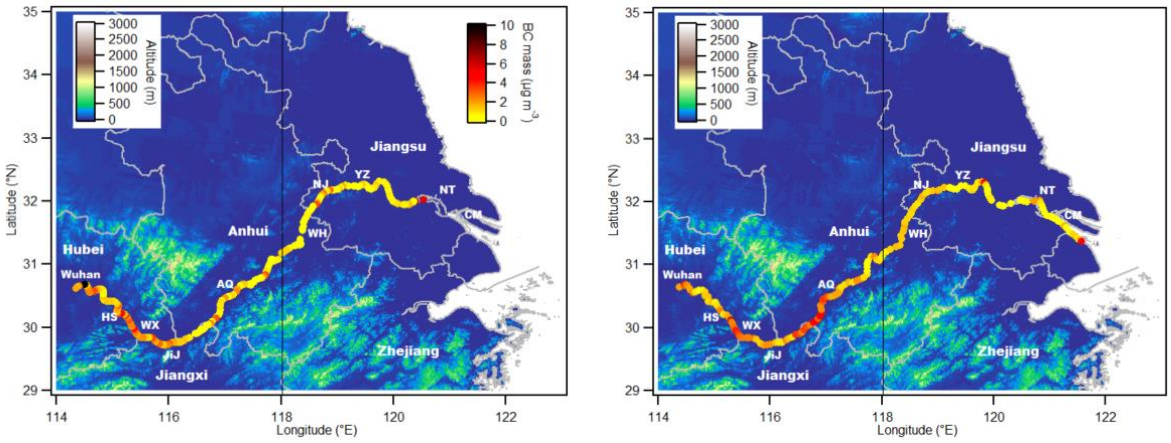

Figure 3. Spatial distribution of BC mass median concentrations back and forth between Shanghai and Wuhan along the Yangtze River from 22/11/2015 to 04/12/2015. Left: departing journey (Shanghai to Wuhan); right: returning journey (Wuhan to Shanghai).

In the regional emission inventory, in China, aggregated by Li et al. (2017), there are four main anthrogenic sources of BC; power, industry, residential and transportation (Figure 4). Figure 4 also shows the back trajectories of the four periods, which present the major sources of BC that the air masses passed through. For the intercomparison, the primary sources of air pollution during the four periods were classified into three catagories, based on the trajectories of the air masses; local sources (including shipping), easterly sources (cleaner) and westerly sources (more polluted sources), as shown in Figure 5. For the depart_I, the air masses mainly came from the east (87.6 ± 4.2 %), which mostly came from the sea and probably brought cleaner air to dilute the air pollution dominated by the local sources (12.4 ± 4.2%) including the carrier ships and surrounding ships emissions. During the depart_II, both local sources (47.9 ± 34.1) and westerly sources (48.0 ± 32.8 %), with similar percentages, significantly contributed to the air pollution with a small portion attributed to the easterly sources (5.2 ± 17.1 %). As for the return_I, when the route was the same as depart_II, only the local sources (56.2 ± 25.5 %) and westerly sources (43.8 ± 25.5 %) contributed to the air pollution without easterly sources. During the return_II period, the local sources that contributed to pollutant concentrations were similar to those during the depart_II. However, westerly sources accounted for 49.7 ± 28.1 % of the air pollutants during the period of return_II with 39.3 ± 26.6 % from the east. It can be noted that the westerly sources contributed greatly to air pollution during the most of the time, except for the depart_I, implying that air quality in the Yangtze river was affected by the transmission of the air pollutants from the inland, where there are diverse sources.

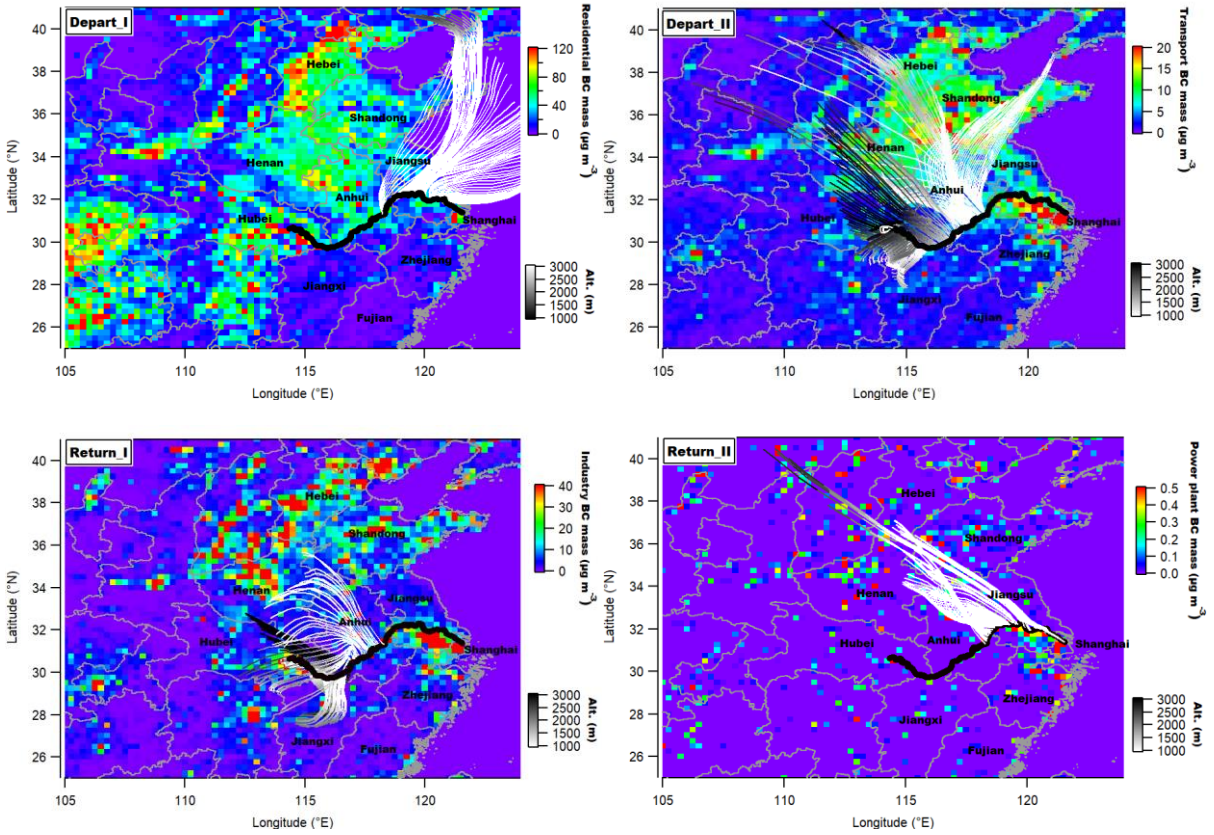

Figure 4. 72h back trajectories simulated by HYSPLIT model constrained at a height of 1000 m a.g.l. (above ground level) for the four periods shown on the BC emission inventories (Li et al., 2017) between Shanghai and Wuhan.

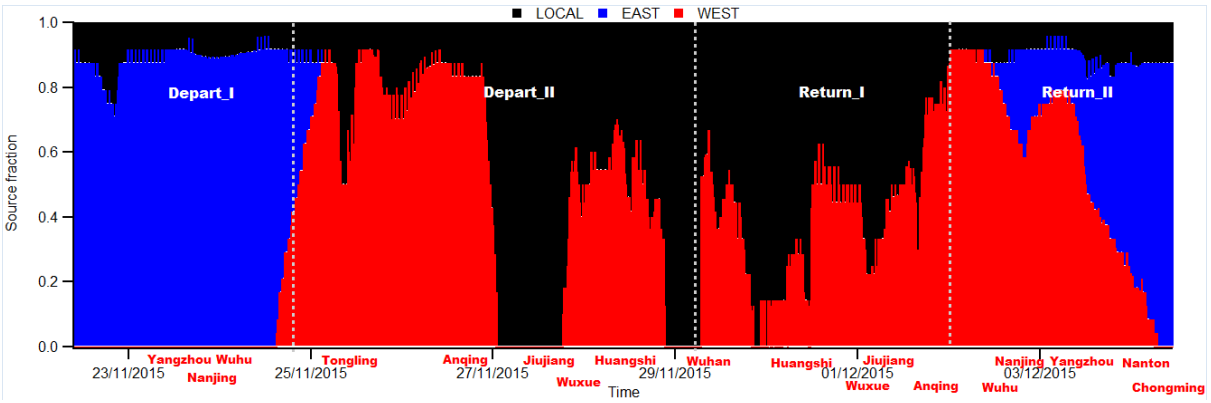

Figure 5. The fraction of the sources according to 24h backward trajectory air mass divided into three regions: East: (>118 °E), West: (<118 °E) and Local (Lat ± 0.25 °E and Lon ± 0.25 °N).

Figure 6 and Figure S1 shows gaseous pollutants, PM_1 and BC-related properties as a function of NO_x, which was one of the main indicators of shipping emissions for the four periods. In general, the air pollution during the depart_I consisted of low SO_2, CO, BC, PM_1 mass concentrations, MMD and coating thickness of BC particles. This suggests fresh emissions from local sources with clean regional transport. In contrast, the return_I period had the highest BC mass/number concentrations, coating thickness of BC particles, PM_1 and

CO, implying the most influence of the regional transport on the background, which were consistent with the air mass coming from the much polluted west. Combined with the outcomes of backward trajectory analysis, the potential sources for each section were summarized as local sources + clean long-range transport (depart_I), local sources + clean long-range transport + polluted long-range transport (dapart_II), local sources + polluted long-range transport (return_I) and local sources + clean long-range transport + polluted long-range transport (return_II). The mass concentration of SO_2, which is also highly related to shipping emissions (Endresen et al., 2003, Wang et al., 2007, Zhao et al., 2013), increased rapidly when NO_x were above the specific concentration of 80 μg m^{-3}, which was regarded as an threshold of shipping emissions. The periods, when NO_x emissions were above the thresholds and corresponded to high SO_2 (> ~10 μg m^{-3}), were considered to be dominated by shipping emissions, whereas the others were considered to be the value of the background. This section will present the overall variation of the pollutants, and the comparison between the background and the shipping emissions will be discussed in the following section.

The significant correlations between NO_x, SO_2 and BC mass and number concentrations implied the source of shipping emissions, however the correlations with PM_1 and CO concentrations were not observed due to the effect of the long-range transport and the longer residence time in the atmosphere (Pfister et al., 2004, Heinizenberg, 1989). Fresher BC for depart_I imposed on cleaner environmental background reflected by low CO and PM_1, when cleaner easterly air mass came from ocean. In addition, more convincible indicator of BC signature was observed from possible fresh shipping emissions, i.e. much smaller core size and thinner coatings. For other periods, depart_II, return_I and return_II, BC is imposed on the polluted background, where showed larger core size and thicker coating of the BC particles.

Air quality over the YR is affected by local sources in almost whole periods (carrier ship, surrounding ships and local sources). However, the characteristics of BC were not significantly affected by the regional sources at Lon.> ~118 °E (red line; marine air mass, cleaner), whereas the others were affected by the distinct sources (petrochemical plants, industry, biomass burning. Urban outflow and coal burning) from more polluted westerly air mass at Lon. < ~118 °E (grey, blue and green lines) with larger core size and thicker coatings.

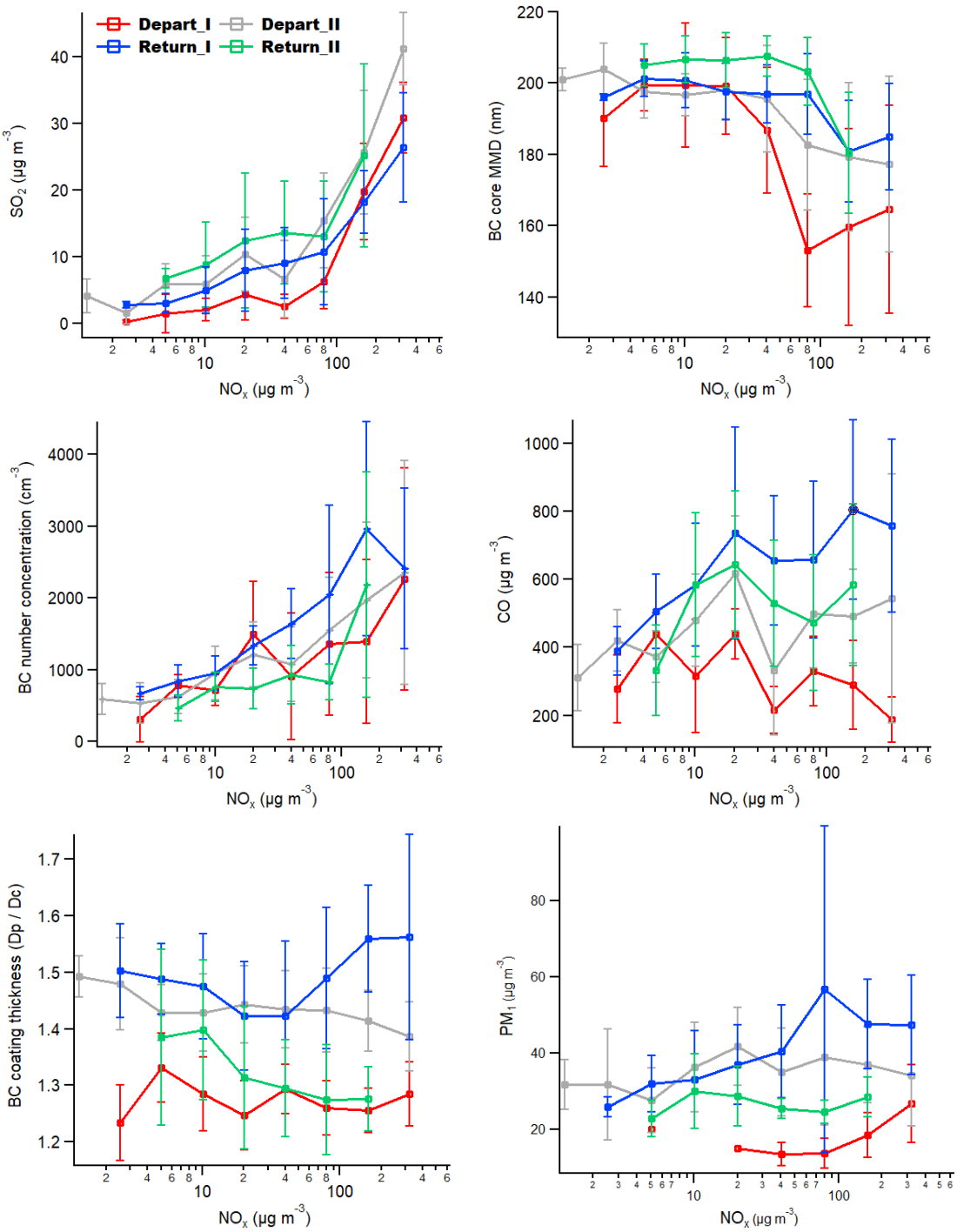

Figure 6. SO_2, CO, PM_1 and BC-related properties as a function of NOx. Red line: depart_I, grey line: depart_II, blue line: return_I, green line: depart_II.

As stated above, the 80 μg m^{-3} of NO_x mass concentration was considered as the division between the value of the background and shipping emissions. The data for each period was subsequently divided into two pollution levels, which were the background with NO_x < 80 μg m^{-3} and high pollution periods with NO_x > 80 μg m^{-3}.

For the cleaner environmental background during depart_I, fresher BC contributed by the shipping emissions was observed by the characteristic indicator of BC properties with much smaller core size of 159.71 ± 26.52 nm and thinner coatings of 1.27 ± 0.05 at high pollution level. Comparing the air pollution in the background and the high pollution levels, when BC mass showed 1.54 ± 1.30 μg m^{-3} in the background and only increased by 5.9 % at the high pollution levels. In terms of the effect of the shipping emissions on the background, SO_2 considerably increased by 721.0 % with the largest decline in BC core MMD of 19.4 % during depart_I. It is noted that in the case of high pollution levels, there was not increase but decrease in the CO mass concentrations, implying that CO from the shipping emissions were much lower than that of the background.

Significant increases in CO, BC and PM_1 mass concentrations were observed during return_I, however the pollutants were not mainly contributed by the shipping emissions as it presented the most influence from the background, consistent with air masses mainly coming from the much polluted west with the greatest increase in the BC coating thickness of 11.26 %. During the four periods, BC core size showed consistent mode at ~180-220nm with a peak diameter of ~ 200 nm at background level, whereas exhibited bimodal mode of BC core size at high pollution level with additional mode at notably smaller size ~120-180nm (Figure 8). Figure S2 shows the distribution of BC core MMD for the period of the SO_2 plumes, which were considered to be mainly contributed by shipping emissions. This BC mode exclusively existed at high pollution level over the river (not at the other pollution levels), thus may be importantly contributed by the shipping emission. Regarding the larger BC core size dominating the background, this might be likely contributed by biomass burning and coal combustion (Huang et al., 2012a, Liu et al., 2014, Wang et al., 2016) transmitted from the surrounding areas. In previous studies, the peak diameter of the rBC mass size distribution was ~210 nm in Shenzhen in southern China (Huang et al., 2012), ~205 nm in Xi'an in western China (Wang et al., 2015) and ~ 200 nm in Shanghai in eastern China (Gong et al., 2016). This similar mass size distribution of rBC suggested that there may be common sources of pollution in different cities in eastern China. Detailed information of the impact of shipping emissions on the background during the four periods is shown in tables S1-S2 in the supplement.

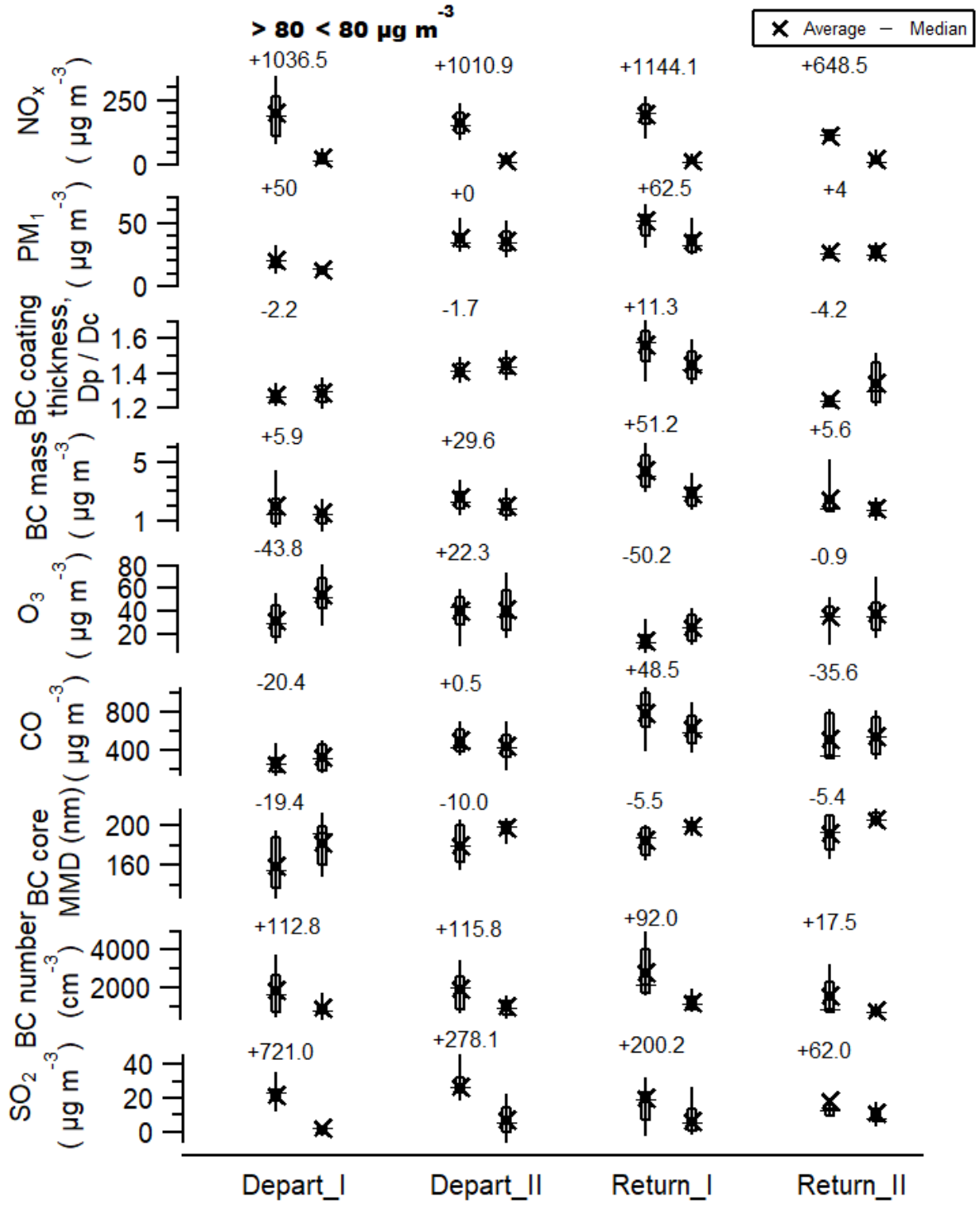

Figure 7. Boxplots of statistical values of the pollutants during the four periods over the Yangtze River, and the increased percentage of the pollutants contributed by ship emissions (unit: %). Left boxes: high pollution period (NO_x > 80 μg m^{-3}); right boxes: background pollution level (NO_x < 80 μg m^{-3})

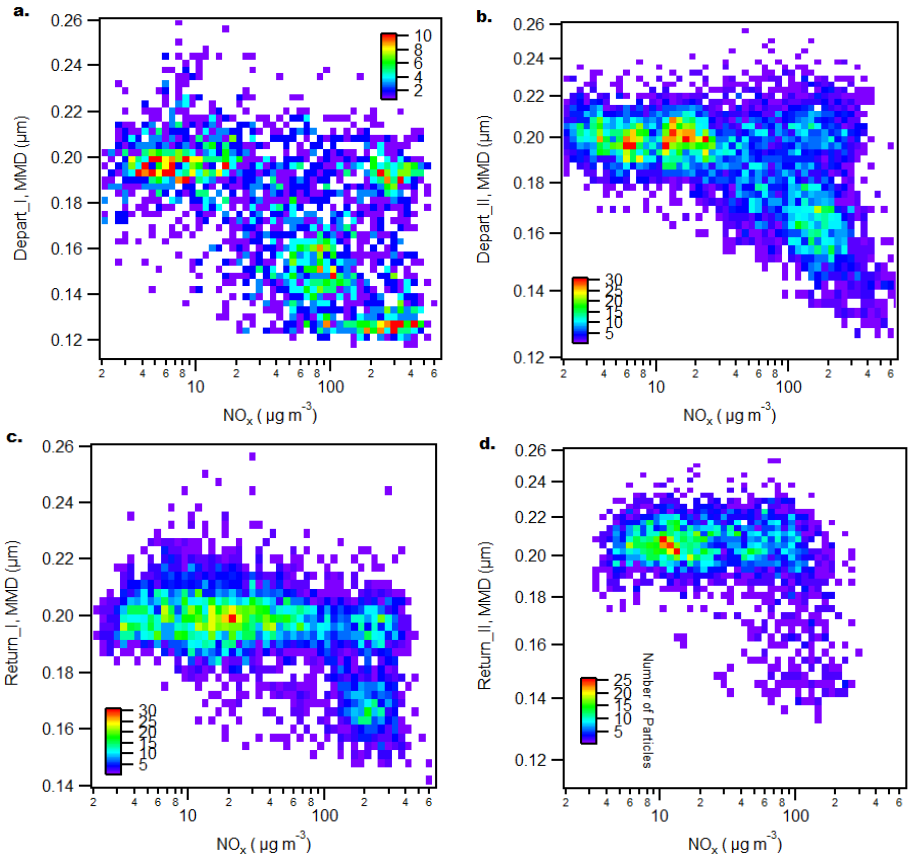

Figure 8. The distribution of BC core MMD as a function of NO_x. a) depart_I. b) depart_II. c) return_I. d) return_II. The color scale represents the BC particle number concentration.

Figure 9 shows the comparison of air pollutants between field measurements on the Yangtze River and the nearest official monitoring site in the coastal cities passed through. With the consistency of the mass concentrations of $PM_{2.5}$, which are contributed by the complex sources and chemical reactions, and the behaviour of a relatively long residence time in the atmosphere that favour regional /long-range transport (Zhang et al., 2008, Ding et al., 2013), it was evident that the regional transport was one of the major sources of the air pollutants in the Yangtze River region, which was consistent with the previous studies indicating that $PM_{2.5}$ pollution has become more frequent on a large regional scale in China (Fu et al., 2008, Hu et al., 2014).

CO and NO_2 concentrations in the coastal cities were mostly higher than that on the river, implying that vehicular emissions in urban areas largely contributed to the air pollution in urban areas (Cheng et al., 2006, Hu et al., 2014). For the period of depart_I, SO_2 concentrations on the river were higher than that in the coastal cities, which might be mainly caused by the local sources dominated by the shipping emissions. However, higher SO_2 concentrations in the coastal cities during the other periods were observed, which

corresponded to the higher NO_2 concentrations. Due to the characteristics of the relatively short-life in the atmosphere (van der A et al., 2017), the high NO_2 and SO_2 concentrations in the coastal cities were probably contributed by the same local sources, which could be power generation plant, industrial emissions, coal combustion and biomass burning (Chen and Xu, 2010). Although NO_x and SO_2 were contributed by more and less the same sources, i.e. the burning of the fossil fuel and coal, the main difference is that traffic is a much more important source for NO_x. Further research of the emission factors of air pollutants is needed to understand how much the air pollution is contributed by the individual sources and its impact on the air quality in a large regional scale.

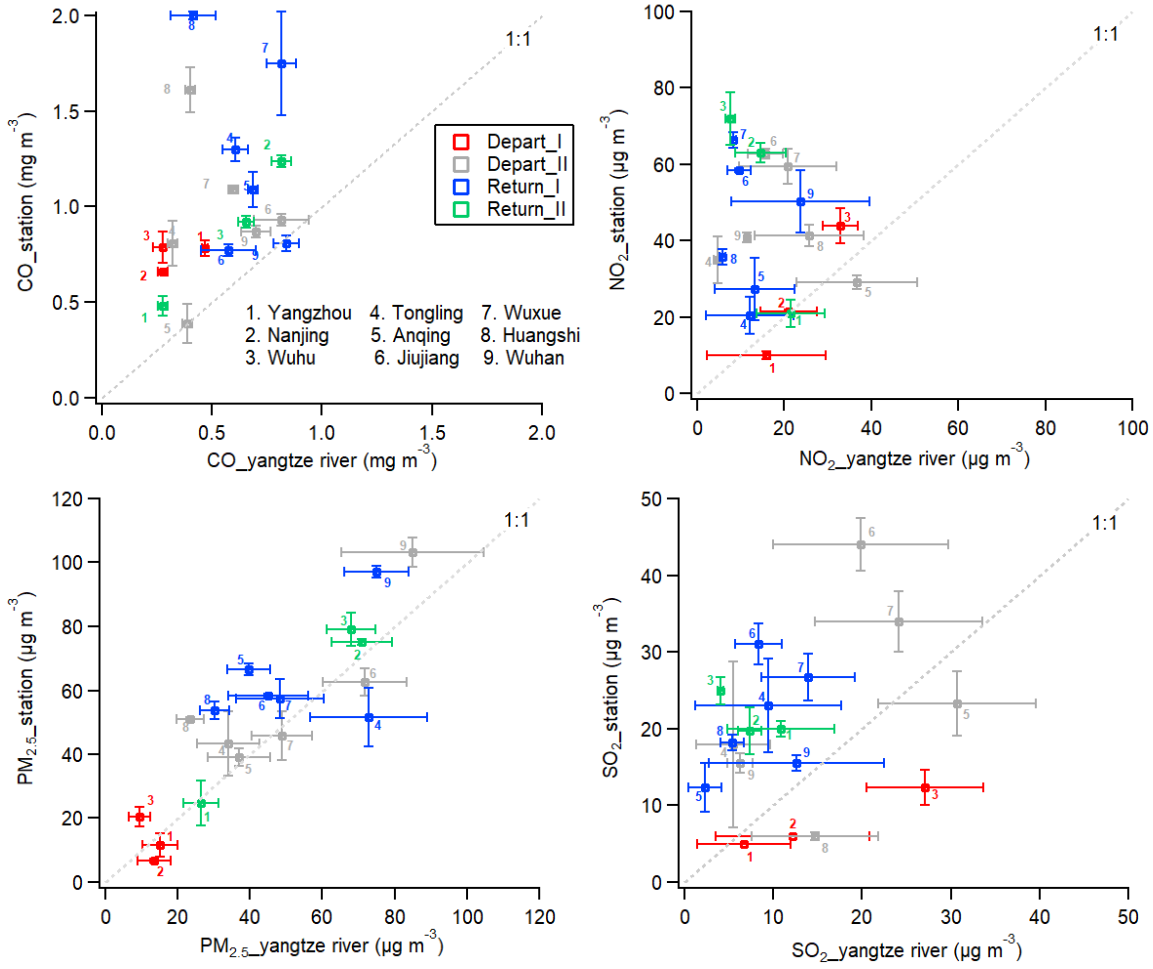

Figure 9. Comparison of the pollutants between the measurements and the monitoring site passed through.

Conclusion

It was the first time to continuously measure rBC, PM_1, $PM_{2.5}$ and gaseous pollutants (NO_x, SO_2, CO, O_3) along the Yangtze River between Shanghai and Wuhan from 21st November and 4th December 2015. The measured data of the round cruising was split into four section according to the boundary of the terrain. Three major source clusters were identified during the cruising based on the air masses obtained from the back trajectory analysis: local sources (including shipping emissions), easterly sources (cleaner air masses) and westerly sources (more polluted air masses).

During the depart_I, local sources were the main sources of air pollutants as the air masses mainly came from the cleaner ocean. The lowest rBC, PM_1, CO, SO_2 mass concentrations, MMD and coatings of rBC particles were observed, indicating the fresh emissions from the local sources and clean air masses from the ocean. However, the air pollutants during the rest of the three periods did not reveal significant characteristics of a certain source, as they were greatly contributed by westerly air masses coming from more polluted inland, which were likely to carry the pollutants originated by a variety of different sources.

Based on the threshold of NO_x concentration of 80 μg m^{-3} used to identify shipping emissions to be the dominating source, NO_x, SO_2, BC mass and number concentrations correlated well with each other during the depart_I, when shipping emissions was the dominating source, but not with CO and PM_1 due to the effect of the long-range transport and the longer lifetime in the atmosphere (Heinizenberg, 1989, Pfister et al., 2004). Moreover, fresh rBC particles, which were likely to be contributed by the shipping emissions, with much smaller core size of ~160 nm and thinner coatings of ~1.27 were also observed during the depart_I. However, rBC, for the other three periods imposed on the polluted background, showed larger core size and thicker coatings. It was found that the shipping emissions caused an increase of 5.9% in BC mass on the background, where the average rBC mass concentration was 1.54 ± 1.30 μg m^{-3}. However, the CO mass concentrations produced by shipping showed no increase in the background, implying that CO in the background were much higher than that from the shipping emissions. The rBC core size showed a consistent mode of ~180-220nm with a peak diameter of ~200nm at the background level, whereas a bimodal mode of rBC core size with an additional mode of ~120-180nm at high NO_x level was observed, indicating the shipping emissions considerably contributed to the rBC with this size range. Moreover, the rBC properties of the larger core size and thicker coating

dominating the background indicated that biomass burning and coal combustion were likely to be the dominant sources (Huang et al., 2012; Liu et al., 2014; Wang et al., 2016).

The comparison between the measured data on the YR and the nearest official monitoring sites in the coastal cities showed the identical $PM_{2.5}$ mass concentrations during the whole period, implying the regional/ longe-range transport was one of the major sources of the air pollutants in the YR region (Fu et al., 2008; Li et al., 2011; Hu et al., 2014). The higher CO and NO_2 mass concentrations in the coastal cities implied that traffic emissions in the cities greatly contributed to the air pollution. The results in this study showed that the regional transport greatly contributed to the rBC and its related gases. However, the specific sources could not be identified due to the same properties of rBC particles contributed by different sources. More work is needed to further investigate the complex sources in YR region and to obtain the contribution of the individual sources for the formulation of the mitigation strategy of the rBC.

Reference

AGRAWAL, H., EDEN, R., ZHANG, X., FINE, P. M., KATZENSTEIN, A., MILLER, J. W., OSPITAL, J., TEFFERA, S. & COCKER III, D. R. 2009. Primary particulate matter from ocean-going engines in the southern California air basin. *Environmental science & technology,* 43**,** 5398-5402.

BAUMGARDNER, D., POPOVICHEVA, O., ALLAN, J., BERNARDONI, V., CAO, J., CAVALLI, F., COZIC, J., DIAPOULI, E., ELEFTHERIADIS, K., GENBERG, P. J., GONZALEZ, C., GYSEL, M., JOHN, A., KIRCHSTETTER, T. W., KUHLBUSCH, T. A. J., LABORDE, M., LACK, D., MULLER, T., NIESSNER, R., PETZOLD, A., PIAZZALUNGA, A., PUTAUD, J. P., SCHWARZ, J., SHERIDAN, P., SUBRAMANIAN, R., SWIETLICKI, E., VALLI, G., VECCHI, R. & VIANA, M. 2012. Soot reference materials for instrument calibration and intercomparisons: a workshop summary with recommendations. *Atmos. Meas. Tech.,* 5**,** 1869- 1887.

BOND, T. C. & BERGSTROM, R. W. 2006. Light Absorption by Carbonaceous Particles: An Investigative Review. *Aerosol Sci. Technol.,* 40**,** 27-67.

BOND, T. C., DOHERTY, S. J., FAHEY, D., FORSTER, P., BERNTSEN, T., DEANGELO, B., FLANNER, M., GHAN, S., KÄRCHER, B. & KOCH, D. 2013. Bounding the role of black carbon in the climate system: A scientific assessment. *J. Geophys. Res.,* 118**,** 5380-5552.

BOND, T. C., STREETS, D. G., YARBER, K. F., NELSON, S. M., WOO, J. H. & KLIMONT, Z. 2004. A technology-based global inventory of black and organic carbon emissions from combustion. *J. Geophys. Res.,* 109.

CAPALDO, K., CORBETT, J. J., KASIBHATLA, P., FISCHBECK, P. & PANDIS, S. N. 1999. Effects of ship emissions on sulphur cycling and radiative climate forcing over the ocean. *Nature,* 400**,** 743.

CHEN, P., WANG, T., HU, X. & XIE, M. 2015. Chemical Mass Balance Source Apportionment of Size-Fractionated Particulate Matter in Nanjing, China. *Aerosol and Air Quality Research,* 15**,** 1855-1867.

CHENG, Y., LEE, S., HO, K., WANG, Y., CAO, J., CHOW, J. & WATSON, J. 2006. Black carbon measurement in a coastal area of south China. *Journal of geophysical research: atmospheres,* 111.

CORBETT, J. J., WINEBRAKE, J. J., GREEN, E. H., KASIBHATLA, P., EYRING, V. & LAUER, A. 2007. Mortality from ship emissions: a global assessment. *Environmental science & technology,* 41**,** 8512-8518.

DENG, J., WANG, T., LIU, L. & JIANG, F. 2010. Modeling heterogeneous chemical processes on aerosol surface. *Particuology,* 8**,** 308-318.

DING, A., HUANG, X., NIE, W., SUN, J., KERMINEN, V. M., PETÄJÄ, T., SU, H., CHENG, Y., YANG, X. Q. & WANG, M. 2016. Enhanced haze pollution by black carbon in megacities in China. *Geophysical Research Letters,* 43**,** 2873-2879.

DING, A. J., FU, C. B., YANG, X. Q., SUN, J. N., PETÄJÄ, T., KERMINEN, V. M., WANG, T., XIE, Y., HERRMANN, E., ZHENG, L. F., NIE, W., LIU, Q., WEI, X. L. & KULMALA, M. 2013. Intense atmospheric pollution modifies weather: a case of mixed biomass burning with fossil fuel combustion pollution in eastern China. *Atmos. Chem. Phys.,* 13**,** 10545-10554.

ENDRESEN, Ø., SØRGÅRD, E., SUNDET, J. K., DALSØREN, S. B., ISAKSEN, I. S., BERGLEN, T. F. & GRAVIR, G. 2003. Emission from international sea transportation and environmental impact. *Journal of Geophysical Research: Atmospheres,* 108.

FAN, Q., ZHANG, Y., MA, W., MA, H., FENG, J., YU, Q., YANG, X., NG, S. K. W., FU, Q. & CHEN, L. 2016. Spatial and Seasonal Dynamics of Ship Emissions over the Yangtze River Delta and East China Sea and Their Potential Environmental Influence. *Environmental Science & Technology,* 50**,** 1322-1329.

FU, Q., ZHUANG, G., WANG, J., XU, C., HUANG, K., LI, J., HOU, B., LU, T. & STREETS, D. G. 2008. Mechanism of formation of the heaviest pollution episode ever recorded in the Yangtze River Delta, China. *Atmospheric Environment,* 42**,** 2023-2036.

FU, X., WANG, S., ZHAO, B., XING, J., CHENG, Z., LIU, H. & HAO, J. 2013. Emission inventory of primary pollutants and chemical speciation in 2010 for the Yangtze River Delta region, China. *Atmospheric Environment,* 70**,** 39-50.

FUGLESTVEDT, J., BERNTSEN, T., EYRING, V., ISAKSEN, I., LEE, D. S. & SAUSEN, R. 2009. Shipping Emissions: From Cooling to Warming of Climate and Reducing Impacts on Health. ACS Publications.

GAO, R. S., SCHWARZ, J. P., KELLY, K. K., FAHEY, D. W., WATTS, L. A., THOMPSON, T. L., SPACKMAN, J. R., SLOWIK, J. G., CROSS, E. S., HAN, J. H., DAVIDOVITS, P., ONASCH, T. B. & WORSNOP, D. R. 2007. A Novel Method for Estimating Light-Scattering Properties of Soot Aerosols Using a Modified Single-Particle Soot Photometer. *Aerosol Science and Technology,* 41**,** 125-135.

GONG, X., ZHANG, C., CHEN, H., NIZKORODOV, S. A., CHEN, J. & YANG, X. 2016. Size distribution and mixing state of black carbon particles during a heavy air pollution episode in Shanghai. *Atmos. Chem. Phys.,* 16**,** 5399-5411.

GRAHAME, T. J., KLEMM, R. & SCHLESINGER, R. B. 2014. Public health and components of particulate matter: The changing assessment of black carbon. *Journal of the Air & Waste Management Association,* 64**,** 620-660.

HEINIZENBERG, J. 1989. Fine particles in the global troposphere. *Tellus,* 418**,** 149-160.

HELLEBUST, S., ALLANIC, A., O'CONNOR, I., JOURDAN, C., HEALY, D. & SODEAU, J. 2010. Sources of ambient concentrations and chemical composition of PM2. 5–0.1 in Cork Harbour, Ireland. *Atmospheric Research,* 95**,** 136-149.

HU, J., WANG, Y., YING, Q. & ZHANG, H. 2014. Spatial and temporal variability of PM2.5 and PM10 over the North China Plain and the Yangtze River Delta, China. *Atmospheric Environment,* 95**,** 598-609.

HUA, Y., CHENG, Z., WANG, S., JIANG, J., CHEN, D., CAI, S., FU, X., FU, Q., CHEN, C., XU, B. & YU, J. 2015. Characteristics and source apportionment of PM2.5 during a fall heavy haze episode in the Yangtze River Delta of China. *Atmospheric Environment,* 123, Part B**,** 380-391.

HUANG, C., CHEN, C. H., LI, L., CHENG, Z., WANG, H. L., HUANG, H. Y., STREETS, D. G., WANG, Y. J., ZHANG, G. F. & CHEN, Y. R. 2011. Emission inventory of anthropogenic air pollutants and VOC species in the Yangtze River Delta region, China. *Atmos. Chem. Phys.,* 11**,** 4105-4120.

HUANG, X.-F., SUN, T.-L., ZENG, L.-W., YU, G.-H. & LUAN, S.-J. 2012a. Black carbon aerosol characterization in a coastal city in South China using a single particle soot photometer. *Atmospheric Environment,* 51**,** 21-28.

HUANG, X.-F., XUE, L., TIAN, X.-D., SHAO, W.-W., SUN, T.-L., GONG, Z.-H., JU, W.-W., JIANG, B., HU, M. & HE, L.-Y. 2013. Highly time-resolved carbonaceous aerosol characterization in Yangtze River Delta of China: Composition, mixing state and secondary formation. *Atmospheric Environment,* 64**,** 200-207.

HUANG, X. F., HE, L. Y., XUE, L., SUN, T. L., ZENG, L. W., GONG, Z. H., HU, M. & ZHU, T. 2012b. Highly time-resolved chemical characterization of atmospheric fine particles during 2010 Shanghai World Expo. *Atmos. Chem. Phys.,* 12**,** 4897-4907.

ISAKSON, J., PERSSON, T. & LINDGREN, E. S. 2001. Identification and assessment of ship emissions and their effects in the harbour of Göteborg, Sweden. *Atmospheric Environment,* 35**,** 3659-3666.

KANDLIKAR, M., REYNOLDS, C. C. & GRIESHOP, A. P. 2009. A perspective paper on black carbon mitigation as a response to climate change. *Copenhagen: Copenhagen Consensus Center*.

KIM, E. & HOPKE, P. K. 2008. Source characterization of ambient fine particles at multiple sites in the Seattle area. *Atmospheric Environment,* 42**,** 6047-6056.

KOELMANS, A. A., JONKER, M. T., CORNELISSEN, G., BUCHELI, T. D., VAN NOORT, P. C. & GUSTAFSSON, Ö. 2006. Black carbon: the reverse of its dark side. *Chemosphere,* 63**,** 365-377.

LABORDE, M., SCHNAITER, M., LINKE, C., SAATHOFF, H., NAUMANN, K. H., MÖHLER, O., BERLENZ, S., WAGNER, U., TAYLOR, J. W., LIU, D., FLYNN, M., ALLAN, J. D., COE, H., HEIMERL, K., DAHLKÖTTER, F., WEINZIERL, B., WOLLNY, A. G., ZANATTA, M., COZIC, J., LAJ, P., HITZENBERGER, R., SCHWARZ, J. P. & GYSEL, M. 2012. Single Particle Soot Photometer intercomparison at the AIDA chamber. *Atmos. Meas. Tech.,* 5**,** 3077-3097.

LI, B., ZHANG, J., ZHAO, Y., YUAN, S., ZHAO, Q., SHEN, G. & WU, H. 2015. Seasonal variation of urban carbonaceous aerosols in a typical city Nanjing in Yangtze River Delta, China. *Atmospheric Environment,* 106**,** 223-231.

LI, M., ZHANG, Q., KUROKAWA, J.-I., WOO, J.-H., HE, K., LU, Z., OHARA, T., SONG, Y., STREETS, D. G. & CARMICHAEL, G. R. 2017. MIX: a mosaic Asian anthropogenic emission inventory under the international collaboration framework of the MICS-Asia and HTAP. *Atmospheric Chemistry and Physics,* 17**,** 935.

LIU, D., ALLAN, J. D., YOUNG, D. E., COE, H., BEDDOWS, D., FLEMING, Z. L., FLYNN, M. J., GALLAGHER, M. W., HARRISON, R. M., LEE, J., PREVOT, A. S. H., TAYLOR, J. W., YIN, J., WILLIAMS, P. I. & ZOTTER, P. 2014. Size distribution, mixing state and source apportionment of black carbon aerosol in London during wintertime. *Atmos. Chem. Phys.,* 14**,** 10061-10084.

LIU, D., FLYNN, M., GYSEL, M., TARGINO, A., CRAWFORD, I., BOWER, K., CHOULARTON, T., JURÁNYI, Z., STEINBACHER, M., HÜGLIN, C., CURTIUS, J., KAMPUS, M., PETZOLD, A., WEINGARTNER, E., BALTENSPERGER, U. & COE, H. 2010. Single particle characterization of black carbon aerosols at a tropospheric alpine site in Switzerland. *Atmos. Chem. Phys.,* 10**,** 7389-7407.

LIU, H., FU, M., JIN, X., SHANG, Y., SHINDELL, D., FALUVEGI, G., SHINDELL, C. & HE, K. 2016. Health and climate impacts of ocean-going vessels in East Asia. *Nature climate change,* 6**,** 1037.

LOHMANN, U. & FEICHTER, J. 2005. Global indirect aerosol effects: a review. *Atmospheric Chemistry and Physics,* 5**,** 715-737.

LONATI, G., CERNUSCHI, S. & SIDI, S. 2010. Air quality impact assessment of at-berth ship emissions: Case-study for the project of a new freight port. *Science of the Total Environment,* 409**,** 192-200.

LU, G., BROOK, J. R., RAMI ALFARRA, M., ANLAUF, K., RICHARD LEAITCH, W., SHARMA, S., WANG, D., WORSNOP, D. R. & PHINNEY, L. 2006. Identification and characterization of inland ship plumes over Vancouver, BC. *Atmospheric Environment,* 40**,** 2767-2782.

MATTHIAS, V., BEWERSDORFF, I., AULINGER, A. & QUANTE, M. 2010. The contribution of ship emissions to air pollution in the North Sea regions. *Environmental Pollution,* 158**,** 2241-2250.

MCMEEKING, G. R., HAMBURGER, T., LIU, D., FLYNN, M., MORGAN, W. T., NORTHWAY, M., HIGHWOOD, E. J., KREJCI, R., ALLAN, J. D., MINIKIN, A. & COE, H. 2010. Black carbon measurements in the boundary layer over western and northern Europe. *Atmos. Chem. Phys.,* 10**,** 9393-9414.

MOT 2015. The Statistical Report on China's Traffic in 2015 (in Chinese).

MOTEKI, N., KONDO, Y. & NAKAMURA, S.-I. 2010. Method to measure refractive indices of small nonspherical particles: Application to black carbon particles. *J. Aerosol Sci.,* 41**,** 513-521.

PETZOLD, A., OGREN, J. A., FIEBIG, M., LAJ, P., LI, S. M., BALTENSPERGER, U., HOLZER-POPP, T., KINNE, S., PAPPALARDO, G., SUGIMOTO, N., WEHRLI, C., WIEDENSOHLER, A. & ZHANG, X. Y. 2013. Recommendations for reporting "black carbon" measurements. *Atmos. Chem. Phys.,* 13**,** 8365-8379.

PFISTER, G., PETRON, G., EMMONS, L., GILLE, J., EDWARDS, D., LAMARQUE, J. F., ATTIE, J. L., GRANIER, C. & NOVELLI, P. 2004. Evaluation of CO simulations and the analysis of the CO budget for Europe. *Journal of Geophysical Research: Atmospheres,* 109.

RAMANATHAN, V. & CARMICHAEL, G. 2008. Global and regional climate changes due to black carbon. *Nature geoscience,* 1**,** 221.

RIEMER, N., WEST, M., ZAVERI, R. & EASTER, R. 2010. Estimating black carbon aging time-scales with a particle-resolved aerosol model. *Journal of Aerosol Science,* 41**,** 143-158.

ROSE, D., GUNTHE, S., SU, H., GARLAND, R., YANG, H., BERGHOF, M., CHENG, Y., WEHNER, B., ACHTERT, P. & NOWAK, A. 2011. Cloud condensation nuclei in polluted air and biomass burning smoke near the mega-city Guangzhou, China–Part 2: Size-resolved aerosol chemical composition, diurnal cycles, and externally mixed weakly CCN-active soot particles. *Atmospheric Chemistry and Physics,* 11**,** 2817-2836.

SHRESTHA, G., TRAINA, S. J. & SWANSTON, C. W. 2010. Black carbon's properties and role in the environment: a comprehensive review. *Sustainability,* 2**,** 294-320.

TAYLOR, J., ALLAN, J., LIU, D., FLYNN, M., WEBER, R., ZHANG, X., LEFER, B., GROSSBERG, N., FLYNN, J. & COE, H. 2015. Assessment of the sensitivity of core/shell parameters derived using the single-particle soot photometer to density and refractive index. *Atmos. Meas. Tech.,* 8**,** 1701-1718.

VAN DER A, R. J., MIJLING, B., DING, J., KOUKOULI, M. E., LIU, F., LI, Q., MAO, H. & THEYS, N. 2017. Cleaning up the air: effectiveness of air quality policy for SO2 and NOx emissions in China. *Atmos. Chem. Phys.,* 17**,** 1775-1789.

WANG, C., CORBETT, J. J. & FIRESTONE, J. 2007. Improving spatial representation of global ship emissions inventories. *Environmental Science & Technology,* 42**,** 193-199.

WANG, J., GE, X., CHEN, Y., SHEN, Y., ZHANG, Q., SUN, Y., XU, J., GE, S., YU, H. & CHEN, M. 2016. Highly time-resolved urban aerosol characteristics during springtime in Yangtze River Delta, China: insights from soot particle aerosol mass spectrometry. *Atmos. Chem. Phys.,* 16**,** 9109-9127.

WANG, Q., HUANG, R., ZHAO, Z., CAO, J., NI, H., TIE, X., ZHU, C., SHEN, Z., WANG, M. & DAI, W. 2017. Effects of photochemical oxidation on the mixing state and light absorption of black carbon in the urban atmosphere of China. *Environmental Research Letters,* 12**,** 044012.

WANG, Q., LIU, S., ZHOU, Y., CAO, J., HAN, Y., NI, H., ZHANG, N. & HUANG, R. 2015. Characteristics of black carbon aerosol during the Chinese Lunar Year and weekdays in Xi'an, China. *Atmosphere,* 6**,** 195-208.

WANG, S. & HAO, J. 2012. Air quality management in China: Issues, challenges, and options. *Journal of Environmental Sciences,* 24**,** 2-13.

WANG, Z., LI, J., WANG, Z., YANG, W., TANG, X., GE, B., YAN, P., ZHU, L., CHEN, X., CHEN, H., WAND, W., LI, J., LIU, B., WANG, X., WAND, W., ZHAO, Y., LU, N. & SU, D. 2014. Modeling study of regional severe hazes over mid-eastern China in January 2013 and its implications on pollution prevention and control. *Science China Earth Sciences,* 57**,** 3-13.

XU, H.-H., PU, J.-J., HE, J., LIU, J., QI, B. & DU, R.-G. 2016. Characteristics of Atmospheric Compositions in the Background Area of Yangtze River Delta during Heavy Air Pollution Episode. *Advances in Meteorology,* 2016**,** 13.

ZHANG, Y., YANG, X., BROWN, R., YANG, L., MORAWSKA, L., RISTOVSKI, Z., FU, Q. & HUANG, C. 2017. Shipping emissions and their impacts on air quality in China. *Science of The Total Environment,* 581-582**,** 186-198.

ZHANG, Y. H., HU, M., ZHONG, L. J., WIEDENSOHLER, A., LIU, S. C., ANDREAE, M. O., WANG, W. & FAN, S. J. 2008. Regional Integrated Experiments on Air Quality over Pearl River Delta 2004 (PRIDE-PRD2004): Overview. *Atmospheric Environment,* 42**,** 6157-6173.

ZHAO, M., ZHANG, Y., MA, W., FU, Q., YANG, X., LI, C., ZHOU, B., YU, Q. & CHEN, L. 2013. Characteristics and ship traffic source identification of air pollutants in China's largest port. *Atmospheric Environment,* 64**,** 277-286.

SUPPORTING INFORMATION

Characterising Black Carbon and gaseous pollutants on the Yangtze River in Eastern China.

Y. Ting[1], D. Liu[1], W.T. Morgan[1], J.D. Allan[1,2], H. Coe[1], C. Li[3], X. Wang[3], X. Ye[3] and J. Chen[3]

[1]School of Earth and Environmental Science, University of Manchester, Manchester, UK

[2]National Centre for Atmospheric Science, Manchester, UK

[3]Department of Environmental Science & Engineering, Fudan University, Shanghai, China

Correspondence: Hugh Coe (hugh.coe@manchester.ac.uk)

Table S1. The average BC mass concentration, number concentration, core MMD and coating thickness, and average mass concentrations of NO_x, SO_2, CO, O_3 and PM_1 for the background (NO_x < 80 μg m^{-3}) and high polluted periods (NO_x > 80 μg m^{-3}).

	Depart_I		Depart_II		Return_I		Return_II	
	NOx > 80.2	< 80.2	> 80.2	< 80.2	> 80.2	< 80.2	> 80.2	< 80.2
NO_x (μg m^{-3})	200.35 ± 88.94	27.04 ± 24.51	163.28 ± 53.15	20.34 ± 18.04	195.51 ± 53.85	21.38 ± 17.66	113.82 ± 21.24	25.56 ± 20.63
SO_2 (μg m^{-3})	21.34 ± 10.82	2.60 ± 2.65	26.63 ± 11.01	7.04 ± 5.31	19.75 ± 8.35	6.58 ± 5.14	17.98 ± 12.97	11.10 ± 8.12
MMD (nm)	159.71 ± 26.52	182.71 ± 24.85	180.04 ± 20.89	196.69 ± 10.71	184.54 ± 15.46	198.67 ± 76.0	191.17 ± 18.13	205.81 ± 7.29
BC number (cm^{-3})	1819.85 ± 1376.03	869.44 ± 577.03	1926.14 ± 1108.43	964.72 ± 537.20	2770.74 ± 1405.85	1199.37 ± 438.78	1565.02 ± 1335.89	754.89 ± 290.24
Coating thickness (D_p/D_c)	1.27 ± 0.05	1.28 ± 0.06	1.41 ± 0.06	1.44 ± 0.07	1.56 ± 0.12	1.45 ± 0.10	1.25 ± 0.05	1.34 ± 0.13
BC mass (μg m^{-3})	2.01 ± 1.56	1.54 ± 1.30	2.54 ± 0.90	2.04 ± 1.24	4.46 ± 1.66	2.83 ± 0.93	2.48 ± 1.45	1.78 ± 0.65
CO (μg m^{-3})	262.48 ± 120.88	322.36 ± 131.13	505.12 ± 198.24	445.70 ± 176.68	784.86 ± 244.05	627.91 ± 244.11	507.10 ± 231.06	544.34 ± 217.31
PM_1 (μg m^{-3})	20.76 ± 8.62	13.31 ± 3.09	37.66 ± 13.63	35.16 ± 11.64	51.95 ± 24.90	35.55 ± 11.74	26.55 ± 4.50	27.29 ± 7.46
O_3 (μg m^{-3})	31.84 ± 18.41	54.89 ± 19.96	39.85 ± 19.20	41.15 ± 21.06	14.75 ± 10.04	26.81 ± 13.08	36.02 ± 12.86	37.94 ± 19.66

Table S2. The increased percentage of the pollutants caused by more localized sources on the Yangtze River. (Unit: %)

	Depart_I	Depart_II	Return_I	Return_II
NO_x	1036.5	1010.9	1144.1	648.5
SO_2	721.0	278.1	200.2	62.0
MMD	-19.4	-10.0	-5.5	-5.4
BC number	112.8	115.8	92.0	17.5
Coating thickness (D_p/D_c)	-2.2	-1.7	11.3	-4.2
BC mass	5.9	29.6	51.2	5.6
CO	-20.4	5.0	48.5	-35.6
PM_1	50	0	62.5	4
O_3	-43.8	22.3	-50.2	-0.9

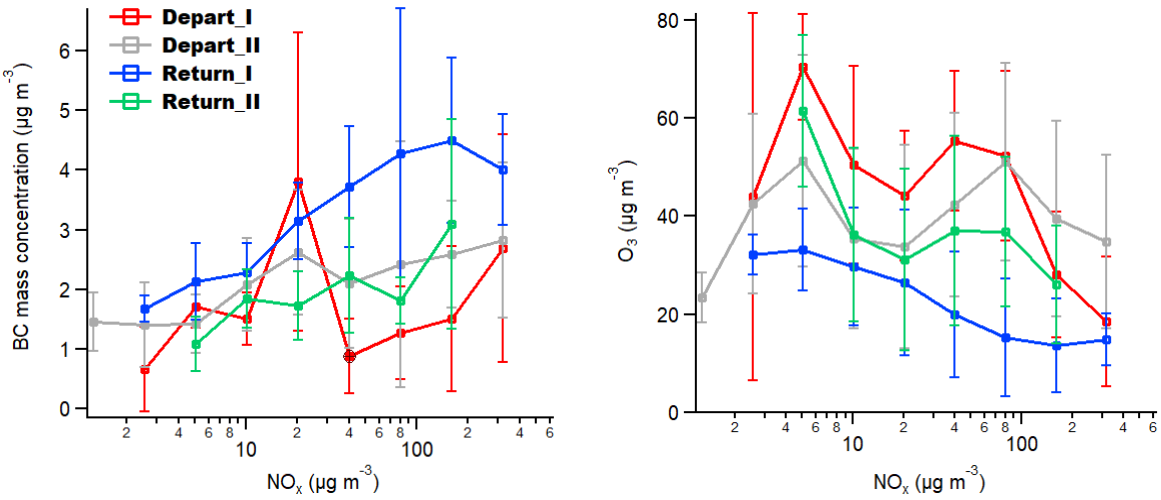

Figure S1. O_3 and BC mass concentrations as a function of NOx. Red line: depart_I, grey line: depart_II, blue line: return_I, green line: depart_II.

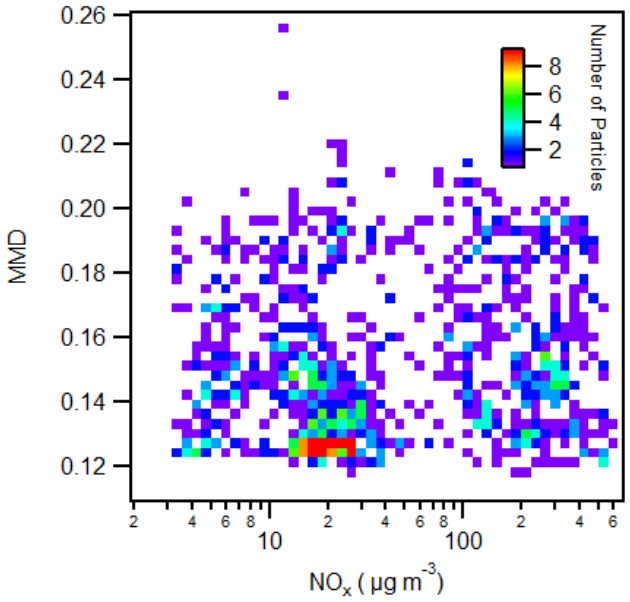

Figure S2. The distribution of BC core MMD as a function of NO_x for the period of the SO_2 plumes.

4.3 Paper III: The Mixing State of Carbonaceous Aerosols of Primary Emissions from 'Improved' African Cookstoves

Authors: Yuchieh Ting, Edward J.S. Mitchell, James D. Allan, Dantong Liu, Dominick V. Spracklen, Alan Williams, Jenny M. Jones, Amanda R. Lea-Langton, Gordon McFiggans, Hugh Coe

Journal: Environmental Science and Technology, 2018, *52* (17), pp 10134–10143

Publication date: August 1, 2018

Research highlights:

- On-line measurements of the solid fuel combustion emissions from cookstoves were performed in a laboratory-based study.
- Organic matter (OM) and black carbon (BC) emissions from different types of solid fuel and stoves were measured by AMS and SP2. Interactions between OM and BC according to modified combustion efficient were investigated.
- The source profile of BC for residential solid fuel burning was generated, which can be used in most of the models to more accurately assess the impact of BC on the regional and global climate.

Author's contribution: I led the data analysis and manuscript preparation.

Co-author contributions: Mitchell and Allan participated in the setup of the instrumentation and the laboratory-based work. Spracklen, Williams, Jones and Lea-Langton provided useful comments for addressing the comments from the reviewers. Liu, Allan, McFiggans and Coe assisted in preparation of the manuscript.

Environmental Science & Technology

Article

Cite This: Environ. Sci. Technol. 2018, 52, 10134−10143

pubs.acs.org/est

Mixing State of Carbonaceous Aerosols of Primary Emissions from "Improved" African Cookstoves

Yuchieh Ting,[†] Edward J. S. Mitchell,[‡] James D. Allan,[*,†,§] Dantong Liu,[†] Dominick V. Spracklen,[∥] Alan Williams,[‡] Jenny M. Jones,[‡] Amanda R. Lea-Langton,[⊥] Gordon McFiggans,[†] and Hugh Coe[†]

[†]School of Earth and Environmental Science, University of Manchester, Manchester M13 9PL, United Kingdom

[‡]School of Chemical and Process Engineering, University of Leeds, Leeds LS2 9JT, United Kingdom

[§]National Centre for Atmospheric Science, University of Manchester, Manchester M13 9PL, United Kingdom

[∥]School of Earth and Environment, University of Leeds, Leeds LS2 9JT, United Kingdom

[⊥]School of Mechanical, Aerospace and Civil Engineering, University of Manchester, Manchester M13 9PL, United Kingdom

Supporting Information

ABSTRACT: Designs of "improved" stoves are introduced recently to benefit the solid fuel consumption of cooking activities in developing countries, but the uncertainties concerning the combustion processes and particulate emissions remain poorly characterized. To help understand this, combustion in three examples of "improved" African cookstoves was investigated in the laboratory. A typical European heating stove was included for comparison purpose. Detailed aerosol emissions were studied in real-time with an Aerosol Mass Spectrometer and Single Particle Soot Photometer, to explore interactions between black carbon (BC) and organic carbon aerosols, which were parametrized according to modified combustion efficiency (MCE), a common metric used within the atmospheric emission community. Greater than 50% of the total organic matter (OM) was found in BC-containing particles when MCE was >0.95 for dry oak and coal fuels, whereas at lower MCE, over 80% of the total OM for most of the fuels existed in particles without detectable BC. When the OM mass fraction of total particulate matter (PM_1) > 0.9, the mass ratio of OM to refractory BC in BC-containing particles was about 2−3, but only ∼0.8 when OM mass fraction <0.9. These findings are not currently included in models and such information should be considered in the future emission scenarios.

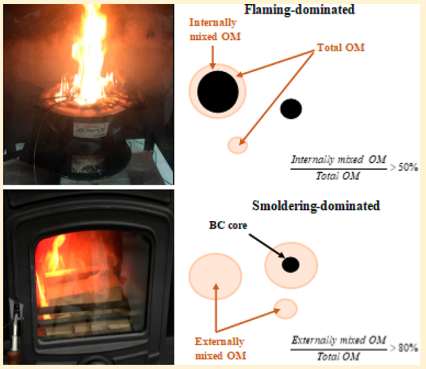

INTRODUCTION

Particulate emissions from the combustion of solid fuel, which is widely used for cooking and heating in developing countries, have severe impacts on human health, air quality, and climate.[1−4] For the year 2010, global burden of disease estimates showed that exposure to household air pollution from cooking resulted in approximately 4 million premature deaths,[5] with the most recent estimates from WHO reporting 4.3 million death for 2012.[6] Household air pollution is also a substantial contributor to outdoor air pollution-related deaths due to emissions into the ambient environment, responsible for around 0.4 million deaths (12%) of the total from ambient air pollution.[7]

Domestic combustion of solid fuels was estimated to contribute to approximate 30% and 70% of global BC and organic carbon (OC) emissions, respectively,[8] although there were big regional differences depending on the operating conditions such as fuel type, appliance type, and fuel loading, which can influence emission compositions considerably.[9−13] BC is the dominant form of light absorbing particulate matter and is estimated to be the most important anthropogenic contributor to instantaneous climate forcing after CO_2.[11] Co-emitted OM also affects the optical properties of emitted BC particles if the components are internally mixed, through coatings and lensing effects.[14−16]

The chemical composition of stove-related combustion emissions was found to vary widely and depend on the fuel type, source loading, and condition, all of which affect combustion conditions.[17−21] Further variations may be expected with the introduction of new technologies designed to reduce fuel consumption and emissions, where the improved combustion efficiency may change the character of the emissions, in addition to the quantity.

Although there have been a number of studies using real-time instrumentation to characterize solid fuel combustion emissions from heating and cooking stoves, most of them focused on particle number concentrations,[22−26] OM composition,[12,13,27−29] and the characterization of BC.[28,30−32] The information about real time emissions of BC and OM and

Received: January 25, 2018
Revised: July 27, 2018
Accepted: August 1, 2018
Published: August 1, 2018

Downloaded via UNIV OF MANCHESTER on September 11, 2018 at 13:41:26 (UTC).
See https://pubs.acs.org/sharingguidelines for options on how to legitimately share published articles.

© 2018 American Chemical Society

DOI: 10.1021/acs.est.8b00456
Environ. Sci. Technol. 2018, 52, 10134−10143

how they are mixed with each other is still lacking.[33,34] The absorption enhancement of BC particles is determined by the mixing state of BC and non-BC materials in a BC-containing particle[14,16,35,36] but this is still uncertain, particularly for solid fuel emissions, and is often largely simplified in models.[37,38] Thus, the unconstrained source profiles of solid fuel emissions limit the ability to accurately simulate the impacts on air quality and climate.[3] The relationship between the emissions from solid fuel combustion and combustion efficiency has been shown in a few studies, but many of the tests were conducted on more idealized and tightly constrained combustion conditions and hence were unable to replicate the diversity of emissions.[10,12,32]

The burning conditions and emissions of the stoves are highly variable and stove performance in the field can be quite different from that in the laboratory.[39−41] While integrated emissions are of use to inform inventories,[42−44] to better understand the exact nature of the emissions, it is important to make high time-resolution measurements of the entire process to have an insight into the evolution of the properties of the emissions. Furthermore, the use of the same type of online instrumentation for emissions and atmospheric measurements enables direct comparison of data sets. In this study, the chemical compositions of nonrefractory species in PM_1 were measured by a compact time-of-flight aerosol mass spectrometer (c-TOF-AMS), and the physical properties of refractory BC (rBC) particles were characterized by using a single particle soot photometer (SP2). The mixing state of rBC and coemitted OM components emitted from the cookstoves was reported and compared to those emitted from a UK heating stove, and their relationships to the MCE and the oxidation level of the emissions, which potentially affects the BC particles, were qualitatively provided for comparability to equivalent atmospheric measurements of air pollutants from wood combustion. To our knowledge, this is the first time to explore the mixing state between OM and BC from solid fuel combustion from both stove types as sources.

MATERIALS AND METHODS

Testing Facility and Combustion Experiments. A series of solid fuel combustion experiments was carried out in the test facility of the University of Leeds. The facility was modified for cookstove testing having been previously used for heating stoves testing.[45] Details of this facility, including the stoves, types of fuel used, and sampling configuration are in the Supporting Information (SI Figures S1 and S2, and Table S1). Three examples of cookstoves used in Africa that could be described as "improved" (better fuel efficiency and lower emissions compared to the traditional cookstoves, such as three stone fires) were used and are named here as Carbonzero,[46] Gyapa,[47] and Lucia.[48] For the sake of comparison, a modern U.K. heating stove[49] was also tested. It should be noted that cookstoves were tested with no cooking pot, which can have a large effect on performance by changing air flow and by quenching flames and combustion gases.

For each combustion experiment except for the Lucia stove, standard ZIP firelighters (http://www.zipfires.co.uk/product-range/fire-lighters/high-performance/) were used to ignite the fuel, which caused ignition of the firelighter immediately and pyrolysis of the solid fuel before consequent burning. Fuel was reloaded manually when the flame on the top of the burning fuel almost died out while the combustion process was ongoing, as would be performed during normal operation. The Lucia stove was a pyrolytic stove with a fundamentally different combustion mechanism. Fuel pellets are pyrolyzed and the resultant gases driven through an outer sheath before combustion at a ring of holes above the fuel bed. The pyrolysis and flow are maintained passively by the heat of the flame, and the initial ignition was provided by 9 g of liquid kerosene.

Different studies have the distinct definitions of the burning phases.[12,23,27,29,50] In this study, the burns for each stove can be qualitatively divided into several phases according to the observed variability of burning conditions and particulate emissions. Typically, these were (i) "fuel reloading", which started when fuel was reloaded on the glowing embers of the proceeding combustion cycle. This included the pyrolysis phase and lasted until BC and the modified combustion efficiency (MCE), calculated as $\Delta CO_2/(\Delta CO + \Delta CO_2)$, increased; (ii) "flaming-dominated", that followed the initial phase of fuel addition and lasted until the MCE and BC emissions dropped; (iii) "poor-burning", which was characterized by a lack of significant dominance in the OM and BC emissions with the fluctuation in MCE over several combustion cycles; (iv) "smoldering-dominated", that occurred only in the combustion cycle with charcoal and coal in this study, during this phase OM emissions were elevated with only nominal BC and little visible flame; and (v) "burn out", which was only observed significantly for the Lucia stove.

Instrumentation and Data Analysis. A cToF-AMS was used for the online measurement of submicron nonrefractory aerosol components, including OM, nitrate (NO_3^-), sulfate (SO_4^{2-}), ammonium (NH_4^+), and chloride (Cl^-). The operating modes of the AMS and detailed descriptions of the cToF-AMS can be found in other publications.[51,52] Details of the data processing and the correction of the mass spectra are in the SI.

The physical and optical properties of individual rBC particles were characterized by a SP2 manufactured by Droplet Measurement Technology (DMT). The operation and data analysis procedures of the SP2 used in these experiments have been described in McMeeking et al.[53] and Liu et al.[54] The SP2 uses incandescence induced by a 1064 nm active laser cavity to obtain rBC mass in individual particles which can be converted to a sphere-equivalent core diameter (Dc) by assuming a density of 1.8 g cm^{-3}.[55] This is done for the sake of comparison with other sizing instruments. A further estimate of overall size can also be provided by inspecting the scattering signal as the particle enters the laser beam, using the "leading edge only" method described by Liu et al.[56] and Taylor et al.[57] A core−shell Mie model was used, assuming a rBC core refractive index of 2.26−1.26i and a coating refractive index of 1.5 + 0i.[58] While it would have been preferable to derive refractive indexes specific to these aerosol, this was not possible with the equipment used here.

The SP2 data were used to estimate the mass of the non-BC material coating on the BC particles from the total volume of the BC particles divided by the total volume of the BC cores as measured within a given time period,[56] as expressed as eq 1. The non-BC material of a BC-containing particle is deemed to be mostly consisted of OM internally mixed with BC. The total organic mass internally mixed with BC in a given time period, OM_{BC}, can then be obtained using the bulk V_P/V_C by assuming the densities of OM and BC as expressed by eq 2:

DOI: 10.1021/acs.est.8b00456
Environ. Sci. Technol. 2018, 52, 10134−10143

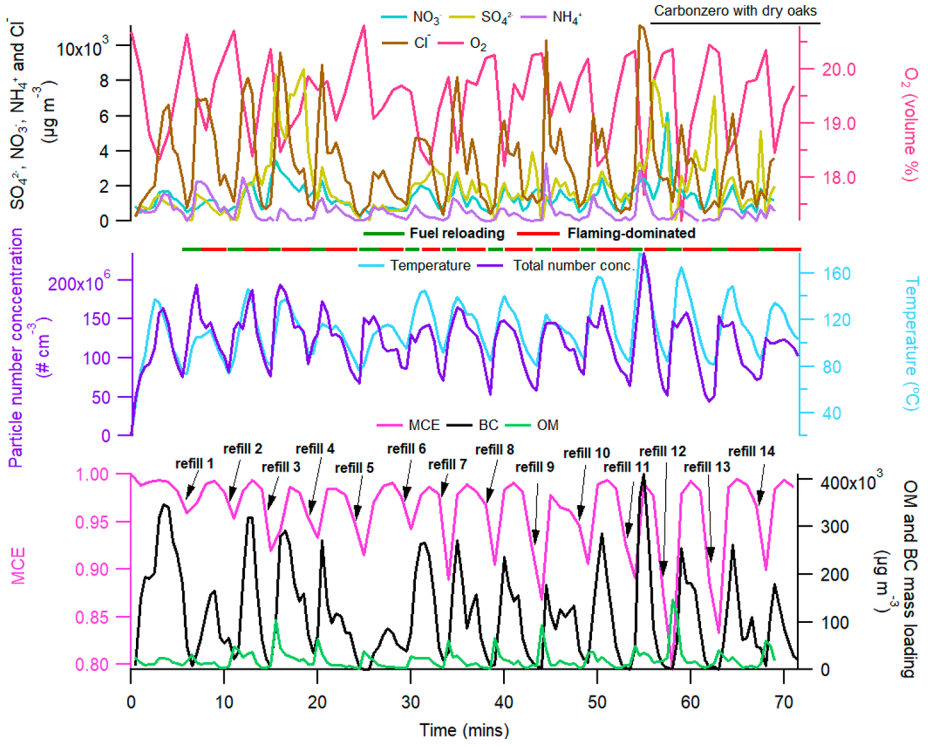

Figure 1. Time series of inorganic aerosol (SO_4^{2-}, NO_3^-, NH_4^+, and Cl^-) concentrations, oxygen volume concentrations, the particle number concentrations, temperature of the flue, modified combustion efficiency (MCE), OM, and BC mass concentrations for an experiment (in this case dry oak using Carbonzero stove), with the timing of refilling the fuels and an indication of the defined burning phases.

$$\frac{V_P}{V_C} = \left(\frac{\sum_i D_{P,i}^3}{\sum_i D_{C,i}^3}\right) \quad (1)$$

$$OM_{BC} = \frac{\left(\frac{V_P}{V_C} - 1\right)}{\rho_{BC}} \times \rho_{OM} \times \sum_i rBC_i \quad (2)$$

where ρ_{OM} and ρ_{BC} are the densities of OM and BC assumed to be 1.2 and 1.8 g cm^{-3}, respectively,[55,59] and $\sum_i rBC_i$ is the total mass of black carbon in a population of i particles, which we later term rBC_{bulk}. A fraction of particles with small BC cores and thin coatings may not be detected by the SP2, though this fraction of coating mass was of minor importance (~5−10%) considering the total coating mass. While it is noted that this method carries uncertainties relating to assumptions concerning shape, density, and refractive index, this still serves as a good comparative metric between stoves and fuels. The lower detection limit of the BC core size from the SP2 is a mass corresponding to around 60 nm diameter.[35] This precludes the ability to identify particles as completely BC-free, i.e., externally mixed with BC, since they can contain some fraction of rBC below the SP2 detection limit (<60 nm). As the mass of the BC emissions from charcoal combustion was too low, this approach was not applicable to the estimation of the coatings in the charcoal experiment.

Given that the AMS is able to detect total OM, the internally mixed OM fraction relative to total OM, denoted as F_{in}, can be obtained by eq 3:

$$F_{in} = \frac{OM_{BC}}{OM_{total}} \quad (3)$$

where OM_{BC} is the OM internally mixed with BC determined by the SP2 measurement, OM_{total} is the total OM measured by the AMS.

The number concentrations and size distribution of submicron particles were measured by a fast response differential mobility spectrometer (DMS500, Cambustion Ltd., Cambridge, U.K.). The soot calibration was performed using a bimodal agglomerate matrix to invert the data.[60] Gaseous emissions in the flue were measured by a Gasmet Dx-4000 Fourier Transform Infrared (FTIR) spectrometer (Temet Instruments OY, Finland) before the second stage dilution and by a Testo 340 analyzer (Testo INC, Lenzkirch, Germany) after the second stage dilution (Figure S1). A number of thermocouples were deployed to measure the temperatures of the flue gas and different positions of the firebox. Two Dekati dilutors (DI-1000, Dekati Ltd., Finland) were placed in series before the AMS and SP2 measurement, giving a third stage of dilution with compressed air (Figure S1). The dilution ratio was nominally set to 100, although this was subsequently found to vary as material collected on the first stage nozzle over the course of the experiment. Due to this and the uncontrolled nature of the dilution from the flue to the extraction tunnel, the dilution factor was derived by comparing the total particle volume derived by the DMS500 (from the flue) measurement and that obtained by the AMS and SP2 (after the two-stage dilutor) (Figure S3). This was applied to obtain the undiluted concentrations. To investigate the relationships between combustion conditions and emissions, the MCE was used to indicate the efficiency of the burn, in keeping with various atmospheric emission studies;[10,13,61−63] however, recent studies on the highly controlled combustion of small wood samples have suggested this may be overly simplistic,[32] as the pyrolysis emissions that occur prior to the

DOI: 10.1021/acs.est.8b00456
Environ. Sci. Technol. 2018, 52, 10134−10143

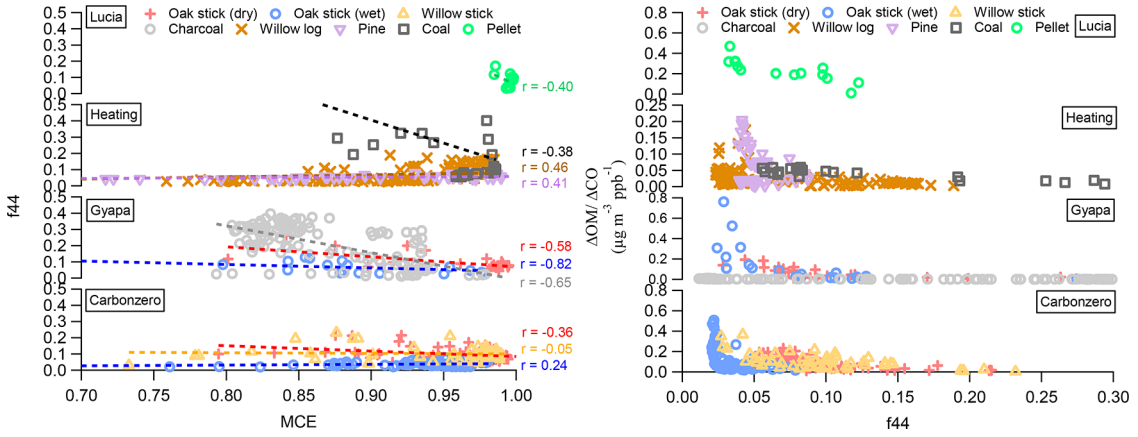

Figure 2. *f44* versus MCE for each combustion cycle (left panel). ΔOM/ΔCO versus *f44* for each combustion cycle (right panel).

local ignition of the fuel may be very significant. The temperature and oxygen measured in the flue were also used as references for combustion conditions. The data from all instruments were averaged to 1 min for the convenience of intercomparison between the different measurements.

The emission ratios (ER) of number concentration of particles with aerodynamic diameter less than 1 μm (PN_1), PM_1 (organics, inorganics and black carbon), OM and BC are normalized to excess CO (i.e., ERx = ΔX/ΔCO, X is the emitted species) to track the relative abundance of the species. The data were not used in this analysis if the OM or BC concentrations were lower than 0.04 μg m^{-3} as the low number included in the coating calculation introduced a large uncertainty. BC mass loadings from charcoal combustion emissions were below 0.04 μg m^{-3} for most of the time and are thus not included in the data analysis.

RESULTS

Real-Time Measurements Resolving Burning Cycle. Figure 1 shows an example of one experiment demonstrating the time series of emissions during burning phases with sequential addition of fuel. The other experiments are shown in SI Figure S4.

As Figure 1 shows, for each burning cycle, OM emissions peaked immediately after fuel addition, which in general correlated with a lower MCE and may be mainly from the pyrolysis process followed by the flaming-dominated phase with a high MCE, consistent with Haslett et al.[32] BC and inorganic particle components peaked at high MCE and temperature, and the MCE dropped each time the fuel refilled as more charcoal accumulated. The non-BC inorganic components (SO_4^{2-}, NO_3^-, and NH_4^+) only contributed to a small mass fraction of the total PM (~5−10%).

There were some differences in other combustion cycles, shown in Figure S4, depending on the fuel and stove used. In the charcoal combustion experiments, the smoldering phase continued through most of the burning cycle and gave dominant emissions of OM and minimum BC. The emissions from solid fuel combustion in the heating stove showed different features, and in most cases, it was not possible to distinguish the burning phases. With the pellet combustion using the Lucia stove, a high correlation between the OM and BC was observed, indicating that pyrolysis and flaming overlapped during the combustion cycle. In addition, the Lucia stove combustion showed a good performance with stable high MCE and produced a relatively lower proportion of OM compared to the others.

Measurements of the number size distribution of dry fuels show a bimodal distribution, whereas that of wet fuels was unimodal (Figure S5(a)). The two dry fuel modes may well arise from different burn phases. The average BC core size distribution are very consistent between the different burns (Figure S5(b)).

Figure S6 illustrates the general decreasing trend of OM mass fraction in total carbonaceous particles OM/(OM + BC) with increasing MCE for all combustions. Apart from the heating stove with coal and Gyapa with dry and wet oaks, the fraction of organic to total carbonaceous species was almost unity for MCE < 0.85. For most of the fuels (apart from pine), the OM fraction started to drop substantially when MCE > 0.85, reducing to around 0.1 when MCE was close to 1. This indicates that above a critical point of MCE, the combustion started to emit a significant amount of BC compared to OM, but below this MCE threshold the OM fraction tended to be higher for most of the fuels but also depended on the stove types. Considering all combustions, at a given MCE, a large variation in OM fraction was observed across the range of different stoves and fuels. This means a single parameter of OM fraction or MCE is unable to fully describe the burning phases in the real world. For this reason, this study uses the MCE as the reference parameter for emission characterization, but does not attempt to unambiguously identify burning phases.

Oxygenation of OM. The degree of oxygenation of OM, as indicated by the fraction of m/z 44 (CO_2^+) in the total organic mass spectra (*f44*),[64] was evaluated against MCE and the ER of OM. For the measurements of OM compositions at the source, changes in *f44* are more likely to reflect the effects of combustion processes rather than subsequent oxidation because of the short aging time involved. However, not only the combustion efficiency, but also the stove types, fuel species, and moisture content may cause the varying *f44*. The correlation between *f44* and MCE, shown in Figure 2 (left panel), appears to be highly dependent on both stove and fuel type. For the dry oak fuel in the Carbonzero and Gyapa cookstoves, the correlations between *f44* and MCE were negative (r = −0.36 and −0.58). However, for the wet oak in the Carbonzero cookstove, the positive correlation was weak (r = 0.24), whereas in the Gyapa stove, a high negative correlation (r = −0.82) was observed. For the combustion cycles in the heating stove, the relationship between *f44* and

DOI: 10.1021/acs.est.8b00456
Environ. Sci. Technol. 2018, 52, 10134−10143

MCE showed dependence on fuel type with a positive correlation for willow log and pine (r = 0.46 and 0.41, respectively), whereas a negative correlation was observed for coal (r = −0.38).

Despite the limited dependence upon the MCE, *f44* reveals a notable relationship with ΔOM/ΔCO over all fuel types. Figure 2 (right panel) shows a near exponential decrease in ΔOM/ΔCO with a wide range of *f44* from around 0.02 up to 0.30 depending on the stoves and fuel types. A range of ΔOM/ΔCO ratios exhibited an *f44* value lower than 0.05, while ΔOM/ΔCO does not exceed 0.20 when *f44* is greater than 0.05. The dry fuels tended to have a larger value of *f44* compared to wet fuels, indicating that the moisture content of fuel not only affect the magnitude of OM emissions but also the oxidation level of OM.

BC Core Size. Figure S7 shows the mass median diameter (MMD) of BC cores as a function of MCE for each experiment. The MMD of average BC mass size distribution for Carbonzero and Gyapa cookstoves show BC core MMD of 188.5 ± 13.6 and 155.1 ± 27.1 nm for dry oak and wet oak, respectively, and these values are independent of MCE (r < 0.1 and 0.4 for Carbonzero and Gyapa cookstoves, respectively). The dependence of MMD on MCE is only found in the heating stove, especially for coal combustion (r = 0.94). This suggests a relatively uniform BC core size for cookstove emissions. The difference of the dependence of MMD on MCE for cookstoves and heating stove may be due to the designs of the stoves, e.g., the heating stove burns fuels in a sealed combustion chamber, whereas the cookstoves are open, thus the residence time of combustion gases in the heating stove may be longer than that in cookstoves, which may cause more significant coagulation of particles in the chamber of the heating stove.

The moisture of fuels only slightly affected the BC core size, such as the MMD of dry oak and willow stick (180.5 ± 18.1 nm), which was slightly larger than that of wet oak (∼160 nm) emissions (p-value <0.001). The coal-emitted BC had the largest and widest range of BC core size (223.8 ± 53.8 nm), and its core MMD was strongly correlated with MCE. This may be consistent with the highly positive correlation between the emission ratios of BC and MCE observed for coal, which may result in the strongest self-coagulation effect of BC for coal combustion. BC particles from the heating stove with coal combustion were mostly emitted when MCE > 0.95, so the averaged MMD ≈ 244 nm at MCE > 0.95 was representative for the majority of BC mass from coal combustion. For the Lucia stove, the BC core MMD was ∼190 nm with high MCE, though MMD was ∼100 nm with a minor contribution of total emitted BC mass.

OM Internally and Externally Mixed with BC-Containing Particles. The coatings on BC are mainly composed of OM, as sulfate and nitrate only accounted for less than 8% of total mass. Figure S8 shows F_{in} as a function of OM/(OM + BC) and MCE. Except for wet oak, F_{in} shows a significant decrease with OM/(OM+BC) from 0.02 to 0.40 for different fuel types, as shown in Figure S8(a). When OM/(OM + BC) exceeded 0.40, most BC-containing particles comprised less than 40% of the total OM except for a few particles with more than 40% of the total OM. With increasing MCE, F_{in} increased from almost no OM internally mixed with the BC (F_{in} = 0) to nearly all OM coated on BC particles (F_{in} = 1), as shown in Figure S8(b). When MCE was larger than 0.95, a wide range of F_{in} from about 0.1 up to 1 was observed. The positive correlation between F_{in} and MCE implies that during efficient burning, the OM emissions are mostly mixed with high BC emissions. Conversely during periods of inefficient burning when OM emissions are high and there is little BC, nearly all the OM is externally mixed with BC particles. A further comparison was performed with the BC coating measurement (see below) to validate the measurement of OM mixed with BC.

Figure 3 reveals the average F_{in} separated into high (>0.95) and low (<0.95) MCE periods. More than half of the OM was

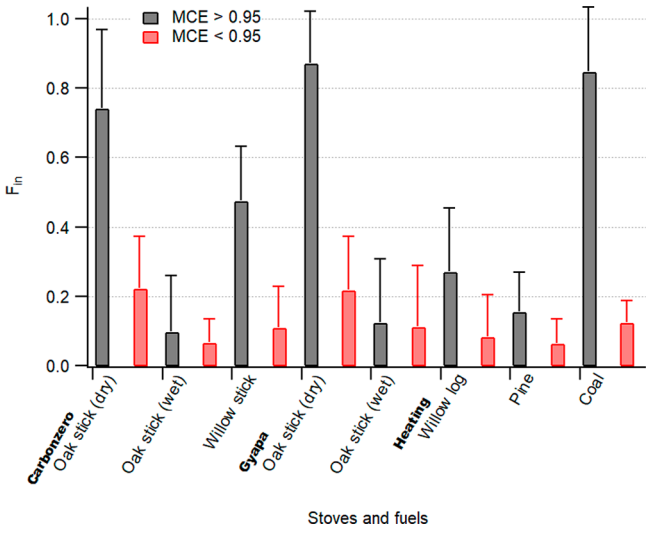

Figure 3. Average ratios of internally mixed OM to total OM (F_{in}) for each stove and fuel type for MCE > 0.95 and MCE < 0.95. The Lucia stove with pellet fuel is not shown here as the OM was completely coated on the BC particles due to the high BC mass loading and efficient combustion. The error bar shows the standard deviation.

coated on the BC particles when MCE > 0.95 during the dry oak and coal experiments, whereas approximately 20% and 12% of the total OM was coated on the BC when MCE < 0.95 for dry oak and coal, respectively. The fuel with higher moisture tended to have a lower F_{in} at the same MCE compared to drier fuel due to the higher OM emission factors. In the heating stove, the coal combustion has higher F_{in} due to the higher BC mass emission ratio.

Mixing State of BC. While the OM_{BC}/rBC_{bulk} ratio does not show consistent correlation with MCE in this study, a certain correlation between the ratio and the OM fraction (OM/(OM + BC)) has been observed, as shown in Figure 4 (left panel). The ratios were mostly lower than 1 when the OM fraction was lower than 0.9; the ratios started to significantly increase when the OM fraction was larger than 0.9, e.g., reaching up to 5 in the cookstoves and 10 for the heating stove. Emissions from the wet fuel had a higher OM fraction than the dry fuel and thus exhibited a higher OM_{BC}/rBC_{bulk} ratio. For an OM fraction larger than 0.9, the OM_{BC}/rBC_{bulk} ratio for the heating stove was much higher than that in the cookstoves, which may be because the dynamics in the enclosed combustion space facilitated the coating process of BC with a higher local concentration of organic vapor.

Figure 4 (right panel) shows that regardless of stoves and fuels, the *f44*/*f43* (*f43*, which the dominant organic ion is $C_2H_3O^+$, denotes the fraction of m/z 43 in the total organic mass spectra) increased with decreased OM_{BC}/rBC_{bulk} ratios in all cases except for the Lucia stove. When the OM_{BC}/rBC_{bulk}

DOI: 10.1021/acs.est.8b00456
Environ. Sci. Technol. 2018, 52, 10134−10143

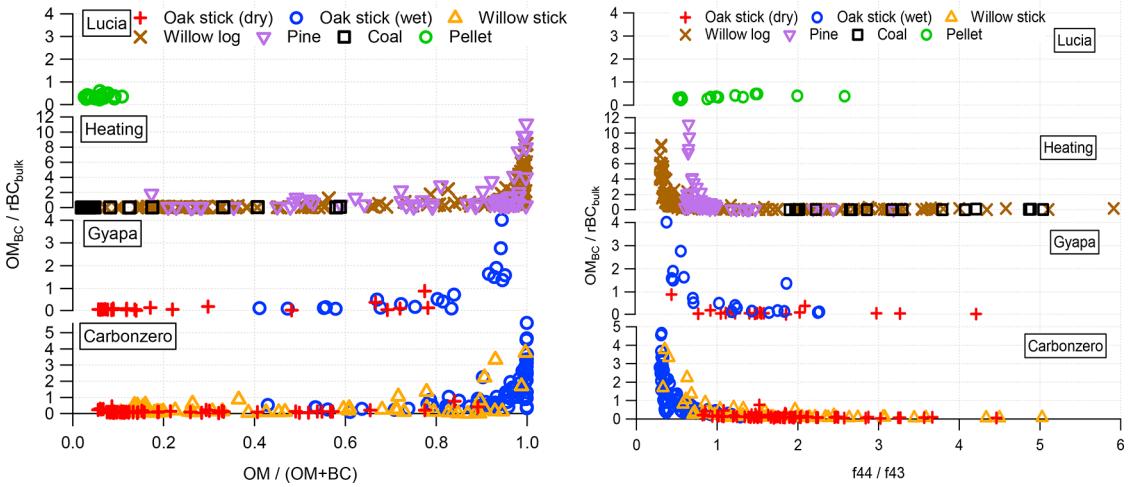

Figure 4. OM_{BC}/rBC_{bulk} as a function of the OM/(OM + BC) ratios (left panel). The OM_{BC}/rBC_{bulk} as a function of *f44*/*f43* ratios (right panel).

ratios were lower than 1, there was a wide range of *f44*/*f43* (larger than 1) and the high OM_{BC}/rBC_{bulk} ratios only arose when *f44*/*f43* < 1. As the combustion process for the Lucia stove is different from the others, which have a pyrolysis stage during the combustion cycle, the OM_{BC}/rBC_{bulk} ratio of the Lucia stove emissions shows near constant of below 1 and no relationship with either OM fraction or *f44*/*f43*, suggesting no enhancement of light absorption results from the BC-containing particles emitted from this kind of stove.

DISCUSSION

With the combination of the AMS and SP2 online measurements, the temporal variability and mixing state of OM and BC over a course of combustion has been observed during different burning phases using a range of cook stoves and fuels. The results here consistently showed an overlap among the phases under the operating conditions unlike those that were observed during more controlled combustion revealing distinguishable burning phases.[31,63] Many studies have used MCE to identify burning phases,[62,63] however the results here show that while trends exist, it is not a complete description, partly because the pyrolysis stage emits large amounts of OM but is not directly represented by a combustion metric.[32]

These experiments found that more complete combustion emitted less OM that was also more oxidized. While *m*/*z* 44 is widely used as an indicator of secondary or aged OM, this shows that primary OM from wood burning exhibits a significant range of *f44*.[27,32] For all the cookstoves tested, negative correlation between *f44* and MCE is shown in Figure 2, consistent with the findings of Weimer et al.[9] In contrast, positive correlations between *f44* and MCE from log and pine combustion were observed in a multifuel heating stove, which may be due to the dominance of hydrocarbon fragments at high MCE. In spite of the difference between *f44* and MCE among the fuel and stove types,[61] a near exponential decline in ΔOM/ΔCO with increased *f44* has been observed in most of the combustion cycles. This is consistent with previous studies where during high MCE, the sufficient supply of oxygen will lead to more oxidation of organics.[61,65] At lower MCEs, the OM emissions were high and the OM was mainly composed of less-oxygenated species, but this differed among fuel types.[61] The relationship between ΔOM/ΔCO and *f44* does show some inconsistency, including the contrasting thresholds between regimes of high and low OM production between different type of fuels and stoves. This is again likely related to the fact that, as found by Haslett et al.,[32] the large emissions from preignition pyrolysis are not related directly to MCE.

The source profile of BC is fundamental to any detailed model when estimating its atmospheric lifetime because mixing state influences loss processes such as in-cloud scavenging. Many global models assume the same BC size for all types of residential solid fuel sources,[37,66] which is consistent with the cookstove data here. However, caution must be taken, as for example, for emissions from the heating stove, the BC core size was dependent on the MCE. The BC concentrations in the heating stove may be important in determining its core size because of the closed combustion chamber. This indicates that combustion in the heating stove during high MCE tends to produce particles with larger BC core size than during low MCE. In general, the intense combustion impedes the efficient transport of oxygen into the flame zone,[67] resulting in the formation of large amounts of small rBC particles. However, since the coagulation rate of particles is approximately proportional to the square of their concentrations,[68] the growth of rBC particles was consequently rapid under high concentrations. In combination with that, the small rBC monomers might easily form agglomerates during high MCE driven by the internally mixed OM when the temperature of flame drops, corresponding to a larger fraction of OM internally mixed with BC. This process may take place in seconds, which occurs too fast to be achievable in ambient measurements.

The mixing state of BC and OM is frequently assumed to be uniform from all sources,[38] and BC is assumed completely externally or internally mixed with coemitted species.[38,69−71] Moreover, the mixing state of BC in models largely relies on the organic carbon (OC)/ elemental carbon (EC)[72] or OM/BC ratio and assumes that all of the coemitted primary OM is internally or externally mixed with BC instantaneously after emission,[70,71] which is likely to overestimate or underestimate the effect of BC-containing particles on radiative forcing.[70] There are numerous different fuels and stoves in actual use emitting BC and OM in potentially different mixing state. However, for the complicated dynamics in burning processes presented, the amount of primary OM emitted as internally or externally mixed with BC shows a certain relationship with MCE. Among combustion events in this study, it was found

DOI: 10.1021/acs.est.8b00456
Environ. Sci. Technol. 2018, 52, 10134−10143

that between 20% and 100% of OM particles contained significant rBC when MCE > 0.95, which should be considered to be internally mixed with BC. When MCE < 0.95, only about 20% of the total OM was internally mixed with BC. These ratios might be useful for improving the accuracy of models in estimating the impact of the mixing state of BC and OM on climate radiative forcing for the regions where the solid fuel combustion from the cookstoves dominates the contributions of carbonaceous species.

The extent to which optical absorption from BC can be theoretically enhanced via lensing, is determined by the mass ratio of non-BC and rBC within a single particle.[35] Liu et al.[35] found that when this ratio was greater than 3, particles displayed an absorption enhancement (E_{abs}) of BC. Our results show a certain consistency that when the OM fraction (OM/(OM + BC)) < 0.9, our bulk OM_{BC}/rBC_{bulk} measurement was less than 1 meaning the BC may have not been significantly coated, so would not result in an absorption enhancement. When the OM fraction >0.9, we found OM_{BC}/rBC_{bulk} was often >3, meaning there is more likely to be a BC absorption enhancement from solid fuel combustion. An OM fraction of 0.9 may therefore be used as a threshold value in models to determine whether the absorption enhancement of BC from solid fuel burning will occur or not. The extent to which the absorption is enhanced also depends on the specific fuel type and stove design. The BC emitted from a cookstove may have a lower E_{abs} compared to the heating stove due to the lower OM_{BC}/rBC_{bulk} ratios. In addition to the effect of the amount of the OM emissions, the oxidation level of OM could also be an indicator of the magnitude of the OM_{BC}/rBC_{bulk} based on *f44*/*f43*, which is related to the volatility of oxygenated organic aerosol (OOA).[73] As the non-BC materials in the BC-containing particles mainly comprise OOA,[74] the consistency in the negative correlation between OM_{BC}/rBC_{bulk} and *f44*/*f43* ratios among the fuels suggests that the internally mixed OM is likely to be less oxidized and more semivolatile (low *f44*/*f43*) for those thickly coated BC, consistent with a large fraction of OM being less volatile when OM emission was high (Figure 2).

The correlation of the OM fraction and *f44*/*f43* with OM_{BC}/rBC_{bulk} ratios derived in this study indicates that the ratio of OM_{BC} and rBC_{bulk} from solid fuel emissions depends not only on the OM fraction but also on the oxygenation level of OM. Our results will help to assess the benefits of reduction in BC from cookstoves and so aid mitigation strategies in the future. While this study provides new insight into the combustion processes, we should stress that the results should be treated as indicative for use in models and more authoritative data will require more work, specifically repeat experiments with other fuel types, stove designs and with a more explicit simulation of cooking activity (e.g., inclusion of a cooking pot).

■ ASSOCIATED CONTENT

Supporting Information

The Supporting Information is available free of charge on the ACS Publications website at DOI: 10.1021/acs.est.8b00456.

Additional details of the sampling configuration; the correction for the silicon tubing contamination; table of emission ratios; figures of images of cookstoves; real-time data of dilution factors and emissions of all combustion cycles; total particle number size distribution; BC particle number and mass size distribution; and F_{in} as a function of MCE (PDF)

■ AUTHOR INFORMATION

Corresponding Author

* E-mail: James.Allan@manchester.ac.uk. Phone: +44 (0)161 306 8532.

ORCID

Yuchieh Ting: 0000-0002-3604-8060
James D. Allan: 0000-0001-6492-4876
Alan Williams: 0000-0002-9841-3203

Notes

The authors declare no competing financial interest.

■ ACKNOWLEDGMENTS

This work has been funded through an EPSRC Pump Priming Grant for Global Challenge Research (grant no. 109602).

■ REFERENCES

(1) Dickau, M.; Olfert, J.; Stettler, M. E. J.; Boies, A.; Momenimovahed, A.; Thomson, K.; Smallwood, G.; Johnson, M. Methodology for quantifying the volatile mixing state of an aerosol. *Aerosol Sci. Technol.* **2016**, *50* (8), 759−772.

(2) Lelieveld, J.; Evans, J. S.; Fnais, M.; Giannadaki, D.; Pozzer, A. The contribution of outdoor air pollution sources to premature mortality on a global scale. *Nature* **2015**, *525* (7569), 367−371.

(3) Kodros, J. K.; Scott, C. E.; Farina, S. C.; Lee, Y. H.; L'Orange, C.; Volckens, J.; Pierce, J. R. Uncertainties in global aerosols and climate effects due to biofuel emissions. *Atmos. Chem. Phys.* **2015**, *15* (15), 8577−8596.

(4) Butt, E. W.; Rap, A.; Schmidt, A.; Scott, C. E.; Pringle, K. J.; Reddington, C. L.; Richards, N. A. D.; Woodhouse, M. T.; Ramirez-Villegas, J.; Yang, H.; Vakkari, V.; Stone, E. A.; Rupakheti, M.; Praveen, P. S.; van Zyl, P. G.; Beukes, J. P.; Josipovic, M.; Mitchell, E. J. S.; Sallu, S. M.; Forster, P. M.; Spracklen, D. V. The impact of residential combustion emissions on atmospheric aerosol, human health, and climate. *Atmos. Chem. Phys.* **2016**, *16* (2), 873−905.

(5) Lim, S. S.; Vos, T.; Flaxman, A. D.; Danaei, G.; Shibuya, K.; Adair-Rohani, H.; AlMazroa, M. A.; Amann, M.; Anderson, H. R.; Andrews, K. G.; Aryee, M.; Atkinson, C.; Bacchus, L. J.; Bahalim, A. N.; Balakrishnan, K.; Balmes, J.; Barker-Collo, S.; Baxter, A.; Bell, M. L.; Blore, J. D.; Blyth, F.; Bonner, C.; Borges, G.; Bourne, R.; Boussinesq, M.; Brauer, M.; Brooks, P.; Bruce, N. G.; Brunekreef, B.; Bryan-Hancock, C.; Bucello, C.; Buchbinder, R.; Bull, F.; Burnett, R. T.; Byers, T. E.; Calabria, B.; Carapetis, J.; Carnahan, E.; Chafe, Z.; Charlson, F.; Chen, H.; Chen, J. S.; Cheng, A. T.-A.; Child, J. C.; Cohen, A.; Colson, K. E.; Cowie, B. C.; Darby, S.; Darling, S.; Davis, A.; Degenhardt, L.; Dentener, F.; Des Jarlais, D. C.; Devries, K.; Dherani, M.; Ding, E. L.; Dorsey, E. R.; Driscoll, T.; Edmond, K.; Ali, S. E.; Engell, R. E.; Erwin, P. J.; Fahimi, S.; Falder, G.; Farzadfar, F.; Ferrari, A.; Finucane, M. M.; Flaxman, S.; Fowkes, F. G. R.; Freedman, G.; Freeman, M. K.; Gakidou, E.; Ghosh, S.; Giovannucci, E.; Gmel, G.; Graham, K.; Grainger, R.; Grant, B.; Gunnell, D.; Gutierrez, H. R.; Hall, W.; Hoek, H. W.; Hogan, A.; Hosgood, H. D.; Hoy, D.; Hu, H.; Hubbell, B. J.; Hutchings, S. J.; Ibeanusi, S. E.; Jacklyn, G. L.; Jasrasaria, R.; Jonas, J. B.; Kan, H.; Kanis, J. A.; Kassebaum, N.; Kawakami, N.; Khang, Y.-H.; Khatibzadeh, S.; Khoo, J.-P.; Kok, C.; Laden, F.; Lalloo, R.; Lan, Q.; Lathlean, T.; Leasher, J. L.; Leigh, J.; Li, Y.; Lin, J. K.; Lipshultz, S. E.; London, S.; Lozano, R.; Lu, Y.; Mak, J.; Malekzadeh, R.; Mallinger, L.; Marcenes, W.; March, L.; Marks, R.; Martin, R.; McGale, P.; McGrath, J.; Mehta, S.; Memish, Z. A.; Mensah, G. A.; Merriman, T. R.; Micha, R.; Michaud, C.; Mishra, V.; Hanafiah, K. M.; Mokdad, A. A.; Morawska, L.; Mozaffarian, D.; Murphy, T.; Naghavi, M.; Neal, B.; Nelson, P. K.; Nolla, J. M.; Norman, R.; Olives, C.; Omer, S. B.; Orchard, J.; Osborne, R.; Ostro, B.; Page, A.; Pandey, K. D.; Parry, C. D. H.;

DOI: 10.1021/acs.est.8b00456
Environ. Sci. Technol. 2018, 52, 10134−10143

Passmore, E.; Patra, J.; Pearce, N.; Pelizzari, P. M.; Petzold, M.; Phillips, M. R.; Pope, D.; Pope, C. A.; Powles, J.; Rao, M.; Razavi, H.; Rehfuess, E. A.; Rehm, J. T.; Ritz, B.; Rivara, F. P.; Roberts, T.; Robinson, C.; Rodriguez-Portales, J. A.; Romieu, I.; Room, R.; Rosenfeld, L. C.; Roy, A.; Rushton, L.; Salomon, J. A.; Sampson, U.; Sanchez-Riera, L.; Sanman, E.; Sapkota, A.; Seedat, S.; Shi, P.; Shield, K.; Shivakoti, R.; Singh, G. M.; Sleet, D. A.; Smith, E.; Smith, K. R.; Stapelberg, N. J. C.; Steenland, K.; Stöckl, H.; Stovner, L. J.; Straif, K.; Straney, L.; Thurston, G. D.; Tran, J. H.; Van Dingenen, R.; van Donkelaar, A.; Veerman, J. L.; Vijayakumar, L.; Weintraub, R.; Weissman, M. M.; White, R. A.; Whiteford, H.; Wiersma, S. T.; Wilkinson, J. D.; Williams, H. C.; Williams, W.; Wilson, N.; Woolf, A. D.; Yip, P.; Zielinski, J. M.; Lopez, A. D.; Murray, C. J. L.; Ezzati, M. A comparative risk assessment of burden of disease and injury attributable to 67 risk factors and risk factor clusters in 21 regions, 1990−2010: a systematic analysis for the Global Burden of Disease Study 2010. *Lancet* **2012**, *380* (9859), 2224−2260.

(6) WHO. WHO Guidelines for Indoor Air Quality: Household Fuel Combustion. World Health Organization: Geneva, Switzerland. 2014.

(7) Smith, K. R.; Bruce, N.; Balakrishnan, K.; Adair-Rohani, H.; Balmes, J.; Chafe, Z.; Dherani, M.; Hosgood, H. D.; Mehta, S.; Pope, D. Millions dead: how do we know and what does it mean? Methods used in the comparative risk assessment of household air pollution. *Annu. Rev. Public Health* **2014**, *35*, 185−206.

(8) Bond, T. C.; Streets, D. G.; Yarber, K. F.; Nelson, S. M.; Woo, J. H.; Klimont, Z. A technology-based global inventory of black and organic carbon emissions from combustion. *J. Geophys. Res.* **2004**, *109* (D14), D14203.

(9) Weimer, S.; Alfarra, M.; Schreiber, D.; Mohr, M.; Prévôt, A.; Baltensperger, U. Organic aerosol mass spectral signatures from wood-burning emissions: Influence of burning conditions and wood type. *J. Geophys. Res.* **2008**, *113* (D10), D10304.

(10) Jetter, J.; Zhao, Y.; Smith, K. R.; Khan, B.; Yelverton, T.; DeCarlo, P.; Hays, M. D. Pollutant Emissions and Energy Efficiency under Controlled Conditions for Household Biomass Cookstoves and Implications for Metrics Useful in Setting International Test Standards. *Environ. Sci. Technol.* **2012**, *46* (19), 10827−10834.

(11) Bond, T. C.; Doherty, S. J.; Fahey, D.; Forster, P.; Berntsen, T.; DeAngelo, B.; Flanner, M.; Ghan, S.; Kärcher, B.; Koch, D. Bounding the role of black carbon in the climate system: A scientific assessment. *J. Geophys. Res.* **2013**, *118* (11), 5380−5552.

(12) Elsasser, M.; Busch, C.; Orasche, J.; Schön, C.; Hartmann, H.; Schnelle-Kreis, J.; Zimmermann, R. Dynamic changes of the aerosol composition and concentration during different burning phases of wood combustion. *Energy Fuels* **2013**, *27* (8), 4959−4968.

(13) Eriksson, A. C.; Nordin, E. Z.; Nyström, R.; Pettersson, E.; Swietlicki, E.; Bergvall, C.; Westerholm, R.; Boman, C.; Pagels, J. H. Particulate PAH Emissions from Residential Biomass Combustion: Time-Resolved Analysis with Aerosol Mass Spectrometry. *Environ. Sci. Technol.* **2014**, *48* (12), 7143−7150.

(14) Liu, S.; Aiken, A. C.; Gorkowski, K.; Dubey, M. K.; Cappa, C. D.; Williams, L. R.; Herndon, S. C.; Massoli, P.; Fortner, E. C.; Chhabra, P. S.; Brooks, W. A.; Onasch, T. B.; Jayne, J. T.; Worsnop, D. R.; China, S.; Sharma, N.; Mazzoleni, C.; Xu, L.; Ng, N. L.; Liu, D.; Allan, J. D.; Lee, J. D.; Fleming, Z. L.; Mohr, C.; Zotter, P.; Szidat, S.; Prevot, A. S. H. Enhanced light absorption by mixed source black and brown carbon particles in UK winter. *Nat. Commun.* **2015**, *6*, 8435−8435.

(15) Saliba, G.; Subramanian, R.; Saleh, R.; Ahern, A. T.; Lipsky, E. M.; Tasoglou, A.; Sullivan, R. C.; Bhandari, J.; Mazzoleni, C.; Robinson, A. L. Optical properties of black carbon in cookstove emissions coated with secondary organic aerosols: Measurements and modeling. *Aerosol Sci. Technol.* **2016**, *50* (11), 1264−1276.

(16) Flato, G.; Marotzke, J.; Abiodun, B.; Braconnot, P.; Chou, S. C.; Collins, W. J.; Cox, P.; Driouech, F.; Emori, S.; Eyring, V. Evaluation of Climate Models. In: Climate Change 2013: The Physical Science Basis. Contribution of Working Group I to the Fifth Assessment Report of the Intergovernmental Panel on Climate Change. *Climate Change 2013* **2013**, *5*, 741−866.

(17) Venkataraman, C.; Sagar, A. D.; Habib, G.; Lam, N.; Smith, K. R. The Indian National Initiative for Advanced Biomass Cookstoves: The benefits of clean combustion. *Energy Sustainable Dev.* **2010**, *14* (2), 63−72.

(18) Gonçalves, C.; Alves, C.; Evtyugina, M.; Mirante, F.; Pio, C.; Caseiro, A.; Schmidl, C.; Bauer, H.; Carvalho, F. Characterisation of PM10 emissions from woodstove combustion of common woods grown in Portugal. *Atmos. Environ.* **2010**, *44* (35), 4474−4480.

(19) Pettersson, E.; Boman, C.; Westerholm, R.; Boström, D.; Nordin, A. Stove Performance and Emission Characteristics in Residential Wood Log and Pellet Combustion, Part 2: Wood Stove. *Energy Fuels* **2011**, *25* (1), 315−323.

(20) Vicente, E. D.; Duarte, M. A.; Calvo, A. I.; Nunes, T. F.; Tarelho, L. A. C.; Custódio, D.; Colombi, C.; Gianelle, V.; Sanchez de la Campa, A.; Alves, C. A. Influence of operating conditions on chemical composition of particulate matter emissions from residential combustion. *Atmos. Res.* **2015**, *166*, 92−100.

(21) Nyström, R.; Lindgren, R.; Avagyan, R.; Westerholm, R.; Lundstedt, S.; Boman, C. Influence of Wood Species and Burning Conditions on Particle Emission Characteristics in a Residential Wood Stove. *Energy Fuels* **2017**, *31* (5), 5514−5524.

(22) Johansson, L. S.; Tullin, C.; Leckner, B.; Sjövall, P. Particle emissions from biomass combustion in small combustors. *Biomass Bioenergy* **2003**, *25* (4), 435−446.

(23) Pagels, J.; Dutcher, D. D.; Stolzenburg, M. R.; McMurry, P. H.; Gälli, M. E.; Gross, D. S. Fine-particle emissions from solid biofuel combustion studied with single-particle mass spectrometry: Identification of markers for organics, soot, and ash components. *J. Geophys. Res.* **2013**, *118* (2), 859−870.

(24) Shen, G.; Gaddam, C. K.; Ebersviller, S. M.; Vander Wal, R. L.; Williams, C.; Faircloth, J. W.; Jetter, J. J.; Hays, M. D. A Laboratory Comparison of Emission Factors, Number Size Distributions, and Morphology of Ultrafine Particles from 11 Different Household Cookstove-Fuel Systems. *Environ. Sci. Technol.* **2017**, *51* (11), 6522−6532.

(25) Hansen, J.; Sato, M.; Ruedy, R.; Kharecha, P.; Lacis, A.; Miller, R.; Nazarenko, L.; Lo, K.; Schmidt, G. A.; Russell, G.; Aleinov, I.; Bauer, S.; Baum, E.; Cairns, B.; Canuto, V.; Chandler, M.; Cheng, Y.; Cohen, A.; Del Genio, A.; Faluvegi, G.; Fleming, E.; Friend, A.; Hall, T.; Jackman, C.; Jonas, J.; Kelley, M.; Kiang, N. Y.; Koch, D.; Labow, G.; Lerner, J.; Menon, S.; Novakov, T.; Oinas, V.; Perlwitz, J.; Perlwitz, J.; Rind, D.; Romanou, A.; Schmunk, R.; Shindell, D.; Stone, P.; Sun, S.; Streets, D.; Tausnev, N.; Thresher, D.; Unger, N.; Yao, M.; Zhang, S. Climate simulations for 1880−2003 with GISS modelE. *Climate Dynamics* **2007**, *29* (7), 661−696.

(26) L'Orange, C.; Volckens, J.; DeFoort, M. Influence of stove type and cooking pot temperature on particulate matter emissions from biomass cook stoves. *Energy Sustainable Dev.* **2012**, *16* (4), 448−455.

(27) Heringa, M. F.; DeCarlo, P. F.; Chirico, R.; Lauber, A.; Doberer, A.; Good, J.; Nussbaumer, T.; Keller, A.; Burtscher, H.; Richard, A.; Miljevic, B.; Prevot, A. S. H.; Baltensperger, U. Time-Resolved Characterization of Primary Emissions from Residential Wood Combustion Appliances. *Environ. Sci. Technol.* **2012**, *46* (20), 11418−11425.

(28) Just, B.; Rogak, S.; Kandlikar, M. Characterization of Ultrafine Particulate Matter from Traditional and Improved Biomass Cookstoves. *Environ. Sci. Technol.* **2013**, *47* (7), 3506−3512.

(29) Kortelainen, A.; Joutsensaari, J.; Hao, L.; Leskinen, J.; Tiitta, P.; Jaatinen, A.; Miettinen, P.; Sippula, O.; Torvela, T.; Tissari, J.; Jokiniemi, J.; Worsnop, D. R.; Smith, J. N.; Laaksonen, A.; Virtanen, A. Real-Time Chemical Composition Analysis of Particulate Emissions from Woodchip Combustion. *Energy Fuels* **2015**, *29* (2), 1143−1150.

(30) Kar, A.; Rehman, I. H.; Burney, J.; Puppala, S. P.; Suresh, R.; Singh, L.; Singh, V. K.; Ahmed, T.; Ramanathan, N.; Ramanathan, V. Real-Time Assessment of Black Carbon Pollution in Indian

DOI: 10.1021/acs.est.8b00456
Environ. Sci. Technol. 2018, 52, 10134−10143

Households Due to Traditional and Improved Biomass Cookstoves. *Environ. Sci. Technol.* **2012**, *46* (5), 2993−3000.
(31) Bruns, E. A.; Krapf, M.; Orasche, J.; Huang, Y.; Zimmermann, R.; Drinovec, L.; Močnik, G.; El-Haddad, I.; Slowik, J. G.; Dommen, J.; Baltensperger, U.; Prévôt, A. S. H. Characterization of primary and secondary wood combustion products generated under different burner loads. *Atmos. Chem. Phys.* **2015**, *15* (5), 2825−2841.
(32) Haslett, S. L.; Thomas, J. C.; Morgan, W. T.; Hadden, R.; Liu, D.; Allan, J. D.; Williams, P. I.; Keita, S.; Liousse, C.; Coe, H. Highly controlled, reproducible measurements of aerosol emissions from combustion of a common African biofuel source. *Atmos. Chem. Phys.* **2018**, *18* (1), 385−403.
(33) Nielsen, I. E.; Eriksson, A. C.; Lindgren, R.; Martinsson, J.; Nyström, R.; Nordin, E. Z.; Sadiktsis, I.; Boman, C.; Nøjgaard, J. K.; Pagels, J. Time-resolved analysis of particle emissions from residential biomass combustion − Emissions of refractory black carbon, PAHs and organic tracers. *Atmos. Environ.* **2017**, *165*, 179−190.
(34) Martinsson, J.; Eriksson, A.; Nielsen, I. E.; Malmborg, V. B.; Ahlberg, E.; Andersen, C.; Lindgren, R.; Nystrom, R.; Nordin, E.; Brune, W. Impacts of combustion conditions and photochemical processing on the light absorption of biomass combustion aerosol. *Environ. Sci. Technol.* **2015**, *49* (24), 14663−14671.
(35) Liu, D.; Whitehead, J.; Alfarra, M. R.; Reyes-Villegas, E.; Spracklen, D. V.; Reddington, C. L.; Kong, S.; Williams, P. I.; Ting, Y.-C.; Haslett, S. Black-carbon absorption enhancement in the atmosphere determined by particle mixing state. *Nat. Geosci.* **2017**, *10* (3), 184−188.
(36) Saliba, G.; Subramanian, R.; Saleh, R.; Ahern, A. T.; Lipsky, E. M.; Tasoglou, A.; Sullivan, R. C.; Bhandari, J.; Mazzoleni, C.; Robinson, A. L. Optical properties of black carbon in cookstove emissions coated with secondary organic aerosols: Measurements and modeling. *Aerosol Sci. Technol.* **2016**, *50* (11), 1264−1276.
(37) Koch, D.; Schulz, M.; Kinne, S.; McNaughton, C.; Spackman, J. R.; Balkanski, Y.; Bauer, S.; Berntsen, T.; Bond, T. C.; Boucher, O.; Chin, M.; Clarke, A.; De Luca, N.; Dentener, F.; Diehl, T.; Dubovik, O.; Easter, R.; Fahey, D. W.; Feichter, J.; Fillmore, D.; Freitag, S.; Ghan, S.; Ginoux, P.; Gong, S.; Horowitz, L.; Iversen, T.; Kirkevaring, G. A.; Klimont, Z.; Kondo, Y.; Krol, M.; Liu, X.; Miller, R.; Montanaro, V.; Moteki, N.; Myhre, G.; Penner, J. E.; Perlwitz, J.; Pitari, G.; Reddy, S.; Sahu, L.; Sakamoto, H.; Schuster, G.; Schwarz, J. P.; Seland, Ø.; Stier, P.; Takegawa, N.; Takemura, T.; Textor, C.; van Aardenne, J. A.; Zhao, Y. Evaluation of black carbon estimations in global aerosol models. *Atmos. Chem. Phys.* **2009**, *9* (22), 9001−9026.
(38) Reddington, C. L.; McMeeking, G.; Mann, G. W.; Coe, H.; Frontoso, M. G.; Liu, D.; Flynn, M.; Spracklen, D. V.; Carslaw, K. S. The mass and number size distributions of black carbon aerosol over Europe. *Atmos. Chem. Phys.* **2013**, *13* (9), 4917−4939.
(39) MacCarty, N.; Still, D.; Ogle, D.; Drouin, T. Assessing cook stove performance: field and lab studies of three rocket stoves comparing the open fire and traditional stoves in Tamil Nadu, India on measures of time to cook, fuel use, total emissions, and indoor air pollution. *Energy Sustainable Dev.* **2008**, http://www.aprovecho.org/web-content/publications/assets/India%20CCT%20Paper_1.7.08.pdf.*14*161
(40) Roden, C. A.; Bond, T. C.; Conway, S.; Osorto Pinel, A. B.; MacCarty, N.; Still, D. Laboratory and field investigations of particulate and carbon monoxide emissions from traditional and improved cookstoves. *Atmos. Environ.* **2009**, *43* (6), 1170−1181.
(41) Preble, C. V.; Hadley, O. L.; Gadgil, A. J.; Kirchstetter, T. W. Emissions and Climate-Relevant Optical Properties of Pollutants Emitted from a Three-Stone Fire and the Berkeley-Darfur Stove Tested under Laboratory Conditions. *Environ. Sci. Technol.* **2014**, *48* (11), 6484−6491.
(42) Lamberg, H.; Sippula, O.; Tissari, J.; Jokiniemi, J. Effects of Air Staging and Load on Fine-Particle and Gaseous Emissions from a Small-Scale Pellet Boiler. *Energy Fuels* **2011**, *25* (11), 4952−4960.
(43) Leskinen, J.; Tissari, J.; Uski, O.; Virén, A.; Torvela, T.; Kaivosoja, T.; Lamberg, H.; Nuutinen, I.; Kettunen, T.; Joutsensaari, J.; Jalava, P. I.; Sippula, O.; Hirvonen, M. R.; Jokiniemi, J. Fine particle emissions in three different combustion conditions of a wood chip-fired appliance − Particulate physico-chemical properties and induced cell death. *Atmos. Environ.* **2014**, *86*, 129−139.
(44) Shen, G.; Chen, Y.; Xue, C.; Lin, N.; Huang, Y.; Shen, H.; Wang, Y.; Li, T.; Zhang, Y.; Su, S.; Huangfu, Y.; Zhang, W.; Chen, X.; Liu, G.; Liu, W.; Wang, X.; Wong, M.-H.; Tao, S. Pollutant Emissions from Improved Coal- and Wood-Fuelled Cookstoves in Rural Households. *Environ. Sci. Technol.* **2015**, *49* (11), 6590−6598.
(45) Mitchell, E. J. S.; Lea-Langton, A. R.; Jones, J. M.; Williams, A.; Layden, P.; Johnson, R. The impact of fuel properties on the emissions from the combustion of biomass and other solid fuels in a fixed bed domestic stove. *Fuel Process. Technol.* **2016**, *142*, 115−123.
(46) CO_2Balance Website; www.co2balance.com.
(47) Gyapa Website; http://www.gyapa.com.
(48) World Stove Website; http://worldstove.com/stoves.
(49) Stanley Website; http://www.waterfordstanley.com/stanley-stoves/stanley-stoves/room-heating/solid-fuel.
(50) Lee, T.; Sullivan, A. P.; Mack, L.; Jimenez, J. L.; Kreidenweis, S. M.; Onasch, T. B.; Worsnop, D. R.; Malm, W.; Wold, C. E.; Hao, W. M.; Collett, J. L. Chemical Smoke Marker Emissions During Flaming and Smoldering Phases of Laboratory Open Burning of Wildland Fuels. *Aerosol Sci. Technol.* **2010**, *44* (9), i−v.
(51) Drewnick, F.; Hings, S. S.; DeCarlo, P.; Jayne, J. T.; Gonin, M.; Fuhrer, K.; Weimer, S.; Jimenez, J. L.; Demerjian, K. L.; Borrmann, S.; Worsnop, D. R. A New Time-of-Flight Aerosol Mass Spectrometer (TOF-AMS)—Instrument Description and First Field Deployment. *Aerosol Sci. Technol.* **2005**, *39* (7), 637−658.
(52) Canagaratna, M. R.; Jayne, J. T.; Jimenez, J. L.; Allan, J. D.; Alfarra, M. R.; Zhang, Q.; Onasch, T. B.; Drewnick, F.; Coe, H.; Middlebrook, A.; Delia, A.; Williams, L. R.; Trimborn, A. M.; Northway, M. J.; DeCarlo, P. F.; Kolb, C. E.; Davidovits, P.; Worsnop, D. R. Chemical and microphysical characterization of ambient aerosols with the aerodyne aerosol mass spectrometer. *Mass Spectrom. Rev.* **2007**, *26* (2), 185−222.
(53) McMeeking, G. R.; Hamburger, T.; Liu, D.; Flynn, M.; Morgan, W. T.; Northway, M.; Highwood, E. J.; Krejci, R.; Allan, J. D.; Minikin, A.; Coe, H. Black carbon measurements in the boundary layer over western and northern Europe. *Atmos. Chem. Phys.* **2010**, *10* (19), 9393−9414.
(54) Liu, D.; Flynn, M.; Gysel, M.; Targino, A.; Crawford, I.; Bower, K.; Choularton, T.; Jurányi, Z.; Steinbacher, M.; Hüglin, C.; Curtius, J.; Kampus, M.; Petzold, A.; Weingartner, E.; Baltensperger, U.; Coe, H. Single particle characterization of black carbon aerosols at a tropospheric alpine site in Switzerland. *Atmos. Chem. Phys.* **2010**, *10* (15), 7389−7407.
(55) Bond, T. C.; Bergstrom, R. W. Light Absorption by Carbonaceous Particles: An Investigative Review. *Aerosol Sci. Technol.* **2006**, *40* (1), 27−67.
(56) Liu, D.; Allan, J. D.; Young, D. E.; Coe, H.; Beddows, D.; Fleming, Z. L.; Flynn, M. J.; Gallagher, M. W.; Harrison, R. M.; Lee, J.; Prevot, A. S. H.; Taylor, J. W.; Yin, J.; Williams, P. I.; Zotter, P. Size distribution, mixing state and source apportionment of black carbon aerosol in London during wintertime. *Atmos. Chem. Phys.* **2014**, *14* (18), 10061−10084.
(57) Taylor, J.; Allan, J.; Liu, D.; Flynn, M.; Weber, R.; Zhang, X.; Lefer, B.; Grossberg, N.; Flynn, J.; Coe, H. Assessment of the sensitivity of core/shell parameters derived using the single-particle soot photometer to density and refractive index. *Atmos. Meas. Tech.* **2015**, *8* (4), 1701−1718.
(58) Moteki, N.; Kondo, Y.; Nakamura, S.-i. Method to measure refractive indices of small nonspherical particles: Application to black carbon particles. *J. Aerosol Sci.* **2010**, *41* (5), 513−521.
(59) Turpin, B. J.; Lim, H.-J. Species contributions to PM2. 5 mass concentrations: Revisiting common assumptions for estimating organic mass. *Aerosol Sci. Technol.* **2001**, *35* (1), 602−610.
(60) Symonds, J. Calibration of Fast Response Differential Mobility Spectrometers. *National Physical Lab., Metrology of Airborne Nanoparticles, Standardisation and Applications, London* **2010**. DOI: 10.13140/2.1.2095.1046

DOI: 10.1021/acs.est.8b00456
Environ. Sci. Technol. 2018, 52, 10134−10143

(61) Jolleys, M. D.; Coe, H.; McFiggans, G.; McMeeking, G. R.; Lee, T.; Kreidenweis, S. M.; Collett, J. L., Jr.; Sullivan, A. P. Organic aerosol emission ratios from the laboratory combustion of biomass fuels. *J. Geophys. Res.* **2014**, *119* (22), 12850−12871.
(62) Collier, S.; Zhou, S.; Onasch, T. B.; Jaffe, D. A.; Kleinman, L.; Sedlacek, A. J.; Briggs, N. L.; Hee, J.; Fortner, E.; Shilling, J. E.; Worsnop, D.; Yokelson, R. J.; Parworth, C.; Ge, X.; Xu, J.; Butterfield, Z.; Chand, D.; Dubey, M. K.; Pekour, M. S.; Springston, S.; Zhang, Q. Regional Influence of Aerosol Emissions from Wildfires Driven by Combustion Efficiency: Insights from the BBOP Campaign. *Environ. Sci. Technol.* **2016**, *50* (16), 8613−8622.
(63) Corbin, J. C.; Keller, A.; Lohmann, U.; Burtscher, H.; Sierau, B.; Mensah, A. A. Organic Emissions from a Wood Stove and a Pellet Stove Before and After Simulated Atmospheric Aging. *Aerosol Sci. Technol.* **2015**, *49* (11), 1037−1050.
(64) Aiken, A. C.; DeCarlo, P. F.; Kroll, J. H.; Worsnop, D. R.; Huffman, J. A.; Docherty, K. S.; Ulbrich, I. M.; Mohr, C.; Kimmel, J. R.; Sueper, D.; Sun, Y.; Zhang, Q.; Trimborn, A.; Northway, M.; Ziemann, P. J.; Canagaratna, M. R.; Onasch, T. B.; Alfarra, M. R.; Prevot, A. S. H.; Dommen, J.; Duplissy, J.; Metzger, A.; Baltensperger, U.; Jimenez, J. L. O/C and OM/OC Ratios of Primary, Secondary, and Ambient Organic Aerosols with High-Resolution Time-of-Flight Aerosol Mass Spectrometry. *Environ. Sci. Technol.* **2008**, *42* (12), 4478−4485.
(65) Reid, J.; Koppmann, R.; Eck, T.; Eleuterio, D. A review of biomass burning emissions part II: intensive physical properties of biomass burning particles. *Atmos. Chem. Phys.* **2005**, *5* (3), 799−825.
(66) Dentener, F.; Kinne, S.; Bond, T.; Boucher, O.; Cofala, J.; Generoso, S.; Ginoux, P.; Gong, S.; Hoelzemann, J.; Ito, A. Emissions of primary aerosol and precursor gases in the years 2000 and 1750 prescribed data-sets for AeroCom. *Atmos. Chem. Phys.* **2006**, *6* (12), 4321−4344.
(67) Jones, J. M.; Lea-Langton, A. R.; Ma, L.; Pourkashanian, M.; Williams, A. *Pollutants Generated by the Combustion of Solid Biomass Fuels*. 2014.
(68) Lee, K. W.; Chen, H. Coagulation Rate of Polydisperse Particles. *Aerosol Sci. Technol.* **1984**, *3* (3), 327−334.
(69) Wang, Y.; Wang, M.; Zhang, R.; Ghan, S. J.; Lin, Y.; Hu, J.; Pan, B.; Levy, M.; Jiang, J. H.; Molina, M. J. Assessing the effects of anthropogenic aerosols on Pacific storm track using a multiscale global climate model. *Proc. Natl. Acad. Sci. U. S. A.* **2014**, *111* (19), 6894−6899.
(70) Klingmüller, K.; Steil, B.; Brühl, C.; Tost, H.; Lelieveld, J. Sensitivity of aerosol radiative effects to different mixing assumptions in the AEROPT 1.0 submodel of the EMAC atmospheric-chemistry−climate model. *Geosci. Model Dev.* **2014**, *7* (5), 2503−2516.
(71) Wiedinmyer, C.; Akagi, S.; Yokelson, R. J.; Emmons, L.; Al-Saadi, J.; Orlando, J.; Soja, A. The Fire INventory from NCAR (FINN): a high resolution global model to estimate the emissions from open burning. *Geosci. Model Dev.* **2011**, *4* (3), 625.
(72) Turpin, B. J.; Saxena, P.; Andrews, E. Measuring and simulating particulate organics in the atmosphere: problems and prospects. *Atmos. Environ.* **2000**, *34* (18), 2983−3013.
(73) Ng, N. L.; Canagaratna, M. R.; Zhang, Q.; Jimenez, J. L.; Tian, J.; Ulbrich, I. M.; Kroll, J. H.; Docherty, K. S.; Chhabra, P. S.; Bahreini, R.; Murphy, S. M.; Seinfeld, J. H.; Hildebrandt, L.; Donahue, N. M.; DeCarlo, P. F.; Lanz, V. A.; Prévôt, A. S. H.; Dinar, E.; Rudich, Y.; Worsnop, D. R. Organic aerosol components observed in Northern Hemispheric datasets from Aerosol Mass Spectrometry. *Atmos. Chem. Phys.* **2010**, *10* (10), 4625−4641.
(74) Cappa, C. D.; Onasch, T. B.; Massoli, P.; Worsnop, D. R.; Bates, T. S.; Cross, E. S.; Davidovits, P.; Hakala, J.; Hayden, K. L.; Jobson, B. T.; Kolesar, K. R.; Lack, D. A.; Lerner, B. M.; Li, S.-M.; Mellon, D.; Nuaaman, I.; Olfert, J. S.; Petäjä, T.; Quinn, P. K.; Song, C.; Subramanian, R.; Williams, E. J.; Zaveri, R. A. Radiative Absorption Enhancements Due to the Mixing State of Atmospheric Black Carbon. *Science* **2012**, *337* (6098), 1078−1081.

DOI: 10.1021/acs.est.8b00456
Environ. Sci. Technol. 2018, 52, 10134−10143

SUPPORTING INFORMATION

The Mixing State of Carbonaceous Aerosols of Primary Emissions from 'Improved' African Cookstoves.

Yuchieh Ting[†], *Edward J.S. Mitchell*[‡], *James D. Allan*[†,§,*], *Dantong Liu*[†], *Dominick V. Spracklen*[¶], *Alan Williams*[‡], *Jenny M. Jones*[‡], *Amanda R. Lea-Langton*[‖], *Gordon McFiggans*[†], *Hugh Coe*[†]

[†]School of Earth and Environmental Science, University of Manchester, M13 9PL, Manchester, UK
[‡]School of Chemical and Process Engineering, University of Leeds, LS2 9JT, Leeds, UK
[§]National Centre for Atmospheric Science, University of Manchester, M13 9PL, Manchester, UK
[¶]School of Earth and Environment, University of Leeds, LS2 9JT, Leeds, UK
[‖]School of Mechanical, Aerospace and Civil Engineering, University of Manchester, M13 9PL, Manchester, UK

Corresponding Author

*E-mail: James.Allan@manchester.ac.uk.

Total Pages: 25

Number of Figures: 8; Number of tables: 2

SI CONTENTS

Sampling Configuration and Testing Method

Each cookstove was placed on an electronic platform scale (Kern DE 300K5DL) inside a customised firebox with dimensions of 750 by 750 mm with a height of 1330 mm. The firebox was designed to allow symmetrical inflow of ambient air through 130mm high space through the bottom of the firebox to the bed and to the main combustion zone. There is evidence that enclosing the stove with forced extraction may affect the combustion conditions – this was an issue in the development of the Water Boiling Test protocol (WBT).[1] However, our firebox was open at the bottom for the flow of the air into the firebox allowing for unforced draft conditions and unimpeded combustion. Some of the air that entered the firebox flowed up to the combustion chamber, and some air circulated around the hot stove due to natural convection (first stage dilution). The air and combustion gases exited the flue from the firebox and then entered a small hood on the extraction duct (second stage dilution). The third stage of dilution for the AMS and SP2 was the two Dekati dilutors placed in series before the measurements.

The dimensions of the combustion chamber of the heating stove are 250*270*190mm (height*width*depth) with a single primary supply of ambient air under the grate manually controlled by a damper. The test system of the heating stove was based on BS EN 13240, as described in detail by Mitchell et al.[2] A 1m insulated flue with a diameter of 125 mm allowed sampling of primary combustion emissions without dilution, as shown in Figure S1. The testing method applied was essentially the WBT protocol, except for not using a cooking pot. The testing end point for each batch was typically where the CO concentration dropped to within the measurement error of the FTIR, since CO spikes to a maximum at the end of test when other pollutants are reducing.

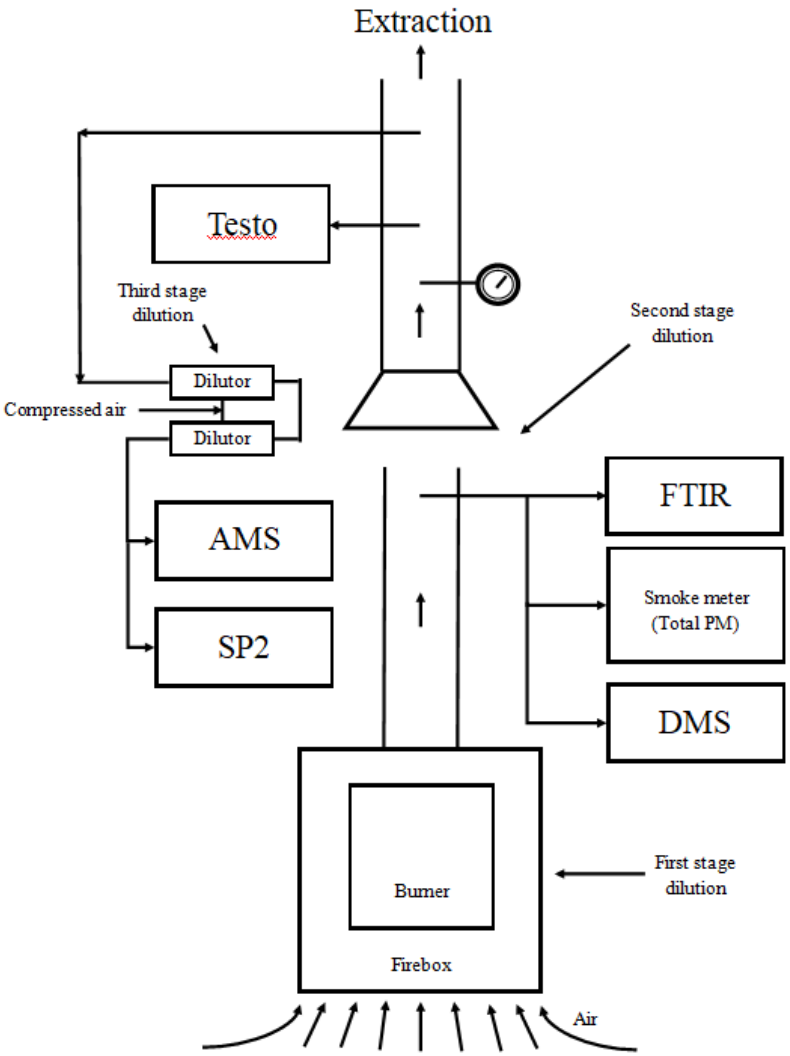

Figure S1. The schematic of the experimental system.

Stove and Fuel Specifications

The Carbonzero stove, with higher efficiency and reduction in the amount of the fuel required compared to the traditional three-stone fires,[3] is an improved rocket-type cook stove designed to burn wood and widely used in Kenya, Uganda and Tanzania [4-6]. The Gyapa stove is a fuel-efficient charcoal burning cook stove widely used in Ghana.[7] The design enables the reduction of the amount of the charcoal needed for cooking.[8] The Lucia stove was designed to be a fuel-efficient and low- emission 'carbon negative' stove,[9] and to be able to produce a consistent temperature with no need to refuel during a cook time using wood pellets.[10] The mass of the pellets was derived from the stove instructions, which require it to be filled with pellets from the base to 1 inch below the top ring of holes. A number of Lucia stove designs ranging in scale and complexity have been developed and one of the smallest and simplest designs is utilized here. A multi-fuel stove (Waterford Stanley Oisin, Ireland) was employed to explore the emissions of solid fuel combustion typically used for domestic heating in the UK, for the sake of comparison. The heating stove was designed to meet the current conditions for multi-fuel combustion.[11] The types of the fuel used in corresponding stoves are shown in Table S1. The sizes of the oak and willow sticks were similar, with diameters and length ranging from 2 to 26mm and 89 to 181 mm respectively. Namibian charcoal used with the Gyapa stove meets the required standard for barbeques in the UK (BS EN 1860-2:2005). Wood pellets used in the Lucia stove were 6 mm in diameter with a maximum length of 23 mm.

Table S1. The moisture, batch mass and the number of loading for all fuels correspond to the stoves.

	CarbonZero Cookstove			Gyapa Cookstove			Heating stove			Lucia Cookstove
	Oak stick (dry)	Oak stick (wet)	Willow stick (dry)	Oak stick (dry)	Oak stick (wet)	Charcoal	Willow log	Pine	Coal	Wood pellet
Moisture (%)	5.1	27.9	5.6	5.1	27.9	3.1	18.5	7.0	7.2	6.5
Volatile matter (% dry basis)	87.1	82.1	82.6	87.1	82.1	16.0	89.0	86.1	39.7	85.5
Ash (%dry basis)	1.4	1.6	1.7	1.4	1.6	13.5	0.1	0.1	4.2	0.4
Batch mass (g)	80-100	100-120	60-80	190-200	190-200	450	800-900	1000	1000	70
Number of loading times	15	6	12	3	3	2	3	1	1	1

a. **b.** **c.**

d.

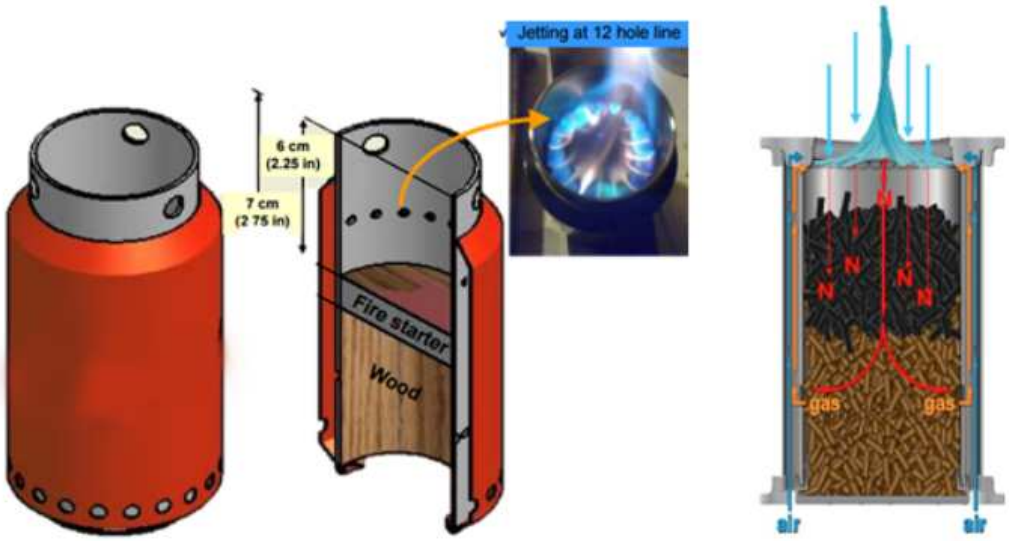

Figure S2. The residential stoves were used in this study. a) Heating stove. b) Carbonzero cookstove. c) Gyapa cookstove. d) Lucia stove.[10]

Data Analysis of Aerosol Mass Spectrometer

For the analysis of the Aerosol Mass Spectrometer (AMS) data, a collection efficiency (CE) value of 1 was used and the concentrations of the particulate OM and mass spectra were averaged as the ensemble of PM_1 with a time resolution of 30 seconds. Although there has been no comprehensive assessment of the collection efficiency for solid fuel combustion, the CE of 1 has been widely used in previous studies regarding solid fuel combustion from residential stoves,[12-14] and a reasonable agreement and linear correlations with other measurements were obtained. The cToF-AMS data were analyzed using standard ToF-AMS analysis toolkit software package (SQUIRREL, SeQUential Igor data RetRiEval) v1.57 within Igor Pro (Wavemetrics). The signal from gas-phase CO_2 can be detected by the AMS to interfere with the contributions of OM at m/z 44.[15] To account for this, the fragmentation table was altered by applying CO_2 concentrations measured in the flue and accounting for dilution.[15] Anhydrous sugars such as levoglucosan, which are thermal decomposition products of cellulose and are found in biomass burning particles have been shown to produce significant mass peaks at m/z 60 and 73.[16] Signals at m/z 73, 147, 207, 221 and 281, which are known as signatures for siloxane, were clearly observed in the mass spectra, which were considered to be contaminated by conductive silicone tubing[16, 17] used in the sampling configuration. The influence of the tubing contamination must therefore be removed from the levoglucosan retrieval. Details for the correction of the silicon tubing effect are shown as below.

Correction of Silicone Tubing Contamination

There are two potential artefacts using silicon tubing for aerosol sampling experiments. One is the CO_2 uptake effect which was nominal as the tubing length is shorter than 15.2 m.[17] Another artefact is siloxane, which has been identified as the key constituent of

146 contamination emitted from the silicone tubing. This study only took the siloxane artefact
147 into account as the tubing length used in the experiments was much shorter than 15.2 m.

148 In this study, the abnormally high signals at m/z 73 and 147 with lower signal at m/z 60
149 were observed in most combustion cycles compared to that of Levoglucosan, and this was
150 most significant during the flaming phase, indicating that most of m/z 73 was contributed by
151 silicone tubing contamination. During the pellet combustion there were no signals at m/z 60
152 but the signals at 73 and 147 were high and it was assumed that these two signals were totally
153 contributed by the siloxane. The ratio of signals at m/z 73 and m/z 147 from pellet
154 combustion emissions during the flaming phase is 5.07:1, which was then applied to the mass
155 spectra signals for the correction of the silicone tubing contamination. The derived mass
156 spectra of combustion cycles using oak fuels showed no signal at m/z 73, which was not
157 consistent with previous studies of the tracer of levoglucosan.[16, 18] The ratio of m/z 60 and 73
158 (1:0.28) observed in the mass spectrum of levoglucosan was applied to account for this and
159 fully remove influence of the contamination from silicone tubing. The methodology of
160 performing the modification of the fragmentation table has been described in detail by Allan
161 et al. [15]

162 **The Calibration of Single Particle Soot Photometer**

163 Regarding the analysis of Single Particle Soot Photometer (SP2) data, monodisperse
164 polystyrene latex spheres were used to calibrate the scattering signal and monitor the
165 intensity of the laser power. The SP2 incandescence signal was calibrated for BC mass using
166 Aquadag® black carbon particle standards (Aqueous Deflocculated Acheson Graphite,
167 manufactured by Acheson Inc.) and corrected for ambient BC with a factor of 0.75.[19, 20]

168

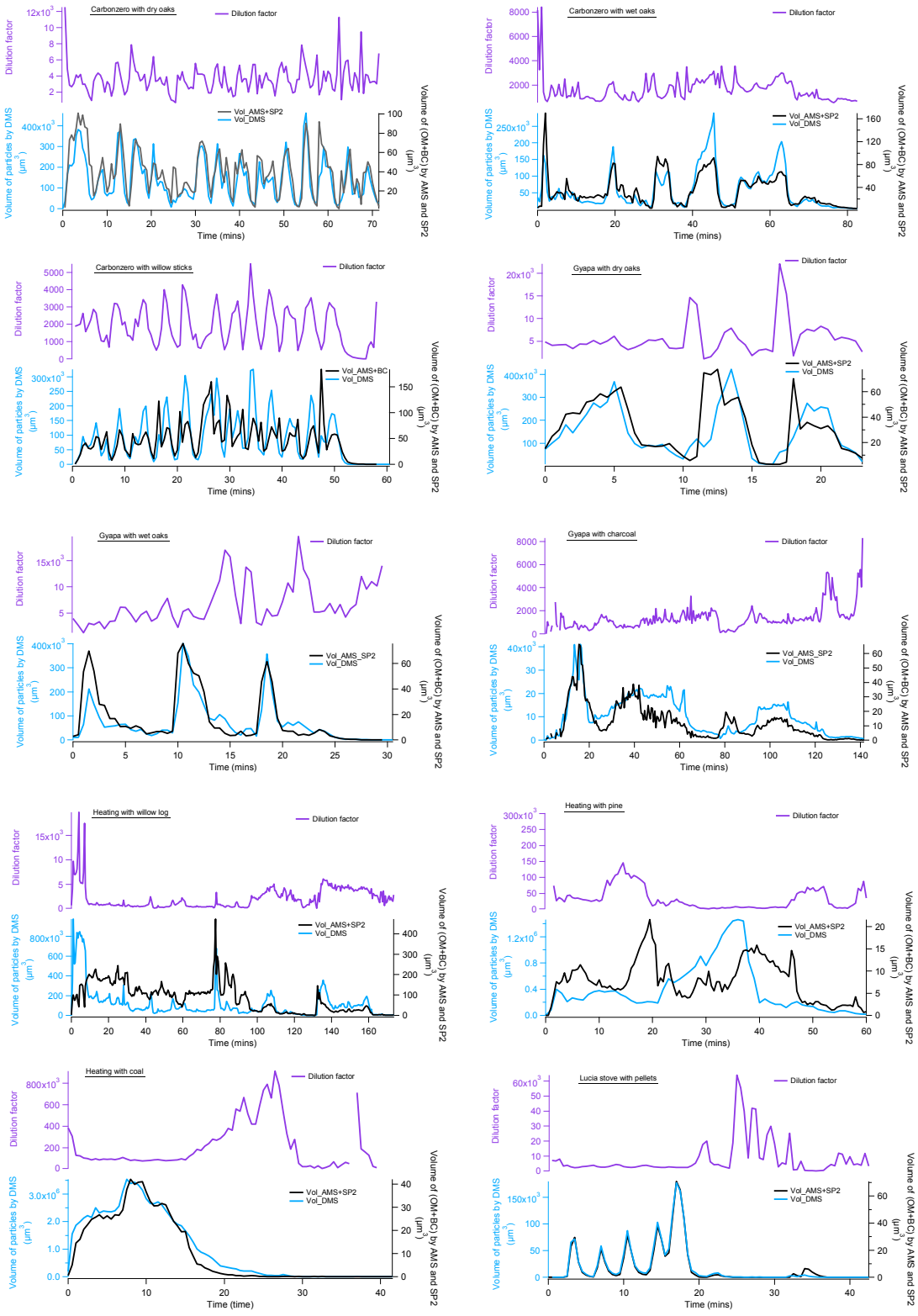

Figure S3. Particle volume derived by DMS (vol_DMS) and AMS+SP2 (vol_AMS+SP2). Dilution factors derived by the ratios of vol_DMS/vol_AMS+SP2 for each combustion cycle.

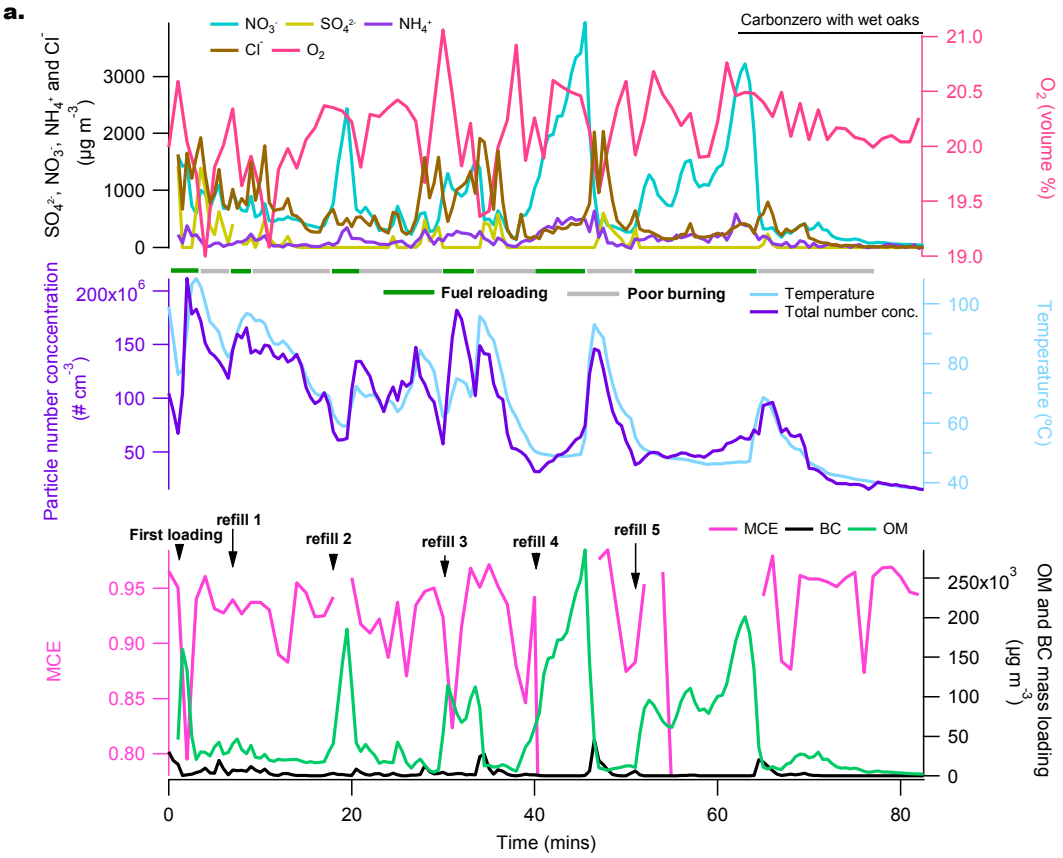
a.
Carbonzero with wet oaks
NO3- SO4 2- NH4+
Cl- O2
SO4 2-, NO3-, NH4+ and Cl- (µg m-3)
O2 (volume %)
Fuel reloading
Poor burning
Temperature
Total number conc.
Particle number concentration (# cm-3)
Temperature (°C)
First loading
refill 1
refill 2
refill 3
refill 4
refill 5
MCE
BC
OM
MCE
OM and BC mass loading (µg m-3)
Time (mins)

176

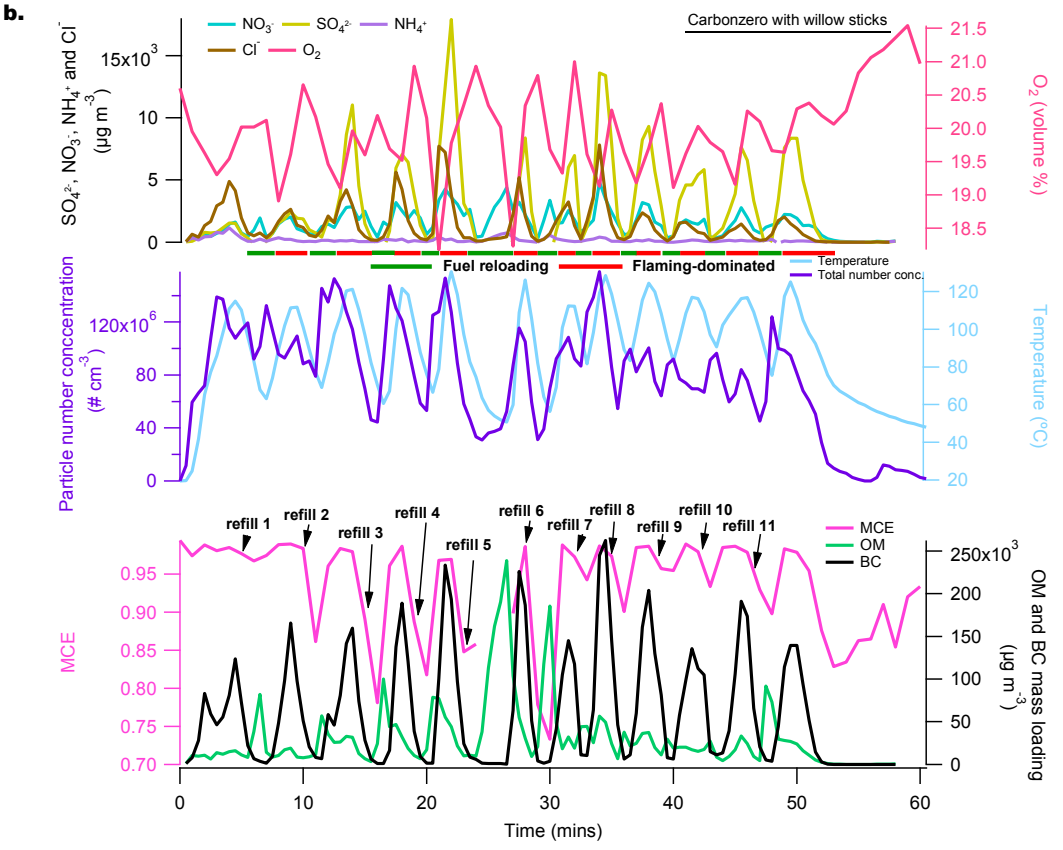
b.
Carbonzero with willow sticks
NO3- SO4 2- NH4+
Cl- O2
SO4 2-, NO3-, NH4+ and Cl- (µg m-3)
O2 (volume %)
Fuel reloading
Flaming-dominated
Temperature
Total number conc.
Particle number concentration (# cm-3)
Temperature (°C)
refill 1
refill 2
refill 3
refill 4
refill 5
refill 6
refill 7
refill 8
refill 9
refill 10
refill 11
MCE
OM
BC
MCE
OM and BC mass loading (µg m-3)
Time (mins)

177

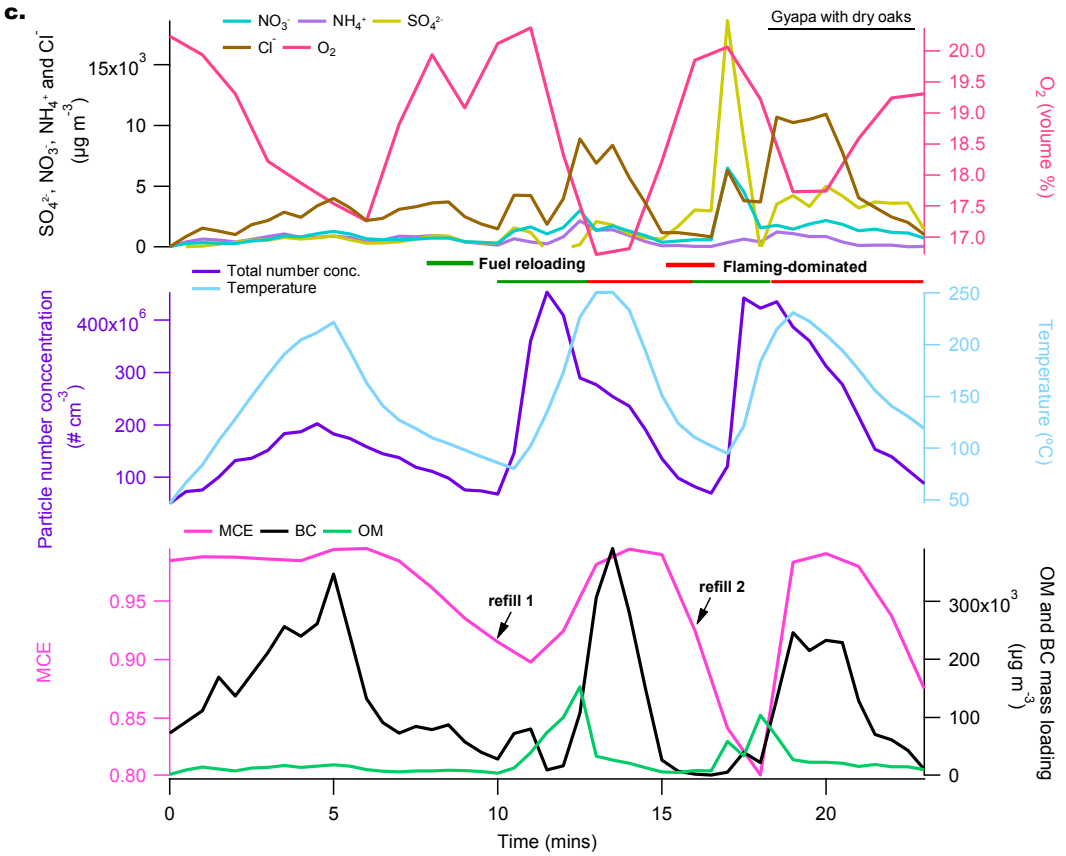
c.
Gyapa with dry oaks
NO3- NH4+ SO4 2-
Cl- O2
SO4 2-, NO3-, NH4+ and Cl-
(µg m-3)
15x10 3
10
5
0
O2 (volume %)
20.0
19.5
19.0
18.5
18.0
17.5
17.0
Total number conc.
Temperature
Fuel reloading
Flaming-dominated
Particle number conccentration
(# cm-3)
400x10 6
300
200
100
Temperature (°C)
250
200
150
100
50
MCE BC OM
refill 1
refill 2
MCE
0.95
0.90
0.85
0.80
OM and BC mass loading
(µg m-3)
300x10 3
200
100
0
0
5
10
15
20
Time (mins)

178

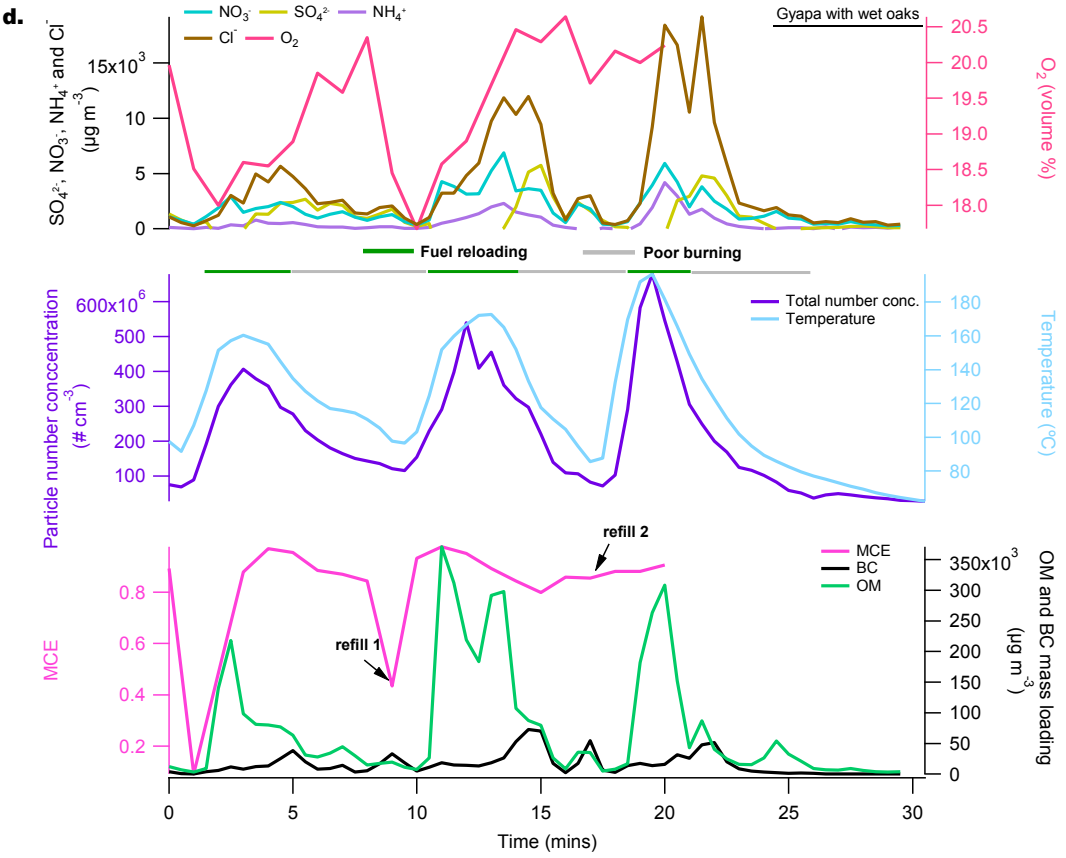
d.
Gyapa with wet oaks
NO3- SO4 2- NH4+
Cl- O2
SO4 2-, NO3-, NH4+ and Cl-
(µg m-3)
15x10 3
10
5
0
O2 (volume %)
20.5
20.0
19.5
19.0
18.5
18.0
Fuel reloading
Poor burning
Total number conc.
Temperature
Particle number conccentration
(# cm-3)
600x10 6
500
400
300
200
100
Temperature (°C)
180
160
140
120
100
80
refill 2
refill 1
MCE
BC
OM
MCE
0.8
0.6
0.4
0.2
OM and BC mass loading
(µg m-3)
350x10 3
300
250
200
150
100
50
0
0
5
10
15
20
25
30
Time (mins)

179

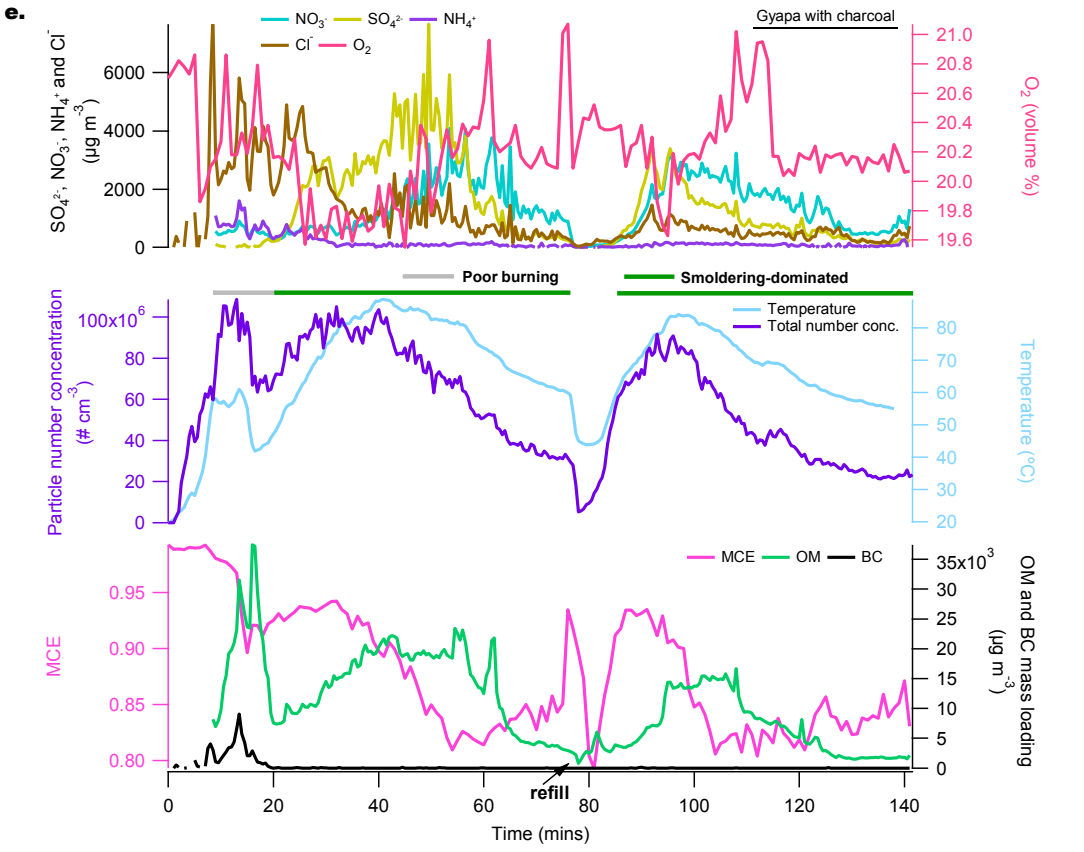
e.
Gyapa with charcoal
NO_3^- SO_4^{2-} NH_4^+ Cl^- O_2
SO_4^{2-}, NO_3^-, NH_4^+ and Cl^- (μg m^{-3})
O_2 (volume %)
Poor burning
Smoldering-dominated
Temperature
Total number conc.
Particle number concentration (# cm^{-3})
Temperature (°C)
MCE
OM
BC
MCE
OM and BC mass loading (μg m^{-3})
refill
Time (mins)

180

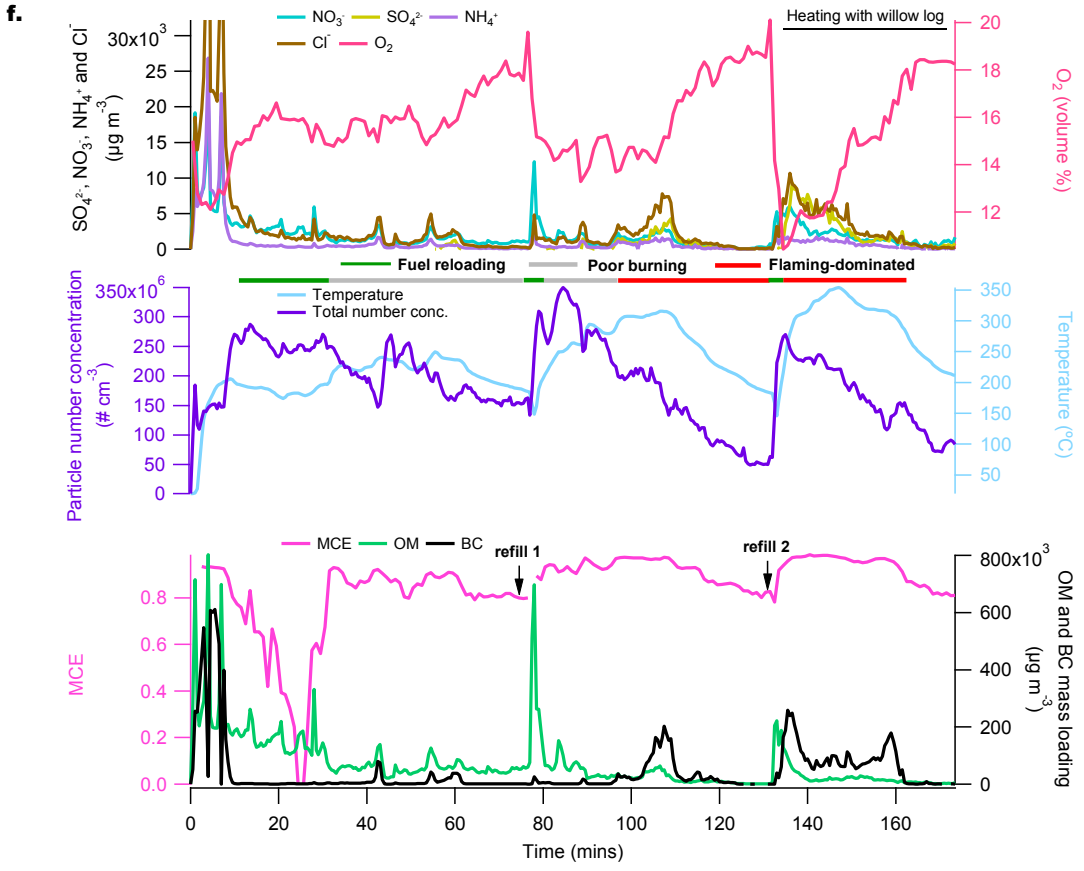
f.
Heating with willow log
NO_3^- SO_4^{2-} NH_4^+ Cl^- O_2
SO_4^{2-}, NO_3^-, NH_4^+ and Cl^- (μg m^{-3})
O_2 (volume %)
Fuel reloading
Poor burning
Flaming-dominated
Temperature
Total number conc.
Particle number concentration (# cm^{-3})
Temperature (°C)
MCE
OM
BC
refill 1
refill 2
MCE
OM and BC mass loading (μg m^{-3})
Time (mins)

181

g.

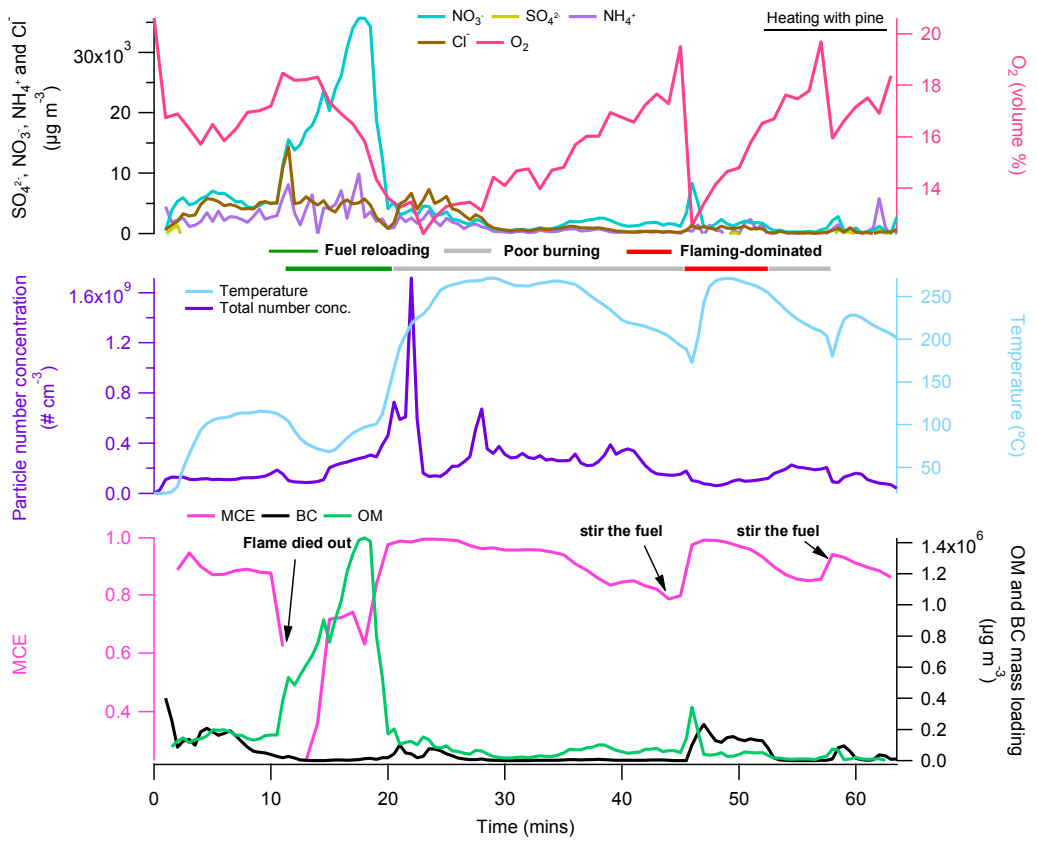
NO3- SO4 2- NH4+
Cl- O2
Heating with pine
SO4 2-, NO3-, NH4+ and Cl- (µg m-3)
O2 (volume %)
Fuel reloading
Poor burning
Flaming-dominated
Temperature
Total number conc.
Particle number concentration (# cm-3)
Temperature (°C)
MCE BC OM
Flame died out
stir the fuel
stir the fuel
MCE
OM and BC mass loading (µg m-3)
Time (mins)

182

h.

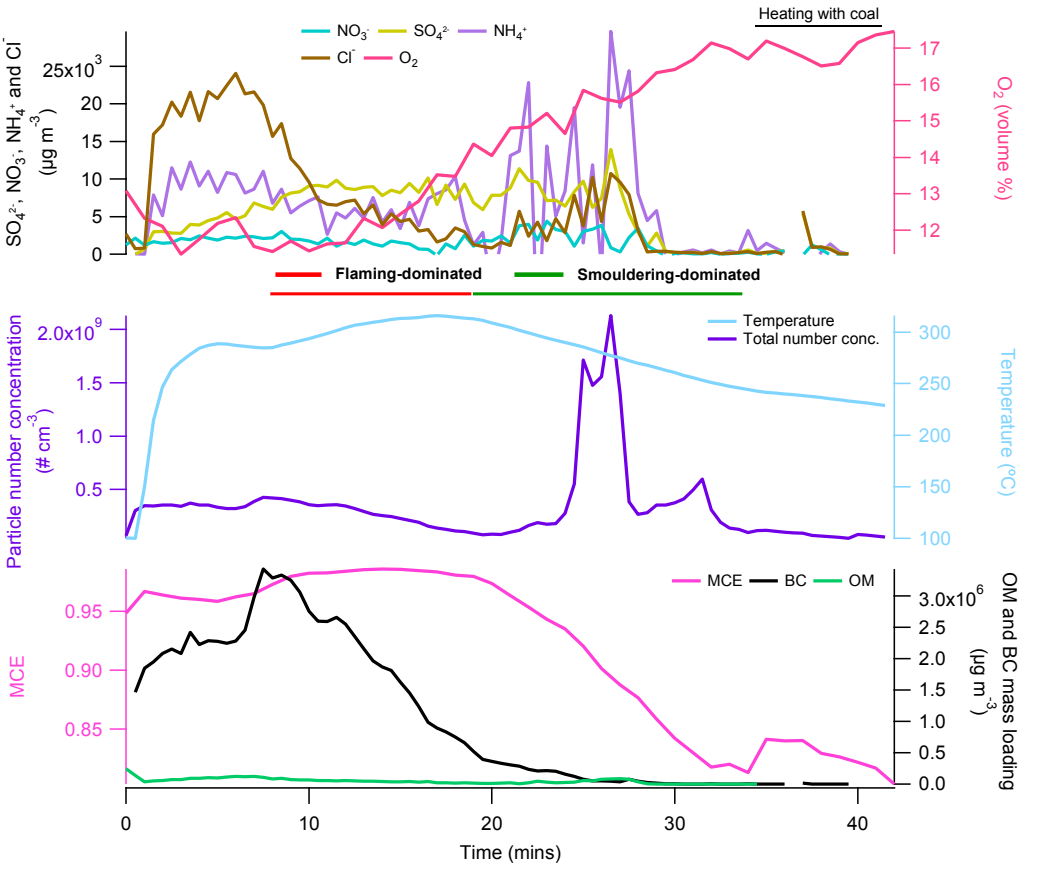
NO3- SO4 2- NH4+
Cl- O2
Heating with coal
SO4 2-, NO3-, NH4+ and Cl- (µg m-3)
O2 (volume %)
Flaming-dominated
Smouldering-dominated
Temperature
Total number conc.
Particle number concentration (# cm-3)
Temperature (°C)
MCE BC OM
MCE
OM and BC mass loading (µg m-3)
Time (mins)

183

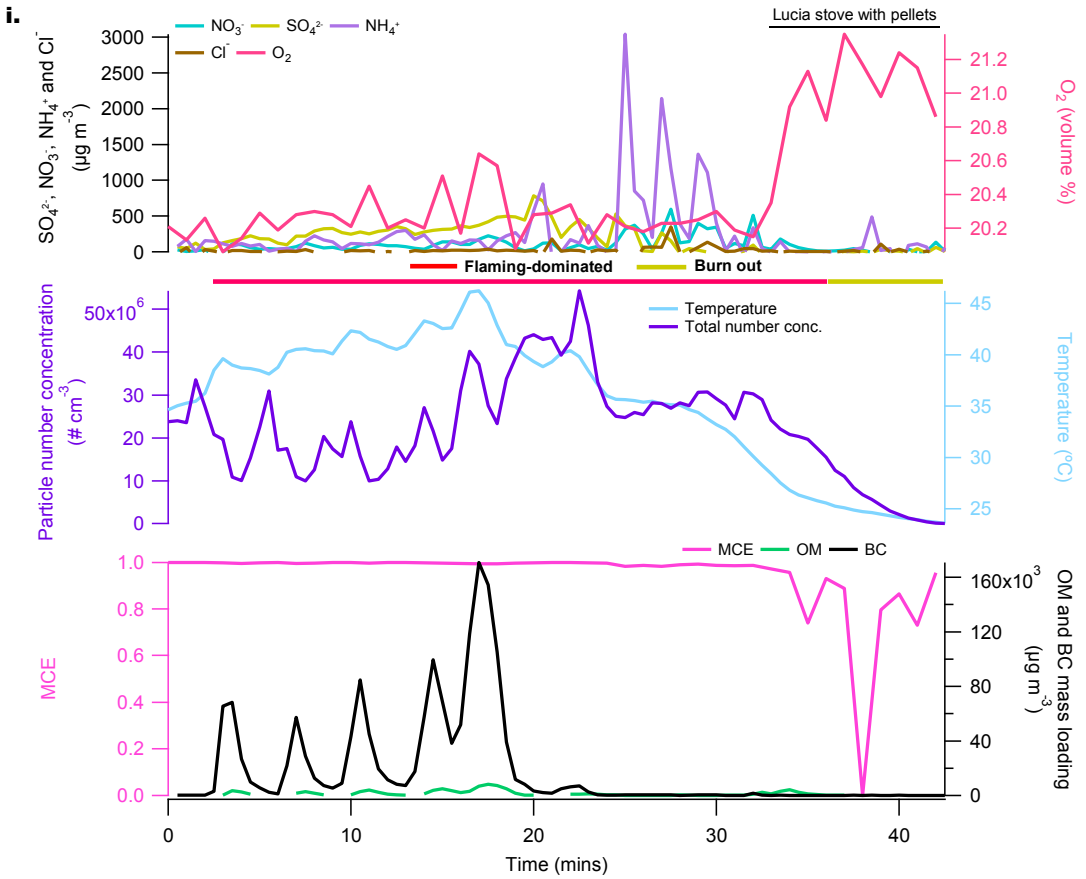

Figure S4. The time series of inorganics (SO_4^{2-}, NO_3^-, NH_4^+ and Cl^-), oxygen, particle number concentrations, temperature, MCE, OM and BC for all experiments. Carbonzero cookstove: a) Wet oak, b) willow stick. Gyapa cookstove: c) dry oak, d) wet oak, e) charcoal. Heating stove: f) willow log, g) pine, h) coal. Lucia stove: i) pellet.

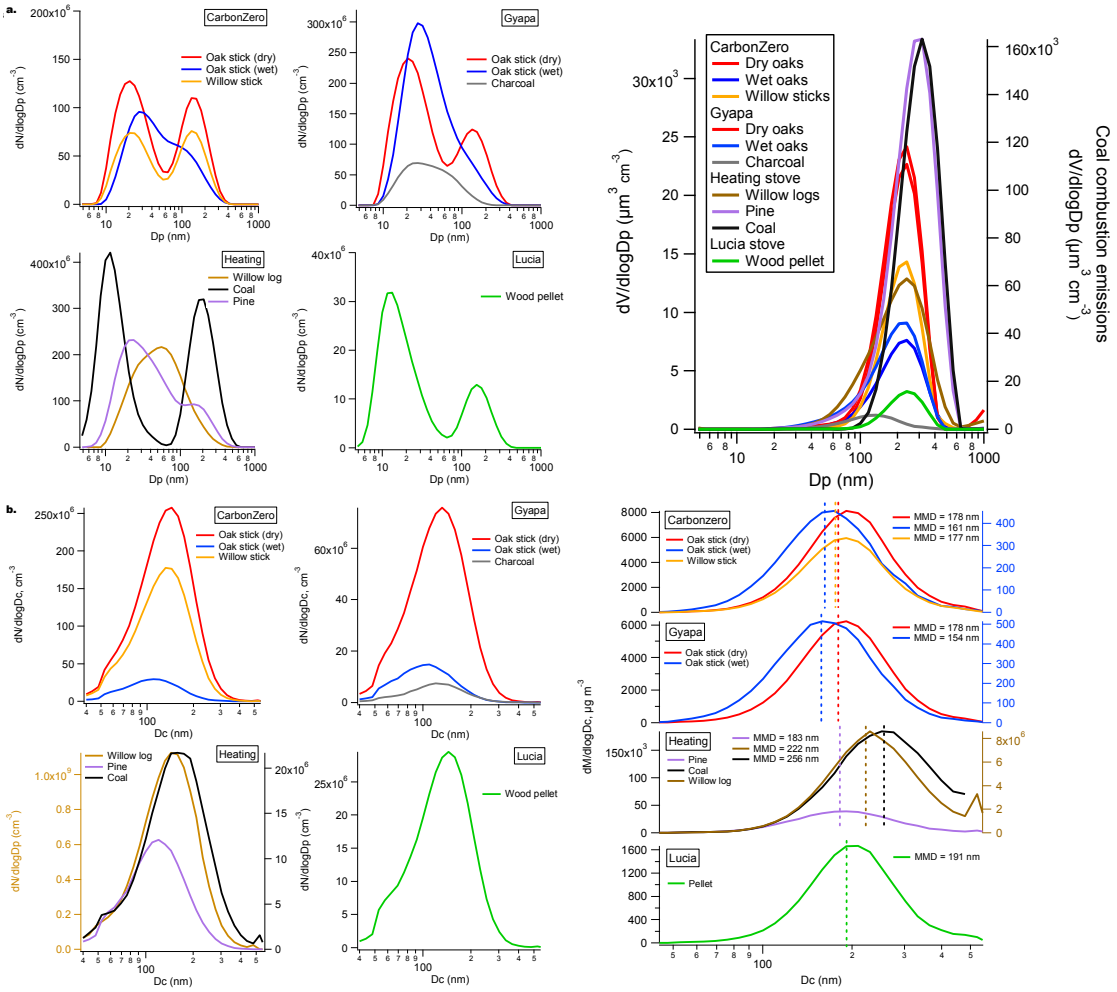

Figure S5. a) Averaged particle number size distribution (left plot) and volume size distribution (right plot) over the full combustion cycle for each of the stoves and fuels. b) Averaged BC particle number size distribution (left plot) and BC core size distribution with the dotted line showing the MMD over each combustion cycle.

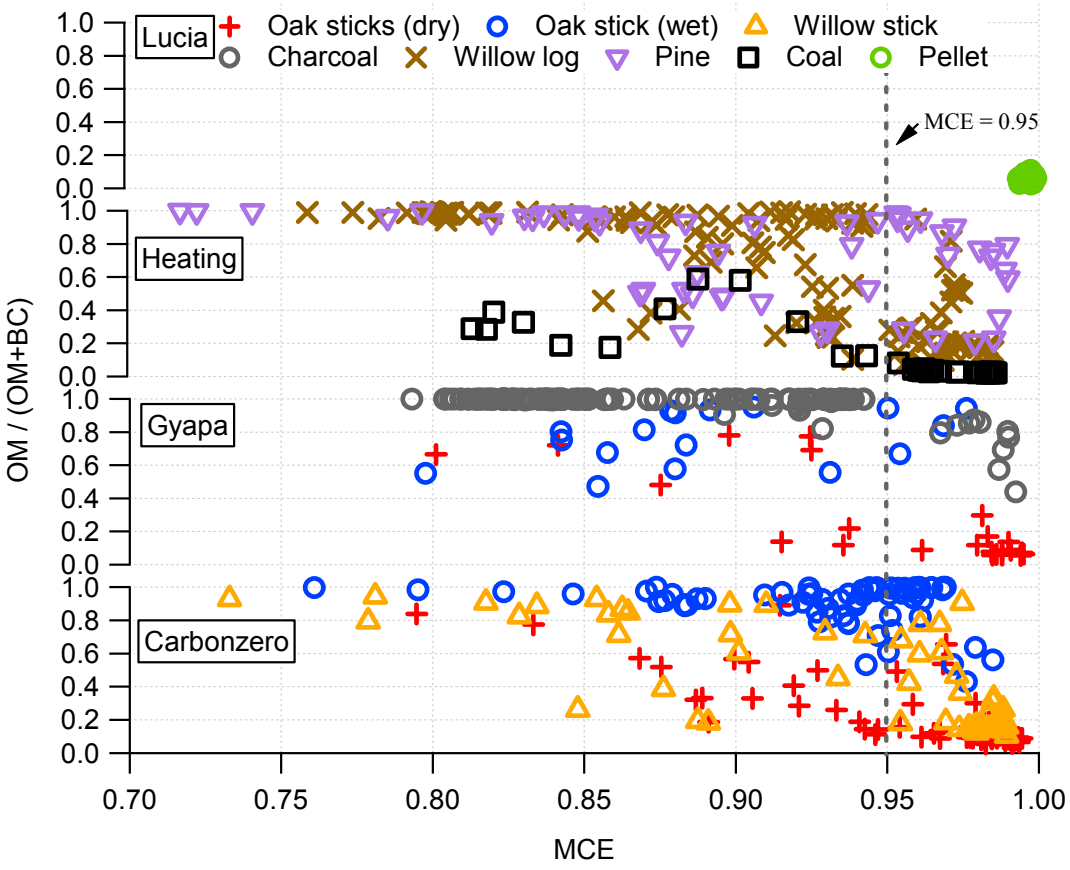

196

197 **Figure S6.** The ratios of OM/(OM+BC) as a function of MCE in different stoves using different fuels.

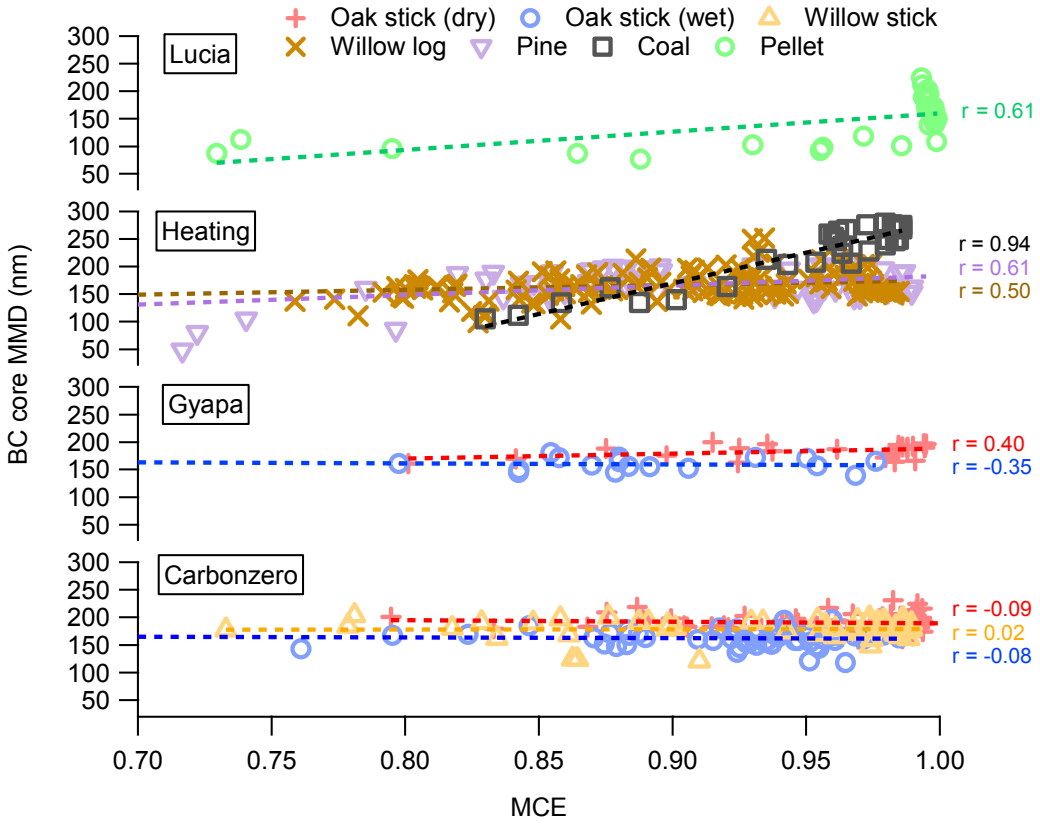

Figure S7. The mass median diameter (MMD) of BC cores for all combustion cycles as a function of MCE; r denotes the correlation between BC core MMD and MCE. The average MMD ± standard deviation for Carbonzero cookstove: 190.2 ± 13.8 (dry oak), 153.4 ± 29.9 (wet oak) and 180.5 ± 18.1 (willow stick); Gyapa cookstove: 183.5 ± 12.2 (dry oak) and 161.2 ± 11.4 (wet oak); heating stove: 162.5 ± 26.9 (willow log), 161.0 ± 37.9 (pine) and 223.8 ± 53.8 (coal); Lucia stove: 145.5 ± 40.8 (pellet).

207 **Emission ratios**

208 Table S2 shows the emission ratios (ER) of PN_1 and BC mass normalised to CO averaged
209 over each combustion cycle. An average ER was reported for periods when MCE was high
210 (>0.95) and low (<0.95) for each parameter. This was selected as a generally representative
211 threshold with different emission characteristics (Figure 3). The emission factors showed
212 positive correlations with the MCE when the MCE was higher than 0.95, whereas the EF was
213 nearly constant when the MCE was lower than 0.95.

214 For the emissions from the carbonzero and gyapa cookstoves at MCE>0.95, ΔBC/ΔCO
215 ratios from dry oak emissions reach 0.89 and 1.03 μg m^{-3} ppb^{-1}, whereas those from wet oak
216 emissions are only 0.02 and 0.03 μg m^{-3} ppb^{-1}. The distinct ΔBC/ΔCO ratios for oak fuels
217 with different moistures are because the CO emission fraction (ΔCO/Total ΔCO) vastly
218 dominated at a lower MCE, i.e. larger fraction of CO emissions were emitted from wet oak
219 compared to that from dry oak combustion. This also causes the emission ratio difference for
220 other species, such as $\Delta PN_1/\Delta CO$ ratios that are 755.8 and 963.5 cm^{-3} ppb^{-1} for dry oaks
221 during the period of MCE>0.95 compared to 249.6 and 572.0 cm^{-3} ppb^{-1} for wet oak,
222 indicating that the higher moisture of the fuel leads to lower $\Delta PN_1/\Delta CO$. The BC/OM ratios
223 are 8.51 and 11.28 μg m^{-3} ppb^{-1} for dry oak, while only 0.24 and 0.20 μg m^{-3} ppb^{-1} for wet
224 oak. This suggests the relative contribution of BC compared to OM is greater at lower
225 moisture content. As for the ER of particulate emissions from both cookstoves at MCE<0.95,
226 the ER for dry oak shows big differences from that when MCE>0.95, whereas the ER for wet
227 oak at MCE<0.95 is close to that at MCE>0.95, indicating that the water content of fuels has
228 an impact on the ER even at the same MCE.

229 For the heating stove, the ER of the willow log and pine are similar. This may result from
230 similar characteristics of both types of wood or the fuel-independent emissions from the

heating stove. Coal emissions, however, showed an extremely high ΔBC/ΔOM of 34.40. The $\Delta PN_1/\Delta CO$ ratios for heating stove emissions are lower than cookstoves since the CO emissions from heating stoves are much higher than those from cookstoves especially so when burning coal. Nevertheless, the emitted number concentrations of particles from the heating stove are still high. Overall, the $\Delta PN_1/\Delta CO$ and ΔBC/ΔCO for the Lucia stove are highest, but this is largely just the result of extremely low CO emissions resulting from a consistently high MCE.

Table S2. Emission ratios (ER) of PN_1 and BC normalised to CO. All results are classified by an MCE threshold of 0.95. The proportion of CO enhancement, OM and BC emitted during each of the high and low MCE periods compared to the total over the burn is also shown as the ratio of BC to OM - ΔBC/ΔOM.

Stove and fuel	ΔPN$_1$/ΔCO (cm^{-3} ppb^{-1})		ΔBC/ΔCO (mg m^{-3} ppb^{-1})		ΔOM/ΔCO (mg m^{-3} ppb^{-1})		ΔCO/Total ΔCO (%)		ΔBC/Total ΔBC (%)		ΔOM/Total ΔOM (%)		ΔBC/ΔOM		ΔCO (ppb)
	MCE>0.95	MCE<0.95	MCE>0.95	MCE<0.95	MCE>0.95	MCE<0.95	MCE>0.95	MCE<0.95	MCE>0.95	MCE<0.95	MCE>0.95	MCE<0.95	MCE>0.95	MCE<0.95	
Carbonzero															
Oak stick (dry)	755.8 ± 421.5	164.9 ± 66.9	0.89 ± 0.78	0.10 ± 0.10	0.10 ± 0.06	0.04 ± 0.03	45.3	54.7	86.2	13.8	61.0	39.0	8.51 ± 3.29	2.50 ± 2.27	342.17 ± 257.96
Oak stick (wet)	249.6 ± 166.6	224.8 ± 94.2	0.02 ± 0.03	0.01 ± 0.01	0.10 ± 0.08	0.07 ± 0.06	28.6	71.4	41.8	58.2	18.1	81.9	0.24 ± 0.38	0.12 ± 0.16	315.92 ± 211.27
Willow stick	460.4 ± 180.4	84.2 ± 73.8	0.41 ± 0.25	0.05 ± 0.06	0.11 ± 0.05	0.05 ± 0.09	36.0	64.0	87.4	12.6	48.4	51.6	4.19 ± 2.07	1.38 ± 1.59	380.27 ± 276.29
Gyapa															
Oak stick (dry)	963.5 ± 391.7	254.1 ± 155.8	1.03 ± 0.66	0.04 ± 0.03	0.09 ± 0.05	0.03 ± 0.04	26.1	73.9	87.6	12.4	47.7	52.3	11.28 ± 4.15	2.46 ± 2.76	537.85 ± 482.41
Oak stick (wet)	572.0 ± 111.4	166.6 ± 85.1	0.03 ± 0.01	0.02 ± 0.01	0.27 ± 0.20	0.11 ± 0.19	10.7	89.3	20.5	79.5	30.6	69.4	0.20 ± 0.20	0.46 ± 0.41	1085.58 ± 493.07
Charcoal	398.3 ± 195.6	49.3 ± 30.1	14.32 ± 7.18	0.17 ± 1.06	0.01 ± 0.00	0.00 ± 0.00	1.2	98.8	51.6	48.4	6.1	93.9	0.23 ± 0.10	0.01 ± 0.02	1181.37 ± 517.13
Heating															
Willow log	116.2 ± 32.1	54.5 ± 23.5	0.05 ± 0.03	0.01 ± 0.03	0.02 ± 0.01	0.02 ± 0.03	13.0	87.0	49.5	50.5	8.9	91.1	3.90 ± 2.86	0.48 ± 1.08	2984.64 ± 1009.14
Pine	172.6 ± 135.8	49.0 ± 18.0	0.05 ± 0.05	0.02 ± 0.03	0.05 ± 0.04	0.06 ± 0.06	18.3	81.7	38.0	62.0	13.6	86.4	0.97 ± 1.33	0.54 ± 0.83	3005.73 ± 1638.25
Coal	203.3 ± 94.5	41.0 ± 33.5	1.41 ± 0.81	0.01 ± 0.02	0.04 ± 0.02	0.01 ± 0.01	23.0	77.0	98.4	0.6	80.9	19.1	34.40 ± 10.59	3.18 ± 2.29	3185.66 ± 2137.03
Lucia															
Pellet	3848.7 ± 3875.0	92.3 ± 69.9	2.94 ± 3.30	0	0.18 ± 0.12	0	50.4	49.6	100	0	100	0	22.28 ± 11.10	0	24.48 ± 29.51

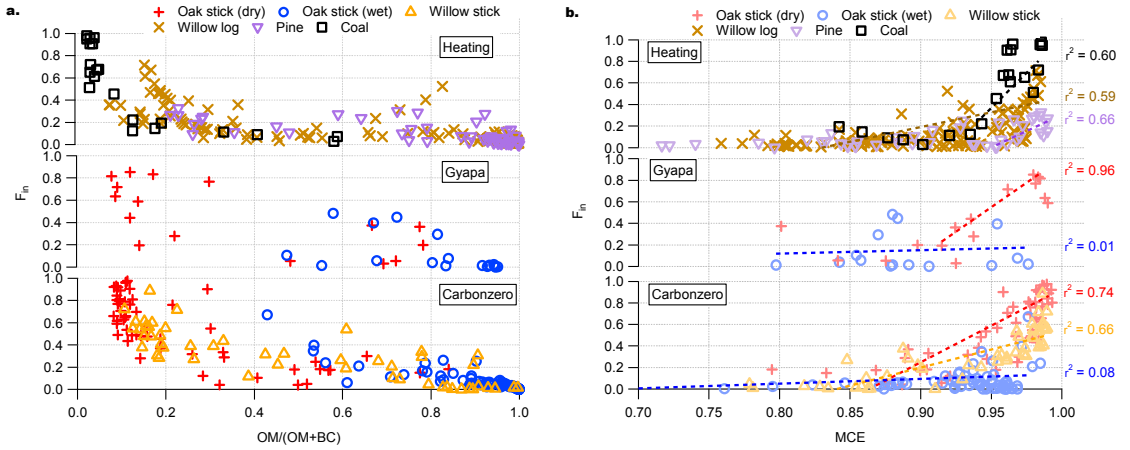

Figure S8. a) F_{in} as a function of OM/(OM+BC). b) F_{in} as a function of MCE. The Lucia stove with pellet fuel is not shown here as the OM was completely coated on BC due to the high BC mass loading. The r^2 denotes the correlation between F_{in} and MCE at MCE>0.95.

References

1. Bailis, P. R.; Ogle, D.; Maccarty, N.; From, D. S. I.; Smith, K. R.; Edwards, R.; Energy, H., The water boiling test (WBT). **2007**.

2. Mitchell, E. J. S.; Lea-Langton, A. R.; Jones, J. M.; Williams, A.; Layden, P.; Johnson, R., The impact of fuel properties on the emissions from the combustion of biomass and other solid fuels in a fixed bed domestic stove. *Fuel Process. Technol.* **2016,** *142*, 115-123.

3. CO2balance Website; www.co2balance.com.

4. Ezzati, M.; Mbinda, B. M.; Kammen, D. M., Comparison of emissions and residential exposure from traditional and improved cookstoves in Kenya. *Environ. Sci. Technol.* **2000,** *34*, (4), 578-583.

5. Loo, J. D.; Hyseni, L.; Ouda, R.; Koske, S.; Nyagol, R.; Sadumah, I.; Bashin, M.; Sage, M.; Bruce, N.; Pilishvili, T., User Perspectives of Characteristics of Improved Cookstoves from a Field Evaluation in Western Kenya. *Int. J. Environ. Res. Public Health* **2016,** *13*, (2), 167.

6. Yip, F.; Christensen, B.; Sircar, K.; Naeher, L.; Bruce, N.; Pennise, D.; Lozier, M.; Pilishvili, T.; Loo Farrar, J.; Stanistreet, D.; Nyagol, R.; Muoki, J.; de Beer, L.; Sage, M.; Kapil, V., Assessment of traditional and improved stove use on household air pollution and personal exposures in rural western Kenya. *Environ. Int.* **2017,** *99*, (Supplement C), 185-191.

7. Gyapa Website; http://www.gyapa.com.

8. Obeng, G.; Mensah, E.; Ashiagbor, G.; Boahen, O.; Sweeney, D., Watching the Smoke Rise Up: Thermal Efficiency, Pollutant Emissions and Global Warming Impact of Three Biomass Cookstoves in Ghana. *Energies* **2017,** *10*, (5), 641.

9. Bates, A., *The biochar solution: carbon farming and climate change*. New Society Publishers: 2010.

10. World Stove Website; http://worldstove.com/stoves.

11. Stanley Website; http://www.waterfordstanley.com/stanley-stoves/stanley-stoves/room-heating/solid-fuel.

12. Heringa, M. F.; DeCarlo, P. F.; Chirico, R.; Lauber, A.; Doberer, A.; Good, J.; Nussbaumer, T.; Keller, A.; Burtscher, H.; Richard, A.; Miljevic, B.; Prevot, A. S. H.; Baltensperger, U., Time-Resolved Characterization of Primary Emissions from Residential Wood Combustion Appliances. *Environ. Sci. Technol.* **2012,** *46*, (20), 11418-11425.

13. Brito, J.; Rizzo, L. V.; Morgan, W. T.; Coe, H.; Johnson, B.; Haywood, J.; Longo, K.; Freitas, S.; Andreae, M. O.; Artaxo, P., Ground-based aerosol characterization during the South American Biomass Burning Analysis (SAMBBA) field experiment. *Atmos. Chem. Phys.* **2014,** *14*, (22), 12069-12083.

14. Haslett, S. L.; Thomas, J. C.; Morgan, W. T.; Hadden, R.; Liu, D.; Allan, J. D.; Williams, P. I.; Keita, S.; Liousse, C.; Coe, H., Highly controlled, reproducible measurements of aerosol emissions from combustion of a common African biofuel source. *Atmos. Chem. Phys.* **2018,** *18*, (1), 385-403.

15. Allan, J. D.; Delia, A. E.; Coe, H.; Bower, K. N.; Alfarra, M. R.; Jimenez, J. L.; Middlebrook, A. M.; Drewnick, F.; Onasch, T. B.; Canagaratna, M. R.; Jayne, J. T.; Worsnop, D. R., A generalised method for the extraction of chemically resolved mass spectra from Aerodyne aerosol mass spectrometer data. *J. Aerosol Sci.* **2004,** *35*, (7), 909-922.

16. Schneider, J.; Weimer, S.; Drewnick, F.; Borrmann, S.; Helas, G.; Gwaze, P.; Schmid, O.; Andreae, M. O.; Kirchner, U., Mass spectrometric analysis and aerodynamic properties of various types of combustion-related aerosol particles. *Int. J. Mass Spectrom.* **2006,** *258*, (1–3), 37-49.

17. Timko, M. T.; Yu, Z.; Kroll, J.; Jayne, J. T.; Worsnop, D. R.; Miake-Lye, R. C.; Onasch, T. B.; Liscinsky, D.; Kirchstetter, T. W.; Destaillats, H., Sampling artifacts from conductive silicone tubing. *Aerosol Sci. Technol.* **2009,** *43*, (9), 855-865.

18. Alfarra, M. R.; Prevot, A. S. H.; Szidat, S.; Sandradewi, J.; Weimer, S.; Lanz, V. A.; Schreiber, D.; Mohr, M.; Baltensperger, U., Identification of the Mass Spectral Signature of Organic Aerosols from Wood Burning Emissions. *Environ. Sci. Technol.* **2007,** *41*, (16), 5770-5777.

19. Baumgardner, D.; Popovicheva, O.; Allan, J.; Bernardoni, V.; Cao, J.; Cavalli, F.; Cozic, J.; Diapouli, E.; Eleftheriadis, K.; Genberg, P. J.; Gonzalez, C.; Gysel, M.; John, A.; Kirchstetter, T. W.; Kuhlbusch, T. A. J.; Laborde, M.; Lack, D.; Muller, T.; Niessner, R.; Petzold, A.; Piazzalunga, A.; Putaud, J. P.; Schwarz, J.; Sheridan, P.; Subramanian, R.; Swietlicki, E.; Valli, G.; Vecchi, R.; Viana, M., Soot reference materials for instrument calibration and intercomparisons: a workshop summary with recommendations. *Atmos. Meas. Tech.* **2012,** *5*, 1869- 1887.

20. Laborde, M.; Schnaiter, M.; Linke, C.; Saathoff, H.; Naumann, K. H.; Möhler, O.; Berlenz, S.; Wagner, U.; Taylor, J. W.; Liu, D.; Flynn, M.; Allan, J. D.; Coe, H.; Heimerl, K.; Dahlkötter, F.; Weinzierl, B.; Wollny, A. G.; Zanatta, M.; Cozic, J.; Laj, P.; Hitzenberger, R.;

Schwarz, J. P.; Gysel, M., Single Particle Soot Photometer intercomparison at the AIDA chamber. *Atmos. Meas. Tech.* **2012,** *5*, (12), 3077-3097.

Chapter 5

Conclusions

Carbonaceous aerosols in PM_1, including OM and BC, contributed by wood burning have increasingly received attention from people in the world due to the association with adverse effects on human health and climate warming. Biomass burning emissions, especially in winter, have been identified to be major sources of the CM. Although there have been several analysis techniques to estimate their contribution to CM, the estimations of these methods exist in a certain degree of uncertainty due to the complexity of characterising the emissions from biomass burning. In this thesis, the causes of the uncertainties is investigated using a comprehensive suite of aerosol measurements conducted at an urban background site in London in order to better estimate the contribution of the biomass burning to the air quality. The wood burning pollution, typically the BC from this source in London during wintertime is investigated to give a comprehensive evaluation of source apportionment approaches.

China is one of the globally largest source of the BC particles not only from the biomass burning but also from a range of combustion sources. In addition, significant uncertainties exist regarding the BC particle burden at the regional scale in China, which complicates the assessments of the impact of the BC emissions upon regional climate and air quality. In this thesis, a state-of-the-art instrumentation was used to characterise the BC particles in the YR region in eastern China. The analyses presented here mainly focus on the identification of the potential sources of BC, with particular emphasis on the BC properties in the PM1 and the effects of the regional transport.

In addition to the importance of the characteristics of BC particles contributed by solid fuel burning in the atmosphere, the understanding of the properties of the BC particle from residential solid fuel burning is also essential as the household emissions considerably contribute to air pollutants, and also the emissions from residential sources is persistent. Furthermore, as the combustion of solid fuel burning adds more complexity of the properties of BC particles due to the different combustion mechanisms and the large fraction of co-emitted OM, the source profile of BC for climate models to estimate its atmospheric lifetime and

the subsequent aging process is needed. Due to the limitation of previous instrumentation, the variety of fuels and burning conditions, the profiles of BC of the solid fuel combustion emissions at source have been scarce and not applied in most of the models. In this thesis, the primary emissions from the cookstoves with a variety of the solid fuels burnt in the laboratory were therefore determined and investigated to provide an insight into the impact on human health and climate forcing.

The following sections will summarise the research findings, discuss their implications, and give the recommendations pertinent to the issues raised in this thesis for the future work.

5.1 Summary of research findings

A comprehensive suite of the measurements were conducted during wintertime, in 2012, at an urban background site in London. Intercomparisons of the estimates of the source contributions from the different source apportionment techniques were presented in Section 4.1. Oxygenated organic aerosols (OOA) and the solid fuel organic aerosols (SFOA) were found to be the substances resulting in the difference between the attributions of BC contributed by biomass burning derived by Aethalometer model and SP2 techniques. The absorption Angstrom exponent for wood burning (α_{wb}) was found that it was essential to be adjusted depending on the behaviours of biomass burning rather than assuming a constant for all the time. With the AMS-PMF, which can identify the contribution of individual sources to OA, and SP2-attributed BC, the contributions of the biomass burning to the CM were better estimated by the Aethalometer model, implying that the estimation of the contribution of biomass burning to the CM in the mostly previous studies was possibly be overestimated due to the non-biomass burning OA attributed to those contributed by the biomass burning.

While the first paper examined the impact of the aerosol constituents on the BC measurements of the instruments, the second served a metric to evaluate the effects of the particulate pollutants from possible shipping emissions and regional pollutants on the air pollution over the YangTze River in wintertime and explored the characteristics of BC using the state-of-the-art instrumentation as presented in Section 4.2. With specific attention to the BC measurements and gaseous pollutants in the Yangtze River region, it was found that the basin was influenced

by complex sources, such as shipping emission, power plants, surrounding industries and regional transport from the cities along the river. NO_x and SO_2 was found to be the important indicators identifying the highly polluted periods (HPP), which indicated more localized emission, e.g. mainly from shipping emission on the river or some local industry sources along the river. These HPP were found to correspond with high BC number concentrations, but have no apparent correlation with CO and PM_1 due to the higher background level and the dominating secondary formation, respectively. For the region in the inner island, mostly influenced by terrain height and regional transport, and outer island, mainly influenced by easterly oceanic or westerly continental air mass, the core size of the rBC particles during the HPP decreased by 5.39-19.41% compared to those of the background. The BC with smaller core size at a mode of mass median diameter (MMD) of 120-180 nm was found to be contributed by the local sources, whereas a more consistent mode of MMD of ~200 nm was attributed to the mixed sources. Overall, the HPP, when the shipping emissions possibly dominated, increased the rBC number by 17.49-115.77% compared to those in the background, but less increase in rBC mass (5.62-51.19%) was found due to the smaller core size. The high consistency of the $PM_{2.5}$ between the measurements on the Yangtze River and the official monitoring stations in the coastal cities showed that the regional transport of the particulate matter had a significant impact on the air pollution in this region.

As the results presented in Section 4.1 and 4.2 illustrated the complexity of the characteristics of the rBC particles emitted by solid fuel combustion, the characteristics of carbonaceous aerosols of the primary emissions from solid fuel combustion were investigated in the laboratory using three examples of 'improved' cookstoves and a typical European heating stove as presented in Section 4.3. The results in this thesis showed that the modified combustion efficiency (MCE), a common metric used within the atmospheric emission community, was not a complete description, partly due to the large amount of OM emitted at the pyrolysis stage, which was not directly represented by a combustion metric.

It was found that the more complete combustion emitted less OM that was more oxidized. Although the difference between the degree of oxygenation of OM, as indicated by the fraction of m/z 44 in the total mass spectra (f44), and MCE

among the stove and fuel types was observed, a near exponential decline in ΔOM/ΔCO with increased *f44* has been observed in most of the combustion cycles. The almost identical BC core size for the cookstove combustion cycles was presented in this work. However, the core size of the rBC particles emitted from the solid fuel combustion in the heating stove was dependent on the MCE. Combustion in the heating stove during high MCE tended to emitted particles with larger BC core size than that during low MCE.

For the complicated dynamics in combustion processes presented, a certain relationship between the mixing state of the carbonaceous aerosols and MCE was presented. Among the combustion cycles in this work, it was found that 20-100% of OM was internally mixed with rBC when MCE > 0.95 depending on the fuel and stove types. When MCE < 0.95, over 80% of the total OM existed without detectable rBC. The mass ration of non-BC, which was considered to be mostly composed of OM in this study, and rBC was investigated and showed a certain consistency with the OM fraction in PM_1. When the OM mass fraction of PM_1 > 0.9, the bulk mass ratio of OM to rBC in BC-containing particles was often > 3, but only about 1 was observed when the OM mass ratio < 0.9. It was also found that the oxidation level of OM could be an indicator of the magnitude of the bulk mass ratio of OM to rBC in BC-containing particles based on *f44*/*f43*, which is related to the volatility of oxygenated organic aerosol (OOA). The internally-mixed OM for those thickly coated BC particles was considered to be less oxidized and more semi-volatile.

5.2 Implication and recommendation

The main findings of this project could be summarized as: intercomparison of different source apportionment techniques, the characteristics of the emissions from complex sources at regional scale in eastern China and the properties of the carbonaceous aerosols from solid fuel combustion from cookstove.

5.2.1 Evaluation of wood burning aerosols

The results presented in Section 6.1 are based on the measurements of the Clean Air for London research project (ClearfLo, www.clearflo.ac.uk, Bohnenstengel et al. (2014)) during wintertime, when the London urban environment is significant influenced by solid fuel burning sources, e.g. wood burning for residential heating (Allan et al., 2010). This section shows that OOA can significantly affect the

Aethalometer measurements, which is consistent with the previous studies indicating that secondary organic aerosols comprise brown carbon (BrC) exhibiting the properties of light absorption at different wavelengths to an extent (Saleh et al., 2013, Wang et al., 2014a). In addition, the absorption Angstrom exponent for wood burning (α_{wb}) is expected to be varied depending on the burning conditions, other non-traffic sources and fuel types rather that an assumption of a constant. There are literatures indicating that BrC is mainly contributed by biomass burning (Washenfelder et al., 2015) and the photo-oxidation of anthropogenic and biogenic volatile organic compounds (Ervens et al., 2011). Thus, the assumption of α_{wb} should depend on these components for a better estimation of BC from wood burning.

Results presented here demonstrate that using the pre-apportioned OM and BC in the Aethalometer model can obtain the more accurate parameters for the estimates of the contribution of wood burning to the carbonaceous matter compared to those in the previous studies (Sandradewi et al., 2008a; Fave et al., 2009, 2010), which may result in the overestimation of the contribution of wood burning to carbonaceous matter. This indicates that the Aethalometer model accompanied with the total carbonaceous matter consisting of the bulk OM and BC will attribute the unassociated wood burning emissions to the wood burning emissions, which leads to an overestimation of the attribution of their emissions to the carbonaceous matter.

The derived parameter for the estimation of the contribution of wood burning is based on the ambient environment in London during wintertime, and it is not necessarily applicable to other areas. Therefore, it is needed to carry out the numbers of the atmospheric measurements in other regions to obtain the accurate parameter for the specific ambient environment, which can underpin the mitigation strategies of air pollution.

5.2.2 Local sources and regional transport of air pollution in the Yangtze River basin

The Yangtze River campaign was carried out along the Yangtze River in winter 2015 in order to characterise rBC and its related gaseous pollution in eastern China. The observation was the first time to measure the shipping emissions and regional transport over the Yangtze River. The results presented in Section 4.2

illustrated that the air pollution in this region was significantly contributed by sulphur-containing fossil fuel combustion, which could be from the shipping emissions, power generation plants and facilities, etc., (Lu et al., 2006). In the different regions, the degree of the influence of local sources, including shipping emissions, and regional transport depended on the origin of the air mass and topography. The source of shipping emissions can be inferred according to the ship's tracking gases, NO_x and SO_2, accompanied with the small BC core and thin coating. In this study, shipping emissions were found to have a significant impact on air pollution in this region. Thus, the reduction in the shipping emissions can effectively decrease the occurrence of high pollution episodes over the river (MOT, 2015, Zhang et al., 2017). While large contribution of the shipping emissions to air pollution in the Yangtze River region can result in high pollution events, the regional transport also considerably contributes to the deterioration of air quality in the inland areas. Furthermore, the consistency of $PM_{2.5}$ between the measurements on the river and at environmental monitoring site in the coastal cities suggested that surrounding areas in the Yangtze River basin were major regional sources of $PM_{2.5}$. For example, the rBC properties of the larger core size and thicker coating dominated the background, which was mainly contributed by the regional transport, and suggested that the biomass burning and coal combustion were most likely to be the dominant sources (Huang et al., 2012; Liu et al., 2014; Wang et al., 2016).

Although the sources of BC have been roughly identified according to the origins of air masses, the specific sources and contribution to particulate matter of BC cannot identified. While Liu et al. (2014) has identified two sources of BC at urban background site in London by using the optical properties of BC with SP2 data, the method is not feasible for identification of the sources in eastern China due to the same properties of BC contributed by various sources. Therefore, it is recommended that a combined measurement with the SP2 and AMS, which can quantify the contribution of the specific sources to the organic matter, is needed to better estimate the contribution of BC sources.

5.2.3 The mixing state of the primary carbonaceous aerosols from solid fuel combustion

The results presented in Section 4.3 provide useful insights into interactions between BC and OM, which were emitted by residential solid fuel combustion with the complex dynamics in the combustion process, by simulating real-world burning conditions in laboratory. There have been a number of studies investigating the link between the variation of carbonaceous aerosols from heating and cooking stoves and the variables affecting the burning conditions, such as fuel and stove types (Heringa et al., 2012, Just et al., 2013, Kortelainen et al., 2015, Haslett et al., 2018). These have proven valuable knowledge of the variability of emission under different burning conditions and the properties of emitted aerosols. However, the source profile of BC for solid fuel combustion, which have been simplified in most global model (Koch et al., 2009; Reddington et al., 2013), is scarce due to the instrumentation limitation, the wide variety of fuels and burning conditions, resulting in the over- or underestimation of the impact of BC on climate forcing. Thus, the source profile of BC for residential solid fuel burning presented in Section 4.3 can be applied in most of the models in order to more accurately assess the impact of BC, produced by residential solid fuel combustion, on the regional and global climate forcing.

Furthermore, the relationship between the OM fraction in PM_1 and the mixing state of BC presented here indicates that the OM fraction can be used in models to determine the impact of BC from solid fuel burning on global warming, when the mixing state of BC is not available. The results here will help to assess the benefits of reduction in BC from domestic solid fuel combustion and so aid mitigation strategies in the future.

While this study provides new insight into the mixing state of BC in the combustion processes, the results here should be treated as indicative for use in models and more authoritative data will need more work, specifically repeat experiments with other stove designs, fuel types and with a more explicit simulation of cooking activities.

5.3 Closing remarks

This project evaluated a variety of BC sources from few representing sources over European, African and Asian countries.

It is highly challenging to identify the sources of atmospheric aerosols and to estimate their contribution to air pollution due to high variability of aerosols in the atmosphere, particularly the complex and uncertain emissions from anthropogenic solid fuel burning. The London study provides an opportunity to evaluate the multiple sources in urban environment by examining a variety of source apportionment techniques, and the results could be widely used in other urban environments even when some of the instrumentations are not always available.

China has been a rapidly developing country and is projected to continue developing at a rapid pace. The large population has a big demand for energy, from which the sources are complex and extensively distributed. Accompanied with the unstable meteorological conditions, it is very difficult to identify the specific sources and to fully understand the characteristics of their emissions. This work provided the characteristics of the emissions in the YR region. The AMS measurement should be added in the future study, and thus the well-developed PMF model can be used to explicitly identify the sources of the air pollutants.

Source profiles of BC for solid fuel combustion vary considerably with stove and fuel types. More work for the establishment of the source files of BC from different stoves and solid fuels is essential to aid climate models in better estimating the impact of the solid fuel combustion emissions on regional and global scale.

Appendix A. Co-authorship in peer reviewed publications

Title: Black-carbon absorption enhancement in the atmosphere determined by particle mixing state

Authors: Dantong Liu, James Whitehead, M. Rami Alfarra, Ernesto Reyes-Villegas, Dominick V. Spracklen, Carly L. Reddington, Shaofei Kong, Paul I.Williams, Yu-Chieh Ting, Sophie Haslett, JonathanW. Taylor, Michael J. Flynn,William T. Morgan, Gordon McFiggans, Hugh Coe and James D. Allan

doi.org/10.1038/ngeo2901

I participated in the measurements and assistance of the manuscript.

Title: Simultaneous aerosol mass spectrometry and chemical ionisation mass spectrometry measurements during a biomass burning event in the UK: insights into nitrate chemistry

Authors: Ernesto Reyes-Villegas, Michael Priestley, Yu-Chieh Ting, Sophie Haslett, Thomas Bannan, Michael Le Breton, Paul I. Williams, Asan Bacak, Michael J. Flynn, Hugh Coe, Carl Percival, and James D. Allan

doi.org/10.5194/acp-2017-605

I participated in the measurements and assistance of the manuscript.

References

ABDALMOGITH, S. S. & HARRISON, R. M. 2006. An analysis of spatial and temporal properties of daily sulfate, nitrate and chloride concentrations at UK urban and rural sites. *Journal of Environmental Monitoring,* 8**,** 691-699.

AIKEN, A., SALCEDO, D., CUBISON, M. J., HUFFMAN, J., DECARLO, P., ULBRICH, I. M., DOCHERTY, K. S., SUEPER, D., KIMMEL, J. & WORSNOP, D. R. 2009. Mexico City aerosol analysis during MILAGRO using high resolution aerosol mass spectrometry at the urban supersite (T0)–Part 1: Fine particle composition and organic source apportionment. *Atmospheric Chemistry and Physics,* 9**,** 6633-6653.

ALFARRA, M. R., COE, H., ALLAN, J. D., BOWER, K. N., BOUDRIES, H., CANAGARATNA, M. R., JIMENEZ, J. L., JAYNE, J. T., GARFORTH, A. A., LI, S.-M. & WORSNOP, D. R. 2004. Characterization of urban and rural organic particulate in the Lower Fraser Valley using two Aerodyne Aerosol Mass Spectrometers. *Atmospheric Environment,* 38**,** 5745-5758.

ALLAN, J. D., DELIA, A. E., COE, H., BOWER, K. N., ALFARRA, M. R., JIMENEZ, J. L., MIDDLEBROOK, A. M., DREWNICK, F., ONASCH, T. B., CANAGARATNA, M. R., JAYNE, J. T. & WORSNOP, D. R. 2004. A generalised method for the extraction of chemically resolved mass spectra from Aerodyne aerosol mass spectrometer data. *J. Aerosol Sci.,* 35**,** 909-922.

ALLAN, J. D., JIMENEZ, J. L., WILLIAMS, P. I., ALFARRA, M. R., BOWER, K. N., JAYNE, J. T., COE, H. & WORSNOP, D. R. 2003. Quantitative sampling using an Aerodyne aerosol mass spectrometer 1. Techniques of data interpretation and error analysis. *Journal of Geophysical Research: Atmospheres (1984–2012),* 108.

ALLAN, J. D., WILLIAMS, P. I., MORGAN, W. T., MARTIN, C. L., FLYNN, M. J., LEE, J., NEMITZ, E., PHILLIPS, G. J., GALLAGHER, M. W. & COE, H. 2010. Contributions from transport, solid fuel burning and cooking to primary organic aerosols in two UK cities. *Atmos. Chem. Phys.,* 10**,** 647-668.

AMATO, F. & HOPKE, P. K. 2012. Source apportionment of the ambient PM2.5 across St. Louis using constrained positive matrix factorization. *Atmospheric Environment,* 46**,** 329-337.

AMEGAH, A. K. & JAAKKOLA, J. J. 2016. Household air pollution and the sustainable development goals. *Bulletin of the World Health Organization,* 94**,** 215.

AN, J., ZHU, B., WANG, H., LI, Y., LIN, X. & YANG, H. 2014. Characteristics and source apportionment of VOCs measured in an industrial area of Nanjing, Yangtze River Delta, China. *Atmospheric Environment,* 97**,** 206-214.

ANDREAE, M. O. & GELENCSÉR, A. 2006. Black carbon or brown carbon? The nature of light-absorbing carbonaceous aerosols. *Atmos. Chem. Phys.,* 6**,** 3131-3148.

ANENBERG, S. C., BALAKRISHNAN, K., JETTER, J., MASERA, O., MEHTA, S., MOSS, J. & RAMANATHAN, V. 2013. Cleaner Cooking Solutions to Achieve Health, Climate, and Economic Cobenefits. *Environmental Science & Technology,* 47**,** 3944-3952.

AQEG 2012. Fine Particulate Matter (PM2.5) in the United Kingdom, Defra, London.
BAEK, B. H., ANEJA, V. P. & TONG, Q. 2004. Chemical coupling between ammonia, acid gases, and fine particles. *Environmental Pollution,* 129**,** 89-98.
BAUMGARDNER, D., POPOVICHEVA, O., ALLAN, J., BERNARDONI, V., CAO, J., CAVALLI, F., COZIC, J., DIAPOULI, E., ELEFTHERIADIS, K., GENBERG, P. J., GONZALEZ, C., GYSEL, M., JOHN, A., KIRCHSTETTER, T. W., KUHLBUSCH, T. A. J., LABORDE, M., LACK, D., MULLER, T., NIESSNER, R., PETZOLD, A., PIAZZALUNGA, A., PUTAUD, J. P., SCHWARZ, J., SHERIDAN, P., SUBRAMANIAN, R., SWIETLICKI, E., VALLI, G., VECCHI, R. & VIANA, M. 2012. Soot reference materials for instrument calibration and intercomparisons: a workshop summary with recommendations. *Atmos. Meas. Tech.,* 5**,** 1869- 1887.
BEEVERS, S. D., KITWIROON, N., WILLIAMS, M. L., KELLY, F. J., ANDERSON, H. R. & CARSLAW, D. C. 2013. Air pollution dispersion models for human exposure predictions in London. *Journal of Exposure Science and Environmental Epidemiology,* 23**,** 647-653.
BOHNENSTENGEL, S. I., HAMILTON, I., DAVIES, M. & BELCHER, S. E. 2014. Impact of anthropogenic heat emissions on London's temperatures. *Quarterly Journal of the Royal Meteorological Society,* 140**,** 687-698.
BOND, T. C. & BERGSTROM, R. W. 2006. Light Absorption by Carbonaceous Particles: An Investigative Review. *Aerosol Sci. Technol.,* 40**,** 27-67.
BOND, T. C., DOHERTY, S. J., FAHEY, D., FORSTER, P., BERNTSEN, T., DEANGELO, B., FLANNER, M., GHAN, S., KÄRCHER, B. & KOCH, D. 2013. Bounding the role of black carbon in the climate system: A scientific assessment. *J. Geophys. Res.,* 118**,** 5380-5552.
BOND, T. C., STREETS, D. G., YARBER, K. F., NELSON, S. M., WOO, J. H. & KLIMONT, Z. 2004. A technology-based global inventory of black and organic carbon emissions from combustion. *J. Geophys. Res.,* 109.
BRITO, J., RIZZO, L. V., MORGAN, W. T., COE, H., JOHNSON, B., HAYWOOD, J., LONGO, K., FREITAS, S., ANDREAE, M. O. & ARTAXO, P. 2014. Ground-based aerosol characterization during the South American Biomass Burning Analysis (SAMBBA) field experiment. *Atmos. Chem. Phys.,* 14**,** 12069-12083.
BROOK, R. D., FRANKLIN, B., CASCIO, W., HONG, Y., HOWARD, G., LIPSETT, M., LUEPKER, R., MITTLEMAN, M., SAMET, J. & SMITH, S. C. 2004. Air pollution and cardiovascular disease: a statement for healthcare professionals from the Expert Panel on Population and Prevention Science of the American Heart Association. *Circulation,* 109**,** 2655-2671.
BRUNEKREEF, B. & HOLGATE, S. T. 2002. Air pollution and health. *The Lancet,* 360**,** 1233-1242.
BRYNER, G. C. 1993. Blue skies, green politics: The clean air act of 1990.
BULLOCK, K. R., DUVALL, R. M., NORRIS, G. A., MCDOW, S. R. & HAYS, M. D. 2008. Evaluation of the CMB and PMF models using organic molecular markers in fine particulate matter collected during the Pittsburgh Air Quality Study. *Atmospheric Environment,* 42**,** 6897-6904.
BUTTERFIELD, D., BECCACECI, S., QUINCEY, P., SWEENEY, B., WHITESIDE, K., FULLER, G., GREEN, D. & GRIEVE, A. 2016. 2014 Annual Report for the UK Black Carbon Network.

CANAGARATNA, M. R., JAYNE, J. T., JIMENEZ, J. L., ALLAN, J. D., ALFARRA, M. R., ZHANG, Q., ONASCH, T. B., DREWNICK, F., COE, H., MIDDLEBROOK, A., DELIA, A., WILLIAMS, L. R., TRIMBORN, A. M., NORTHWAY, M. J., DECARLO, P. F., KOLB, C. E., DAVIDOVITS, P. & WORSNOP, D. R. 2007. Chemical and microphysical characterization of ambient aerosols with the aerodyne aerosol mass spectrometer. *Mass Spectrometry Reviews,* 26**,** 185-222.

CANONACO, F., CRIPPA, M., SLOWIK, J. G., BALTENSPERGER, U. & PREVOT, A. S. H. 2013. SoFi, an IGOR-based interface for the efficient use of the generalized multilinear engine (ME-2) for the source apportionment: ME-2 application to aerosol mass spectrometer data. *Atmospheric Measurement Techniques,* 6**,** 3649-3661.

CHARRON, A., HARRISON, R. M. & QUINCEY, P. 2007. What are the sources and conditions responsible for exceedences of the 24 h PM10 limit value (50 µg m−3) at a heavily trafficked London site? *Atmospheric Environment,* 41**,** 1960-1975.

CHEN, L. W. A., WATSON, J. G., CHOW, J. C., DUBOIS, D. W. & HERSCHBERGER, L. 2011. PM2.5 Source Apportionment: Reconciling Receptor Models for U.S. Nonurban and Urban Long-Term Networks. *Journal of the Air & Waste Management Association,* 61**,** 1204-1217.

CHEN, P., WANG, T., HU, X. & XIE, M. 2015. Chemical Mass Balance Source Apportionment of Size-Fractionated Particulate Matter in Nanjing, China. *Aerosol and Air Quality Research,* 15**,** 1855-1867.

CHEN, T., DENG, S., GAO, Y., QU, L., LI, M. & CHEN, D. 2017. Characterization of air pollution in urban areas of Yangtze River Delta, China. *Chinese Geographical Science,* 27**,** 836-846.

CHENG, Z., WANG, S., FU, X., WATSON, J. G., JIANG, J., FU, Q., CHEN, C., XU, B., YU, J., CHOW, J. C. & HAO, J. 2014. Impact of biomass burning on haze pollution in the Yangtze River delta, China: a case study in summer 2011. *Atmos. Chem. Phys.,* 14**,** 4573-4585.

CHINA, M. 2012. Ambient air quality standards. GB 3095-2012. *China Environmental Science Press, Beijing*.

COLLAUD COEN, M., WEINGARTNER, E., APITULEY, A., CEBURNIS, D., FIERZ-SCHMIDHAUSER, R., FLENTJE, H., HENZING, J., JENNINGS, S. G., MOERMAN, M. & PETZOLD, A. 2010. Minimizing light absorption measurement artifacts of the Aethalometer: evaluation of five correction algorithms. *Atmospheric Measurement Techniques,* 3**,** 457-474.

CRILLEY, L. R., BLOSS, W. J., YIN, J., BEDDOWS, D. C. S., HARRISON, R. M., ALLAN, J. D., YOUNG, D. E., FLYNN, M., WILLIAMS, P., ZOTTER, P., H. PREVOT, A. S., HEAL, M. R., BARLOW, J. F., HALIOS, C. H., LEE, J. D., SZIDAT, S. & MOHR, C. 2014. Sources and contributions of wood smoke during winter in London: assessing local and regional influences. *Atmos. Chem. Phys. Discuss.,* 14**,** 27459-27530.

CRILLEY, L. R., BLOSS, W. J., YIN, J., BEDDOWS, D. C. S., HARRISON, R. M., ALLAN, J. D., YOUNG, D. E., FLYNN, M., WILLIAMS, P., ZOTTER, P., PREVOT, A. S. H., HEAL, M. R., BARLOW, J. F., HALIOS, C. H., LEE, J. D., SZIDAT, S. & MOHR, C. 2015. Sources and contributions of wood smoke during winter in London: assessing local and regional influences. *Atmos. Chem. Phys.,* 15**,** 3149-3171.

CROSIER, J., ALLAN, J., COE, H., BOWER, K., FORMENTI, P. & WILLIAMS, P. 2007. Chemical composition of summertime aerosol in the

Po Valley (Italy), northern Adriatic and Black Sea. *Quarterly Journal of the Royal Meteorological Society,* 133**,** 61-75.
DECARLO, P. F., KIMMEL, J. R., TRIMBORN, A., NORTHWAY, M. J., JAYNE, J. T., AIKEN, A. C., GONIN, M., FUHRER, K., HORVATH, T., DOCHERTY, K. S., WORSNOP, D. R. & JIMENEZ, J. L. 2006. Field-Deployable, High-Resolution, Time-of-Flight Aerosol Mass Spectrometer. *Analytical Chemistry,* 78**,** 8281-8289.
DEFRA 2017. (Department for Environment, Food and Rural Affairs) Family Food 2015. *Available at: www.gov.uk/government/uploads/system/uploads/attachment_data/file/597667/Family_*.
DING, A., FU, C., YANG, X., SUN, J., ZHENG, L., XIE, Y., HERRMANN, E., NIE, W., PETÄJÄ, T. & KERMINEN, V.-M. 2013. Ozone and fine particle in the western Yangtze River Delta: an overview of 1 yr data at the SORPES station. *Atmospheric Chemistry and Physics,* 13**,** 5813-5830.
DOCHERTY, K. S., STONE, E. A., ULBRICH, I. M., DECARLO, P. F., SNYDER, D. C., SCHAUER, J. J., PELTIER, R. E., WEBER, R. J., MURPHY, S. M., SEINFELD, J. H., GROVER, B. D., EATOUGH, D. J. & JIMENEZ, J. L. 2008. Apportionment of Primary and Secondary Organic Aerosols in Southern California during the 2005 Study of Organic Aerosols in Riverside (SOAR-1). *Environmental Science & Technology,* 42**,** 7655-7662.
DOUMBIA, E. H. T., LIOUSSE, C., GALY-LACAUX, C., NDIAYE, S. A., DIOP, B., OUAFO, M., ASSAMOI, E. M., GARDRAT, E., CASTERA, P., ROSSET, R., AKPO, A. & SIGHA, L. 2012. Real time black carbon measurements in West and Central Africa urban sites. *Atmospheric Environment,* 54**,** 529-537.
DREWNICK, F., HINGS, S., ALFARRA, M., PREVOT, A. & BORRMANN, S. 2009. Aerosol quantification with the Aerodyne Aerosol Mass Spectrometer: detection limits and ionizer background effects. *Atmospheric Measurement Techniques,* 2**,** 33-46.
DREWNICK, F., HINGS, S. S., DECARLO, P., JAYNE, J. T., GONIN, M., FUHRER, K., WEIMER, S., JIMENEZ, J. L., DEMERJIAN, K. L., BORRMANN, S. & WORSNOP, D. R. 2005. A New Time-of-Flight Aerosol Mass Spectrometer (TOF-AMS)—Instrument Description and First Field Deployment. *Aerosol Sci. Technol.,* 39**,** 637-658.
DRINOVEC, L., MOČNIK, G., ZOTTER, P., PRÉVÔT, A. S. H., RUCKSTUHL, C., COZ, E., RUPAKHETI, M., SCIARE, J., MÜLLER, T., WIEDENSOHLER, A. & HANSEN, A. D. A. 2015. The "dual-spot" Aethalometer: An improved measurement of aerosol black carbon with real-time loading compensation. *Atmospheric Measurement Techniques,* 8**,** 1965-1979.
EDMONDS, R. L. 1999. The environment in the People's Republic of China 50 years on. *The China Quarterly,* 159**,** 640-649.
ERVENS, B., TURPIN, B. J. & WEBER, R. 2011. Secondary organic aerosol formation in cloud droplets and aqueous particles (aqSOA): a review of laboratory, field and model studies. *Atmospheric Chemistry and Physics,* 11**,** 11069-11102.
FAN, Q., ZHANG, Y., MA, W., MA, H., FENG, J., YU, Q., YANG, X., NG, S. K. W., FU, Q. & CHEN, L. 2016. Spatial and Seasonal Dynamics of Ship Emissions over the Yangtze River Delta and East China Sea and Their

Potential Environmental Influence. *Environmental Science & Technology,* 50**,** 1322-1329.

FAVEZ, O., EL HADDAD, I., PIOT, C., BOREAVE, A., ABIDI, E., MARCHAND, N., JAFFREZO, J. L., BESOMBES, J. L., PERSONNAZ, M. B., SCIARE, J., WORTHAM, H., GEORGE, C. & D'ANNA, B. 2010. Inter-comparison of source apportionment models for the estimation of wood burning aerosols during wintertime in an Alpine city (Grenoble, France). *Atmospheric Chemistry and Physics,* 10**,** 5295-5314.

FLATO, G., MAROTZKE, J., ABIODUN, B., BRACONNOT, P., CHOU, S. C., COLLINS, W. J., COX, P., DRIOUECH, F., EMORI, S. & EYRING, V. 2013. Evaluation of Climate Models. In: Climate Change 2013: The Physical Science Basis. Contribution of Working Group I to the Fifth Assessment Report of the Intergovernmental Panel on Climate Change. *Climate Change 2013,* 5**,** 741-866.

FU, Q., ZHUANG, G., WANG, J., XU, C., HUANG, K., LI, J., HOU, B., LU, T. & STREETS, D. G. 2008. Mechanism of formation of the heaviest pollution episode ever recorded in the Yangtze River Delta, China. *Atmospheric Environment,* 42**,** 2023-2036.

FU, X., WANG, S., ZHAO, B., XING, J., CHENG, Z., LIU, H. & HAO, J. 2013. Emission inventory of primary pollutants and chemical speciation in 2010 for the Yangtze River Delta region, China. *Atmospheric Environment,* 70**,** 39-50.

FUZZI, S., ANDREAE, M. O., HUEBERT, B. J., KULMALA, M., BOND, T. C., BOY, M., DOHERTY, S. J., GUENTHER, A., KANAKIDOU, M., KAWAMURA, K., KERMINEN, V. M., LOHMANN, U., RUSSELL, L. M. & PÖSCHL, U. 2006. Critical assessment of the current state of scientific knowledge, terminology, and research needs concerning the role of organic aerosols in the atmosphere, climate, and global change. *Atmos. Chem. Phys.,* 6**,** 2017-2038.

FUZZI, S., BALTENSPERGER, U., CARSLAW, K., DECESARI, S., DENIER VAN DER GON, H., FACCHINI, M., FOWLER, D., KOREN, I., LANGFORD, B. & LOHMANN, U. 2015. Particulate matter, air quality and climate: lessons learned and future needs. *Atmospheric chemistry and physics,* 15**,** 8217-8299.

GAO, R. S., SCHWARZ, J. P., KELLY, K. K., FAHEY, D. W., WATTS, L. A., THOMPSON, T. L., SPACKMAN, J. R., SLOWIK, J. G., CROSS, E. S., HAN, J. H., DAVIDOVITS, P., ONASCH, T. B. & WORSNOP, D. R. 2007. A Novel Method for Estimating Light-Scattering Properties of Soot Aerosols Using a Modified Single-Particle Soot Photometer. *Aerosol Science and Technology,* 41**,** 125-135.

GARLAND, C., DELAPENA, S., PRASAD, R., L'ORANGE, C., ALEXANDER, D. & JOHNSON, M. 2017. Black carbon cookstove emissions: A field assessment of 19 stove/fuel combinations. *Atmospheric Environment,* 169**,** 140-149.

GENG, F., ZHANG, Q., TIE, X., HUANG, M., MA, X., DENG, Z., YU, Q., QUAN, J. & ZHAO, C. 2009. Aircraft measurements of O3, NOx, CO, VOCs, and SO2 in the Yangtze River Delta region. *Atmospheric Environment,* 43**,** 584-593.

GIANINI, M. F. D., PIOT, C., HERICH, H., BESOMBES, J. L., JAFFREZO, J. L. & HUEGLIN, C. 2013. Source apportionment of PM10, organic carbon and elemental carbon at Swiss sites: An intercomparison of different approaches. *Science of The Total Environment,* 454–455**,** 99-108.

GLOVER, D. M., HOPKE, P. K., VERMETTE, S. J., LANDSBERGER, S. & D'AUBEN, D. R. 1991. Source Apportionment with Site Specific Source Profiles. *Journal of the Air & Waste Management Association,* 41**,** 294-305.

GOLDSTEIN, A. H. & GALBALLY, I. E. 2007. Known and Unexplored Organic Constituents in the Earth's Atmosphere. *Environmental Science and Technology***,** 1515-1521.

GONG, X., ZHANG, C., CHEN, H., NIZKORODOV, S. A., CHEN, J. & YANG, X. 2016. Size distribution and mixing state of black carbon particles during a heavy air pollution episode in Shanghai. *Atmos. Chem. Phys.,* 16**,** 5399-5411.

GRAHAME, T. J., KLEMM, R. & SCHLESINGER, R. B. 2014. Public health and components of particulate matter: The changing assessment of black carbon. *Journal of the Air & Waste Management Association,* 64**,** 620-660.

HAMILTON, J. F., WEBB, P. J., LEWIS, A. C., HOPKINS, J. R., SMITH, S., DAVY, P., HAMILTON, J. F., WEBB, P. J., LEWIS, A. C., HOPKINS, J. R., SMITH, S. & DAVY, P. 2004. Partially oxidised organic components in urban aerosol using GCXGC-TOF/MS. *Atmospheric Chemistry and Physics,* 4**,** 1279-1290.

HANSEN, A. D. A., ROSEN, H. & NOVAKOV, T. 1984. The aethalometer — An instrument for the real-time measurement of optical absorption by aerosol particles. *Science of The Total Environment,* 36**,** 191-196.

HARRISON, R. M., BEDDOWS, D. C. S., HU, L. & YIN, J. 2012. Comparison of methods for evaluation of wood smoke and estimation of UK ambient concentrations. *Atmos. Chem. Phys.,* 12**,** 8271-8283.

HARRISON, R. M., BEDDOWS, D. C. S., JONES, A. M., CALVO, A., ALVES, C. & PIO, C. 2013. An evaluation of some issues regarding the use of aethalometers to measure woodsmoke concentrations. *Atmospheric Environment,* 80**,** 540-548.

HARRISON, R. M., STEDMAN, J. & DERWENT, D. 2008. New Directions: Why are PM 10 concentrations in Europe not falling? *Atmospheric Environment,* 42**,** 603-606.

HASLETT, S. L., THOMAS, J. C., MORGAN, W. T., HADDEN, R., LIU, D., ALLAN, J. D., WILLIAMS, P. I., KEITA, S., LIOUSSE, C. & COE, H. 2018. Highly controlled, reproducible measurements of aerosol emissions from combustion of a common African biofuel source. *Atmos. Chem. Phys.,* 18**,** 385-403.

HEINTZENBERG, J., RAES, F., SCHWARTZ, S., ACKERMANN, I., ARTAXO, P., BATES, T., BENKOVITZ, C., BIGG, K., BOND, T., BRENGUIER, J.-L., EISELE, F., FEICHTER, J., FLOSSMAN, A., FUZZI, S., GRAF, H.-F., HALES, J., HERRMANN, H., HOFFMANN, T., HUEBERT, B., HUSAR, R., JAENICKE, R., KÄRCHER, B., KAUFMAN, Y., KENT, G., KULMALA, M., LECK, C., LIOUSSE, C., LOHMANN, U., MARTICORENA, B., MCMURRY, P., NOONE, K., O'DOWD, C., PENNER, J., PSZENNY, A., PUTAUD, J.-P., QUINN, P., SCHURATH, U., SEINFELD, J., SIEVERING, H., SNIDER, J., SOKOLIK, I., STRATMANN, F., VAN DINGENEN, R., WESTPHAL, D., WEXLER, A., WIEDENSOHLER, A., WINKER, D. & WILSON, J. 2003. Tropospheric Aerosols. *In:* BRASSEUR, G., PRINN, R. & PSZENNY, A. P. (eds.) *Atmospheric Chemistry in a Changing World.* Springer Berlin Heidelberg.

HENRY, R. C., CHANG, Y.-S. & SPIEGELMAN, C. H. 2002. Locating nearby sources of air pollution by nonparametric regression of atmospheric concentrations on wind direction. *Atmospheric Environment,* 36**,** 2237-2244.

HEO, J., DULGER, M., OLSON, M. R., MCGINNIS, J. E., SHELTON, B. R., MATSUNAGA, A., SIOUTAS, C. & SCHAUER, J. J. 2013. Source apportionments of PM2.5 organic carbon using molecular marker Positive Matrix Factorization and comparison of results from different receptor models. *Atmospheric Environment,* 73**,** 51-61.

HERINGA, M. F., DECARLO, P. F., CHIRICO, R., LAUBER, A., DOBERER, A., GOOD, J., NUSSBAUMER, T., KELLER, A., BURTSCHER, H., RICHARD, A., MILJEVIC, B., PREVOT, A. S. H. & BALTENSPERGER, U. 2012. Time-Resolved Characterization of Primary Emissions from Residential Wood Combustion Appliances. *Environ. Sci. Technol.,* 46**,** 11418-11425.

HOPKE, P. K. 1985. *Receptor modeling in environmental chemistry*, John Wiley & Sons.

HOPKE, P. K. 2003. Recent developments in receptor modeling. *Journal of Chemometrics,* 17**,** 255-265.

HOPKE, P. K., ITO, K., MAR, T., CHRISTENSEN, W. F., EATOUGH, D. J., HENRY, R. C., KIM, E., LADEN, F., LALL, R., LARSON, T. V., LIU, H., NEAS, L., PINTO, J., STOLZEL, M., SUH, H., PAATERO, P. & THURSTON, G. D. 2006. PM source apportionment and health effects: 1. Intercomparison of source apportionment results. *J Expos Sci Environ Epidemiol,* 16**,** 275-286.

HU, J., WANG, Y., YING, Q. & ZHANG, H. 2014. Spatial and temporal variability of PM2.5 and PM10 over the North China Plain and the Yangtze River Delta, China. *Atmospheric Environment,* 95**,** 598-609.

HUA, Y., CHENG, Z., WANG, S., JIANG, J., CHEN, D., CAI, S., FU, X., FU, Q., CHEN, C., XU, B. & YU, J. 2015. Characteristics and source apportionment of PM2.5 during a fall heavy haze episode in the Yangtze River Delta of China. *Atmospheric Environment,* 123, Part B**,** 380-391.

HUANG, C., CHEN, C. H., LI, L., CHENG, Z., WANG, H. L., HUANG, H. Y., STREETS, D. G., WANG, Y. J., ZHANG, G. F. & CHEN, Y. R. 2011. Emission inventory of anthropogenic air pollutants and VOC species in the Yangtze River Delta region, China. *Atmos. Chem. Phys.,* 11**,** 4105-4120.

HUANG, X.-F., SUN, T.-L., ZENG, L.-W., YU, G.-H. & LUAN, S.-J. 2012a. Black carbon aerosol characterization in a coastal city in South China using a single particle soot photometer. *Atmospheric Environment,* 51**,** 21-28.

HUANG, X.-F., XUE, L., TIAN, X.-D., SHAO, W.-W., SUN, T.-L., GONG, Z.-H., JU, W.-W., JIANG, B., HU, M. & HE, L.-Y. 2013. Highly time-resolved carbonaceous aerosol characterization in Yangtze River Delta of China: Composition, mixing state and secondary formation. *Atmospheric Environment,* 64**,** 200-207.

HUANG, X. F., HE, L. Y., XUE, L., SUN, T. L., ZENG, L. W., GONG, Z. H., HU, M. & ZHU, T. 2012b. Highly time-resolved chemical characterization of atmospheric fine particles during 2010 Shanghai World Expo. *Atmos. Chem. Phys.,* 12**,** 4897-4907.

HUFFMAN, J. A., JAYNE, J. T., DREWNICK, F., AIKEN, A. C., ONASCH, T., WORSNOP, D. R. & JIMENEZ, J. L. 2005. Design, modeling, optimization, and experimental tests of a particle beam width probe for the

aerodyne aerosol mass spectrometer. *Aerosol Science and Technology,* 39**,** 1143-1163.

HYVÄRINEN, A. P., KOLMONEN, P., KERMINEN, V. M., VIRKKULA, A., LESKINEN, A., KOMPPULA, M., HATAKKA, J., BURKHART, J., STOHL, A., AALTO, P., KULMALA, M., LEHTINEN, K. E. J., VIISANEN, Y. & LIHAVAINEN, H. 2011. Aerosol black carbon at five background measurement sites over Finland, a gateway to the Arctic. *Atmospheric Environment,* 45**,** 4042-4050.

JANSSEN, N., GERLOFS-NIJLAND, M., LANKI, T., SALONEN, R., CASSEE, F., HOEK, G., FISCHER, P., BRUNEKREEF, B. & KRZYZANOWSKI, M. 2012. Health effects of black carbon, The WHO European Centre for Environment and Health, Bonn, Germany. *World Health Organisation Regional Office for Europe, Copenhagen, Denmark.*

JAYNE, J. T., LEARD, D. C., ZHANG, X., DAVIDOVITS, P., SMITH, K. A., KOLB, C. E. & WORSNOP, D. R. 2000. Development of an Aerosol Mass Spectrometer for Size and Composition Analysis of Submicron Particles. *Aerosol Science and Technology,* 33**,** 49-70.

JI, D., WANG, Y., WANG, L., CHEN, L., HU, B., TANG, G., XIN, J., SONG, T., WEN, T., SUN, Y., PAN, Y. & LIU, Z. 2012. Analysis of heavy pollution episodes in selected cities of northern China. *Atmospheric Environment,* 50**,** 338-348.

JIMENEZ, J. L., CANAGARATNA, M. R., DONAHUE, N. M., PREVOT, A. S. H., ZHANG, Q., KROLL, J. H., DECARLO, P. F., ALLAN, J. D., COE, H., NG, N. L., AIKEN, A. C., DOCHERTY, K. S., ULBRICH, I. M., GRIESHOP, A. P., ROBINSON, A. L., DUPLISSY, J., SMITH, J. D., WILSON, K. R., LANZ, V. A., HUEGLIN, C., SUN, Y. L., TIAN, J., LAAKSONEN, A., RAATIKAINEN, T., RAUTIAINEN, J., VAATTOVAARA, P., EHN, M., KULMALA, M., TOMLINSON, J. M., COLLINS, D. R., CUBISON, M. J., E., DUNLEA, J., HUFFMAN, J. A., ONASCH, T. B., ALFARRA, M. R., WILLIAMS, P. I., BOWER, K., KONDO, Y., SCHNEIDER, J., DREWNICK, F., BORRMANN, S., WEIMER, S., DEMERJIAN, K., SALCEDO, D., COTTRELL, L., GRIFFIN, R., TAKAMI, A., MIYOSHI, T., HATAKEYAMA, S., SHIMONO, A., SUN, J. Y., ZHANG, Y. M., DZEPINA, K., KIMMEL, J. R., SUEPER, D., JAYNE, J. T., HERNDON, S. C., TRIMBORN, A. M., WILLIAMS, L. R., WOOD, E. C., MIDDLEBROOK, A. M., KOLB, C. E., BALTENSPERGER, U. & WORSNOP, D. R. 2009. Evolution of Organic Aerosols in the Atmosphere. *Science,* 326**,** 1525-1529.

JIMENEZ, J. L., JAYNE, J. T., SHI, Q., KOLB, C. E., WORSNOP, D. R., YOURSHAW, I., SEINFELD, J. H., FLAGAN, R. C., ZHANG, X. & SMITH, K. A. 2003. Ambient aerosol sampling using the aerodyne aerosol mass spectrometer. *Journal of Geophysical Research: Atmospheres (1984–2012),* 108.

JUST, B., ROGAK, S. & KANDLIKAR, M. 2013. Characterization of Ultrafine Particulate Matter from Traditional and Improved Biomass Cookstoves. *Environ. Sci. Technol.,* 47**,** 3506-3512.

KAN, H., CHEN, B. & HONG, C. 2009. Health impact of outdoor air pollution in China: current knowledge and future research needs. *Environmental health perspectives,* 117**,** A187.

KANAKIDOU, M., SEINFELD, J. H., PANDIS, S. N., BARNES, I., DENTENER, F. J., FACCHINI, M. C., VAN DINGENEN, R., ERVENS, B., NENES, A., NIELSEN, C. J., SWIETLICKI, E., PUTAUD, J. P.,

BALKANSKI, Y., FUZZI, S., HORTH, J., MOORTGAT, G. K., WINTERHALTER, R., MYHRE, C. E. L., TSIGARIDIS, K., VIGNATI, E., STEPHANOU, E. G. & WILSON, J. 2005. Organic aerosol and global climate modelling: a review. *Atmos. Chem. Phys.,* 5**,** 1053-1123.

KAR, A., REHMAN, I. H., BURNEY, J., PUPPALA, S. P., SURESH, R., SINGH, L., SINGH, V. K., AHMED, T., RAMANATHAN, N. & RAMANATHAN, V. 2012. Real-Time Assessment of Black Carbon Pollution in Indian Households Due to Traditional and Improved Biomass Cookstoves. *Environ. Sci. Technol.,* 46**,** 2993-3000.

KIRCHSTETTER, T. W., NOVAKOV, T. & HOBBS, P. V. 2004. Evidence that the spectral dependence of light absorption by aerosols is affected by organic carbon. *Journal of Geophysical Research: Atmospheres (1984–2012),* 109.

KOCH, D., SCHULZ, M., KINNE, S., MCNAUGHTON, C., SPACKMAN, J., BALKANSKI, Y., BAUER, S., BERNTSEN, T., BOND, T. C. & BOUCHER, O. 2009. Evaluation of black carbon estimations in global aerosol models. *Atmospheric Chemistry and Physics,* 9**,** 9001-9026.

KORTELAINEN, A., JOUTSENSAARI, J., HAO, L., LESKINEN, J., TIITTA, P., JAATINEN, A., MIETTINEN, P., SIPPULA, O., TORVELA, T., TISSARI, J., JOKINIEMI, J., WORSNOP, D. R., SMITH, J. N., LAAKSONEN, A. & VIRTANEN, A. 2015. Real-Time Chemical Composition Analysis of Particulate Emissions from Woodchip Combustion. *Energy & Fuels,* 29**,** 1143-1150.

KULMALA, M., ASMI, A., LAPPALAINEN, H. K., BALTENSPERGER, U., BRENGUIER, J. L., FACCHINI, M. C., HANSSON, H. C., HOV, Ø., O'DOWD, C. D., PÖSCHL, U., WIEDENSOHLER, A., BOERS, R., BOUCHER, O., DE LEEUW, G., DENIER VAN DER GON, H. A. C., FEICHTER, J., KREJCI, R., LAJ, P., LIHAVAINEN, H., LOHMANN, U., MCFIGGANS, G., MENTEL, T., PILINIS, C., RIIPINEN, I., SCHULZ, M., STOHL, A., SWIETLICKI, E., VIGNATI, E., ALVES, C., AMANN, M., AMMANN, M., ARABAS, S., ARTAXO, P., BAARS, H., BEDDOWS, D. C. S., BERGSTRÖM, R., BEUKES, J. P., BILDE, M., BURKHART, J. F., CANONACO, F., CLEGG, S. L., COE, H., CRUMEYROLLE, S., D'ANNA, B., DECESARI, S., GILARDONI, S., FISCHER, M., FJAERAA, A. M., FOUNTOUKIS, C., GEORGE, C., GOMES, L., HALLORAN, P., HAMBURGER, T., HARRISON, R. M., HERRMANN, H., HOFFMANN, T., HOOSE, C., HU, M., HYVÄRINEN, A., HÕRRAK, U., IINUMA, Y., IVERSEN, T., JOSIPOVIC, M., KANAKIDOU, M., KIENDLER-SCHARR, A., KIRKEVÅG, A., KISS, G., KLIMONT, Z., KOLMONEN, P., KOMPPULA, M., KRISTJÁNSSON, J. E., LAAKSO, L., LAAKSONEN, A., LABONNOTE, L., LANZ, V. A., LEHTINEN, K. E. J., RIZZO, L. V., MAKKONEN, R., MANNINEN, H. E., MCMEEKING, G., MERIKANTO, J., MINIKIN, A., MIRME, S., MORGAN, W. T., NEMITZ, E., O'DONNELL, D., PANWAR, T. S., PAWLOWSKA, H., PETZOLD, A., PIENAAR, J. J., PIO, C., PLASS-DUELMER, C., PRÉVÔT, A. S. H., PRYOR, S., REDDINGTON, C. L., ROBERTS, G., ROSENFELD, D., SCHWARZ, J., SELAND, Ø., SELLEGRI, K., et al. 2011. General overview: European Integrated project on Aerosol Cloud Climate and Air Quality interactions (EUCAARI) – integrating aerosol research from nano to global scales. *Atmos. Chem. Phys.,* 11**,** 13061-13143.

LABORDE, M., MERTES, P., ZIEGER, P., DOMMEN, J., BALTENSPERGER, U. & GYSEL, M. 2012a. Sensitivity of the Single Particle Soot Photometer to different black carbon types. *Atmos. Meas. Tech.,* 5**,** 1031-1043.

LABORDE, M., SCHNAITER, M., LINKE, C., SAATHOFF, H., NAUMANN, K. H., MÖHLER, O., BERLENZ, S., WAGNER, U., TAYLOR, J. W., LIU, D., FLYNN, M., ALLAN, J. D., COE, H., HEIMERL, K., DAHLKÖTTER, F., WEINZIERL, B., WOLLNY, A. G., ZANATTA, M., COZIC, J., LAJ, P., HITZENBERGER, R., SCHWARZ, J. P. & GYSEL, M. 2012b. Single Particle Soot Photometer intercomparison at the AIDA chamber. *Atmos. Meas. Tech.,* 5**,** 3077-3097.

LACK, D. A., MOOSMÜLLER, H., MCMEEKING, G. R., CHAKRABARTY, R. K. & BAUMGARDNER, D. 2014. Characterizing elemental, equivalent black, and refractory black carbon aerosol particles: a review of techniques, their limitations and uncertainties. *Analytical and bioanalytical chemistry,* 406**,** 99-122.

LANZ, V. A., ALFARRA, M. R., BALTENSPERGER, U., BUCHMANN, B., HUEGLIN, C., SZIDAT, S., WEHRLI, M. N., WACKER, L., WEIMER, S., CASEIRO, A., PUXBAUM, H. & PREVOT, A. S. H. 2008. Source Attribution of Submicron Organic Aerosols during Wintertime Inversions by Advanced Factor Analysis of Aerosol Mass Spectra. *Environmental Science & Technology,* 42**,** 214-220.

LEE, S., LIU, W., WANG, Y., RUSSELL, A. G. & EDGERTON, E. S. 2008. Source apportionment of PM2.5: Comparing PMF and CMB results for four ambient monitoring sites in the southeastern United States. *Atmospheric Environment,* 42**,** 4126-4137.

LEI, Y., ZHANG, Q., HE, K. & STREETS, D. 2011. Primary anthropogenic aerosol emission trends for China, 1990–2005. *Atmospheric Chemistry and Physics,* 11**,** 931-954.

LEWIS, K., ARNOTT, W. P., MOOSMÜLLER, H. & WOLD, C. E. 2008. Strong spectral variation of biomass smoke light absorption and single scattering albedo observed with a novel dual-wavelength photoacoustic instrument. *Journal of Geophysical Research: Atmospheres (1984–2012),* 113.

LI, B., ZHANG, J., ZHAO, Y., YUAN, S., ZHAO, Q., SHEN, G. & WU, H. 2015a. Seasonal variation of urban carbonaceous aerosols in a typical city Nanjing in Yangtze River Delta, China. *Atmospheric Environment,* 106**,** 223-231.

LI, L., AN, J. Y., ZHOU, M., YAN, R. S., HUANG, C., LU, Q., LIN, L., WANG, Y. J., TAO, S. K., QIAO, L. P., ZHU, S. H. & CHEN, C. H. 2015b. Source apportionment of fine particles and its chemical components over the Yangtze River Delta, China during a heavy haze pollution episode. *Atmospheric Environment,* 123, Part B**,** 415-429.

LI, L., CHEN, C. H., FU, J. S., HUANG, C., STREETS, D. G., HUANG, H. Y., ZHANG, G. F., WANG, Y. J., JANG, C. J., WANG, H. L., CHEN, Y. R. & FU, J. M. 2011. Air quality and emissions in the Yangtze River Delta, China. *Atmos. Chem. Phys.,* 11**,** 1621-1639.

LIN, W., XU, X., GE, B. & LIU, X. 2011. Gaseous pollutants in Beijing urban area during the heating period 2007–2008: variability, sources, meteorological, and chemical impacts. *Atmos. Chem. Phys.,* 11**,** 8157-8170.

LIU, D., ALLAN, J. D., YOUNG, D. E., COE, H., BEDDOWS, D., FLEMING, Z. L., FLYNN, M. J., GALLAGHER, M. W., HARRISON, R. M., LEE,

J., PREVOT, A. S. H., TAYLOR, J. W., YIN, J., WILLIAMS, P. I. & ZOTTER, P. 2014. Size distribution, mixing state and source apportionment of black carbon aerosol in London during wintertime. *Atmos. Chem. Phys.,* 14**,** 10061-10084.

LIU, D., TAYLOR, J. W., YOUNG, D. E., FLYNN, M. J., COE, H. & ALLAN, J. D. 2015. The effect of complex black carbon microphysics on the determination of the optical properties of brown carbon. *Geophysical Research Letters,* 42**,** 2014GL062443.

LIU, D., WHITEHEAD, J., ALFARRA, M. R., REYES-VILLEGAS, E., SPRACKLEN, D. V., REDDINGTON, C. L., KONG, S., WILLIAMS, P. I., TING, Y.-C. & HASLETT, S. 2017. Black-carbon absorption enhancement in the atmosphere determined by particle mixing state. *Nat. Geosci.,* 10**,** 184-188.

LIU, P., ZIEMANN, P. J., KITTELSON, D. B. & MCMURRY, P. H. 1995. Generating particle beams of controlled dimensions and divergence: I. Theory of particle motion in aerodynamic lenses and nozzle expansions. *Aerosol Science and Technology,* 22**,** 293-313.

LIU, X.-H., ZHANG, Y., CHENG, S.-H., XING, J., ZHANG, Q., STREETS, D. G., JANG, C., WANG, W.-X. & HAO, J.-M. 2010. Understanding of regional air pollution over China using CMAQ, part I performance evaluation and seasonal variation. *Atmospheric Environment,* 44**,** 2415-2426.

LIU, X., LIN, B. & ZHANG, Y. 2016. Sulfur dioxide emission reduction of power plants in China: current policies and implications. *Journal of Cleaner Production,* 113**,** 133-143.

LIU, Y., CHEN, R., SHEN, X. & MAO, X. 2004. Wintertime indoor air levels of PM10, PM2.5 and PM1 at public places and their contributions to TSP. *Environment International,* 30**,** 189-197.

LU, G., BROOK, J. R., RAMI ALFARRA, M., ANLAUF, K., RICHARD LEAITCH, W., SHARMA, S., WANG, D., WORSNOP, D. R. & PHINNEY, L. 2006. Identification and characterization of inland ship plumes over Vancouver, BC. *Atmospheric Environment,* 40**,** 2767-2782.

MARMUR, A., MULHOLLAND, J. A. & RUSSELL, A. G. 2007. Optimized variable source-profile approach for source apportionment. *Atmospheric Environment,* 41**,** 493-505.

MARTINSSON, J., ERIKSSON, A., NIELSEN, I. E., MALMBORG, V. B., AHLBERG, E., ANDERSEN, C., LINDGREN, R., NYSTROM, R., NORDIN, E. & BRUNE, W. 2015. Impacts of combustion conditions and photochemical processing on the light absorption of biomass combustion aerosol. *Environ. Sci. Technol.,* 49**,** 14663-14671.

MIDDLEBROOK, A. M., BAHREINI, R., JIMENEZ, J. L. & CANAGARATNA, M. R. 2012. Evaluation of composition-dependent collection efficiencies for the aerodyne aerosol mass spectrometer using field data. *Aerosol Science and Technology,* 46**,** 258-271.

MING, L., JIN, L., LI, J., FU, P., YANG, W., LIU, D., ZHANG, G., WANG, Z. & LI, X. 2017. PM2.5 in the Yangtze River Delta, China: Chemical compositions, seasonal variations, and regional pollution events. *Environmental Pollution,* 223**,** 200-212.

MONKS, P. S., GRANIER, C., FUZZI, S., STOHL, A., WILLIAMS, M. L., AKIMOTO, H., AMANN, M., BAKLANOV, A., BALTENSPERGER, U., BEY, I., BLAKE, N., BLAKE, R. S., CARSLAW, K., COOPER, O. R., DENTENER, F., FOWLER, D., FRAGKOU, E., FROST, G. J.,

GENEROSO, S., GINOUX, P., GREWE, V., GUENTHER, A., HANSSON, H. C., HENNE, S., HJORTH, J., HOFZUMAHAUS, A., HUNTRIESER, H., ISAKSEN, I. S. A., JENKIN, M. E., KAISER, J., KANAKIDOU, M., KLIMONT, Z., KULMALA, M., LAJ, P., LAWRENCE, M. G., LEE, J. D., LIOUSSE, C., MAIONE, M., MCFIGGANS, G., METZGER, A., MIEVILLE, A., MOUSSIOPOULOS, N., ORLANDO, J. J., O'DOWD, C. D., PALMER, P. I., PARRISH, D. D., PETZOLD, A., PLATT, U., PÖSCHL, U., PRÉVÔT, A. S. H., REEVES, C. E., REIMANN, S., RUDICH, Y., SELLEGRI, K., STEINBRECHER, R., SIMPSON, D., TEN BRINK, H., THELOKE, J., VAN DER WERF, G. R., VAUTARD, R., VESTRENG, V., VLACHOKOSTAS, C. & VON GLASOW, R. 2009. Atmospheric composition change – global and regional air quality. *Atmospheric Environment,* 43**,** 5268-5350.

MOT 2015. The Statistical Report on China's Traffic in 2015 (in Chinese).

MOTEKI, N., KONDO, Y. & NAKAMURA, S.-I. 2010. Method to measure refractive indices of small nonspherical particles: Application to black carbon particles. *J. Aerosol Sci.,* 41**,** 513-521.

NI, M., HUANG, J., LU, S., LI, X., YAN, J. & CEN, K. 2014. A review on black carbon emissions, worldwide and in China. *Chemosphere,* 107**,** 83-93.

NIELSEN, I. E., ERIKSSON, A. C., LINDGREN, R., MARTINSSON, J., NYSTRÖM, R., NORDIN, E. Z., SADIKTSIS, I., BOMAN, C., NØJGAARD, J. K. & PAGELS, J. 2017. Time-resolved analysis of particle emissions from residential biomass combustion – Emissions of refractory black carbon, PAHs and organic tracers. *Atmos. Environ.,* 165**,** 179-190.

NYSTRÖM, R., LINDGREN, R., AVAGYAN, R., WESTERHOLM, R., LUNDSTEDT, S. & BOMAN, C. 2017. Influence of Wood Species and Burning Conditions on Particle Emission Characteristics in a Residential Wood Stove. *Energy & Fuels,* 31**,** 5514-5524.

OKAMOTO, S. I., WANGKIAT, A., PONGKIATKUL, P., NAKKHWAN, C. & OANH, N. T. K. 2012. Comparative Study on the CMB-8 and PMF Models for a Coastal Industrial Area. *International Journal of Environmental Protection*.

ONASCH, T., TRIMBORN, A., FORTNER, E., JAYNE, J., KOK, G., WILLIAMS, L., DAVIDOVITS, P. & WORSNOP, D. 2012. Soot particle aerosol mass spectrometer: development, validation, and initial application. *Aerosol Science and Technology,* 46**,** 804-817.

PAATERO, P. 1997. Least squares formulation of robust non-negative factor analysis. *Chemometrics and Intelligent Laboratory Systems,* 37**,** 23-35.

PAATERO, P. 1999. The Multilinear Engine—A Table-Driven, Least Squares Program for Solving Multilinear Problems, Including the n-Way Parallel Factor Analysis Model. *Journal of Computational and Graphical Statistics,* 8**,** 854-888.

PAATERO, P. & HOPKE, P. K. 2009. Rotational tools for factor analytic models. *Journal of Chemometrics,* 23**,** 91-100.

PAATERO, P., HOPKE, P. K., SONG, X.-H. & RAMADAN, Z. 2002. Understanding and controlling rotations in factor analytic models. *Chemometrics and Intelligent Laboratory Systems,* 60**,** 253-264.

PAATERO, P. & TAPPER, U. 1994. Positive matrix factorization: A non-negative factor model with optimal utilization of error estimates of data values. *Environmetrics,* 5**,** 111-126.

PAATERO, P., TAPPER, U., AALTO, P. & KULMALA, M. 1991. Matrix factorization methods for analysing diffusion battery data. *Journal of Aerosol Science,* 22, Supplement 1**,** S273-S276.

PATHAK, R. K., WU, W. S. & WANG, T. 2009. Summertime PM2.5 ionic species in four major cities of China: nitrate formation in an ammonia-deficient atmosphere. *Atmospheric Chemistry and Physics,* 9**,** 1711-1722.

PETTERSSON, E., BOMAN, C., WESTERHOLM, R., BOSTRÖM, D. & NORDIN, A. 2011. Stove Performance and Emission Characteristics in Residential Wood Log and Pellet Combustion, Part 2: Wood Stove. *Energy & Fuels,* 25**,** 315-323.

PETZOLD, A., OGREN, J. A., FIEBIG, M., LAJ, P., LI, S. M., BALTENSPERGER, U., HOLZER-POPP, T., KINNE, S., PAPPALARDO, G., SUGIMOTO, N., WEHRLI, C., WIEDENSOHLER, A. & ZHANG, X. Y. 2013. Recommendations for reporting "black carbon" measurements. *Atmos. Chem. Phys.,* 13**,** 8365-8379.

PÖSCHL, U. 2005. Atmospheric aerosols: composition, transformation, climate and health effects. *Angewandte Chemie International Edition,* 44**,** 7520-7540.

PUI, D. Y. H., CHEN, S.-C. & ZUO, Z. 2014. PM2.5 in China: Measurements, sources, visibility and health effects, and mitigation. *Particuology,* 13**,** 1-26.

QUINCEY, P. 2007. A relationship between Black Smoke Index and Black Carbon concentration. *Atmospheric Environment,* 41**,** 7964-7968.

QUINCEY, P., BUTTERFIELD, D., GREEN, D., COYLE, M. & CAPE, J. N. 2009. An evaluation of measurement methods for organic, elemental and black carbon in ambient air monitoring sites. *Atmospheric Environment,* 43**,** 5085-5091.

QUINN, P., BATES, T., COFFMAN, D., ONASCH, T., WORSNOP, D., BAYNARD, T., DE GOUW, J., GOLDAN, P., KUSTER, W. & WILLIAMS, E. 2006. Impacts of sources and aging on submicrometer aerosol properties in the marine boundary layer across the Gulf of Maine. *Journal of Geophysical Research: Atmospheres,* 111.

RAMANATHAN, V. & CARMICHAEL, G. 2008. Global and regional climate changes due to black carbon. *Nature geoscience,* 1**,** 221.

REDDINGTON, C. L., MCMEEKING, G., MANN, G. W., COE, H., FRONTOSO, M. G., LIU, D., FLYNN, M., SPRACKLEN, D. V. & CARSLAW, K. S. 2013. The mass and number size distributions of black carbon aerosol over Europe. *Atmos. Chem. Phys.,* 13**,** 4917-4939.

ROBINSON, A. L., SUBRAMANIAN, R., DONAHUE, N. M., BERNARDO-BRICKER, A. & ROGGE, W. F. 2006. Source Apportionment of Molecular Markers and Organic Aerosol. 3. Food Cooking Emissions. *Environmental Science & Technology,* 40**,** 7820-7827.

ROHDE, R. A. & MULLER, R. A. 2015. Air pollution in China: mapping of concentrations and sources. *PloS one,* 10**,** e0135749.

SAARIKOSKI, S., CARBONE, S., DECESARI, S., GIULIANELLI, L., ANGELINI, F., CANAGARATNA, M., NG, N. L., TRIMBORN, A., FACCHINI, M. C., FUZZI, S., HILLAMO, R. & WORSNOP, D. 2012. Chemical characterization of springtime submicrometer aerosol in Po Valley, Italy. *Atmos. Chem. Phys.,* 12**,** 8401-8421.

SALEH, R., HENNIGAN, C. J., MCMEEKING, G. R., CHUANG, W. K., ROBINSON, E. S., COE, H., DONAHUE, N. M. & ROBINSON, A. L.

2013. Absorptivity of brown carbon in fresh and photo-chemically aged biomass-burning emissions. *Atmos. Chem. Phys.*, 13**,** 7683-7693.
SALIBA, G., SUBRAMANIAN, R., SALEH, R., AHERN, A. T., LIPSKY, E. M., TASOGLOU, A., SULLIVAN, R. C., BHANDARI, J., MAZZOLENI, C. & ROBINSON, A. L. 2016. Optical properties of black carbon in cookstove emissions coated with secondary organic aerosols: Measurements and modeling. *Aerosol Sci. Technol.*, 50**,** 1264-1276.
SANDRADEWI, J., PRÉVÔT, A. S. H., SZIDAT, S., PERRON, N., ALFARRA, M. R., LANZ, V. A., WEINGARTNER, E. & BALTENSPERGER, U. 2008b. Using Aerosol Light Absorption Measurements for the Quantitative Determination of Wood Burning and Traffic Emission Contributions to Particulate Matter. *Environmental Science & Technology,* 42**,** 3316-3323.
SANDRADEWI, J., PRÉVÔT, A. S. H., WEINGARTNER, E., SCHMIDHAUSER, R., GYSEL, M. & BALTENSPERGER, U. 2008a. A study of wood burning and traffic aerosols in an Alpine valley using a multi-wavelength Aethalometer. *Atmospheric Environment,* 42**,** 101-112.
SCHWARZ, J., GAO, R., FAHEY, D., THOMSON, D., WATTS, L., WILSON, J., REEVES, J., DARBEHESHTI, M., BAUMGARDNER, D. & KOK, G. 2006. Single-particle measurements of midlatitude black carbon and light-scattering aerosols from the boundary layer to the lower stratosphere. *Journal of Geophysical Research: Atmospheres (1984–2012),* 111.
SCHWARZ, J., GAO, R., SPACKMAN, J., WATTS, L., THOMSON, D., FAHEY, D., RYERSON, T., PEISCHL, J., HOLLOWAY, J. & TRAINER, M. 2008a. Measurement of the mixing state, mass, and optical size of individual black carbon particles in urban and biomass burning emissions. *Geophysical Research Letters,* 35.
SCHWARZ, J. P., SPACKMAN, J. R., FAHEY, D. W., GAO, R. S., LOHMANN, U., STIER, P., WATTS, L. A., THOMSON, D. S., LACK, D. A., PFISTER, L., MAHONEY, M. J., BAUMGARDNER, D., WILSON, J. C. & REEVES, J. M. 2008b. Coatings and their enhancement of black carbon light absorption in the tropical atmosphere. *Journal of Geophysical Research: Atmospheres,* 113**,** D03203.
SEINFELD, J. H. & PANDIS, S. N. 2006. Atmospheric chemistry and physics: from air pollution to climate change.
SEINFELD, J. H. & PANDIS, S. N. 2012. *Atmospheric chemistry and physics: from air pollution to climate change*, John Wiley & Sons.
SHIRAIWA, M., YEE, L. D., SCHILLING, K. A., LOZA, C. L., CRAVEN, J. S., ZUEND, A., ZIEMANN, P. J. & SEINFELD, J. H. 2013. Size distribution dynamics reveal particle-phase chemistry in organic aerosol formation. *Proceedings of the National Academy of Sciences,* 110**,** 11746-11750.
SLOWIK, J. G., CROSS, E. S., HAN, J.-H., DAVIDOVITS, P., ONASCH, T. B., JAYNE, J. T., WILLIAMS, L. R., CANAGARATNA, M. R., WORSNOP, D. R. & CHAKRABARTY, R. K. 2007. An inter-comparison of instruments measuring black carbon content of soot particles. *Aerosol Science and Technology,* 41**,** 295-314.
SMITH, K. R., JERRETT, M., ANDERSON, H. R., BURNETT, R. T., STONE, V., DERWENT, R., ATKINSON, R. W., COHEN, A., SHONKOFF, S. B., KREWSKI, D., POPE, C. A., THUN, M. J. & THURSTON, G. 2009. Public health benefits of strategies to reduce greenhouse-gas emissions: health implications of short-lived greenhouse pollutants. *The Lancet,* 374**,** 2091-2103.

SONG, Y., DAI, W., SHAO, M., LIU, Y., LU, S., KUSTER, W. & GOLDAN, P. 2008. Comparison of receptor models for source apportionment of volatile organic compounds in Beijing, China. *Environmental Pollution,* 156**,** 174-183.

STEPHENS, M., TURNER, N. & SANDBERG, J. 2003. Particle identification by laser-induced incandescence in a solid-state laser cavity. *Applied Optics,* 42**,** 3726-3736.

STONE, E. A., SNYDER, D. C., SHEESLEY, R. J., SULLIVAN, A. P., WEBER, R. J. & SCHAUER, J. J. 2008. Source apportionment of fine organic aerosol in Mexico City during the MILAGRO experiment 2006. *Atmospheric Chemistry and Physics,* 8**,** 1249-1259.

TAKEGAWA, N., MIYAZAKI, Y., KONDO, Y., KOMAZAKI, Y., MIYAKAWA, T., JIMENEZ, J., JAYNE, J., WORSNOP, D., ALLAN, J. & WEBER, R. 2005. Characterization of an Aerodyne Aerosol Mass Spectrometer (AMS): Intercomparison with other aerosol instruments. *Aerosol Science and Technology,* 39**,** 760-770.

TAULER, R., VIANA, M., QUEROL, X., ALASTUEY, A., FLIGHT, R. M., WENTZELL, P. D. & HOPKE, P. K. 2009. Comparison of the results obtained by four receptor modelling methods in aerosol source apportionment studies. *Atmospheric Environment,* 43**,** 3989-3997.

TOPPING, D., COE, H., MCFIGGANS, G., BURGESS, R., ALLAN, J., ALFARRA, M., BOWER, K., CHOULARTON, T., DECESARI, S. & FACCHINI, M. C. 2004. Aerosol chemical characteristics from sampling conducted on the Island of Jeju, Korea during ACE Asia. *Atmospheric Environment,* 38**,** 2111-2123.

TURPIN, B. J., SAXENA, P. & ANDREWS, E. 2000. Measuring and simulating particulate organics in the atmosphere: problems and prospects. *Atmos. Environ.,* 34**,** 2983-3013.

VENKATARAMAN, C., SAGAR, A. D., HABIB, G., LAM, N. & SMITH, K. R. 2010. The Indian National Initiative for Advanced Biomass Cookstoves: The benefits of clean combustion. *Energy Sustain. Dev.,* 14**,** 63-72.

VIANA, M., KUHLBUSCH, T. A. J., QUEROL, X., ALASTUEY, A., HARRISON, R. M., HOPKE, P. K., WINIWARTER, W., VALLIUS, M., SZIDAT, S., PRÉVÔT, A. S. H., HUEGLIN, C., BLOEMEN, H., WÅHLIN, P., VECCHI, R., MIRANDA, A. I., KASPER-GIEBL, A., MAENHAUT, W. & HITZENBERGER, R. 2008. Source apportionment of particulate matter in Europe: A review of methods and results. *Journal of Aerosol Science,* 39**,** 827-849.

VICENTE, E. D., DUARTE, M. A., CALVO, A. I., NUNES, T. F., TARELHO, L. A. C., CUSTÓDIO, D., COLOMBI, C., GIANELLE, V., SANCHEZ DE LA CAMPA, A. & ALVES, C. A. 2015. Influence of operating conditions on chemical composition of particulate matter emissions from residential combustion. *Atmos. Res.,* 166**,** 92-100.

WANG, M., CAO, C., LI, G. & SINGH, R. P. 2015. Analysis of a severe prolonged regional haze episode in the Yangtze River Delta, China. *Atmospheric Environment,* 102**,** 112-121.

WANG, Q., SCHWARZ, J. P., CAO, J., GAO, R., FAHEY, D. W., HU, T., HUANG, R. J., HAN, Y. & SHEN, Z. 2014a. Black carbon aerosol characterization in a remote area of Qinghai–Tibetan Plateau, western China. *Science of The Total Environment,* 479–480**,** 151-158.

WANG, X., HEALD, C. L., SEDLACEK, A. J., DE SÁ, S. S., MARTIN, S. T., ALEXANDER, M. L., WATSON, T. B., AIKEN, A. C., SPRINGSTON,

S. R. & ARTAXO, P. 2016. Deriving Brown Carbon from Multi-Wavelength Absorption Measurements: Method and Application to AERONET and Surface Observations. *Atmos. Chem. Phys. Discuss.,* 2016**,** 1-33.
WANG, Z., LI, J., WANG, Z., YANG, W., TANG, X., GE, B., YAN, P., ZHU, L., CHEN, X., CHEN, H., WAND, W., LI, J., LIU, B., WANG, X., WAND, W., ZHAO, Y., LU, N. & SU, D. 2014b. Modeling study of regional severe hazes over mid-eastern China in January 2013 and its implications on pollution prevention and control. *Science China Earth Sciences,* 57**,** 3-13.
WASHENFELDER, R., ATTWOOD, A., BROCK, C., GUO, H., XU, L., WEBER, R., NG, N., ALLEN, H., AYRES, B. & BAUMANN, K. 2015. Biomass burning dominates brown carbon absorption in the rural southeastern United States. *Geophysical Research Letters,* 42**,** 653-664.
WATSON, J. G. 2002. Visibility: Science and regulation. *Journal of the Air & Waste Management Association,* 52**,** 628-713.
WATTS, J. 2012. Air pollution could become China's biggest health threat, expert warns. *The Guardian,* 16.
WEIMER, S., DREWNICK, F., HOGREFE, O., SCHWAB, J. J., RHOADS, K., ORSINI, D., CANAGARATNA, M., WORSNOP, D. R. & DEMERJIAN, K. L. 2006. Size-selective nonrefractory ambient aerosol measurements during the Particulate Matter Technology Assessment and Characterization Study–New York 2004 Winter Intensive in New York City. *Journal of Geophysical Research: Atmospheres,* 111.
WEINGARTNER, E., SAATHOFF, H., SCHNAITER, M., STREIT, N., BITNAR, B. & BALTENSPERGER, U. 2003. Absorption of light by soot particles: determination of the absorption coefficient by means of aethalometers. *Journal of Aerosol Science,* 34**,** 1445-1463.
WHO 2014. WHO Guidelines for Indoor Air Quality: Household Fuel Combustion, Geneva, Switzerland, World Health Organisation.
WONG, E. 2013. China's Smog Toll Put at 1.2 Million. *International Herald Tribune,* 5.
WROTH, C. & WILES, A. 2009. Population and vital statistics by area of usual residence in the United Kingdom, 2007. *Office for National Statistics, Newport, UK,* series vs no 34, ppi no 30.
WU, Y., WANG, X., TAO, J., HUANG, R., TIAN, P., CAO, J., ZHANG, L., HO, K.-F., HAN, Z. & ZHANG, R. 2017. Size distribution and source of black carbon aerosol in urban Beijing during winter haze episodes. *Atmospheric Chemistry and Physics,* 17**,** 7965-7975.
XU, H.-H., PU, J.-J., HE, J., LIU, J., QI, B. & DU, R.-G. 2016. Characteristics of Atmospheric Compositions in the Background Area of Yangtze River Delta during Heavy Air Pollution Episode. *Advances in Meteorology,* 2016**,** 13.
YANG, G., WANG, Y., ZENG, Y., GAO, G. F., LIANG, X., ZHOU, M., WAN, X., YU, S., JIANG, Y., NAGHAVI, M., VOS, T., WANG, H., LOPEZ, A. D. & MURRAY, C. J. L. 2013. Rapid health transition in China, 1990–2010: findings from the Global Burden of Disease Study 2010. *The Lancet,* 381**,** 1987-2015.
YIN, J., CUMBERLAND, S. A., HARRISON, R. M., ALLAN, J., YOUNG, D. E., WILLIAMS, P. I. & COE, H. 2015. Receptor modelling of fine

particles in southern England using CMB including comparison with AMS-PMF factors. *Atmos. Chem. Phys.*, 15**,** 2139-2158.
YOUNG, D., ALLAN, J., WILLIAMS, P., GREEN, D., FLYNN, M., HARRISON, R., YIN, J., GALLAGHER, M. & COE, H. 2015. Investigating the annual behaviour of submicron secondary inorganic and organic aerosols in London. *Atmospheric Chemistry and Physics,* 15**,** 6351-6366.
YOUNG, D. E., ALLAN, J. D., WILLIAMS, P. I., GREEN, D. C., FLYNN, M. J., HARRISON, R. M., YIN, J., GALLAGHER, M. W. & COE, H. 2014. Investigating the annual behaviour of submicron secondary inorganic and organic aerosols in London. *Atmos. Chem. Phys. Discuss.*, 14**,** 18739-18784.
ZHANG, Q., GENG, G., WANG, S., RICHTER, A. & HE, K. 2012. Satellite remote sensing of changes in NO x emissions over China during 1996–2010. *Chinese Science Bulletin,* 57**,** 2857-2864.
ZHANG, Q., JIMENEZ, J. L., CANAGARATNA, M. R., ALLAN, J. D., COE, H., ULBRICH, I., ALFARRA, M. R., TAKAMI, A., MIDDLEBROOK, A. M., SUN, Y. L., DZEPINA, K., DUNLEA, E., DOCHERTY, K., DECARLO, P. F., SALCEDO, D., ONASCH, T., JAYNE, J. T., MIYOSHI, T., SHIMONO, A., HATAKEYAMA, S., TAKEGAWA, N., KONDO, Y., SCHNEIDER, J., DREWNICK, F., BORRMANN, S., WEIMER, S., DEMERJIAN, K., WILLIAMS, P., BOWER, K., BAHREINI, R., COTTRELL, L., GRIFFIN, R. J., RAUTIAINEN, J., SUN, J. Y., ZHANG, Y. M. & WORSNOP, D. R. 2007. Ubiquity and dominance of oxygenated species in organic aerosols in anthropogenically-influenced Northern Hemisphere midlatitudes. *Geophysical Research Letters,* 34**,** L13801.
ZHANG, Q., JIMENEZ, J. L., CANAGARATNA, M. R., ULBRICH, I. M., NG, N. L., WORSNOP, D. R. & SUN, Y. 2011. Understanding atmospheric organic aerosols via factor analysis of aerosol mass spectrometry: a review. *Analytical and Bioanalytical Chemistry,* 401**,** 3045-3067.
ZHANG, X., SMITH, K. A., WORSNOP, D. R., JIMENEZ, J., JAYNE, J. T. & KOLB, C. E. 2002. A numerical characterization of particle beam collimation by an aerodynamic lens-nozzle system: Part I. An individual lens or nozzle. *Aerosol Science & Technology,* 36**,** 617-631.
ZHANG, X., SMITH, K. A., WORSNOP, D. R., JIMENEZ, J. L., JAYNE, J. T., KOLB, C. E., MORRIS, J. & DAVIDOVITS, P. 2004. Numerical characterization of particle beam collimation: Part II integrated aerodynamic-lens–nozzle system. *Aerosol Science and Technology,* 38**,** 619-638.
ZHANG, Y., SHEESLEY, R. J., SCHAUER, J. J., LEWANDOWSKI, M., JAOUI, M., OFFENBERG, J. H., KLEINDIENST, T. E. & EDNEY, E. O. 2009. Source apportionment of primary and secondary organic aerosols using positive matrix factorization (PMF) of molecular markers. *Atmospheric Environment,* 43**,** 5567-5574.
ZHANG, Y., TANG, L., YU, H., WANG, Z., SUN, Y., QIN, W., CHEN, W., CHEN, C., DING, A., WU, J., GE, S., CHEN, C. & ZHOU, H.-C. 2015. Chemical composition, sources and evolution processes of aerosol at an urban site in Yangtze River Delta, China during wintertime. *Atmospheric Environment,* 123, Part B**,** 339-349.
ZHANG, Y., YANG, X., BROWN, R., YANG, L., MORAWSKA, L., RISTOVSKI, Z., FU, Q. & HUANG, C. 2017. Shipping emissions and

their impacts on air quality in China. *Science of The Total Environment,* 581-582**,** 186-198.
ZHUANG, B. L., WANG, T. J., LIU, J., LI, S., XIE, M., YANG, X. Q., FU, C. B., SUN, J. N., YIN, C. Q., LIAO, J. B., ZHU, J. L. & ZHANG, Y. 2014. Continuous measurement of black carbon aerosol in urban Nanjing of Yangtze River Delta, China. *Atmospheric Environment,* 89**,** 415-424.